
# Defining the role of exercise in prostate cancer bone metastasis

A thesis submitted in fulfilment of the requirements
for the degree of Doctor of Philosophy

by

Hector Manuel Arredondo Carrera

March 2022

Department of Oncology and Metabolism
The University of Sheffield

## List of contents

## List of figures

### Chapter 1

**Chapter 2**



**Chapter 3**

**Chapter 4**



**Chapter 5**

**Chapter 6**

**Chapter 7**



**Chapter 8**

## List of tables

### Chapter 2



### Chapter 3



### Chapter 5



### Chapter 6

**Chapter 7**



**Chapter 8**

**Appendix A**

# List of abbreviations

| | |
|---|---|
| **ADT** | Androgen depravation |
| **AE** | Aerobic exercise |
| **AI** | Androgen-independent |
| **ALP** | Alkaline phosphatase |
| **ATF4** | Activating-transcription factor 4 |
| **ATP** | Adenosine triphosphate |
| **BCa** | Breast cancer |
| **BLCs** | Bone lining cells |
| **BM** | Bone marrow |
| **BMC** | Bone mineral content |
| **BMD** | Bone mineral density |
| **BMPs** | Bone morphogenetic proteins |
| **BMU** | Basic multicellular unit |
| **BSD** | Basolateral secretory domain |
| **BSP** | Bone sialoprotein |
| **BV** | Bone volume |
| **BV/TV** | Trabecular bone volume fraction |
| **CCD** | Charged coupled device |
| **CDK** | Cyclin dependent kinase |
| **CGRP** | Calcitonin gene-related peptide |
| **Cl** | Chloride |
| **CRF** | Cardioresporatory fitness |
| **CSF2** | Colony stimulating factor 2 |
| **CTX** | Carboxy-terminal telopeptide of type 1 collagen |
| **CVD** | Cardiovascular diseases |
| **CXCL12** | Chemokine ligand 12 |
| **CXCR** | Chemokine receptor |
| **DA** | Degree of anisotropy |

| | |
|---|---|
| **DAP12** | DNAX-activation protein 12 |
| **DC-STAMP** | Dendritic-cell specific transmembrane protein |
| **DMEM** | Dulbecco’s modified Eagle’s medium |
| **DMP-1** | Dentin matrix protein 1 |
| **DSPP** | Dentin sialophoshoprotein |
| **EDTA** | Ethylenediaminetetraacetic acid |
| **EGF** | Epidermal growth factor |
| **EMT** | Epithelial to mesenchymal transition |
| **ERK** | Extracellular signal-related protein kinase |
| **FAK** | Focal adhesion kinase |
| **FCS** | Foetal calf serum |
| **FE** | Finite elements |
| **FGF-23** | Fibroblast growth factor 23 |
| **FGFR** | Fibroblast growth factor receptor |
| **GAS6** | Growth factor growth arrest-specific 6 |
| **HSCs** | Hematopoietic stem cells |
| **IGF-1** | Insulin like growth factor-1 |
| **IGFBP-1** | Growth factor binding protein 1 |
| **IVIS** | In vivo imaging system |
| **KO** | Knock out |
| **LAPC-9** | Los Angeles Prostate Cancer-9 |
| **LMHFV** | Low-magnitude high-frequency vibration |
| **MAPK** | Mitogen-activated protein kinase |
| **M-CSF** | Macrophage colony-stimulating factor |
| **MEPE** | Matrix extracellular phosphoglycoprotein |
| **MET** | Metabolic equivalent task |
| **Micro-CT** | Micro Computed Tomography |
| **MMP** | Matrix metalloproteinase |
| **MRI** | Magnetic resonance imaging |
| **MSCs** | Mesenchymal cells |

| | |
|---|---|
| **MTS** | Multi time series |
| **N.Ob/B.Pm** | Number of osteoblasts |
| **N.Oc/B.Pm** | Number of osteoclasts |
| **NBF** | Neutral buffered formalin |
| **NCPs** | Non-collagenous proteins |
| **NDRG1** | N-myc downstream-regulated gene 1 |
| **NFATc1** | Nuclear Factor Of Activated T Cells 1 |
| **NO** | Nitric oxide |
| **Ob.Pm/B.Pm** | Perimeter occupied by osteoblasts |
| **Oc.Pm/B.Pm** | Perimeter occupied by osteoclasts |
| **OCN** | Osteocalcin |
| **OFF** | Oscillatory fluid flow |
| **OPG** | Osteoprotegrin |
| **OSCAR** | Osteoclast-associated receptor |
| **P1NP** | Amino-terminal propeptide |
| **PANTERA** | Prostate cancer novel therapy |
| **PBS** | Phosphate-buffered saline |
| **PCa** | Prostate cancer |
| **PDGF** | Platelet-derived growth factor |
| **PDX** | Patient derived xenograft |
| **Pen-strep** | Penicillin-Streptomycin |
| **PGE** | Prostaglandin |
| **PHEX** | Metalloendopeptidase homolog PEX |
| **PPL** | Procedure Project License |
| **PTHrP** | Parathyroid hormone-related protein |
| **QoL** | Quality of life |
| **RANKL** | Nuclear factor-κB ligand |
| **RB** | Ruffled border |
| **RCT** | Randomized controlled trial |
| **RE** | Resistance exercise |

| | |
|---|---|
| **RER** | Rough endoplasmic reticulum |
| **RIA** | Radioimmunoassay |
| **ROI** | Region of interest |
| **RT** | Room temperature |
| **RUNX2** | Runt-related transcription factor 2 |
| **S249/T252** | Serine-249 and threonine-252 |
| **SCID** | Severe combined immunodeficient |
| **SCID** | Severely compromised immunodeficient |
| **SMI** | Structure model index |
| **SP** | Substance P |
| **SRE** | Skeletal related events |
| **SZ** | Sealing zone |
| **Tb. Pf** | Trabecular bone pattern factor |
| **Tb.N** | Trabecular number |
| **Tb.Sp** | Trabecular separation |
| **Tb.Th** | Trabecular thickness |
| **TGF-β** | Transforming growth factor β |
| **TRAMP** | Transgenic adenocarcinoma of the mouse prostate |
| **TRAP** | Tartrate-resistant acid phosphatase |
| **TWIST2** | Twist homolog 2 |
| **TYRO** | Tyrosine kinase-binding protein |
| **VIP** | Vasoactive intestinal peptide |
| **WASp** | Wiskott-Aldrich syndrome protein |
| **WBVP** | Whole body vibration platform |
| **WT** | Wild type |

# Acknowledgments

First of all, I would like to express my gratitude to Dr. Ning Wang for the invaluable support he has given me since I started my master's degree in 2016 by his side. I have been able to learn so much and enjoy the scientific field thanks to his enthusiasm and joyful spirit. Thank you for the opportunities you have offered me, to travel to congresses and present my research project, being part of your lab group, contribute to articles, reviews, and book chapters. Thank you for pushing me to be better each day and pursue greatness and most importantly, happiness.

To my second supervisor Professor Alison Gartland. Thank you for being a truly inspiration to become a good scientist. Thank you for depth-in knowledge in bone cancer, your collaboration, and your kindness. To Dr. Karan Shah, Dr. Ameera Jailani, Dr. Paris Avgoustou, Dr. Jessica Warrington, Dr. Gareth Richards for teaching me how to be a great scientist while keeping it fun. I want to mention a special gratitude to PhD-to-be Alex Sprules. Thank you so much for all your help, I would have been lost without you. You became an amazing scientist and friend during this time. If I am half as good as you, I would consider myself the best scientist ever!

I am also grateful with Prostate Cancer UK and CONACYT. Their funding opportunity allowed me to be part of this project and provide evidence useful for the world.

To all my friends who I left in Mexico and the ones who I made here in the UK: Rebeca, Ary, Gerson, Ana, Chofis, Neto, Mariana, Idalia, Kari, Iván, Claudia, Manuel, Sandy, Victor, Carlos, Giovana, Brenda, Sebastiano, Marguerita and lot more. My life in the UK would have been very different without you guys. You became my family. To Jack Semmence for keeping me sane and happy during all these months of writing.

Finally, I will be forever grateful to my family for their love and support they have given me my entire life. To my dad, mom, and my sister. I love you and miss you, but I know it's all worth it. I'm here thanks to you.

# Publications

## Articles

Zhou, Y., **Arredondo, H. M.,** & Wang, N. (2022). P2Y Receptors in Bone - Anabolic, Catabolic, or Both? Frontiers in endocrinology, 12, 818499. https://doi.org/10.3389/fendo.2021.818499

He, J., Zhou, Y., **Arredondo Carrera, H. M**., Sprules, A., Neagu, R., Zarkesh, S. A., Eaton, C., Luo, J., Gartland, A., & Wang, N. (2020). Inhibiting the P2X4 Receptor Suppresses Prostate Cancer Growth In Vitro and In Vivo, Suggesting a Potential Clinical Target. Cells, 9(11), 2511. https://doi.org/10.3390/cells9112511

Roberts, B. C., **Arredondo Carrera, H. M**., Zanjani-Pour, S., Boudiffa, M., Wang, N., Gartland, A., & Dall'Ara, E. (2020). PTH(1-34) treatment and/or mechanical loading have different osteogenic effects on the trabecular and cortical bone in the ovariectomized C57BL/6 mouse. Scientific reports, 10(1), 8889. https://doi.org/10.1038/s41598-020-65921-1

## Abstracts

Ning Wang, **Hector M. Arredondo**, Alexandria R. Sprules, Colby L. Eaton. Continuous load bearing exercise inhibits the development of prostate cancer bone metastasis [abstract]. In: Proceedings of the Annual Meeting of the American Association for Cancer Research 2020; 2020 Apr 27-28 and Jun 22-24. Philadelphia (PA): AACR; Cancer Res 2020;80(16 Suppl):Abstract nr 3481.

**ARREDONDO, Hector**, SPRULES, Alexandria, EATON, Colby and WANG, Ning (2020). Different prostate cancer bone metastasis models respond differently to treadmill exercise. Bone Reports, 13, p. 100309.

**Hector Arredondo**, Colby Eaton, Ning Wang. Defining the role of P2X7 receptor in the dormant population of prostate cancer cells. The Mellanby Centre for Bone Research, Department of Oncology & Metabolism, Sheffield, United Kingdom. Journal of Bone Oncology, Volume 13, November 2018, pages 11-54.

**Book chapters**

Dormancy in cancer bone metastasis. **Hector M. Arredondo Carrera**, Ning Wang, in Bone Sarcomas and Bone Metastases - From Bench to Bedside (Third Edition), 2022. Pages 393-410.

# Abstract

Prostate cancer (PCa) is one of the most common cancers diagnosed in men of western countries. It is estimated that ~70% of patients with PCa will develop bone metastasis, in which the disease is considered to be incurable. Therefore, alternative therapies are in need to be evaluated. Exercise has been shown to be safe and tolerable for patients with PCa, and have positive outcomes, such as reduced cancer-related fatigue, improvement in quality of life, and increased strength and bone mass. However, there are no evidence related to the effect of exercise in patients with PCa bone metastasis. As exercise is a known factor to induce an osteogenic response and improve the bone health, we hypothesize that physical exercise interferes in the development of PCa skeletal metastases through promoting osteogenic response.

To test this overarching hypothesis and examine the effect of exercise in PCa bone metastasis, we used PCa xenograft and syngeneic murine models and applied three different exercise regimens: tibial mechanical loading which mimics load-bearing exercise, treadmill running and whole-body high frequency low magnitude vibration platform. Firstly, the tibial mechanical loading not only effectively induced an osteogenic response within the first week of loading (3 loads) but also caused the spatial re-distribution of osteoblasts and osteoclasts cells in the loaded tibias. The arrival of PCa cells into bone was not enhanced by the osteogenic response induced by mechanical loading examined using quantitative multiphoton microscopy *ex vivo*. Furthermore, continuous tibial mechanical loading reduced the PCa bone metastasis incidence and tumour burden and preserved the bone structure parameters in the intracardiac injected xenograft and syngeneic PCa models and in the intra-tail artery injected xenograft model. This effect might be mediated by breakage of the vicious cycle due to the osteoclast's inhibition, and the alteration of the profile of pro-metastatic cytokines such as DKK1 and RANTES. Interestingly, treadmill running and whole-body vibration platform stimulus did not affect the development of PCa bone metastasis, a result possibly caused by these exercise regimens being insufficient to generate an osteogenic response.

These findings support our original hypothesis and provide invaluable information for future research and clinical trials in applying appropriate exercise regimens as an alternative therapeutic strategy in patients already with or in risk of developing PCa bone metastasis.

# CHAPTER 1:

## Introduction

## 1.1. Introduction

Prostate cancer (PCa) is a leading cause of mortality in men in the UK with a predilection to metastasise the bone tissue. Once PCa has been established in bone, it is considered to be incurable. In addition, it is estimated that more than 70% of the patients with PCa will develop skeletal metastasis, making the identification of mechanisms involved in bone metastasis and finding a cure, imperative (Florencio-silva et al. 2015; Nørgaard et al. 2010). Bone metastasis alters bone remodelling, a process to maintain bone health by resorption of old tissue and deposition of new bone matrix. In advanced stages, bone metastasis can lead to pain in bone, pathological fractures and spinal cord compression, pathologies known as skeletal related events (SRE) (Nørgaard et al. 2010). On the other hand, exercise is an important anabolic stimulus that improves bone formation and strength (Yuan et al. 2016). The aim of this project is to study the effect of exercise in PCa bone metastasis, using three modalities of exercise: mechanical loading which mimics load-bearing exercise, treadmill running and vibration platform. Here, we discuss the basics of bone biology, followed by PCa bone metastasis and colonisation into bone, the benefits of exercise in PCa, and evidence that has assessed the effect of mechanical loading in other types of cancer.

## 1.2. Basics of Bone Biology

### 1.2.1. Human skeletal system

The skeletal system is an organized set of pieces where bone and cartilage are the principal units. At birth, the skeletal system is comprised of approximately 300 bones that fuse together through age to reach a final number of 206 in a human adult. The skeleton is divided into axial and appendicular. The spine, ribs cage and the skull form the axial skeleton while the upper and lower limb constitute the appendicular skeleton. After full development, the bone does not maintain static features, but continues to renew itself, where internal stimulus like hormones, cytokines and external stimulus such as mechanical loading and strain are essential to maintain a healthy bone tissue structure (Cavendish 2010).

### 1.2.2. Bone

Bone is a specialized connective tissue comprised mainly of four cell types: osteoblasts, osteoclasts, osteocytes and bone lining cells (BLCs), also including a mineralized extracellular matrix, figure 1.1. The main element in bone matrix is collagen type I followed by proteoglycans (decorin and biglycan) and non-collagen proteins like osteonectin and osteopontin. Mineralisation of the extracellular matrix occurs by calcium deposition in the form of hydroxyapatite crystals, resulting in a hard tissue playing important roles (Florencio-silva et al. 2015).

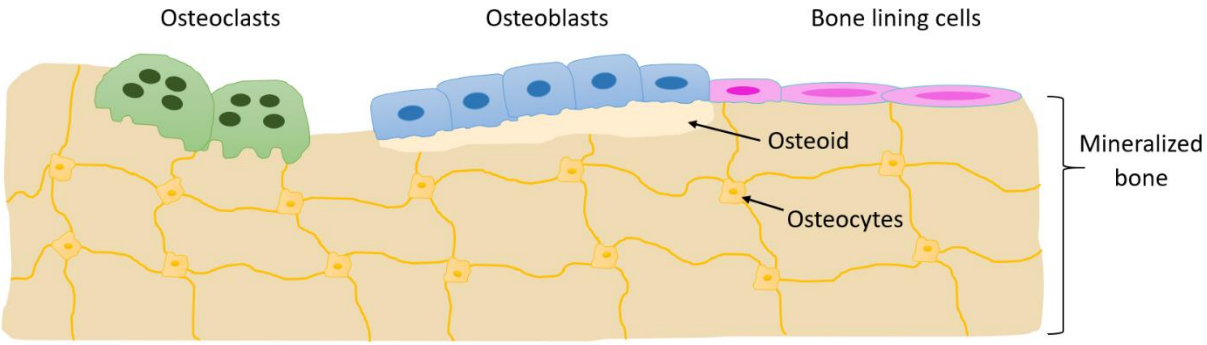


**Figure 1. 1. Distribution of bone cells**. *Four cell types are found in bone tissue: osteoclasts, osteoblasts, and bone lining cell, mainly located on bone surface. The fourth cell is the osteocyte, embedded in the bone matrix.*

Bone functions are described in six categories: 1) support of the body weight, 2) protection of vital organs, 3) locomotion, acting as inserts for muscles, 4) haematopoiesis, taking place in the bone marrow (BM), 5) storehouse for minerals such as calcium and phosphate, therefore, it is also involved in calcium metabolism, 6) as an endocrine organ by producing fibroblast growth factor 23 (FGF-23) and osteocalcin. The FGF-23 and osteocalcin have roles in phosphate and glucose metabolism, respectively (Florencio-silva et al. 2015).

### 1.2.3. Bone anatomy

Bones are classified according to their size and shape into long, short, flat, and irregular. The femur and tibia are typical examples of long bones while carpal and tarsal bones fall into the short bone category. Bones of the skull, sternum and ribs illustrate the flat bones group. The vertebrae, sacrum and coccyx are known as irregular bones. (Clarke 2008).

At a macroscopic level, the bone is constituted by a cortical and a trabecular tissue. The cortical bone is a high compact structure with roles in bone strength and mechanical load bearing. Trabecular bone has a porous light structure composed of struts and plates, conferring internal support in the event of mechanical loading while conferring a light bone architecture (Burr & Allen 2013).

Three anatomic regions are found in a typical long bone: the epiphysis, metaphysis, and diaphysis. The epiphysis is located at the top of the bone, it has a rounded-like shape covered by cartilage that contacts neighbouring bones which creates the joint. The diaphysis is predominantly composed of cortical bone, which provides weight bearing function and contains the BM within the medullary cavity. The metaphysis lies between the epiphysis and diaphysis, consisting mainly of trabecular bone and transmit the bear loading force to the diaphysis (Clarke 2008).

The growth plate is another important region found between the epiphysis and metaphysis. Overtime, the cartilaginous growth plate gets replaced by cortical tissue making it responsible for longitudinal bone development. Evidence suggests that

mechanical loading is an important stimulus to the growth plate to achieve bone formation (Stokes et al. 2002).

### 1.2.4. Bone histology: cells and function

#### *Osteoblasts*

Osteoblasts are the cells responsible for bone formation. They produce the osteoid matrix which later becomes mature bone tissue. In this process some osteoblasts become sequestrated to form the osteocyte cells or undergo quiescence in the bone surface to become BLCs. Histologically, they are single-nucleated cells with a large Golgi complex and a hypertrophic endoplasmic reticulum associated with the production of bone matrix proteins (Dudley & Spiro 1961).

When mature, osteoblasts secrete several proteins that regulate bone formation. One of the most important is collagen type 1, where the hydroxyapatite crystals (formed by calcium and phosphate) are deposited. Moreover, the osteoblasts produce other non-collagenous proteins (NCPs) imperative for bone matrix integrity: osteonectin, osteopontin, osteocalcin (OCN), bone sialoprotein (BSP) I/II and proteoglycans like decorin and biglycan. Expression of the enzyme alkaline phosphatase (ALP) is also important in osteoblasts function. Although the precise role of ALP is not yet elucidated, has been implicated in bone mineralisation by degradation of the mineralisation inhibitor: pyrophosphatase (Lynch et al. 1995; Midura et al. 1994; Whyte 1994).

Osteoblasts are derived from a group of pluripotent cells known as mesenchymal cells (MSCs). The osteoblastogenesis initiates when MSCs become committed to pre-osteoblast via runt-related transcription factor 2 (RUNX2) and ALP (Kuo et al. 2016). After pre-osteoblast differentiation, the full osteoblasts maturation is completed when osterix, a downstream gene of RUNX2, and bone mineralization factors such as activating-transcription factor 4 (ATF4), OCN, osteopontin, BSPs are expressed. Finally, osteoblasts fate could end as BLCs, osteocytes or follow apoptosis, figure 1.2. (Tang et al. 2011)

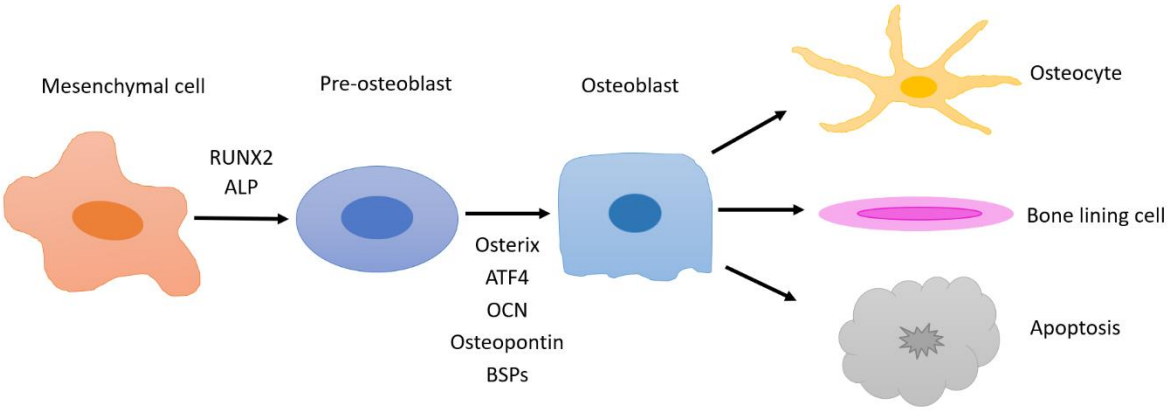


**Figure 1. 2. Osteoblastogenesis.** *Mesenchymal cells differentiate into pre-osteoblasts by RUNX2 and ALP action. Fully mature osteoblasts display markers like Osterix, ATF4, OCN, Osteopontin and BSPs. After fulfilling their function, osteoblasts become osteocytes, bone lining cells or undergo apoptosis.*

### *Osteoclasts*

Bone resorption is mediated by osteoclasts. They are large multinucleated cells with exclusive physical properties which are exhibited when polarized or mature. These histologic characteristics are a sealing zone (SZ) (or clear zone), the ruffled border (RB) and a basolateral secretory domain (BSD) (Baron et al. 1985).

The bone degradation process begins when the osteoclasts become highly attached to the bone area which will be resorb by the SZ. The components of the SZ are F-actin-binding proteins including cortactin, gelsolin, Wiskott-Aldrich syndrome protein (WASp) and Arp2/3, integrins and linkage-associated proteins such as vinculin, talin, Pyk2 and filamin, all of which ensure the isolation of the osteoclast from the external cell (Hurst et al. 2004; Tehrani et al. 2006). After cell adhesion, lysosomal enzymes containing hydrogen ions ($H^+$) and Chloride ($Cl^-$) ions and proteinases like matrix metalloproteinase 9 (MMP9) and Cathepsin K are released throughout the RB. The $H^+$ ions are expelled by vacuolar $H^+$-ATPase and $Cl^-$ through chloride channels located in the RB. The $H^+$ plus $Cl^-$ create hydrochloric acid, favouring collagen type 1 degradation in hand with MMP9 and Cathepsin K. The bone matrix residues are then endocytosed and transported by transcytosis to the BSD where they are finally secreted (Mulari et al. 2003; Oshiro et al. 2001).

The osteoclasts originate in hematopoietic stem cells from the monocyte/macrophage lineage through stimulation of the macrophage colony-stimulating factor (M-CSF) and the receptor activator of nuclear factor-κB ligand (RANKL). First, M-CSF binding to c-Fms receptors in osteoclast precursors activates the PI3K/Akt and ERK pathways, resulting in proliferation and survival of osteoclast cells. Several factors like RANKL (expressed by osteoblasts), the dendritic-cell specific transmembrane protein (DC-STAMP), the vacuolar $H^+$-ATPase subunit D2, the tyrosine kinase-binding protein (TYRO) and DNAX-activation protein 12 (DAP12) stimulate the mononucleated pre-osteoclasts to fuse together and create the multinucleated osteoclast (Burr & Allen 2013). Osteoclast's differentiation is induced when RANKL binds RANK receptor in osteoclasts. The RANKL signalling stimulates NF-κB and c-Fos, to activate the osteoclastogenic marker nuclear factor of activated T cells 1 (NFATc1). At the end,

NFATc1 mediates the expression of genes found only in osteoclasts such as tartrate-resistant acid phosphatase (TRAP), osteoclast-associated receptor (OSCAR), and cathepsin K. More recently, it has been suggested that osteoclasts undergo recycling by fission into daughter cells, named osteomorphs. This was evidenced by the group of Mcdonald et al. (2021) where they tracked the osteoclast's fate *in vivo* by means of small conditional RNA (scRNA) and intravital imaging. The osteomorphs where shown to re-fuse with osteoclasts, by this manner "recycling" the osteoclasts cells. This fission cell products displayed a unique cell profile comprised of AXL, CCR3, VCAM1, CD74, and CAM1 which was detected by scRNA. This study suggests that osteoclasts recycle through osteomorphs as an alternate fate to apoptosis and supports the long-life spam of osteoclasts and precursors described by others (Jacome-galarza et al. 2019). In addition, osteomorphs are thought to undergo a less aggressive bone resorption with reduced acidity and increased motility as they would require reduced mitochondrial activity and metabolism (Søe & Delaissé 2017). Furthermore, osteoclastogenesis is supressed by osteoprotegrin (OPG), a factor produced by osteoblasts that binds to RANKL as a decoy receptor, disrupting the RANK downstream pathway, figure 1.3 (Matsumoto et al. 2004; Karst et al. 2015).

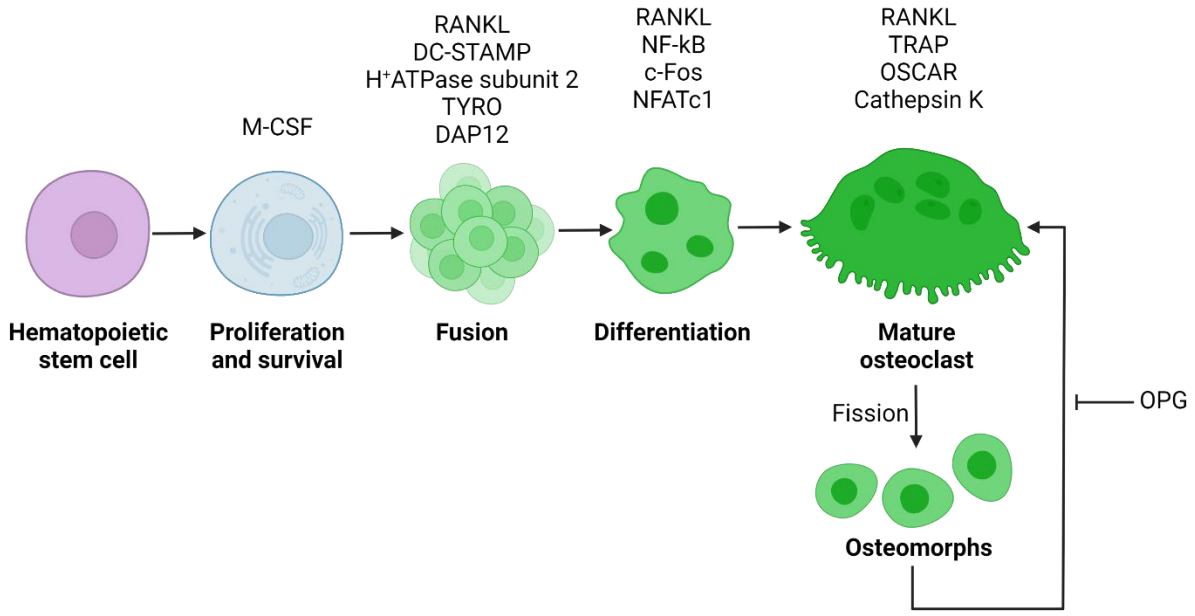


**Figure 1. 3. Osteoclast differentiation.** *Osteoclast precursors proliferate when M-CSF stimulates hematopoietic stem cells. The committed osteoclasts fuse to develop the multinucleated osteoclasts. Fusion is mediated through RANKL, DC-STAMP, H+-ATPase subunit D2, TYRO, DAP12. Later, RANKL signals NF-κB and c-Fos to activate NFATc1 which in turn mediates the expression of TRAP, OSCAR and Cathepsin K, found in fully polarized osteoclasts. Mature osteoclasts can undergo fission into daughter cells named osteomorphs as a matter for recycling which can be re-fused into mature osteoclasts.*

### *Osteocytes*

In the mature bone, osteocytes are the principal bone cells accounting for 90-95% of all cells within the bone tissue. The osteocytes have a long-life expectancy of ~25 years (Franz-Odendaal et al. 2006). They have a dendritic shape which lies within an ovalized region known as lacunae, surrounded by calcified bone matrix (Rochefort et al. 2010).

The transition from osteoblast to osteocyte begins when the osteoblast becomes internalized in the osteoid region. After this, the cell is known as osteoid-osteocyte and starts to develop dendritic processes. The dendritic processes genesis is believed to be orchestrated by the protein E11/gp38 (podoplanin). Other molecules with a role in osteoblast-osteocyte differentiation are CapG and destrin, mediating skeleton rearrangement. At the end, the mature osteocyte has decreased expression of osteoblast biomarkers and in turn displays osteocyte markers like metalloendopeptidase homolog PEX (PHEX), dentin matrix protein 1 (DMP-1), matrix extracellular phosphoglycoprotein (MEPE) and sclerostin (Guo et al. 2010).

Although osteocytes were considered an inert cell, recent evidence suggest their role in local and systemic mineralization. Osteocyte expression of PHEX and DMP-1 correlates with hydroxyapatite development and mineral deposition whereas MEPE activity downregulates mineralization. FGF-23 is a hormone produced by osteocytes with direct effects on phosphorus and vitamin D metabolism. Increased levels of FGF-23 lead to low-serum vitamin D, minor calcium deposition and osteomalacia. In contrast, hypercalcification and hyperostosis result from low FGF-23 levels (Feng et al. 2007; Rowe et al. 2005). Another function of osteocytes is the osteoblast inhibition via sclerostin, a protein encoded by *SOST* gene. Patients with disrupted *SOST* gene acquire sclerosteosis, a condition characterised by abnormal bone mass production (Balemans et al. 2001). Finally, osteocytes play a pivotal role as mechanical-sensing cells. This function is described in 1.2.6.

### *Bone lining cells*

BLCs are quiescent cells localised in the surface of inactive (lack of remodelling) bone surface derived from osteoblasts after mineral deposition. Morphologically, they display a large-flattened shape and nucleus, a median-size rough endoplasmic reticulum (RER) and Golgi apparatus and low vesicles number. They are in immediate contact with each other by gap junctions and to other cells like osteocytes by linkage of their cytoplasmic processes through the canalicular bone matrix channels (Miller et al. 1980).

BLCs were first thought to create a cell barrier between the extracellular fluid and bone compartment, due to the different concentration of calcium and phosphate, mediating mineral homeostasis (Talmage 1970). Recently, Matic et al. (2017) also suggests a proliferative activity of BLCs after osteoblasts depletion *in vivo*, suggesting their role in bone formation when osteoblasts are absent. Interestingly, BLCs function was significantly supressed by glucocorticoid treatment, an osteoblast-inhibiting compound associated with osteoporosis incidence, further supporting BLCs' role in bone development. In bone remodelling, after osteoclast bone resorption, there are some nonmineralized collagen remains which are absorbed by BLCs via MMP13. Finally, the BLCs deposit a collagen layer at the bottom of the lacunae, preparing the territory for osteoblast bone deposition (Everts et al. 2002).

### 1.2.5. Bone physiology: modelling and remodelling

#### *Bone modelling*

Bone modelling refers to the overall growth of bone mass and shape adaptation, a process governed by mechanical stimuli. This process is representative of childhood and puberty, where bone development and mineralization are key features, ending with the ossification of the growth plate. The daily mechanical stress applied to bone improves the gain of bone mass, leading to the strengthening of bone tissue. In this case, the addition or resorption of bone tissue are not coupled, osteoblastic and osteoclastic activity take place in different bone locations, which is a major difference between modelling and remodelling (Burr & Allen 2013).

#### *Bone remodelling*

The renewal of bone tissue is known as remodelling or turnover. This process is essential to maintain bone health by repairing bone structure damage, replace old tissue and maintain mineral homeostasis. Bone remodelling is carried out by the “basic multicellular unit” (BMU), a complex of osteoclasts and osteoblasts localised in the region to remodel. Firstly, a mechanical or hormonal stimulus activates (activation phase) osteoclasts to resorb bone tissue (resorption phase) in the needed area. After resorption, BLCs clean any debris followed by a shift from bone degradation to formation (reversal phase) where osteoblasts are recruited to synthesize new bone matrix (formation phase) figure1.4. The aim of remodelling is to maintain the bone structure integrity rather than an extra-gain in bone mass as is the case in bone modelling (Florencio-silva et al. 2015).

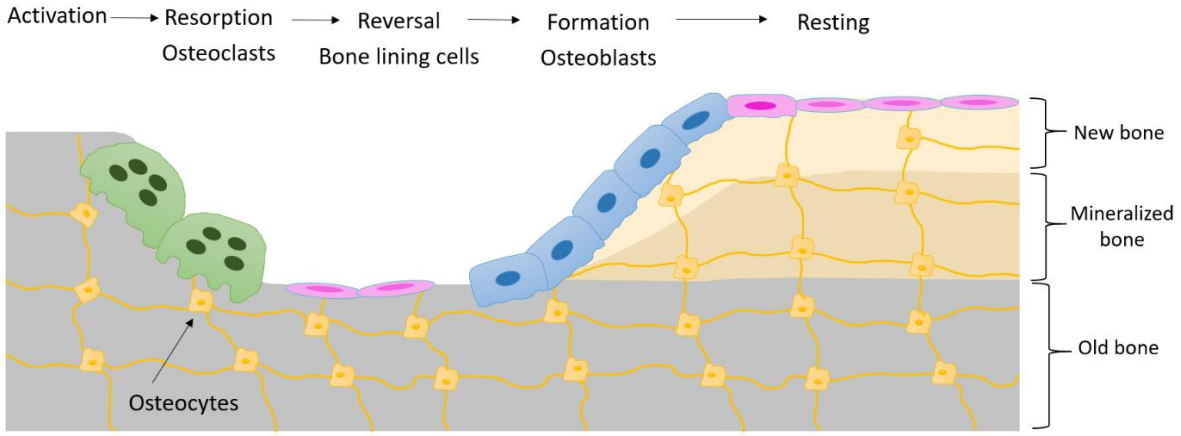


**Figure 1. 4. Bone remodelling process.** *A stimulus initiates osteoclasts-mediated bone resorption. Bone lining cells clean bone remains to give place to osteoblasts, performing bone deposition. At the end, new bone is created, and bone enters a resting phase until a new stimulus activates bone remodelling.*

### 1.2.6. Mechanical stimulus and bone response

The bone is a dynamic tissue; therefore, it adapts and improves its strength to withstand the mechanical forces it encounters daily. The first observations of mechanical loading and bone response were performed by Wolff in 1892. According to Wolff's law the bone regions subjected to mechanical loading stress will improve its mass and architecture in order to adapt themselves to these loading forces (Frost 2001a). Wolff's law seemed incomplete, since it only stated that mechanical forces affect bone but did not expand on the process that resulted in bone architecture modification. Therefore, it could not be translated into clinical applications. To overcome this issue, the Utah's paradigm emerged with propositions explaining how mechanical loading influences bone structure (Frost 2001b).

The first proposition describes the aim of physical bone design which is to bear voluntary mechanical loads, achieving bone strength, health and avoiding fractures. The second Utah's proposition states bone cells as the designers of bone structure which are guided by mechanical loadings and strains. The main concept in which the Utah's paradigm is based on is known as mechanostat. The latter applies bone modelling and remodelling as the dynamics that govern bone design according to the resulted strain by loading, the greater the loading the greater the strain. Bone strength will improve if the strain is strong enough to exceed a modelling threshold. On the contrary, strain below the remodelling threshold would lead to bone tissue loss, figure 1.5. In this way, mechanical loading and the resulting strain boost bone health and strength (Frost 2001b).

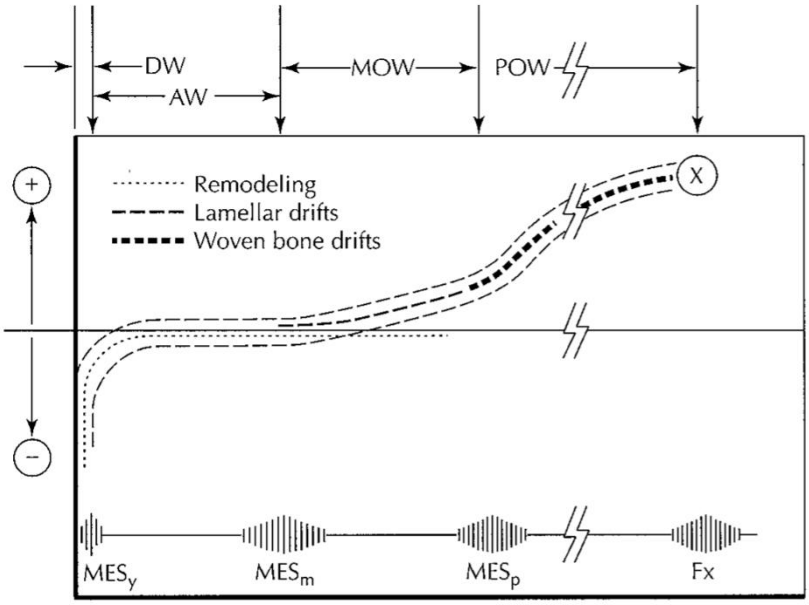


**Figure 1. 5. Modelling and remodelling effect on bone strength and architecture**. *The lower line represents three different peak bone strains thresholds or minimum effective strain (MES) range, from left to right: remodelling (MESr), modelling (MESm), microdamage (MESp). The last threshold is the fracture (Fx) strain. Each threshold is comprised of a microstrain value that range from 50-100, ~1,000, ~3,000 and ~25,000 microstrain for MESr, MESm, MESp and Fx respectively (Frost 2001b). The upper horizontal line shows a neutral strength set where there is neither gain nor bone loss. Lack of activity would result in bone removal as shown by the dotted line below the axis. On the contrary, physical activity would maintain bone strength and mass. To improve bone strength through modelling drifts, the strain must overtake the MESm value, as suggested by the upper dashed line curve. The combined effect of modelling and remodelling is illustrated by the dashed outlines. Physiologically, if great and continuous strain results on bone, woven bone would be created instead of lamellar, in a rush to compensate bone formation when the strain exceeds the MESp threshold. When the strain surpasses the Fx value, the bone will fracture. Above the figure, four windows illustrate the strain threshold: DW: Disuse window, AW: adapted window, MOW: mild overload window, POW: pathological overload window. Figure reproduced from Frost (2001) with publisher permission: John Wiley and Sons.*

Biologically, osteocytes are the main cells governing the mechanosensory function through their canalicular system, translating physical activity into biological signals that lead to bone formation. Some mechanisms have been proposed to explain how osteocytes sense mechanical loadings. One of these is a complex between polycystin 1, 2 and cilia extensions expressed by osteoblasts and osteocytes, mediating bone development and structure. Another signal comes from the focal adhesion kinase (FAK) and its interaction with integrins such as paxillin, vinculin and talin. Several factors are produced by osteocytes in response to mechanical forces including nitric oxide (NO), adenosine triphosphate (ATP), $Ca^{2+}$ and prostaglandins $E_2$ and $I_2$ ($PGE_2$, $PGI_2$), leading to bone anabolic response (Florencio-silva et al. 2015).

One known factor that causes great mechanical loading response and improves bone health is exercise. Evidence suggests a beneficial role of exercise not only to maintain a healthy-life style, but also as part of the treatment for bone loss diseases like osteoporosis. For instance, elderly patients clinically diagnosed with osteoporosis were subjected to weight-bearing and non-weight bearing exercises to assess the effect of different type of physical activities on osteoporosis (Shanb & Youssef 2014). The results suggested an improvement in bone mineral density (BMD) for both exercises, with greater BMD for weight-bearing training. This study provides evidence in the clinical applications of bone response to exercise, paving the way for novel treatments in conditions where bone is highly affected. The force of the loading applied in bone due to exercise creates a strain, which can further influence the bone structure. For instance, increased BMD and bone mineral content (BMC) is generated in gymnastics or jump skippers, attributable to the high strains generated in bone (Taaffe et al. 1997; Pettersson et al. 2000). The proposed strain could be above 1500 με, as this range is suggested to promote bone formation (Frost 1987). One disease that mainly disrupts bone health and integrity is cancer bone metastases or cancer induced bone diseases.

### 1.3. Prostate Cancer and bone metastasis

PCa is one of the most common cancers diagnosed in UK, with an incidence of 47,000 cases and a mortality of ~11,000 individuals each year. Once diagnosed, the treatment consists of androgen depravation therapy (ADT), radical prostatectomy, chemotherapy and radiotherapy (Namiki et al. 2012). However, they are inefficient to treat the PCa bone metastasis in advanced stages. PCa bone metastasis affects ~70% of patients and represents the main issue of this disease as at this stage is considered to be uncurable. For instance, it is estimated that patients diagnosed with primary PCa (no bone metastasis) have a survival rate of 87% that drops to 55% after 5 years of diagnosis. This survival rate decreases alarmingly from 47% to 3% in patients with PCa bone metastasis and from 40% to 0.7% in patients with bone metastasis and skeletal related events (SRE), such as spinal cord compression and pathological fractures (Nørgaard et al. 2010). The clinical implications of bone metastases include pain, cancer-derived fractures, spinal cord compression and hypercalcemia. Understanding the biological steps that orchestrate PCa cells to invade bone are essential to create new therapeutics against these factors (Ye et al. 2007).

PCa metastases is a multi-stage process that begins with a cancerous cell population known as metastasis-initiating cells. These cancerous cells abandon the primary tumour and migrate towards blood vessels by acquiring an epithelial to mesenchymal transition (EMT) phenotype, gaining migratory and invasive features. Subsequently, PCa cells invade blood/lymphatic vessels and travel through the system until they extravasate from the circulation to nest the bone tissue. Once arrived into the bone, the cancerous cells can remain dormant for up to ~10 years, until they regain mitotic activity and develop clinical metastases (Ye et al. 2007; Wang et al. 2015).

An important characteristic of PCa is its predilection to metastasise to bone tissue. This tropism to bone can be explained using the Paget's "seed and soil" theory. In 1889, Paget proposed why cancerous cells (the seeds) tend to nest a particular organ (the soil), explaining that this predilection is a consequence of favourable conditions found only in certain tissues that attract the cancer cells and assures their survival

(Paget 1889). In the case of PCa, several markers expressed in PCa cells and bone exemplify this affinity.

The osteoblastic lesions PCa generates in bone is another feature different from other cancer types which are mainly osteolytic. Osteosclerotic metastases are the result of factors that promote osteoblast activity. When the PCa cells exit their dormant status, they secrete pro-osteoblast factors such as ET-1, bone morphogenetic proteins (BMPs) and platelet-derived growth factor (PDGF), promoting osteoblast recruitment and bone matrix deposition. The new bone matrix represents a source of growth factors for PCa cells such as transforming growth factor β (TGF-β) and NCPs, attracting PCa cells to the bone environment and enhancing the tumour survival and proliferation. Eventually, expression of RANKL by cancerous cells and osteoblasts promotes osteoclast activity, leading to bone resorption and further release of growth factors, resulting in a vicious cycle, with a mixed osteolytic/osteosclerotic lesions, the latter being predominant (Ye et al. 2007).

### 1.3.1. PCa cells target osteoblastic lineages to establish footholds

Osteoblasts are part of the endosteal niche that maintains the HSCs niches inactive. The quiescent status of HSCs niches is governed by many molecules that include the CXCL12/CXCR4 axis. The CXCL12 is expressed by osteoblasts and CXCR4 by PCa cells, therefore, the CXCL12/CXCR4 axis is suggested to play a role in the PCa cells HSCs niche localisation in bone (Song et al. 2010).

Based on the latter, Wang et al. (2014) assessed the localisation of PCa cells into bone at early stages of this disease. The authors found a predominant location of PCa cells in the lateral endocortical bone surface compared to the medial side. This preferential location of PCa cells was linked to the great number of osteoblasts occupying this surface. In addition, the cancerous cells were found close or even in contact with osteoblasts, suggesting PCa cells target osteoblastic lineages in the early events of metastasis. Following the study, the chemokine receptor CXCR4 was found overexpressed in the metastasis-initiating population of PCa cells (N. Wang, Docherty, Hannah K. Brown, et al. 2015). Additionally, TaqMan array gene analysis revealed

increase CXCR4 expression in the dormant population versus proliferative cells. Osteoblasts are known to express the ligand CXCL12 which binds to CXCR4. Application of AMD3100, an CXCR4/CXCL12 antagonist *in vivo,* resulted in mobilisation of the dormant cells away from bone surface, further suggesting the colonisation of osteoblastic lineages by PCa cells.

### 1.4. Exercise and PCa

Given the suggested predilection of PCa to nest the osteoblasts, exercise which induces an osteogenic response may be counterproductive for patients with PCa, as the PCa cells may be attracted due to the enhanced osteoblast activity. On the other hand, lack of mechanical loading is suggested to enhance osteoclast activity leading to bone resorption which could trigger the PCa bone metastasis vicious cycle, increase tumour growth, SRE and decrease survival rate (Frost 2001a; Guise 2002). In medical practice, studies suggest ineffective education and lack of specific guidelines for healthcare professionals in the exercise training field, resulting in low provision and impaired assessment of exercise for PCa patients (Liam Bourke, Turner, Greasley, Sutton, Steed, Smith, Brown, Kelly, Hulme, Greenfield, Persad, Farrin, Hewison & Derek J Rosario 2018).

Currently, there are three well-stablished risk factors for PCa development: black ethnicity background, 55 years old or more of age and a family history of relatives who have had PCa (Gann 2002). Other risk factors are associated with the patient's lifestyle and therefore are modifiable. From the life-style risk factors, obesity has been linked with decreased propensity to develop localized PCa, but significant increase in advance PCa development in a meta-analysis performed by Discacciati et al. (2012). Other studies have found a significant decrease in PCa development in subjects who performed occupational and recreational physical activities (19% and 5% risk reduction respectively), suggesting that men should remain physically active and perform exercise if they are able to do so (Liu et al. 2011). These studies support the hypothesis that patients with PCa should perform exercise as part of their cancer treatment.

As exercise is highly recommended for patients with PCa, more clinical trials have assessed its role in this condition, studying aerobic and resistance (weight-bearing) exercises.

### 1.4.1. PCa and aerobic exercise

In order to generate energy, cells follow the aerobic and anaerobic metabolic pathways. In the aerobic pathway, carbohydrates, lipids, and proteins are reduced into water and carbon dioxide, and the resulting product is energy in the form of ATP. This process requires the presence of oxygen, that is why it is known as aerobic. In low oxygen levels (the anaerobic pathway), glucose is metabolized into ATP and lactic acid (Patel and Bhise. 2017).

According to The American College of Sports Medicine, aerobic exercise (AE) is “any activity that uses large muscle groups, can be maintained continuously, and is rhythmic in nature”. Examples of AE are walking, jogging, running, swimming (Patel et al. 2017). Benefits from AE have been shown by Patel and Bhise (2017), such as decreased cancer-related fatigue, improvement in the quality of life (QoL) and physical performance in patients with diagnostic of either gastrointestinal, breast, gynaecological, head and neck cancer performing treadmill routines.

A study carried out by Uth et al. (2018), assessed the effect of AE in patients with PCa. Eleven men with PCa diagnostic undergoing ADT treatment performed football training for a period of 5 years. At the end of the assessment, these authors found an increased BMD in the right femoral neck. This is of importance, as ADT has been associated with osteoporosis in PCa patients, suggesting AE could counteract the detrimental bone effect of ADT.

Recently, a clinical trial named the Prostate Cancer Novel Therapy (PANTERA) conducted by Bourke et al. (2018) assessed the feasibility of aerobic training as primary treatment in PCa. Patients who performed aerobic training showed an improvement in body mass, QoL and reduction in diastolic and systolic blood pressure. The cardiovascular benefit of aerobic exercise should be highlighted since it has been shown that cardiovascular diseases (CVD) are cause of approximately three times

more mortality in patients with localised PCa, rather than PCa itself (Hamdy et al. 2016).

The treadmill exercise is one of the best examples of AE. In the case of breast cancer (BCa), the effect of treadmill running was studied in F344 rats who were treated with the carcinogen 1-methyl-1-nitrosourea (MNU) to induce mammary carcinogenesis (Thompson et al. 1995). One week after treatment inoculation, the rats were subjected to three modalities of treadmill exercise based on the $VO_2$ max consumption either at 35%, 70% or 100%. The treadmill exercise at these three modalities achieved significant protection against mammary cancer incidence and number, while the 1% $VO_2$ modality showed enhanced mammary tumour. This was one of the first studies suggesting the importance of the exercise intensity and its impact in cancer development. Similarly, Peel et al. (2009) assessed the correlation between cardiorespiratory fitness (CRF) (measured as maximal exercise in a treadmill regimen) and BCa mortality. The results of this study showed that women subjected to moderate and high CRF had a 33% and 55% lower risk of BCa mortality. Also, women with an exercise capacity lower than 8 metabolic equivalent task value (which is the energy used compared to the one at a resting status) showed a three-fold higher risk of BCa mortality while dose with equal or greater 8 metabolic equivalent task had a protective effect against BCa mortality, suggesting that the intensity of the treadmill exercise is dose-dependent to have an effect in BCa survival.

More recently, Vainshelboim et al. (2021) studied the association between CRF, cancer incidence and cancer mortality in patients with history of CVD, as cancer and CVD have a negative impact in the CRF while higher CRF has a protective effect against cancer. Importantly, PCa was one of the cancer types included in this study. The authors reported that higher CRF was associated with lower risk of cancer mortality and extended survival rate. These findings are in line with previous studies which emphasize the importance of exercise training and its role in maintaining a positive functional capacity in cancer treatment and its protection in cancer mortality (Howden et al. 2019; Stamatakis et al. 2018; Saeidifard et al. 2019)

In a pre-clinical model of PCa, rats' xenografts subjected to treadmill running showed a reduced PCa tumour size, inhibition of the Ki67 proliferation marker which was linked

to blockage of the ERK protein (Gueritat et al. 2014). Also, the expression of enzymatic antioxidant defences was increased while a reduction in oxidative DNA damage and lipid peroxidation was achieved with treadmill running, suggesting a protective role of treadmill running in PCa growth. Another study conducted by McCullough et al. (2013), revealed that treadmill running applied for 5-7 weeks is able to increase the tumour microvascular $PO_2$ and reduced the tumour hypoxia, suggesting that this type of exercise affects the tumour microenvironment, reduces tumour hypoxia and could lead to a less aggressive PCa phenotype. Finally, treadmill running has been shown to reduce the levels of pro-inflammatory cytokines such as IL-6, macrophage chemoattractant protein-1 (MCP-1), and increased the hypoxia inducible factor 1α, vascular endothelial growth factor and the apoptotic marker caspase-3 (Jones et al. 2012; Murphy et al. 2012; Zheng et al. 2008).

### 1.4.2. PCa and resistance exercise

The American College of Sports Medicine defines resistance exercise (RE) as "exercise that causes muscles to work or hold against an applied force or weight" (Chodzko-Zajko et al. 2009). Positive outcomes have been associated with RE in several health conditions: increase in muscle mass, body fat loss, greater physical function, lower propensity to develop type 2 diabetes, reduced incidence of CVD, BMD improvement and mental health wellness (Westcott 2012). Given this evidence, the effect of RE has been studied in PCa.

Recently, a meta-analysis published by Keilani et al. (2017) analysed the efficacy of RE in patients with PCa. In this study, a significant improvement was identified in the upper and lower body strength in patients who performed bench or chest press and leg press, respectively. In regards of the body composition, there was a significant decrease in body fat mass and trunk fat mass while achieving a significant increase in the body lean mass.

Another study conducted by Cormie et al. (2013) assessed patients with PCa bone metastasis in RE regimens. Importantly, the exercise regimen was carefully designed to avoid high impact in skeletal regions where metastasis had been established. The

results showed no adverse effects associated with RE. Moreover, the significant attendance and the compliance for each session suggested that RE is safe and tolerable for patients with bone metastatic lesions. In addition, RE lead to improvement in muscle strength, submaximal AE capacity, and ambulation.

The effect of high-impact exercise in PCa specific-related deaths and overall mortality was studied by Kenfield et al. (2011). In this study, 2,705 patients with PCa but no metastasis (to avoid complications related to metastasis) were subjected to vigorous and non-vigorous exercises evaluated for 18 years. These exercises were classified according to a metabolic equivalent task value, which is the energy used compared to the one at a resting status. Exercises with a value lower than 6 were categorized as non-vigorous while those with equal or higher 6 value as vigorous. Non-vigorous activities included walking as exercise or walking to work, outdoor work like digging or chopping, weight-free lifting or in machine, and stair climbing while vigorous exercises were cycling (including stationary), tennis, calisthenics, rowing, running, jogging, swimming and squash or racquetball. According to the results, individuals who did more than 5 hours per week (h/wk) of non-vigorous exercises had a significant decrease in overall mortality, compared to those with less than 1 h/wk training. In vigorous activity, overall mortality was reduced in patients performing ≥ 3 h/wk compared to those with less than 1 h/wk. Furthermore, PCa specific-related mortality was decreased in patients executing ≥ 3 h/wk in comparison with less than 1h/wk.

A number of randomised trial control (RTC) were analysed in a meta-analysis assessing RE and AE, searching for data indicating if those activities can overcome or attenuate ADT adverse effects (Yunfeng et al. 2017). The selected publication included patients who had started ADT treatment alone, after prostatectomy or in combination with radiotherapy, subjected to individual or mixed AE and RE trainings. Positive results were seen in BMI for patients exercising for a period of 6 months. Upper and lower body strength was improved as well for patients performing chest and leg press trainings. Exercise tolerance was measured as $VO_2$ peak with a significant improvement after 6 months training. Fatigue was overcome in the exercise group performing more than 6 months exercise.

Another RTC conducted by Newton et al. (2019) tested the effect of exercise in the adverse effects (bone loss, and decreased muscle strength) caused by ADT (Smith et al. 2002; Galvão et al. 2008). 159 patients who were undergoing ADT were subjected to impact loading (jumping, hopping, leaping) + resistance exercise (i.e., chest press, seated row, shoulder press) or aerobic exercise (walking/jogging on a treadmill, cycling, rowing). The BMD loss at the spine and femoral neck was lower in the impact loaded group versus the aerobic exercised patients, −0.6% vs −1.8% BMD in the spine at 12 months and −1.0% vs −2.0% BMD in the femoral neck at 6 months. This RTC provides evidence on the importance of adding impact loading exercises to preserve the BMD in patients undergoing ADT.

Overall, exercise seems to be safe and tolerable even for patients who have skeletal metastasis. The QoL is also improved as well as body composition parameters: lower body fat mass, increased body lean mass in hand with upper and lower body strength. Furthermore, specific-PCa mortality and fatigue caused by PCa are significantly decreased. However, most of the studies are focused on patients who are in early stages of PCa which does not correlate with the most common outcome in the progression of this condition: the bone metastasis. Only one study (Cormie et al. 2013) took the bone metastasis as a parameter to measure. Another issue is the lack of explanation about how these benefits are modulated physiologically in the patients, there is a lack of knowledge about the interaction of PCa cells and the patient's organism. To further understand the biology behind PCa and exercise, some studies have applied *in vitro* and *in vivo* experiments.

### 1.4.3. PCa and exercise: *In vitro* and *in vivo* studies

Up to date, a limited number of studies have given possible molecular explanations of the positive effects of exercise in PCa. Jones et al. (2012) studied AE in an orthotopic murine PCa model. A group of 59 C57BL/6 male mice were orthotopically inoculated with C-1 murine PCa cells. From the study sample, 28 had access to a treadmill 24 hr/day and the rest were used as controls. The mice were assessed for up to 53 days and before culling, magnetic resonance imaging (MRI) was performed to measure blood perfusion on the developed tumours. Tumour growth was significantly

decreased in the exercised mice while a tendency towards diminished tumour weight and number of metastases was detected in the trained mice versus controls. To complement this result, gene expression was analysed in the tumours, finding increased expression of pro-metastatic genes related to angiogenic development such as HIF-1α, VEGF, MMP-9, and CXCR4 in the trained mice. Although this result seems contradictory for the diminish metastasis, it is believed that exercise stabilizes the tumour blood flow, which in resting conditions is usually impaired and surrounded by a hypoxic environment that leads to major expression of HIF-1α, creation of deficient blood vessels, more hypoxia and metastasis. Finally, the MRI revealed increased blood perfusion in the tumours, that could create a healthy environment in the tumour and decreased metastasis. This study is in line with the findings of McCullough et al. (2013), in which an orthotopic PCa mice model was subjected to treadmill exercise, finding increase $PO_2$ and reduced tumour hypoxia.

The study of Rundqvist et al. (2013) examined the effect of AE on the growth of PCa cells. To test this, 10 males performed AE as bicycle training for 60 minutes at high intensity. Serum samples from arterial blood vessels were taken before (resting serum) and after (exercise serum) bicycle performance. The PCa cell lines LNCaP, Du145 and 22rv1 were incubated for 96 hours with resting or exercise serum. PCa cells incubated with exercise serum showed significantly decreased proliferation for the LNCaP and Du145 cell lines and a trend towards diminish proliferation in the 22rv1 cell line. Furthermore, LNCaP cells treated with exercise and resting serum were injected subcutaneously *in vivo* to assess tumour formation. The results revealed no tumour incidence at day 14 post-injection in mice treated with exercise serum pre-incubated LNCaP cells, but a 20% incidence was seen in the control group. Analysis of molecular factors revealed 35% increase of ınsulin like growth factor binding protein 1 (IGFBP-1) and 18% reduced epidermal growth factor (EGF) levels after exercise. EGF is associated with PCa tumour growth, while IGFBP-1 negatively affects insulin like growth factor -1 (IGF-1) viability, which is also related to PCa risk and progression.

Although the mentioned experiments have assessed the role of exercise in PCa, there is scarce literature about the interaction of PCa cells and bone when exercise stimulus is applied. Therefore, models of exercise and cancer bone metastasis are needed, as a matter to elucidate the impact of exercise in bone and how the osteogenic response,

due to exercise, may affect cancer progression. To date, exercise models and osteolytic cancer models have been assessed by some authors.

### 1.5. Models of exercise and cancer bone metastasis

One of the first studies to test the effect of mechanical loading in bone metastasis was the one performed by Lynch et al. (2013). The results of Lynch et al. (2013), suggested that mechanical loading could inhibit the development of established bone metastasis in a BCa murine xenograft model. Osteolytic lesions were developed, showing ~70% bone destruction in non-loaded mice tibia. In contrast, reduced tumour metastasis was observed in loaded bones (tibial compression of 1200 cycles at 4 Hz, 5 days per week) as well as improvement in bone structure parameters. In the loaded bones, only 29% had detectable tumour formation compared to non-loaded tibias. In addition, identification of activated osteoblasts was noted in the loaded tibias and osteoclasts in the non-loaded samples. Another finding was a decreased expression of RUNX2 in a 3D culture model mediated by mechanical response. In the BCa vicious cycle, RUNX2 promotes PTHrP expression which stimulates RANKL and consequent osteoclast activity.

In line with Lynch et al. (2013), Rummler et al. (2021) subjected a multiple myeloma (MM) syngeneic model to mechanical tibial loading. The tibias stimulated with loading improved the trabecula microstructure and cortical thickness and showed less cortical porosity while non-loaded tibias had increased bone resorption as observed by almost total loss of all the trabecula tissue and decreased cortical tissue thickness. The MM tumour burden was found significantly lower in loaded mice models compared to controls at the end of the experiment as evidenced by bioluminescence assay and serum measurement of the M315-specific MM protein. Another similar study carried out by Wang et al. (2021), tested three exercise regimens in a syngeneic BCa *in vivo* model: 2 modalities of tibial mechanical loading (applied at 4.5N or 8N) and treadmill exercise. Mechanical loading at 4.5N and treadmill running protected the bone structure and delayed the progression of BCa. In contrast, mechanical loading applied at 8N showed detrimental bone structure and increase BCa progression, possibly by overuse of the bone tissue as evidenced by woven bone development and increased

HIF-1α in osteocytes, a marker associated with damaging due to loading as suggested by others (Tomlinson & Silva 2015).

These studies exemplify the relationship between osteolytic cancer models and bone cells, providing information regarding their behaviour under mechanical loading stimulus or treadmill exercise. It is important to observe how the loading force applied or the type of exercise performed could either benefit or worsen the cancer bone metastasis as a matter to apply the appropriate loading/exercise regimen protect the bone from lesions and cancer progression. Of interest, one hypothesis to explain the reduced bone metastasis is a faster bone anabolic response in favour of osteoblast activity and bone formation that may disrupt the vicious cycle of cancer (Guise 2002). The osteogenic response observed in the mentioned studies may counteract the vicious cycle of cancer from the osteoclastic pathway, as it was suggested to be inhibited resulting in increased bone formation. In contrast, PCa has a different nature as it is an osteoclerotic type of cancer and no current evidence has tested the osteogenic response due to exercise in PCa bone metastasis.

## 1.6. Additional osteogenic stimulus: Whole-body vibration platform

The whole-body vibration platform (WBVP) is an alternative to induce an osteogenic response in patients with bone diseases who are not able to perform extenuating exercise routines (Marín-Cascales et al. 2018). It involves a mechanical stimulus generated by vertical oscillatory magnitudes at certain frequency which enables an osteogenic response (Rauch et al. 2010). The effectiveness of the WBVP stimulus in bone and cancer has been evaluated in several studies.

A meta-analysis conducted by Marín-Cascales et al. (2018), found that WBVP applied at frequencies >20 Hz and amplitudes >5 mm or 8 g improved the BMD lumbar spine in postmenopausal women. This in accordance with other studies that suggest that vibration stimulus at high frequencies and low magnitudes are required to send an effective signal to the spine and hip, thus recommending frequencies higher than 20 Hz (Rubin et al. 2003). The duration of the WBV session also affected the bone mass, as a tendency to significance was observed in sessions ≥600 seconds. Other studies have shown that longer WBV sessions have positive impact in bone mass (Ruan et al. 2008; Verschueren et al. 2009). WBVP has been shown to increase the levels of adiponectin, transforming growth factor-beta1, and 17% nitric oxide an reduce the levels of osteopontin, interleukin-1 beta, and tumour necrosis factor-alpha, leading to an improvement in bone mass due to increase osteoblast activity and reduce osteoclast activity (Humphries et al. 2009).

In regards to cancer, WBVP has been shown to improve mobility and jumping height in hospitalized cancer patients undergoing intensive or high-dose chemotherapy, induces muscle activation in BCa survivors, and increases the maximal workload in patients with lung cancer and mesothelioma at stage I-III when combined with AE (Pahl et al. 2018; Ruymbeke et al. 2014, Salhi et al. 2015). However, it has been suggested that occupations and jobs exposed to WBV such as drivers of heavy vehicles (forest machines, tractors), crane and loader operators and helicopter pilot have an increased risk of developing PCa. Such assumption needs to be further addressed as many occupations could be exposed to toxins or any other carcinogens, which would clear whether WBV indeed increases the risk of developing PCa (Alavanja et al. 2003; Hardell et al. 2006; Jakobsson et al. 1997). In fact, more recent

studies have not found a correlation of WBV and PCa development (Krstev & Knutsson 2019; Jones et al. 2014).

### 1.7 Exercise and the immune system

The immune system is comprised of cytokines and cells aimed to protect the host from diseases, external microorganisms, and promote wound healing (Simpson et al. 2015). It is divided into innate and adaptative immune responses. The innate immune system is comprised of a number of cells such as macrophages, dendritic cells, mast cells, neutrophils, eosinophils and natural killer cells (Turvey & Broide 2010). The adaptative immune response is characterised by B and T lymphocytes. In regards of exercise, short periods of exercise are associated with leucocytosis which returns to basal levels after ~6h-24h (Simpson et al. 2015). At recovery, there is a neutrophilia period and lymphocytopenia, which can drop to until clinical-low levels ($<1{\cdot}10^{9}$/L) (Walsh et al. 2011). Acute exercise is also linked to mobilisation of cytotoxic cells such as $CD8^{+}$, NK cells, and γδ T-cells (Anane et al. 2009). The cytotoxicity of NK cells during the recovery period, is suggested to be transiently suppressed, an effect caused by the lower number of NK cells (Nieman et al. 1993). In terms of high-intensity or long-term exercise, an immunosuppressive response is displayed. For instance, runners show a lower level of lymphocytes at a resting phase and swimmers and cyclists a lower NK cells number (Baj et al. 1994; Gleeson et al. 2000; Pyne & Barnes 2010). The levels of pro and anti-inflammatory cytokines, intimately linked to the immune cells' response, is also found impaired in extraneous exercise training as well as increased levels of stress hormones like cortisol (Hough et al. 2013). The immune system has been suggested to mediate the anti-cancer response; however, the immune effect against cancer would be affected by the type, duration, and intensity of the exercise performed (Pandya et al. 2016; Lombardi et al. 2019) This suggest that an appropriate exercise regimen should be applied to patients to achieve the beneficial effect of exercise against cancer progression, particularly patients with bone metastasis, as not all exercise regimens would be suitable for patients at this stage of the disease.

## 1.8. Project rationale and hypothesis

Overall, exercise has been evidenced to achieve positive outcomes in PCa. The benefits of exercise depend on the type performed (AE or RE), the intensity, frequency, and duration. which should be individualized for each patient and the disease stage.

Several *in vivo* studies have found improved bone structure and decreased bone metastasis and metastasis tumour growth when applying mechanical loading in osteolytic cancer models. The decreased bone metastasis growth was hypothesised to be a consequence of enhanced osteoblastic activity and osteoclast inhibition, resulting in disruption of the cancer vicious cycle

In addition, other literature has assessed the nature of PCa cells, suggesting a predilection for PCa cells to target osteoblastic niches. Therefore, the enhanced osteogenic response as a consequence of exercise, may present a risk in attracting more PCa cells into bone. This project aims to clarify the events that take place between bone environment and PCa cells when mechanical loading is applied.

## 1.9. Project hypothesis and aims

The main hypothesis of this project is: **load-bearing exercise interferes in the development of PCa skeletal metastases through promoting osteogenic response.**

The main hypothesis gives rise to three detailed hypotheses:

**1.- Load-bearing exercise enhances the arrival of PCa cells in bone via enlarging the osteoblastic niche.**

**2.- Load-bearing exercise inhibits PCa bone metastasis by disrupting the cancer vicious cycle.**

**3.- Whole-body exercise (treadmill and vibration platform) could affect the progression of PCa bone metastasis by promoting an osteogenic response.**

To test this hypotheses, six aims will be performed:

1. To study the effect of mechanical loading on bone remodelling using naïve mice. (Chapter 3)
2. To determine the effect of mechanical loading on the arrival of PCa cells into bone marrow. (Chapter 4)
3. To examine the effect of continuous and interrupted mechanical loading in the development of PCa bone metastasis in xenograft models. (Chapter 5)
4. Determine whether treadmill exercise affects the growth of PCa bone metastasis in xenograft mice models. (Chapter 6)
5. Study whether the high-frequency low-magnitude vibration platform stimulus inhibits PCa bone metastasis. (Chapter 7)
6. Evaluate the cytokine profile of mice subjected to different exercise regimens and its role in PCa bone metastasis. (Chapter 8)

# CHAPTER 2:

## Materials & methods

## 2.1. Materials used in this project

The materials and reagents are described in Appendix A

## 2.2. Tissue culture and patient derived xenograft (PDX) organoids

**Table 2. 1. Cell lines used in this project**

| Cell lines | Description | Source | References |
|---|---|---|---|
| **PC3** | A bone-seeking human androgen-independent (AI) PCa cell line obtained from a lumbar vertebral metastasis. Luciferase gene transfection was performed to identify them by bioluminescent techniques. | ATCC Corporation (Manassas, Virginia, USA) | (Kaighn et al. 1979). (Sobel & Sadar 2005). (Wang et al. 2014). |
| **C4-2B4** | This cell line was derived from the LNCaP PCa cell line. Its androgen-independence and metastatic osteoclerotic lesions mimics the late stage of PCa that occurs in patients, making it suitable for this project. | ATCC Corporation (Manassas, Virginia, USA) | (Thalmann et al. 1994). |
| **RM1** | A murine PCa cell line obtained by intracardiac injection in a mice model and isolated from the mouse bone tissue, achieving a PCa murine cell model with bone metastatic potential. | ATCC Corporation (Manassas, Virginia, USA) | (Power et al. 2009) |
| **MG-63** | The MG-63 cell line is a pre-osteoblast cell line which expresses mesenchymal markers such as ALDH, Oct4 and Nanog. It also shows chemoresistance as stem-cell. This cell line is useful to study one of the osteoblasts differentiation stages. | ATCC Corporation (Manassas, Virginia, USA) | (Honoki et al. 2010; Siclari & Qin 2010). |

| | | | |
|---|---|---|---|
| **SaOS2** | The SaOS2 cell line is a fully differentiated osteoblast cell line. It expresses ALP, the core binding factor alpha1 (Cbfa1), Osterix (SP7), osteocalcin, bone sialoprotein (BSP), decorin, collagen I and III and mineralisation activity comparable to osteoblasts. | ATCC Corporation (Manassas, Virginia, USA) | (Czekanska et al. 2012; Clover & Gowenf 1994; Pautke et al. 2004; Saldaña et al. 2011). |

**Table 2. 2. PDX organoids used in this project.**

| PDX organoid | Description | Source | References |
|---|---|---|---|
| **LAPC-9** | The LAPC-9 is a novel androgen-dependent (AD), prostate-specific antigen (PSA) secreting PCa xenograft. Upon androgen absence, a small cell population undergoes apoptosis, while the majority remains dormant and could re-enter the cell cycle as AI. | Kind gift of Dr. Marianna Kruithof-de Julio (University of Bern, Switzerland). | (Craft et al. 1999). |

### 2.2.1. Tissue culture

Cell lines were cultured in T75 size tissue culture flasks with Dulbecco's modified Eagle's medium (DMEM) supplemented with 10% foetal calf serum (FCS) and 1 % Penicillin-Streptomycin (pen-strep) at 37°C, 5% $CO_2$. Cell monolayer confluence was estimated at 10x magnification using an Olympus CK2 microscope (Olympus, Tokyo, Japan).

The cells were passed into a new T75 flask whenever they reached ~80-90% confluence at 1:10 or 1:5 concentration.

### 2.2.2. Cell harvesting and counting

To achieve cell culture harvesting, the DMEM from the T75 flask was removed, the cell monolayer washed with 10 ml of phosphate-buffered saline (PBS) buffer and treated with 1 ml of trypsin-Ethylenediaminetetraacetic acid (EDTA) for 5 mins at 37°C. Then, 9 ml of pre-warmed DMEM was added to neutralize the trypsin reagent resulting in a 10 ml sample that was centrifuged at 1,000 rpm for 5 mins. After centrifugation, the DMEM/trypsin media was discarded followed by resuspension of the resulting cell pellet in 10 ml FCS containing DMEM media. From the 10 ml suspension, a certain quantity was seeded in a new T75 flask pre-added with 10-11 ml of DMEM.

According to the experiment, the cell sample was counted using a haemocytometer (Thermo Fisher Scientific, Waltham, Massachusetts), taking 10 µl from the 10 ml suspension before centrifugation. This was applied in experiments where a specific cell number was needed.

### 2.2.3. Tissue dissociation protocol

Briefly, the LAPC-9 organoids were thawed from -80°C at room temperature (RT). When defrosted, a blade was used to cut the sample into small pieces to facilitate its dissociation. Advanced DMEM (1% pen-strep, 1% GlutaMAX, 1% Hepes) (Thermo Fisher Scientific, Waltham, Massachusetts) was then added to the tumour chops in hand with enzyme mix for digestion (5mg/ml Collagenase type 2, 15 µg DNAse, 10µg Y-27632 inhibitor reagent) followed by 1-hour incubation at 37°C. Then, the tumour sample was passed through a 100 µm cell strainer, washed with 5 ml of Advanced DMEM and centrifuged at 1,100 rpm. After centrifugation, the supernatant was discarded, and the resulting cell pellet treated with 5 ml of lysis buffer (150 mM $NH_4Cl$, 10 mM $KHCO_3$, 0.1 mM EDTA) at 4° C for 10 mins. To end, the sample was centrifuged at 1,100 rpm for 5 mins, and the sample resuspended at $1x10^6$ cells/ml using advanced DMEM to be injected intracardiacally (IC) into NOD severely compromised immunodeficient (SCID) mice.

## 2.3. Animals

BALB/c nude, NOD SCID, BNDG and C57BL/6 mice obtained from Charles River Laboratories, Inc. (Wilmington, Massachusetts, USA) were used in this project. The BALB/c nude, NOD SCID and BNDG mice strains are athymic-immunocompromised mice, making them suitable as PCa xenograft models. The BALB/c nude mice, deficient for T immune cells, were used in experiments related to PC3 and C4-2B4 cells. For the LAPC-9 organoid, a NOD SCID xenograft model was utilised, which lacks B and T immune cells and could avoid an immune response against the patient tumour sample. The BNDG mice was applied in a novel intra-tail artery metastasis model as an additional model of bone metastasis. To study the immune system response against the PCa bone metastasis we applied a syngeneic model by using the immunocompetent C57BL/6 murine mice. The mice strains were kept in RB-3 sterile cages at optimum conditions for laboratory mice: 19-23°C temperature, 45-55 relative humidity, 350-400 lux at a light/dark 12hr cycle. Their dietary conditions consisted of free access to Teklad Global 18% Protein Rodent Diet (Envigo, Huntingdon, UK) and water. General mice healthcare was performed by the “Biological Services: The University of Sheffield, UK” staff members. All the scientific experiments were performed under the Procedure Project License (PPL) 70/8799 and PF61050A3 and Procedure Individual License IB19890F9. All the procedures were analysed and approved by the Animal Welfare and Ethical Review Body of The University of Sheffield, UK and accomplished the UK Animals (Scientific Procedures) Act 1986 standards.

PCa cells were injected IC by Dr. Ning Wang in all experiments. An additional metastasis model was used where the cancer cells were inoculated by intra-tail artery injection by Dr. Ottewell and Dr. Puppo (Yu et al. 2016; Kuchimaru et al. 2018; Zhong et al. 2020). According to the experiment, the PCa cells were pre-stained with Vibrant DiD® (Thermo Fisher Scientific, Waltham, Massachusetts), according to the manufacturer’s instructions. Vibrant DiD is a lipophilic dye that allows tracking of cells at 665 nm stimulus.

Load-bearing exercise was mimicked by applying mechanical loading compression into mice right tibia while the left tibia was used as internal control. The arrival of PCa

cells into BM and tumour growth between the loaded and non-loaded tibia was analysed by multiphoton microscopy and In Vivo Imaging System (IVIS) bioluminescence assay, respectively. The tumour growth in mice subjected to treadmill exercise and WBVP stimulus was analysed by bioluminescence assay weekly as well. At the end of the procedure, the mice were sacrificed, their tibias dissected, soft tissue removed and fixed into 10% neutral buffered formalin (NBF) to perform further analysis related to bone architecture (section 2.7) and histological changes (section 2.8).

## 2.4. Mechanical Loading in vivo

The concept of “mechanostat” proposed by Frost (2001b) states that bone mass and strength will improve if sufficient strains are created into bone as a result of external forces or loading. To test Frost’s theory and study the osteogenic response, many animal models have been developed under artificial loading conditions. The first experiments that addressed bone strain changes *in vivo* were carried out by Lanyon & Smith (1969). This team implanted strain electrical gauges in bones of diverse animals like sheeps, horses, dogs and even humans, recording strain bone dynamics in a series of exercises. Interestingly, the strains were very alike across all the species where the long bones had been treated with load-bearing activities; finding values of ~2–3000 με, suggesting the necessary strain rate associated with bone adaptative response and formation. Studies to control the bone strain due to mechanical loading were next performed. This was first carried out by Goodship et al. (1979). Goodship and co-workers implanted strain gauges in pigs bone radius and removed the ulna, by this manner increasing the strain in the contralateral radius and promoting the bone remodelling process. After three months of study, the values between the radius and the contralateral limb were not different. This method was useful to achieve a control limb; however, the strain cannot be fully controlled, only recorded. Hert et al. (1971) avoided the issues faced by Goodship et al. (1979) by implanting transfixing pins into rabbit’s tibia which developed electromagnetically controlled loading forces (Lisková & Hert 1971; Hert, Sklenská, et al. 1971). Hert, et al. (1971) found a method to manipulate the loading forces into bone, but they could not assess the resulting strain. Lanyon and his team resolved this problem by using the properties of the strain gauges and the transfixing pins in conjunction in sheeps and avian animal models. The most useful model was the avian (rooster and turkey) due to its long ulna, suitable to transplant the pins and strain gauges. The avian ulna is externally loaded through two metal caps which are placed in the top and bottom of the ulna bone and manipulated with metal pins in each cap. This method is useful to apply a certain strain and document the resulting bone response; however, the surgery results in a local bone response where the caps are place. Also, the caps disrupt the trabecula architecture, and this cannot be analysed. Finally, the surgery is invasive and can result in distress and infections (O’Connor et al. 1982; Rubin & Lanyon 1984; Lanyon & Rubin 1984). Therefore, non-invasive mechanical loading regimens have been created. The first

non-invasive protocol was developed by Turner et al. (1991). Their experiment consisted of a four-point bending device where the right tibia of rats was placed. The loading force direction started from the lateral to the medial tibia side. Bone formation occurred in the loaded vs the non-loaded (left) tibia overcoming the invasive surgical problems. Disadvantages included that the bending point had most of their effect on the periosteal region which developed periosteal woven bone formation, therefore, the endosteal region was the one suitable for analysis only. Later, Gross et al. (2002) created a cantilever model by placing the knee and ankle of a mice between two cups and applying the loading in the distal part of the tibia, generating a antero-posterior loading in the tibia midshaft. This loading was successful to generate bone formation in the periosteal and endosteal surface, but the trabecula was not loaded, and the anterior-posterior loading did not correlate with the axial loading that bone encounters daily. After all the previous studies, the current method to control the mechanical loading force and the resulting strain is to place the knee and ankle of the mice between two specially designed cups, figure 2.1. The upper cup applies the loading force in an axial direction through bone while the lower cup is connected to a load cell by this manner transmitting the force into electrical measurable values. This method accurately controls the loading applied, it is not invasive and the bone formation is achieved in the cortical and trabecular bone tissue (De Souza et al. 2005; Lee et al. 2002; Sugiyama et al. 2010).

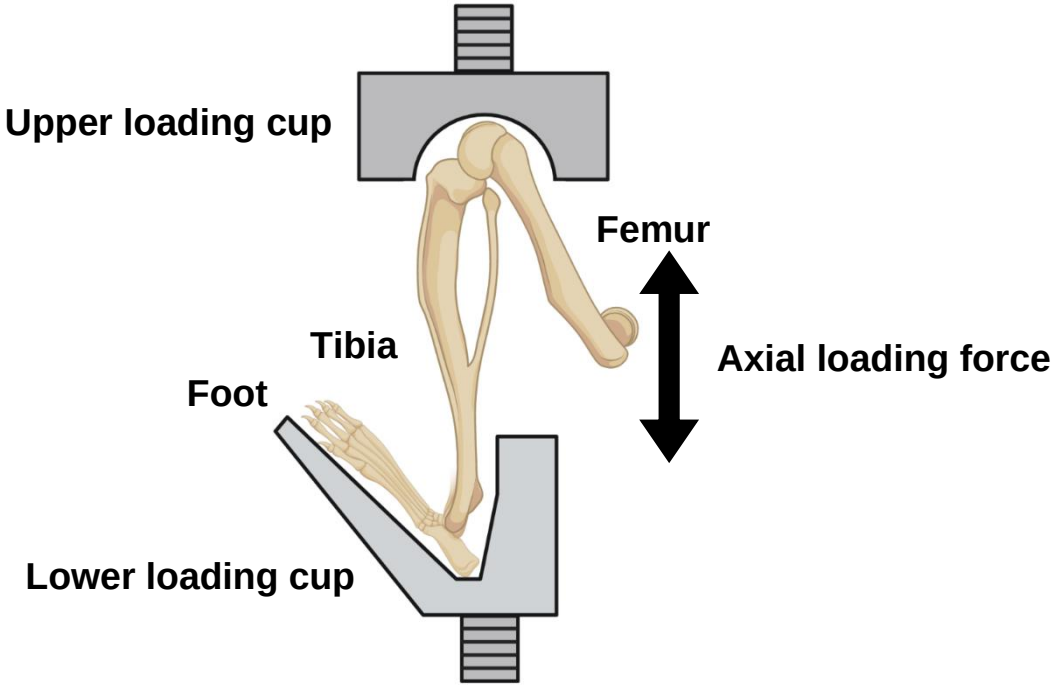


**Figure 2. 1**. **Non-invasive mechanical loading in mice tibia.** *The mice tibia is placed between an upper and lower cup connected to a load cell apparatus that axially applies the desired mechanically loading force.*

In this project, we used the non-invasive mechanical loading method to determine whether mechanical loading: improves bone formation in naïve mice, affects the arrival of PCa cells into bone marrow and inhibits the growth of PCa bone metastasis. Depending on the experiment, 8/12-week-old BALB/c, 8-week-old C57BL/6, 12-week-old NOD SCID or 8-week-old BNDG mice were anaesthetised with isoflurane (Parsippany, New Jersey, U.S.) at 1.5-2 L/m oxygen levels using an anaesthetic machine (Burtons, Turnbridge, UK). While mice were anaesthetised, their right tibia was placed between the upper and lower cups of the Bose ElectroForce 5500 Test apparatus (TA instruments, New Castle, Delaware, USA). To tighten up the tibia a 2 N force was applied, followed by a continuous 12 N loading. Some studies suggest 12 N as the appropriate force to be applied axially into mice tibias to develop 1200 με and achieve an osteogenic response; hence, this compression force was used (Sugiyama et al. 2008; Sugiyama, et al. 2010). Furthermore, a loading force of 9N-12N has been shown to induce 1200-1500με, which is similar to uphill zigzag running or 26cm jumping exercise in humans . These exercises improve the bone mass and can be mimicked in our mechanical loading protocol as a matter to translate this loading protocol into clinical settings (De Souza, Matsuura, et al. 2005; Burr et al. 1996; Milgrom et al. 2000). Following the previous evidence, the mice right tibia was pre-loaded at 2 N followed by 10 N dynamic loads at a rate of 160,000 N/s. Therefore, the loading regimen consisted of 40 trapezoidal waveform loading cycles (12 N hold at 0.2 s) with a 10 sec rest period between each cycle for up to three weeks. A loading force of 12N was applied in 12-week-old naïve BALB/c nude mice experiments (chapter 3) and in the multiphoton microscopy to identify pre-stain cancer cells in BALB/c nude, C57BL/6 and NOD SCID mice models (chapter 4). The 9N force was applied in the longitudinal studies of mechanical loading (3 weeks of loading) in 8-week-old BALB/c nude, C57BL/6 and BNDG mice (chapter 5). At the end of the experiment, the mice were sacrificed, both tibias dissected and fixed into 10% NBF to perform micro-CT and histomorphometry analysis. The contralateral non-loaded left tibia was used as internal control in all the mechanical loading regimens.

## 2.5. Treadmill exercise

The effect of whole-body exercise was evaluated by means of treadmill exercise. Running is a well-known weight-bearing stimulus which promotes a healthy lifestyle (Williams 2009; Schneider et al. 2009) . In regards of patients with PCa, a study carried out by Kenfield et al. (2011), assessed the effect of vigorous vs non-vigorous exercise in patients with localised PCa (non-metastatic). Vigorous exercises included aerobic exercises routines such as running (10 min/mile or faster), jogging (slower than 10 min/mile), lap swimming, bicycling, squash, or racquetball. Non-vigorous exercises were walking to work and weightlifting. The authors found that patients who engaged ≥ 3 hours per week of vigorous activity had a 61% lower risk of death due to PCa when compared to those patients who performed <1 hour per week of vigorous exercise. A follow-up study assessed the effect of vigorous activity and walking at a brisk pace, finding a reduction in PCa progression of 37% and 57%, respectively (Richman et al. 2011). In regards of animal's models, only a few studies have assessed the effect of running exercise into the development of PCa. In the study of Esser et al. (2009), a male mice strain which develop spontaneous prostate cancer known as transgenic adenocarcinoma of the mouse prostate (TRAMP) where subjected to voluntary wheel running to assess the effect of running into PCa development. According to the results, the dorsolateral prostate of mice which run more than 5km/day was classified histologically as "within normal levels" (83%) while those which ran less than 5km/day presented 43% of dorsolateral prostate as "within normal levels". Additionally, 43% of the dorsolateral prostate of mice which ran less than 5km/day was categorised as prostatic intraepithelial neoplasia (PIN) while there was a 65% reduction of PIN in the ventrolateral prostate of mice which ran more than 5km/day . In another experiment, severe combined immunodeficient (SCID) male mice, were subjected to voluntary treadmill running (1.38±0.21 miles/day) one week before the subcutaneous injection of PC3 cells. The treadmill running lasted for 63 days and there was found a 32% reduction in the ratio of the percent mitotic cells/apoptotic cells in the PC3 subcutaneous tumours compared to controls (Zheng et al. 2008). The study of Pedersen et al. (2016), found that voluntary treadmill running achieved a 60% reduction of tumour incidence in 5 cancer xenograft models. Such reduction in tumour incidence was thought to be mediated by epinephrine, which mobilized IL-6 sensitive NK cells into the tumour . The mentioned studies provide evidence that aerobic

exercise, particularly running, is able to affect the progression of PCa. However, there is a lack of knowledge concerning the effect of running into the development of PCa bone metastasis. In order to clarify the effect of running exercise into the development of PCa bone metastasis, we applied a running protocol which has been suggested to induce an osteogenic response in a naïve mice models (Wallace et al. 2007) . In the study of Wallace et al. (2007), 8-week-old male C57BL6/129 mice were subjected to treadmill running at a speed of 12 meters/minute, 5° incline for 30 minutes/day, 7 days/week for 21 consecutive days. The tibia of the mice showed significantly increase cortical area, medial-lateral width in the mid-diaphysis, increase periosteal and endocortical perimeters as well as greater bone mineral density.

As the mentioned study showed that their treadmill running protocol was sufficient to induce an osteogenic response in C57BL6/129 mice, to study the effect of treadmill running into bone in other mouse strains, we subjected naïve 8-week-old BALB/c nude, C57BL/6 and NSG mice (n≥5) to the following treadmill protocol: 12 meters/minute, 5° incline for 30 minutes/day, 5 days/week for 3 weeks, using a LE8708 mouse treadmill (Stoelting). Furthermore, to evaluate the effect of running exercise into the development of PCa bone metastasis, 8-week-old BALB/c nude and C57BL/6 mice (n≥8) were intracardiacally injected with PC3 and RM1 cells (~$1x10^5$ cells/injection), respectively and subjected to treadmill exercise the following day under the same conditions, figure 2.2. A shock grid at the end of each lane provided an electric shock (0-2mA) to stimulate the mice to the running regimen, only when required. The treadmill exercised group was compared to sedentary controls (n=10) of the same strain and age. The tumour growth was investigated weekly by means of bioluminescence assay and the structure of the left tibia by Micro-CT technique *ex vivo*. After 3 weeks of exercise, the mice were sacrificed, blood serum collected and stored at -80°C. The lower limbs were freed of soft tissue, stored in 10% formalin for a week to be later changed into 70% ethanol and stored at room temperature (for histological and Micro-CT technique analysis).

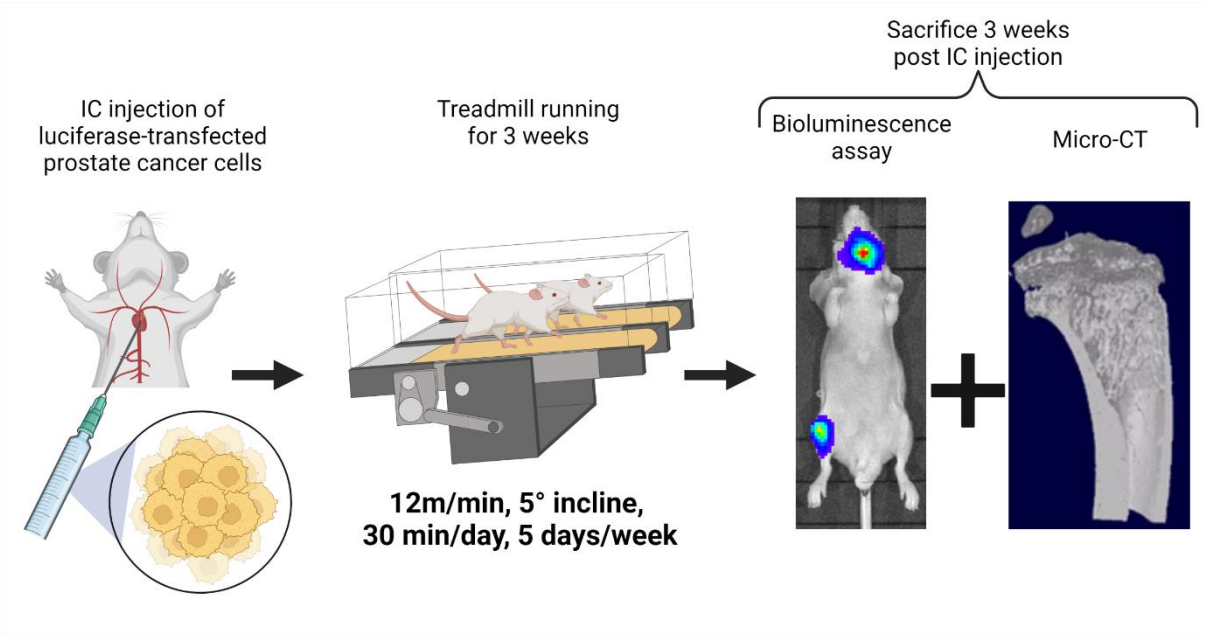


**Figure 2. 2. Schematic outline of mice xenograft model subjected to treadmill running exercise.** *The mice were inoculated intracardiacally with luciferase tagged PCa cells (PC3), followed by B) treadmill exercise for 3 weeks. Tumour growth was monitored weekly by bioluminescence assay and bone structure using Micro-CT technique.*

## 2.6. Vibration platform

The safety and efficacy of exercise into patients with PCa bone metastasis has been evaluated by some authors (Galvão et al. 2006; Stacey A. Kenfield et al. 2011; Newton et al. 2018). However, some clinical trials still exclude patients with PCa bone metastasis as the exercise regimen could put in greater risk the bone structure and increase the odds of SRE and consequently the mortality (Courneya & Friedenreich 2011). Therefore, a safer alternative method such as whole-body vibration (WBV) platform, could be applied into patients with PCa bone metastasis in order to reduce the negative prognosis into the skeleton. The WBV works based on the principle of the piezoelectric theory, which is described as the ability of solid materials to create an electric field in response to a mechanical stimulus (Pohanka 2018). Within the bone tissue, the piezoelectricity effect was first described by Fukada and Yasuda in 1957. These authors observed a negative electrical charge in bone regions subjected to compression while the areas subjected to traction displayed a positive electrical charge (Fukada & Yasuda 1957). At a cellular level, the piezoelectric effect due to mechanical stress into the collagen is sensed by the osteocytes. The compressive force in the collagen leads to the generation of negative charges, opening the voltage-gated calcium channel in these cells, and allowing the influx of calcium, activating calmodulin and in turn the calcineurin. The calcineurin activates Ras and the extracellular signal-related protein kinase (ERK) signalling pathway which induces Runx2 production and in consequence stimulates growth factors production such as TGF-β and BMP. The growth factors (Xu et al. 2009; Zayzafoon 2006) would induce bone formation and are considered to be safe, as long as appropriate parameters such as frequency, amplitude, peak-to-peak distance, and peak acceleration are applied (Rauch et al. 2010; Sá-caputo et al. 2014). Low-magnitude high-frequency vibration (LMHFV) (45 Hz, 0.6g for 20 min/day, 5 days/week for 3 weeks) has been shown to stimulate the trabecular microstructure in female mice models by increasing 38% of the trabecula stiffness compared to non-stimulated controls (Ozcivici et al. 2007). In a sheep animal model, the application of 0.3g, 30 Hz, 20 min/day for 5 days stimulus, induced an anabolic bone response indicated by increase in trabecular bone volume, trabecular number and reduce trabecular space of 32%, 45% and 36% respectively (C. Rubin et al. 2001).

For purposes of this project, we applied the high-frequency low magnitude vibration platform stimulus into xenograft mice models under the following parameters: 20 minutes/day, 5 days/week for 3 weeks with 0.3 g peak-to-peak acceleration and a frequency of 45Hz, using the Juvent vibration platform. We adapted the previous LMHFV stimulus from the study of Wehrle et al. (2015), which induced bone formation (637%) and major flexural rigidity (+1398%) in ovariectomised mice. Eight-week-old male BALB/c nude and C57BL/6 mice were (n=10) were intracardiacally injected with PC3 and RM1 cells (~$1x10^5$ cells/injection), respectively. The following day, the mice were placed into the Juvent vibration platform following the mentioned protocol. We applied the same technique for tumour growth analysis and *ex vivo* tissue collection as in the treadmill study, figure 2.3.

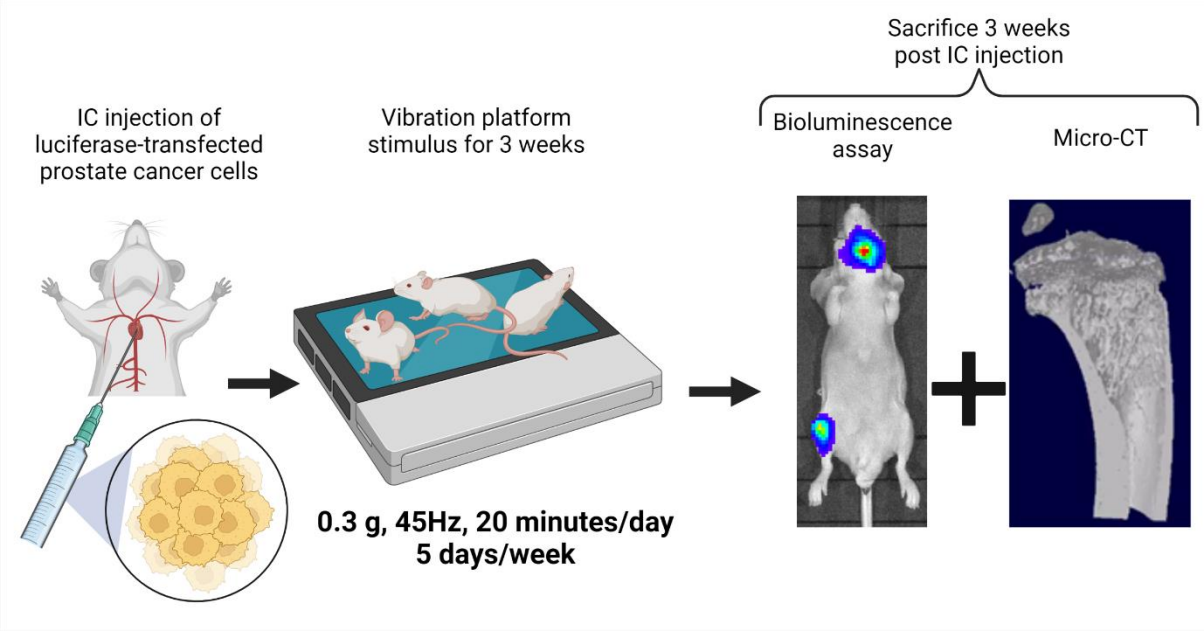


**Figure 2. 3. Schematic outline of mice xenograft model subjected to vibration platform stimulus**. *The mice were inoculated intracardiacally with luciferase tagged PCa cells (PC3), followed by vibration platform for 3 weeks. Tumour growth was monitored weekly by bioluminescence assay and bone structure using Micro-CT technique.*

## 2.7. Micro Computed Tomography

The Micro Computed Tomography (Micro-CT) is a technique which working principle was based on the CT scanner used in hospitals. Just as CT scanners, the Micro-CT projects X-ray beams into a sample of interest to create a final 3D object which can be analysed using different paramethers while maintaining the integrity of the original sample (Clark & Badea 2014). Micro-CT was first introduced by (Elliott & Dover 1982), when they determined a 15 µm resolution into a 0.5 mm snail shell diameter. Since the pixel resolution is set in the micrometer range it is called “Micro”.

The Micro-CT system is composed of three main components: a X-ray source, a rotation stage (turntable) where the sample is placed on and the X-ray detector Figure 2.4. To analyse the sample of interest, several hundred 2D pictures of the sample are taken while the sample rotates on its own axis to avoid internal and external structure overlapping and scan the whole sample. The 2D images are then processed as cross-sectional pictures, a procedure named “reconstruction”. Finally, the “reconstructed” image can be analysed selecting a region of interest (ROI) and modelled as 3D pictures (Bouxsein et al. 2010).

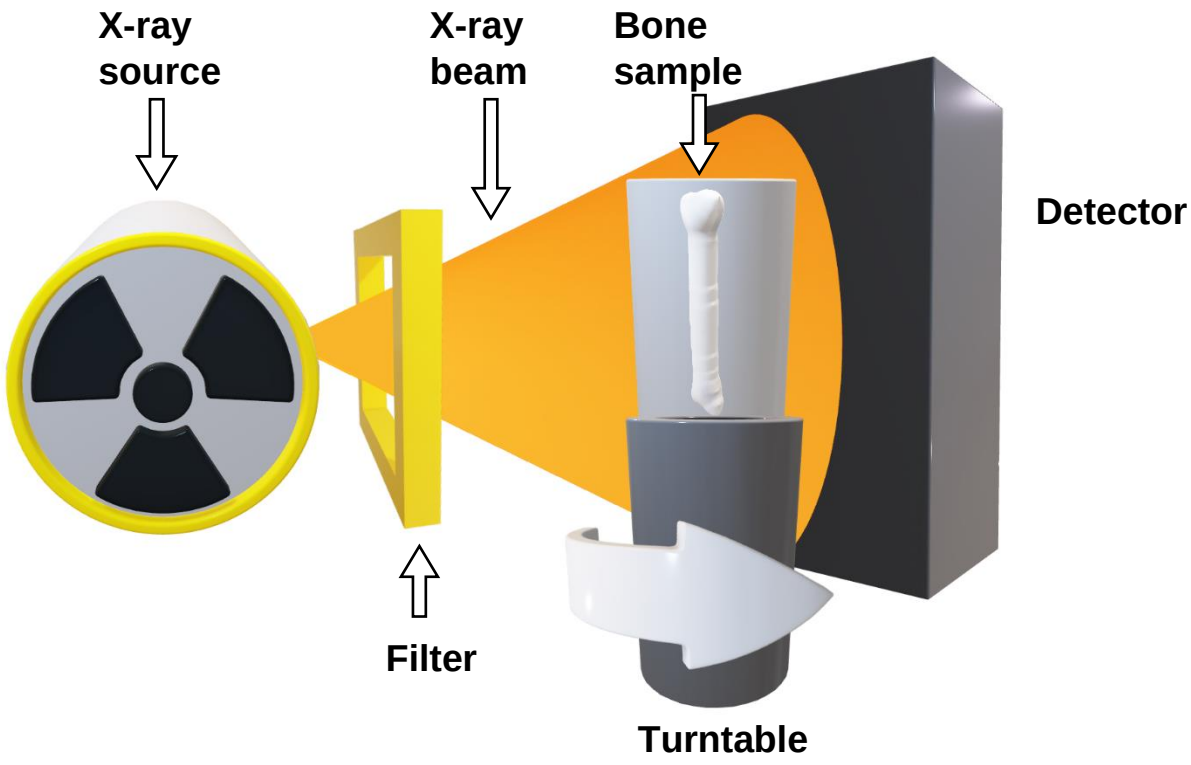


**Figure 2. 4. Schematic representation of Micro-CT working principle.** *An X-ray beam passes through a filter to be directed to a sample which pictures are recorded in an X-ray detector. At the moment of scanning, the sample rotates 180° or 360° using a turntable to fully scan the internal and external sample structure, by this manner obtaining a highly detailed final picture suitable for analysis.*

For the purpose of bone structure analysis, the Skyscan 1272 scanner (Bruker, Billerica, Massachusetts, USA) was used. The X-ray source emmited a 50 voltage and 200 µA with a 0.5 mm aluminium filter. Approximately every 0.66° a 2D picture sample was taken until 180°, finishing with 272 2D images that were later “reconstructed” using the NRecon software. The Micro-CT settings are illustrated in table 2.3.

**Table 2. 3. Micro-CT settings applied in the mice bone scanning**

| Bone sample | Mice strain | Scan resolution | Rotation | NRecon threshold | CTan threshold | ROI off set (mm) | ROI height (mm) |
|---|---|---|---|---|---|---|---|
| **Tibia Trabecula** | BALB/c | 4.3 µm | 180° | 0-0.14 | 90-255 | 0.198 | 0.998 |
| | C57BL/6 | | | | | | |
| | NOD SCID | | | | | | |
| | BNDG | | | | | | |
| **Tibia Cortical tissue** | BALB/c | | | | 90-255 | 0.499 | 0.998 |
| | C57BL/6 | | | | | | |
| | NOD SCID | | | | | | |
| | BNDG | | | | | | |

For Micro-CT analysis of loaded and non-loaded tibias, the tibias were dissected free of all soft tissue, fixed into 10% NBF for 1 week and then maintained at 70% ethanol. The scanning was performed as indicated in table 2.3 with the tibia wraped into cling film into a straw to keep the sample in position while scanning was taking process. After scanning, a ROI was selected for trabecula or cortical tissue using the CTan software, figure 2.5. The bone paramethers analysed were: trabecular bone volume fraction (BV/TV), trabecular thickness (Tb.Th), trabecular number (Tb.N), trabecular separation (Tb.Sp), trabecular bone pattern factor (Tb.Pf), structure model index (SMI), degree of anisotropy (DA) and cortical bone volume (Ct. BV).

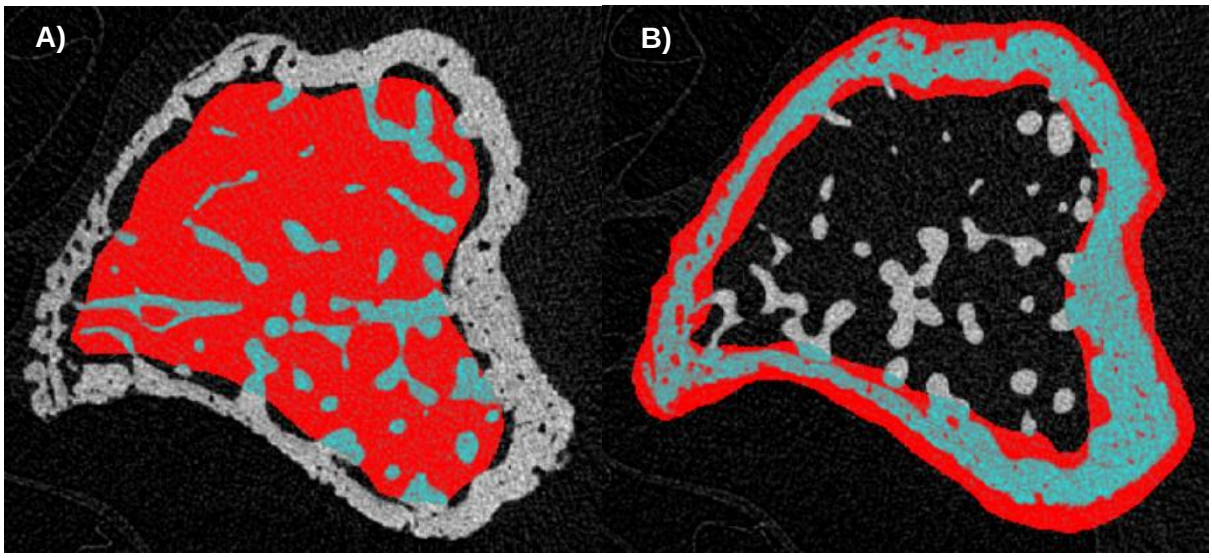


**Figure 2. 5. Schematic representation of ROI selected for trabecula and cortical tissue.** *The ROI for trabecula (a) and cortical (b) tissue, coloured in red, had a height of ~1mm and an offset of 0.2 and 0.5mm from the growth plate respectively.*

## 2.8. Histomorphometry

### 2.8.1. Mice tibia sections

To study the cellular events that took place under mechanical loading, bone sections of the tibias were stained to “coloured” bone tissue and identify bone cells. The bone sections were kindly prepared by Mr. Mark Kinch (skelet.AL, University of Sheffield). Mice tibias were fixed into NBF for one week and then placed into 70% ethanol. After this, they were decalcified with EDTA changing the EDTA media every 3$^{rd}$ day for 4 weeks. Then, the decalcified bones were placed in a cassette and embedded into Paraffin wax. The cassette was placed into a RM2265 microtome (Leica, Wetzlar, Germany) and cut until revealing the head of the tibia. The cut bone sample was frozen down in an ice block for 60 minutes. One bone section of 3 µm was cut and drifted in a distilled water bath at 45°C for 30 minutes to tighten up the bone section. Once the sample was flat it was mounted in a Superfrost Plus Slides (Thermo Fisher). The samples were dried out on a hot plate for 30 minutes and then in an oven overnight at 37°C. The following day, they were maintained at room temperature and finally kept at 4°C.

### 2.8.2. TRAP staining

TRAP is an enzyme expressed in fully developed osteoclasts. Therefore, it is effective as a marker for bone histology analysis. The staining method is an azo dye coupling reaction where the TRAP enzyme reacts with a naphthol AS-BI phosphate substrate, resulting in a primary product that is later treated with a diazonium salt (hexazotised pararosaniline). The final product is a red precipitate that can be visualised under light microscopy (Janckila et al. 2001; Galão et al. 2011).

Bone samples were TRAP-stained to visualise and study bone cells. Prior to staining, Acetate-tartrate buffer was prepared by adding sodium tartrate (Sigma S-4797) into acetate buffer (Sodium acetate trihydrate, Sigma S-9513, 0.2M, pH 5.2) and warmed at 37°C for 2-3 hours. Bone sections were next dewaxed through ethanol to distilled water and placed in Acetate-tartrate buffer at 37°C for 5 minutes. Solution A was then

prepared by mixing 50 ml Acetate-tartrate-buffer to 1ml naphthol/dimethylformamide solution, previously prepared with 20mg naphthol AS-BI phosphate (Sigma N-2250) into 1 ml dimethylformamide (Fisher D/3841/08). The bone sections were incubated for 30 minutes at 37° C in solution A. Solution B was prepared by adding 2 ml pararosaniline stock (50mg/ml, Sigma P-3750) to 2 ml of 4% sodium nitrite (Sigma S-2252) solution and let it stand for 5 minutes, this hexazotises the pararosaniline. Before use, 2.5 ml of the hexazotised solution were added to 50 ml Acetate-tartrate buffer in prewarmed bottle. Then, bone sections were incubated in solution B for 15 minutes and washed twice through distilled water. Sections were counterstained in Gill's II haematoxylin and blue for 20 seconds, treated with ethanol to dehydrate them, cleared in xylene and mounted with DPX mounting medium.

### 2.8.3. Osteomeasure

After TRAP staining, it was possible to identify and quantify bone cells. The osteoclasts were coloured in red while the osteoblasts had a cuboidal form, figure 2.6.

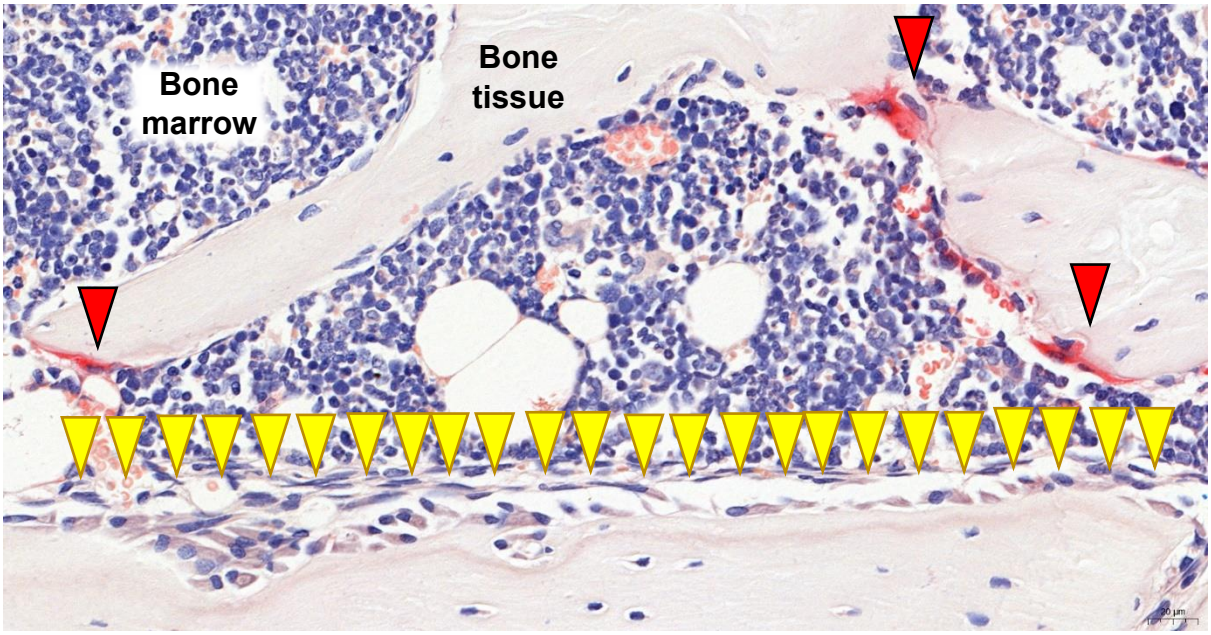


**Figure 2. 6. Bone sections after TRAP staining.** *Pink-cuboidal cells placed on the endocortical bone surface were recognized as osteoblasts (yellow arrows) whilst large multinucleated red cells were identified as osteoclasts (red arrows).*

Two parameters were measured in the bone sections: number of osteoblasts (N.Ob/B.Pm) and osteoclasts (N.Oc/B.Pm) in the lateral, medial and trabecula endocortical bone surface as well as the perimeter occupied by osteoblasts (Ob.Pm/B.Pm) and osteoclasts (Oc.Pm/B.Pm). The analysed surface was 3.6 mm for medial and lateral endocortical bone and 0.72 $mm^2$ trabecula area. The half of growth plate (GP) was taken as reference point for the ROI, figure 2.7. All the bone sections were analysed using a DMRB microscope (Leica, Wetzlar, Germany) at 20x magnification with the Osteomeasure7 v4.2.0.1 (OsteoMetrics) software.

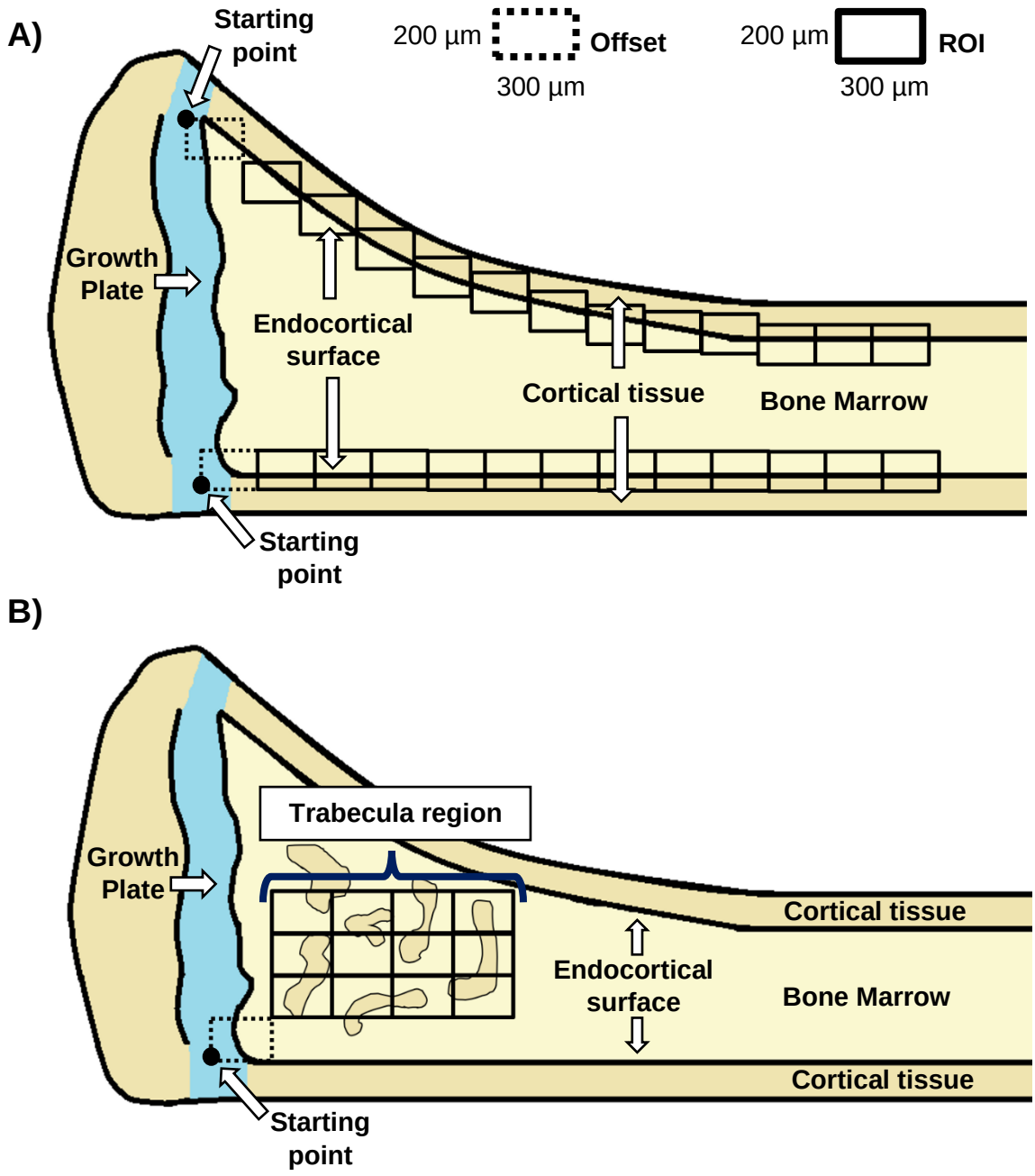


**Figure 2. 7. ROI measured in mice tibia sections using the Osteomeasure software.** *A) The 300 µm offset was placed in the middle of the growth plate to start a quantification of 12 fields (3.6 mm) in the lateral and medial endocortical bone surface. B) Trabecula bone was analysed taking the same reference point as in the medial surface but directed to the trabecula region. Twelve fields (200x300 µm) placed 150 µm below growth plate and 200 µm away from the medial endocortical surface, were analysed as trabecula region (0.72 mm$^2$).*

## 2.9. Multi-photon confocal microscopy

Confocal and multi-photon microscopy are novel tools useful to acquire high quality-3D images of biological samples. Since its invention by Minsky (1988), confocal microscopy has been widely applied in biomedical research, particularly for fluorescent-labelled samples (Rigby & Goldie 1999). In a confocal microscope, a laser beam passes through an objective lens, excites a fluorescent sample located in a focal plane which the fluorescent emission travels through the lens and a pinhole, to end in a detector. The fluorescent light out of the focal plane is blocked by the pinhole, by this manner, eliminating background noise and providing a high-resolution sample image, figure 2.8. Another advantage is the 3D reconstruction of the sample, that is achieved by scanning sample sections which are later reconstructed in a high-quality 3D image (Paddock 2000).

In conventional laser excitation, a single photon carrying certain energy excites a fluorescent molecule that in response emits a fluorescent signal with half the original energy required to excite it, this is known as linear excitation. The larger the wavelength, the lower the energy and vice-versa (Ustione & Piston 2011). For instance, a 488 nm wavelength photon excites a GFP-labelled molecules to emit 507 nm fluorescent signal (Day & Davidson 2009). In multi-photon microscopy, two photons with lower energy are directed simultaneously to the molecule (non-linear excitation); as an example, to excite a GFP molecule, two photons of 976 nm wavelength would hit the molecule at a femtosecond scale. Furthermore, the multi-photon beam takes place only in the focal point, diminishing any out of focus signal, which means there is no need to use a pinhole as in the confocal microscope, figure 2.8. Finally, different fluorescent probes within a sample can be identified with multi-photon microscopy using only one energy wavelength (Ustione & Piston 2011). All the mentioned advantages make multi-photon microscopy a great tool to be applied in samples which are usually not easy to image such as bone, due to its tendency to scatter light (Strupler et al. 2007).

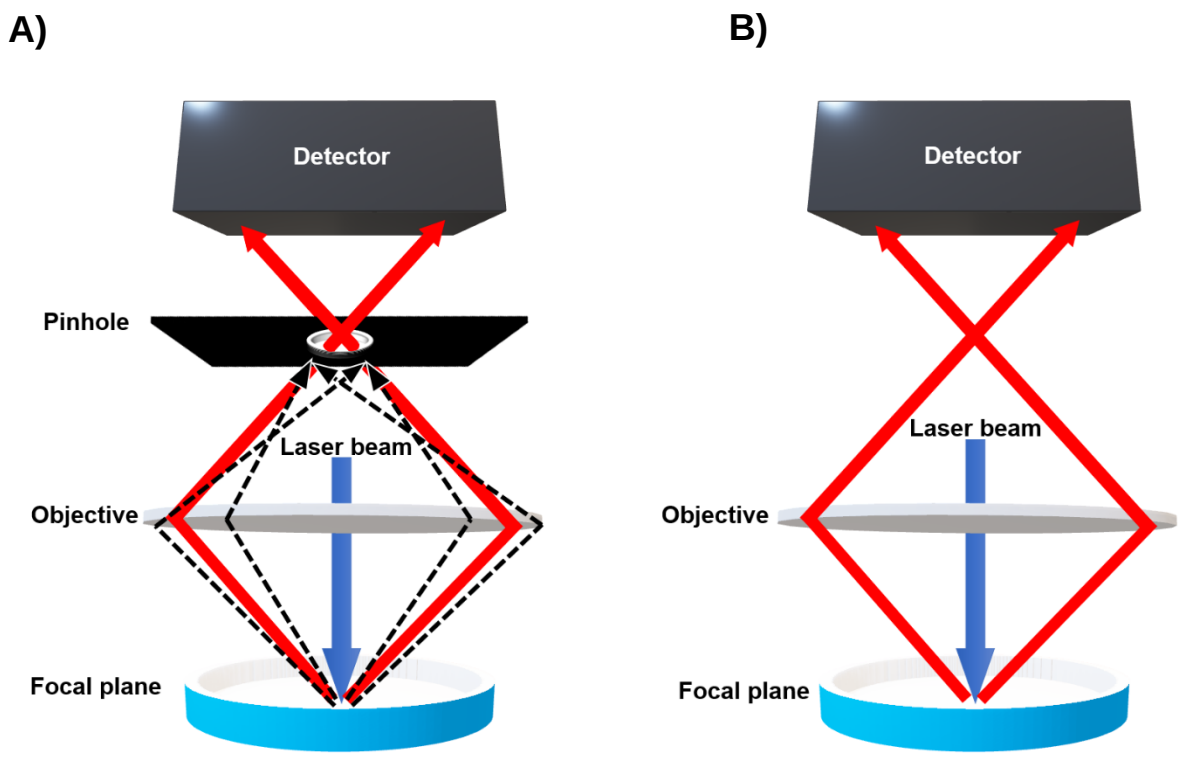


**Figure 2. 8. Working principle comparison between confocal and multiphoton microscopy.** *A) In confocal microscopy, the fluorescent emission (red arrows) from a sample stimulated by a single-photon laser beam will travel through a pinhole to end in a detector. All out of focus signal (dashed arrows) will be blocked by the pinhole, providing a high-quality image. B) In multi-photon microscopy, no pinhole is needed since the multi-photon beam takes places only in the focal point.*

The multiphoton microscopy was applied to identify and analyse the Vibrant DiD pre-stained PCa cells injected IC into xenograft models. These cells were analysed *ex vivo* in the tibia bone marrow of the mice and will be described in the following section.

### 2.9.1. Bone samples preparation for multi-photon

The tibias sample preparation consisted of embedding the tibia in Bright Cryo-M-Bed (Bright Instrument Co Ltd, Huntingdon, UK) and snap-freezing it in liquid nitrogen, obtaining a frozen sample block that was cut longitudinally until BM was revealed using a Bright OTF Cryostat with a 3020 microtome (Bright Instruments Ltd). The tibia was placed in a Nunc™ Glass Base Dish (Thermo Fisher Scientific, Waltham, Massachusetts) with the exposed BM facing the glass dish. A 22x22 mm coverslip (Menzel-Gläser, Saarbrückener, Germany) was placed on top of the tibia using blu-tack (Bostik, La Défense, Paris, France) to ensure the sample was flat, tight and did not move during the scanning. In the two-photon microscope, the glass dish was placed upside down with the BM facing the lens.

### 2.9.2. Multi-photon scanning

In the two-photon microscope, bone tissue was scanned using a Chameleon laser set at 900 nm (Coherent, Santa Clara, CA, USA) while a HeNe laser at 633 nm was used to identify the DiD-labelled PCa cells. Depth of the image (Z-stack) was selected according to the weakest laser signal. Laser depth capacity is 130 and 100 µm for 900 nm Chameleon and 633 nm HeNe laser, respectively. Therefore, to maintain the HeNe laser capacity, a 78 µm Z-stack was set with 3 µm distance between each slide. After selecting the appropriate Z-stack, the BM area was fully covered by selecting a 5x6 tile blocks, representing an area of 2104x2525 µm. Bone imaging was finally performed with high quality settings: 512 frame size, mean pixel depth at 4, maximum scanning speed at 9 and 0.82x0.82x3 µm scaling. Prior to scanning, all the settings were loaded in a Multi Time Series (MTS) software (Carl Zeiss, Jena, Germany). The final 3D and a temporary image were also saved using this software. With the mentioned settings, each scan took ~3 hours to be completed.

### 2.9.3. Bone marrow analysis

The 3D bone tissue images were analysed using the Volocity 3D Image Analysis software (PerkinElmer, Cambridge, UK). With this software, qualitative and quantitative data of the 3D picture can be performed. The “3D opacity” setting was selected to acquire representative bone tissue pictures, since it allows changing the pseudocolour of either bone tissue or DiD-labelled cells as well as controlling the sample brightness and contrast. A greyscale was applied for bone tissue while a red colour was maintained for PCa cells. Quantitative data analysis was performed under “extended focus” mode. Any object scanned at 900 nm with a minimum 500 $\mu m^3$ size was considered bone while objectives detected with the 633 nm HeNe laser with a minimum 250 $\mu m^3$ size and a 90-255 threshold were recognized as PCa DiD-labelled cells. After setting up the protocol, a ROI was drawn, delimitating the BM area. The number of PCa cells within the bone marrow, size, and distance to bone were analysed using this methodology.

## 2.10. In Vivo imaging

Bioluminescence is a biochemical process where visible light is produced in a living being, such as the light emitted by fireflies. This feature has been artificially manufactured into cells and tissues to assess biological mechanisms that take place in vivo, due to its feasible and non-invasive properties. The bioluminescent process requires an enzyme and a substrate. Several bioluminescent enzymes have been identified in living beings such as aequorea in jellyfish or renilla in sea pansy; however, the most used is the luciferase (FLuc) enzyme from the *Photinus pyralis* North American firefly (Sadikot & Blackwell 2005).

The firefly luciferase was first cloned by de Wet et al. (1985) and then used in research to investigate the luciferase luminescent reaction in mammalian cell lysates, establishing this enzyme as a high-efficient reporter gene, particularly for *in vivo* studies (Nguyen et al. 1988). The luciferase reaction releases photons in the presence of ATP, Magnesium, and the luciferase substrate luciferin. The luciferin-luciferase complex produces a 562nm wavelength luminescent signal, which is enough to pass

through soft tissues' thickness and be detectable by charged coupled device (CCD) cameras, the function of which is to convert the produced photons into electron signals that are later converted into images representing the location and intensity of the signal. A red/yellow picture would represent a high-intensity signal while a blue/violet would correspond to a lower signal (Zinn et al. 2008;Close et al. 2011).

In our experimental design, we measured tumour burden weekly after treating the mice with 100µl of D-luciferin (30 mg/kg, Thermo Fisher Scientific, Waltham, Massachusetts) subcutaneously. Dorsal and ventral pictures were taken to be later analysed using the Living Image 4.3.1 software. The tumour burden signal was measured as photons/second and normalized using a colour scale.

### 2.11. Bone tumour area analysis

To provide an additional method to analyse the tumour burden in the bone samples, we applied the QuPath 0.3.0 software (Bankhead et al. 2017). This software allows the analysis of histologic samples according to specific regions of interest, making it useful to select the tumour area developed in the *in vivo* models and obtain further results of the PCa tumour progression in bone at a histological level. Briefly, the TRAP-stained bone sections were scanned using the Pannoramic 250 Flash III - 3D-HISTECH slide scanner machine. Then, the tumour and bone marrow of the digitalised bone sample was drawn by selecting the "brush" option in the software, allowing the quantification of the area of interest ($\mu^2$). Finally, the tumour area was normalised into the bone marrow area of the corresponding sample.

### 2.12. ELISAs

The enzyme-linked immunosorbent assay (ELISA) is a quantitative biochemistry assay which allows the detection of a number of proteins in biological samples, applicable for research purposes as well as clinical diagnostics (Wu 2006). The first immunoassay that described an antibody-bound radioisotope signal to measure the insulin levels in patients was created by Yalow and Berson in 1960. The immunoassay was named radioimmunoassay (RIA) (Yalow & Berson 1960). Years later, enzyme-

substrates complexes were linked to antibodies, in order to avoid the health-risks of using radioactivity (Enzymes et al. 1969). Finally, in 1971, the group of Engvall and Perlmann and the group of Van Weeman and Schurs, independently published the development of (Engvall & Perlmann 1971; Weemen & Schuurs 1971). The principle of an ELISA is based on the antigen-antibody immune reaction, an important system of immune defence against pathogens where antibodies produced by B cells recognizes external antigens (Hoffman et al. 2016) .To detect such antigens, an antigen or antibody is bound to an enzyme, being alkaline phosphatase (ALP), horseradish peroxidase (HRP), and β-galactosidase the most commonly used (Avrameas et al. 1978; Nakane & Kawaoi 1974; Craven et al. 1965). Firstly, the antigen located in the sample is added into a solid surface coated with a specific antibody against the antigen of interest, by this manner creating the antigen-antibody reaction and immobilizing the antigen. Afterwards, an enzyme-linked secondary antibody reacts with the coating primary antibody, and by adding a specific substrate, a coloured/fluorescent signal is produced, which is proportional to the quantity of the antigen contained in the sample (Crowther 2009). For instance, chromogenic substrates such as o-phenylenediamine (OPD) are catalysed by HRP, producing an orange-yellow colour (Fornera & Walde 2010). The optical density of the signal is finally measured using a microtiter plate reader, providing data regarding the antigen quantity within the sample.

To date, we can classify four types of ELISAs according to the method applied to detect the antigen of interest, figure 2.9:

1.- **Direct ELISA:** The first step is to add the sample containing the antigen of interest into the ELISA plate, allowing for the antigen to coat the plate by incubation for a certain period and temperature (i.e., 37°C for one hour or 4°C overnight). After the incubation step, any unbound antigen is removed by using a wash buffer followed by blockage of unbound antigen-sites within the plate. The unbound sites are commonly blocked by applying BSA or casein. Once again, the plate is washed, followed by the addition of an enzyme-linked primary antibody directed against the antigen. After another washing step to remove any unbound primary antibody, a substrate is added,

creating a colour change which corresponds to the antigen quantity within the plate, figure 2.9 A (Engvall 2010; Shah & Maghsoudlou 2016; Kohl & Ascoli 2017a).

2.- **Indirect ELISA**: The indirect ELISA is very similar to the direct ELISA, with the difference of an additional secondary antibody. After addition of the primary antibody and wash step, a secondary enzyme-linked antibody is added. This secondary antibody is directed against the primary antibody, therefore, identifying the antigen of interest in an indirect manner. The final steps such as a wash step and substrate addition to develop a coloured signal remain the same, figure 2.9 B (Engvall 2010; Shah & Maghsoudlou 2016; Kohl & Ascoli 2017c).

3.- **Sandwich ELISA**: This type of ELISA receives its name due to the antigen of interest being captured between two antibodies. Firstly, the antibody is coated and incubated into the plate. After a washing step, the antibody is blocked using BSA or other protein. The plate is washed once again to add the sample containing the antigen which will be bound to the capture antibody. The plate is washed again followed by addition of the primary antibody, incubated, washed and finally, the enzyme-linked secondary antibody is added. As in the direct and indirect ELISA, a colour signal is produced by addition of a substrate to be later quantified using a plate reader, figure 2.9 C (Engvall 2010; Shah & Maghsoudlou 2016; Kohl & Ascoli 2017b).

4.- **Competitive ELISA**: The primary antibody is incubated with a sample containing the antigen to study and making antigen-antibody complexes with it. Then, the sample is transferred into a well plate pre-coated with the antigen. The antibodies which did not bound to the antigens in the sample will bind those antigens located in the well. Therefore, if in the initial sample many antigen-antibody complexes were formed, less antibodies will bind in the well plate. This is the competition step, where the antigens in the sample “compete” with those in the well to bind the antibodies. After an incubation, washing and blocking step, a secondary antibody is added which binds the primary antibody. Finally, a substrate is added. The test result is inversely proportional to the quantity of colour signal produced. For instance, if a higher colour signal is produced it means the antigen within the sample is low or absent, as the other enzyme-linked antibody bound the antigen. Opposite, if the colour signal is low the test is positive for the antibody, figure 2.9 D (Engvall 2010; Kohl & Ascoli 2017a).

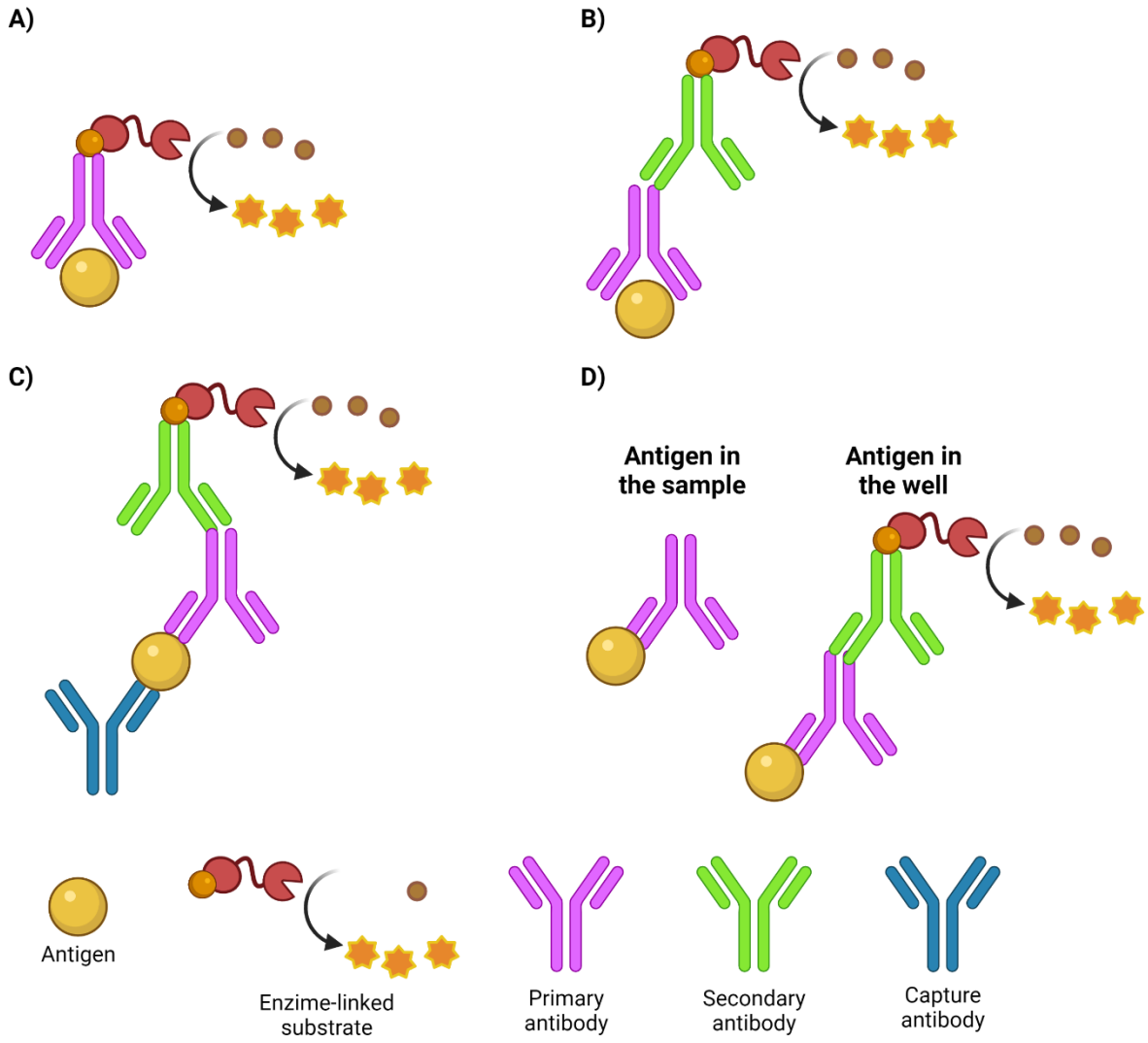


**Figure 2. 9. The different types of ELISAs.** *A) Direct ELISA illustrating the antigen-antibody complex and the substrate-coloured production. B) Indirect ELISA showing the primary and secondary antibody binding. C) Sandwich ELISA. The antigen is trapped between the capture antibody and primary/secondary antibody. D) Competitive ELISA. The antigens in the sample bind the added antibodies and are later removed by washing steps while other antibodies bind the antigens in well, due to lack of antigens in the sample.*

In this project we made use of the sandwich ELISA technique to detect the cytokines of interest in 3 formats: A membrane-based immunoassay, a well-plate ELISA sandwich assay and a magnetic multiplex assay.

### 2.12.1. Proteome Profiler Human XL Cytokine Array

The Proteome Profiler Human XL Cytokine Array is a membrane-based antibody array useful for the detection of 105 cytokines and chemokines in each sample. This membrane array kit was applied to detect cytokines in culture media samples. Briefly, the membranes are blocked using an array buffer for 1 hour at room temperature. Later, the samples are diluted at 1.5ml final volume using an array buffer and placed into the membranes to be incubated overnight at 4°C. The next day, the membranes are washed and treated with a detection antibody cocktail (previously diluted in an array buffer), for one hour. After a washing step, a Streptavidin-HRP reagent is added for 30 minutes, washed, and a chemiluminescent detection reagent applied to produce a signal corresponding to the quantity of protein bound to the membrane-antibodies (in duplicate). The membranes were exposed to X-ray for ~20 minutes and quantified using the Image Lab 6.1 software. The readings were normalised to the control dots.

### 2.12.2. Mouse DKK1 Immunoassay

The Mouse DKK1 Quantikine Immunoassay (R&D systems) was applied to quantify the levels of DKK1 cytokine in mice serum samples. This immunoassay makes use of a 96-well plate pre-coated with DKK1 monoclonal antibody. Firstly, the mice serum samples were 10-fold pre-diluted using 20µl of serum sample with 180µL of Calibrator Diluent RD5-26. Then, 50 µl of Assay diluent added into the well plate followed by 50 µl of standards, controls, and samples to be later incubated at room temperature for 2 hours. The well plates were later washed using 400 µl of Wash Buffer 4 times. After the washing step, 100 µl of Mouse DKK1 Conjugate were added to the respective wells and incubated again for 2 hours. After incubation,100 µl of Substrate Solution were added into the respective wells, incubated for 30 minutes and then the reaction was stopped using 100 µl of stop solution. A wavelength set at 450nm with correction

at 540nm was used to quantify the DKK1 cytokine quantity using a SpectraMax M5 microplate reader.

### 2.12.3. Magnetic multiplex immunoassay

The Bio-Plex® multiplex immunoassay system uses the xMAP technology (licensed from Luminex) to allow the multiplexing of up to 100 analytes using magnetic beads in a single experiment. The working principle of the multiplex assay begins with magnetic beads coloured at different ratios using two different fluorescent dyes (red and infrared, figure 2.10. The beads are further linked to an antibody specific for the analyte of interest while the secondary antibody is enzyme-conjugated and is used to detect the quantity of analyte in the sample. In simple terms, is a sandwich ELISA type that takes place in a magnetic bead. To analyse the quantity of analytes in the beads, a flow cytometer is applied with two channels, one is directed to identify the bead colour and the second one quantifies the analyte concentration (Graham et al. 2019; Houser 2012).

The Bio-Plex Pro Mouse Cytokine 23-plex Assay was applied to analyse 23 cytokines in mice serum samples. This assay was performed with the help of Dr. Josephine Pickworth (The University of Sheffield). Firstly, the mice serum was diluted at 1:4 (12.5µl into 37.5µl of Bio-Plex sample diluent) as recommended by the manufacturer's instructions. Then, the 10x coupled beads were diluted (575µl into 5,175µl of assay buffer) and 50 µl added into each well. The plate was then washed twice with 100 µl of wash buffer. The wash steps were carried out using a magnetic 96-well separator (Thermo Fisher) by placing the 96-well plate into the well separator, let it stand for 1 minute to let the magnetic beads adhere to the well and then the wash buffer dropped, maintaining the beads saved into the plate. Later, 50µl of standards and samples were added to the corresponding wells, covered with a sealing tape, and placed int a shaker at 850±50rpm for 30 minutes. After incubation, the plate was washed again 3 times and the detection antibodies diluted (300ul of detection antibodies into 2,700µl of diluent HB) and then 25µl added into each well. The well plate was again placed into the shaker, washed and 50 µl of Streptavidin-Phycoerythrin (SA-PE, 60 µl diluted into 5,940 µl of assay buffer) added. After another incubation and washing step, the beads

were resuspended in 125 µl of assay buffer, placed into the shaker at the mentioned speed and the well plate read using the Luminex 200 machine.

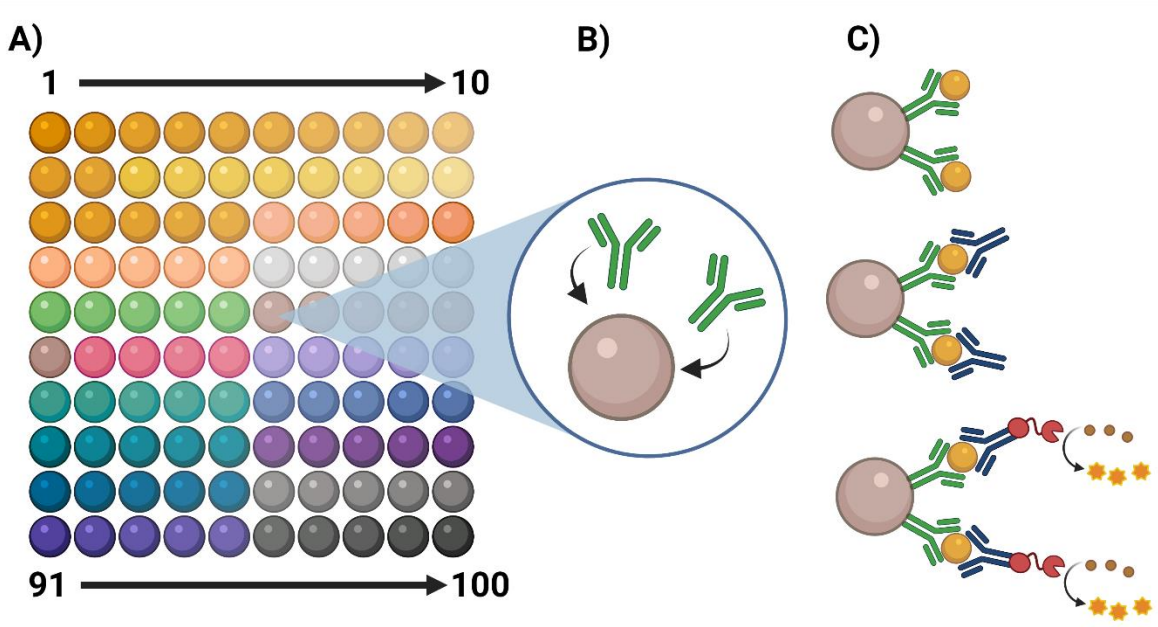


**Figure 2. 10. Multiplex immunoassay technology.** *A) The magnetic nanobeads are coloured using red and infrared dyes, resulting in 100 bead regions which are later conjugated B) with an antibody specific for the analyte to analyse. C) A second enzyme-linked antibody is added to detect the quantity of the analyte of interest.*

## 2.13. Retrospective study

To analyse the expression level of *DKK1* at different stages of PCa, a retrospective study was performed using the Gene Expression Omnibus (NCBI, https://www.ncbi.nlm.nih.gov/geo/) database. To search for PCa human samples, the term “prostate cancer” was used, showing 71 related databases from which, 8 were analysed in human PCa samples (GDS1439, GDS4824, GDS5072, GDS4109, GDS2545, GDS3289, GDS1746, GDS2171). Three out of the 8 databases provided information regarding primary and metastatic PCa sample stages: the “Prostate cancer progression” GDS1439 accession number, the “Prostate cancer progression at the cellular level” GDS3289 accession number, and the “Metastatic prostate cancer” GDS2545 accession number. The “Prostate cancer progression” study, analysed the expression of 54,675 genes using the Affymetrix Human Genome U133 Plus 2.0 Array in 19 samples (13 from cells of individual patients and 6 from tissue pools) (Varambally et al. 2005). In the “Prostate cancer progression at the cellular level” study, 104 samples were analysed using the Chinnaiyan Human 20K Hs6 platform (Tomlins et al. 2006). The “Metastatic prostate cancer” study analysed 171 samples from patients with localised and metastatic PCa using the Affymetrix Human Genome U95 Version 2 Array (Yu et al. 2004; Chandran et al. 2007).

## 2.14. Atomic force microscopy

The atomic force microscopy (AFM) is a type of scanning probe microscope (SPM), at a nanometres scale, providing a high-resolution scanning (Vahabi et al. 2013). The AFM working principle is based on the forces sensed by a probe attached to a cantilever and the sample of interest, figure 2.11. The probe is passed through the sample, by this manner creating forces recorded by the AFM system according to the defection of the cantilever (also known as stiffness of the cantilever) (Fotiadis et al. 2002). The stiffness is measured by the Hooke law, a physics law of elasticity which states that the force required to extend or compress a material is directly proportional to the distance of the extension or compression applied in the material (Cappella & Dietler 1999). A laser hits the cantilever, and its signal is reflected into a mirror to be

directed into a photo-diode detector. Finally, the stiffness measured is recorded and visualised in a computer in real time (Vahabi et al. 2013).

AFM was applied to measure the stiffness of bone samples subjected to mechanical loading, as several evidence suggest a role of the tumour microenvironment stiffness into tumour progression (Winkler et al. 2020; Pickup et al. 2014). Briefly, the tibia obtained from one 8-week-old C57BL/6 mice subjected to one week of mechanical loading (9N loading force, 3 loading cycles) was analysed using the JPK NanoWizard III AFM by Dr. Xinyue Chen at the University of Sheffield. The force map size and resolution were 30 µm × 30 µm, 30 pixels × 30 pixels, respectively. The heat maps represented the Young's modulus from the Hertz-Sneddon fitting, a model to measure elastic deformation between two cylinders and a conical probe into a flat surface, respectively (Han & Chen 2021). The stiffness is measures as Pascals (Pa) with a colour bar ranging from 1 to 1 to $10^6$ log scale. A lower Young's modulus represents a less stiffened surface.

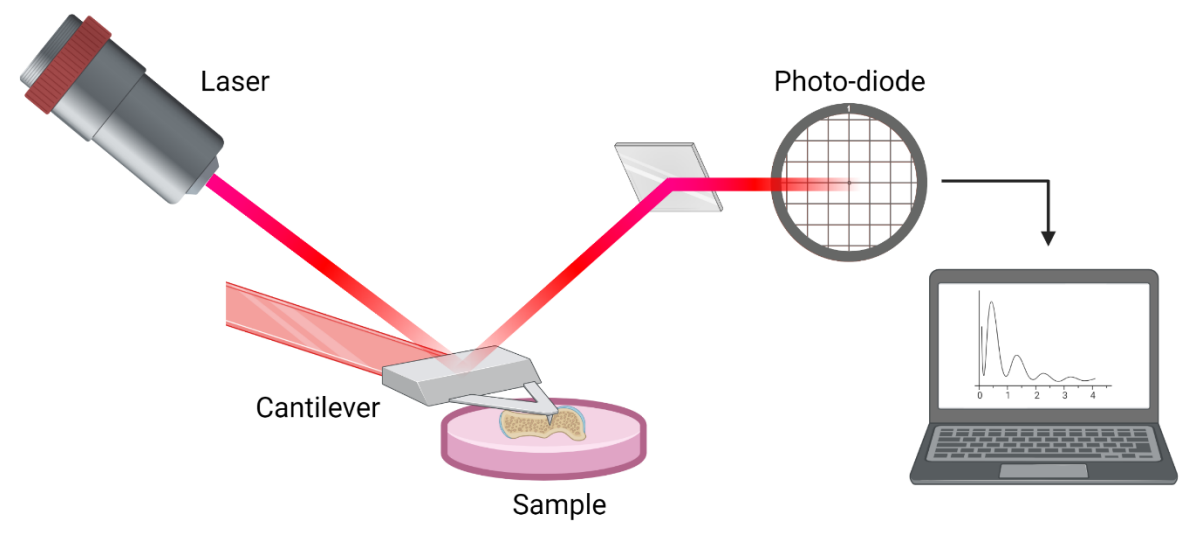


**Figure 2. 11. Principle of atomic force microscopy.** *A probe placed in a cantilever deflects according to the surface of the sample to analyse. A laser projects into the cantilever, and its deflection is recorded as forces and the signal detected by a photodiode to be analysed in a computer system.*

## 2.15. Statistical analysis

Values are presented as mean±SEM. Significance between data was analysed applying paired or unpaired t-test, One-Way ANOVA, chi-square and linear correlation using the GraphPad Prism 7.02 software (San Diego, California, USA). Coding: **p<0.05, **p<0.01, ***p <0.001, ****p<0.0001.*

# CHAPTER 3:

## Osteogenic response and bone formation under mechanical loading stimulus.

## 3.1. Introduction

The bone is a dynamic tissue that preserves its structure through the bone remodelling process (Florencio-silva et al. 2015). Bone remodelling is governed by the coupled activity of osteoblasts, known as the bone forming osteoblasts and bone resorbing osteoclasts, while osteocytes act as the bone mechanosensory cells. Individuals with low physical activity show decreased bone mass and strength. The opposite is seen in subjects with high physical activity, exercise being the best example. From all the types of exercises, resistance or weight-bearing exercise is highly suggested to improve bone mass due to the mechanical loading forces applied on bone during training (Skerry 1997; Guadalupe-Grau et al. 2009).

According to Wolff's law and Utah's paradigm, bone is designed to bear mechanical loading forces and it changes its structure according to the mechanical stimulation applied on it (Frost 2001b). If the mechanical loading force is strong enough to create a strain that exceeds a certain remodelling threshold, bone mass will improve. At the cellular level, the mechanical loading and the consequent strain created will stimulate the bone remodelling cycle, enhancing osteoblast activity to create new bone, and inhibiting bone resorption, which results in greater bone mass and a stronger bone. To study the osteogenic response achieved by mechanical loading, several authors have tried to develop loading protocols using *in vivo* models (Meakin et al. 2014).

The first studies were directed to measure the strains developed in bone under several activities and species, using bone-implanted strain electrical gauges, finding a similar strain peak (~2000–3000 με) for all the species (Lanyon & Smith 1969).Years later, the goal was to control the mechanical loading force and strain, successfully assessed by Lanyon & Rubin (1984). This team implanted transfixing pins on avian ulna metaphysis to apply mechanically controlled loadings in hand with electrical strain gauges to measure the resulting strain. Nowadays, non-invasive methods have been developed to mechanically load bone and achieve bone formation. When using mice models, the mice tibia is placed between two loading cups and the desired loading force axially applied. With these methods, the mechanical loading force and strain are fully controlled, and are safer than invasive models, avoiding distress or infections.

In this chapter, we applied a non-invasive, axial mechanical loading protocol to study the osteogenic response of 12-week-old immunocompromised BALB/c nude mice (De Souza et al. 2005; Sugiyama et al. 2010). The mechanical loading force was applied on the mice right tibia, using cohorts of mice (6 mice each) to study the effects of various lengths of loading stimulus (0, 1, 2 and 3 weeks). Micro-CT and histomorphometry analysis were applied *ex vivo* to study bone remodelling patterns and bone cellular changes after loading stimulus, respectively. These studies provided baseline results to understand the osteogenic response that takes place in load-bearing exercise and link this information to further experiments where PCa cells will interact with resident bone cells under mechanical loading stimulus.

## 3.2. Results

### 3.2.1. Mechanical loading improves osteogenic response and bone formation within 3 loading cycles

#### 3.2.1.1. Whole tibia

Thirty BALB/c nude mice were subjected to non-invasive axial mechanical loading regimens on the right tibia:12 N onto a 2 N pre-load, using the Bose ElectroForce 5500 Test Instrument, 40 loading cycles with a 10 second rest intervals 3 times per week for up to 3 weeks. The left tibia was used as internal non-loaded control. Cohorts of mice (n=6) were euthanised at day 0, 7, 14 and 21 after the loading treatment. Micro-CT analysis revealed significant bone formation in the loaded tibias versus the non-loaded, as demonstrated in the bone remodelling parameters for trabecula and cortical bone tissue. Representative 3D models of the tibia structure at week 0 and week 3 of mechanical loading were created using the CTvol software to show increased trabecula and cortical bone mass over time, figure 3.1.

#### 3 2.1.2 Trabecula tissue

Seven parameters were analysed for the trabecula tissue: Trabecular bone volume fraction (BV/TV%), trabecula thickness (Tb.Th), trabecula number (Tb.N), trabecula separation (Tb.Sp), trabecula bone pattern factor (Tb. Pf), structure model index (SMI) and degree of anisotropy (DA). At the baseline level, the right and left tibia show no significant differences in any of the bone parameters analysed by Micro-CT (Figure 3.2). After one week of loading treatment (3 loading cycles) the trabecula bone volume fraction was significantly improved ~31% compared to the contralateral tibia figure 3.2 A, $p<0.0001$. The trabecula thickness was also significantly increased (figure 3.2 B, ~22%, $p=0.0006$) after the same treatment period. The trabecula number was significantly higher after one week of loading, figure 3.2 C, ~8%, $p=0.003$). A lower trabecula separation correlates with increase volume while decresed levels in trabecula pattern factor are associated with a well-connected structure. Both parametters where significantly decreased in loaded tibias after one and three weeks,

figure 3.2 D and E, $p$=0.002 and $p$=0.0009, respectively. The SMI was also significantly different after 2 weeks of loading, figure 3.2 F, $p$=0.001. The quantitative data is presented in table 3.1 and representative 3D models of the trabecula tissue under loading stimulus are presented in figure 3.3.

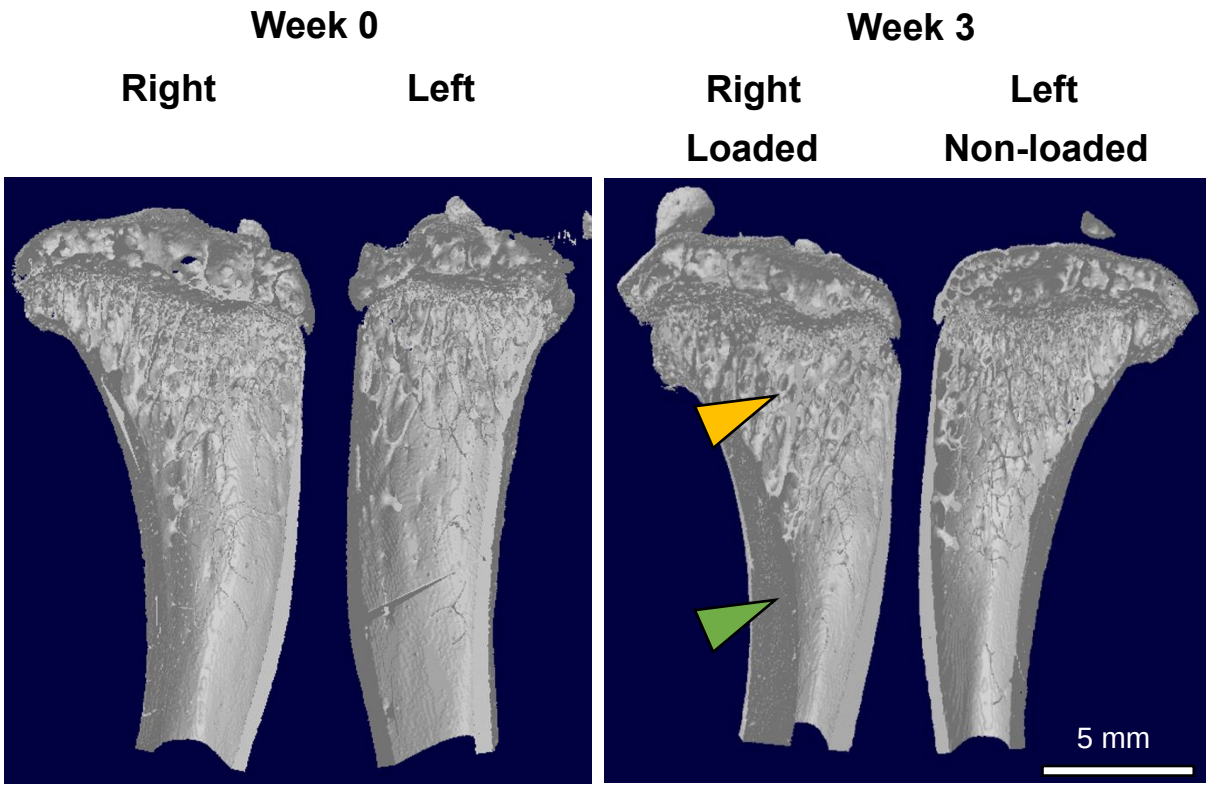


**Figure 3. 1. Mice tibia 3D model before and after mechanical loading treatment.** *Three-dimensional models of the tibias were created using the CTvol software. Notice that at week 0, the right and left mice tibias show similar cortical and trabecula volume. After 3 weeks of loading stimulus, the right-loaded tibia shows increase trabecula (yellow arrow) and cortical (green arrow) tissue volume compared to the non-loaded left tibia, scale bar= 5mm.*

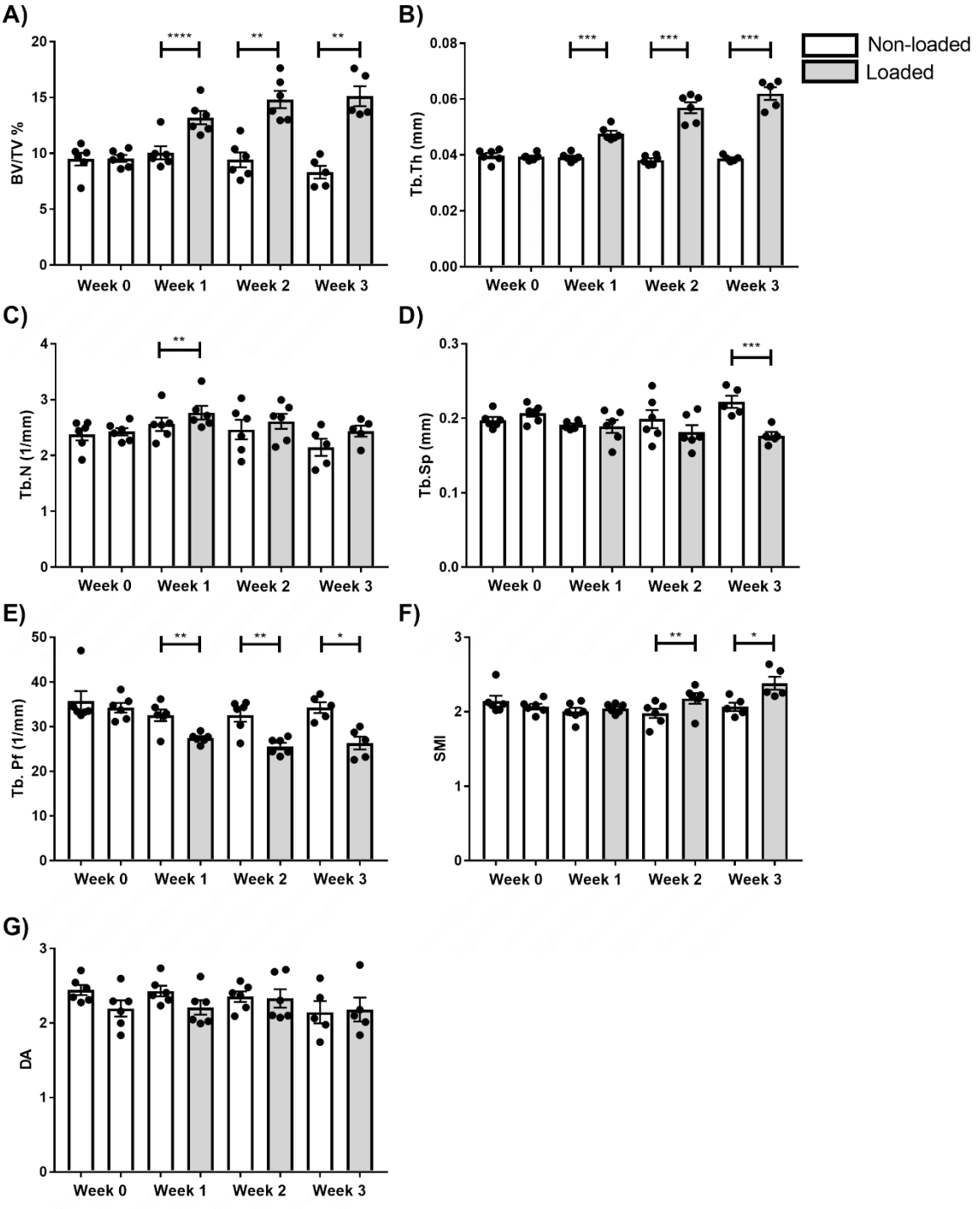


**Figure 3. 2. Mechanical loading improves bone structures parameters after one week of loading stimulus.** *Thirty 12-week-old BALB/c nude mice were subjected to mechanical loading treatment, applying the loading stimulus into their right tibia, using the left tibia (non-loaded) as internal control. The loading regimen was carried out for up to 3 weeks. Cohorts of mice (6 mice each) were culled at day 0, 7, 14 and 21. Mice tibias were scanned at 4.3 µm resolution using the Skyscan 1272 scanner. Bone remodelling parameters were analysed: (A) trabecula bone volume fraction, (B)*

*trabecula thickness, (C) trabecula number, (D) trabecula separation, (E) trabecula pattern factor, (F) structure model index and (G) degree of anisotropy. The bone remodelling parameters were compared among the loaded and non-loaded tibias. All data is presented as mean±SEM,n≥5, paired t-test,*p< 0.05, **p<0.01, ***p<0.001, and ****p<0.0001.*

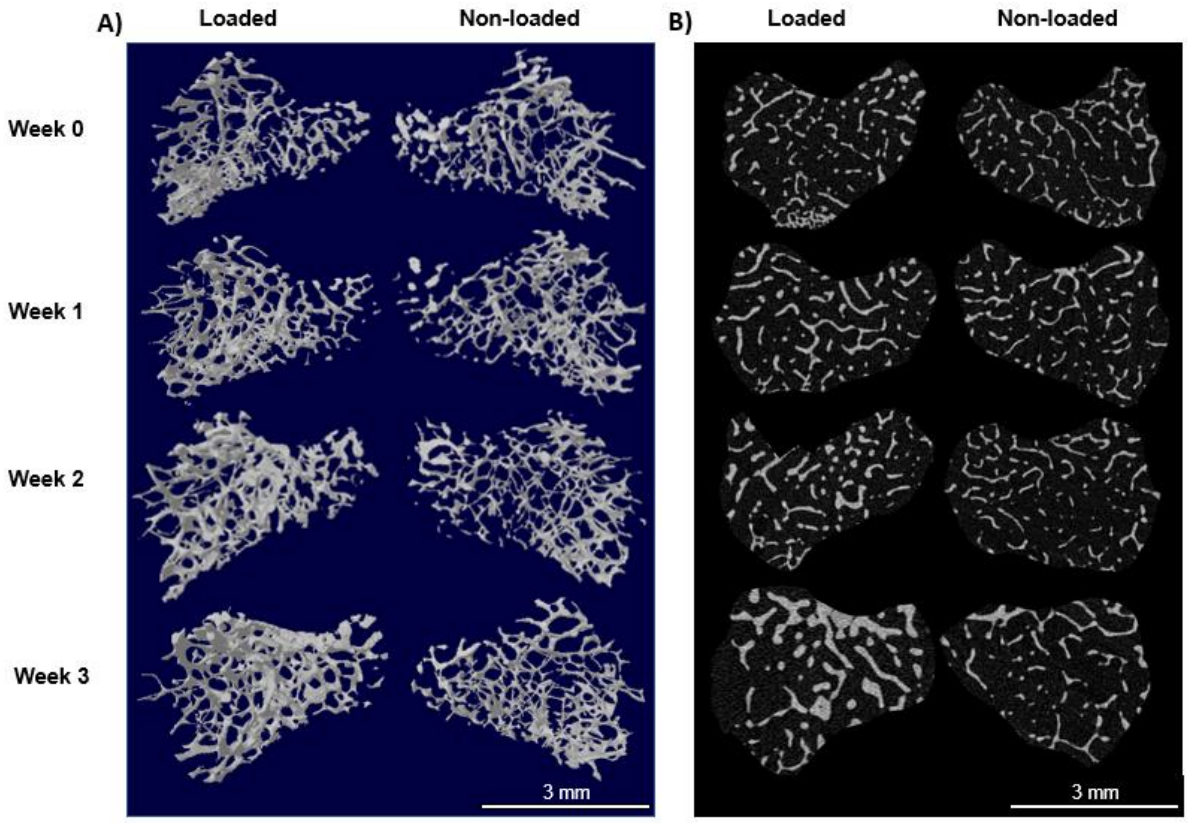


**Figure 3. 3. Three-Dimensional model of loaded versus non-loaded trabecula tissue.** *Three-dimensional models of the trabecula tissue were created with 0.2 mm offset below the growth plate with 1 mm in height. A) The 3D models of the trabeculae tissue and B) the cross-section picture of the corresponding trabecula region. The trabecula tissue under mechanical stimulus becomes thicker each week compared to the non-loaded trabecula tissue, scale bar= 3 mm.*

**Table 3. 1. Quantitative results of tibial trabecula tissue parameters by Micro-CT analysis.**

| | Week 0 | | | |
|---|---|---|---|---|
| | Non-loaded | Non-loaded | Percentage changes | P value |
| | n=6 | n=6 | | |
| **BV/TV %** | 9.48±0.56 | 9.54±0.306 | 0.61 | NS |
| **Tb.Th (mm)** | 0.039±0.0009 | 0.03±0.0004 | -1.16 | NS |
| **Tb.N (1/mm)** | 2.37±0.10 | 2.42±0.066 | 2.10 | NS |
| **Tb.Sp (mm)** | 0.19±0.004 | 0.20±0.004 | 4.63 | NS |
| **Tb. Pf (1/mm)** | 35.69±2.28 | 34.21±1.08 | -4.32 | NS |
| **SMI** | 2.14±0.07 | 2.06±0.036 | -3.62 | NS |
| **DA** | 2.44±0.06 | 2.19±0.10 | -11.29 | NS |

| | Week 1 | | | |
|---|---|---|---|---|
| | Non-loaded | Loaded | Percentage changes | P value |
| | n=6 | n=6 | | |
| **BV/TV %** | 10.06±0.57 | 13.2±0.59 | 23.78 | **** |
| **Tb.Th (mm)** | 0.03±0.0005 | 0.04±0.0009 | 17.84 | *** |
| **Tb.N (1/mm)** | 2.56±0.11 | 2.76±0.12 | 7.44 | ** |
| **Tb.Sp (mm)** | 0.19±0.002 | 0.18±0.008 | -1.004 | NS |
| **Tb. Pf (1/mm)** | 32.52±1.3 | 27.42±0.45 | -18.59 | ** |
| **SMI** | 2.001±0.051 | 2.04±0.02 | 2.15 | NS |
| **DA** | 2.42±0.072 | 2.21±0.09 | -9.90 | NS |

| | Week 2 | | | |
|---|---|---|---|---|
| | Non-loaded | Loaded | Percentage changes | P value |
| | n=6 | n=6 | | |
| **BV/TV %** | 9.41±0.66 | 14.83±0.78 | 36.50 | ** |
| **Tb.Th (mm)** | 0.03±0.0006 | 0.05±0.001 | 32.80 | *** |
| **Tb.N (1/mm)** | 2.46±0.17 | 2.61±0.13 | 5.62 | NS |
| **Tb.Sp (mm)** | 0.19±0.01 | 0.18±0.009 | -9.52 | NS |
| **Tb. Pf (1/mm)** | 32.57±1.45 | 25.62±0.74 | -27.12 | ** |
| **SMI** | 1.97±0.06 | 2.17±0.071 | 9.18 | ** |
| **DA** | 2.35±0.071 | 2.33±0.12 | -0.98 | NS |

| | Week 3 | | | |
|---|---|---|---|---|
| | Non-loaded | Loaded | Percentage changes | P value |
| | n=5 | n=5 | | |
| **BV/TV %** | 8.31±0.57 | 15.12±0.88 | 44.98 | ** |
| **Tb.Th (mm)** | 0.038±0.0004 | 0.06±0.002 | 37.44 | *** |
| **Tb.N (1/mm)** | 2.14±0.15 | 2.43±0.096 | 11.89 | NS |
| **Tb.Sp (mm)** | 0.22±0.008 | 0.17±0.005 | -25.87 | *** |
| **Tb. Pf (1/mm)** | 34.27±1.19 | 26.3±1.47 | -30.30 | * |
| **SMI** | 2.06±0.05 | 2.38±0.08 | 13.22 | * |
| **DA** | 2.14±0.14 | 2.18±0.15 | 1.69 | NS |

Values are mean ± SEM

NS: Non-significant

Percentage changes = (Loaded mean – Non-loaded mean)/Non-loaded mean × 100

* *p<0.05* (Student's paired t-test)

** *p<0.01* (Student's paired t-test)

*** *p<0.001* (Student's paired t-test)

**** *p<0.0001* (Student's paired t-test)

### 3.2.1.3. Cortical tissue

The cortical area analysed for tibias using Micro-CT (0.5mm offset from growth plate and 1mm in height) showed a significant increase in bone volume (BV) for the loaded tibias compared to controls after one week of treatment, ($p=0.0006$, figure 3.4). The tibias subjected to mechanical loading improved ~15% their cortical bone volume in the first week, followed by ~25% in the second week ($p=0.0018$) and 35% in the third week of loading ($p=0.0001$) when compared to non-loaded controls. 3D models of the tibial cortical tissue are presented in figure 3.5, illustrating the change in cortical volume as a result of the mechanical loading stimulus and the quantitative data is presented in table 3.2.

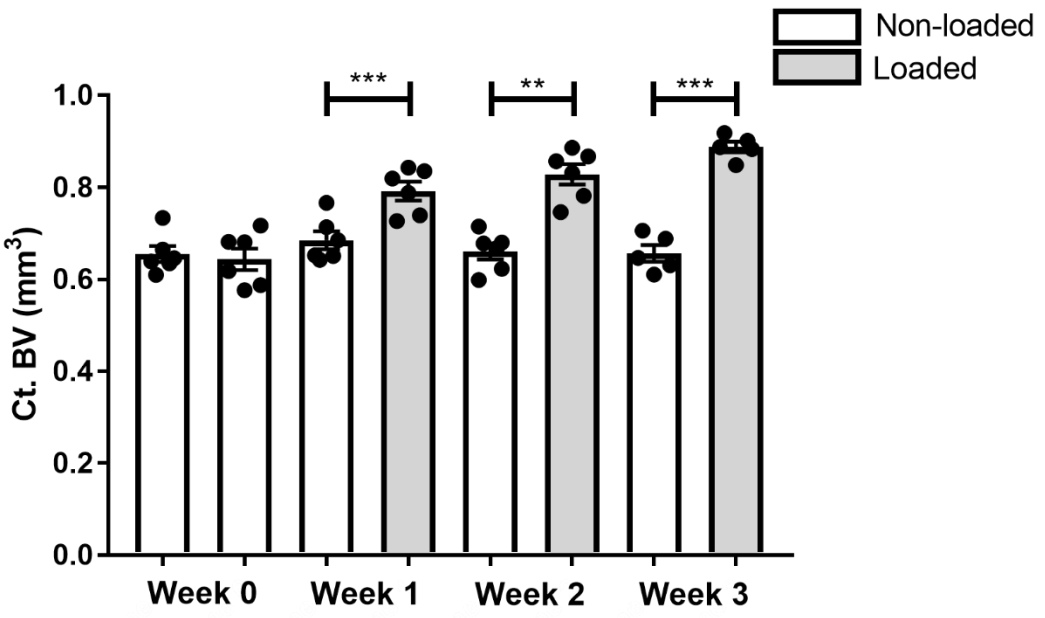


**Figure 3. 4. The effect of mechanical loading in the cortical bone volume of naïve immunocompromised mice**. *The cortical bone volume (Ct. BV) of 12-week-old BALB/c nude mice subjected to mechanical loading was analysed 0.5 mm below the growth plate in 1mm length. All data is presented as mean±SEM, n≥5, paired t-test, **p<0.01, ***p<0.001.*

.

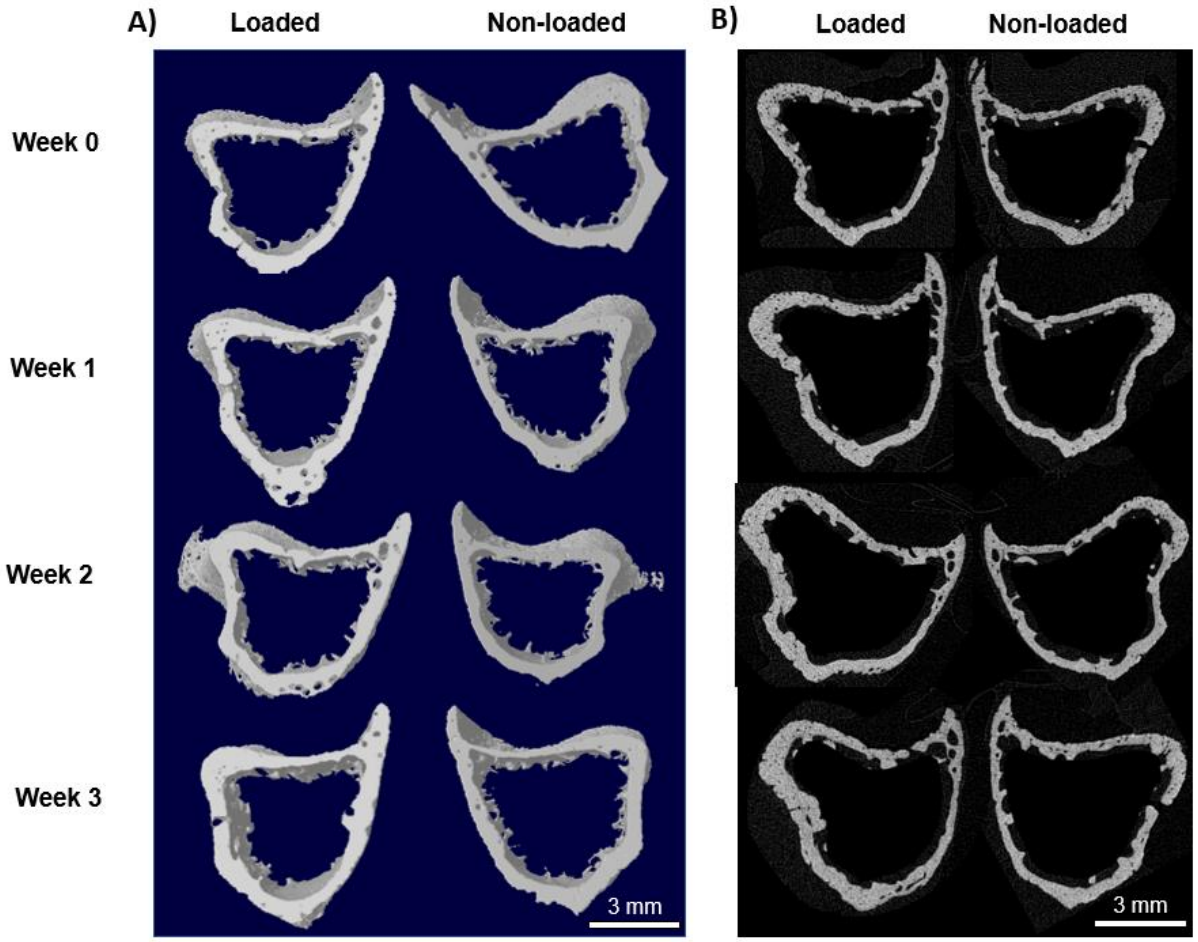


**Figure 3. 5. Three-dimensional models of cortical tissue comparing loaded versus non-loaded tibias.** *Cortical tissue 3D models were built at 0.5mm offset below the growth plate with 1 mm in height. Increase in cortical bone volume can be appreciated along the loaded tibias when compared to the non-loaded tibias, scale bar= 3 mm*

**Table 3. 2. Quantitative results of tibial cortical tissue volume by Micro-CT analysis.**

| | Week 0 | | | |
|---|---|---|---|---|
| | Non-loaded | Non-loaded | Percentage changes | P value |
| | n=6 | n=6 | | |
| **Ct. BV ($mm^3$)** | 0.65±0.017 | 0.64±0.02 | -1.74 | NS |

| | Week 1 | | | |
|---|---|---|---|---|
| | Non-loaded | Loaded | Percentage changes | P value |
| | n=6 | n=6 | | |
| **Ct. BV ($mm^3$)** | 0.68±0.019 | 0.79±0.02 | 13.48 | *** |

| | Week 2 | | | |
|---|---|---|---|---|
| | Non-loaded | Loaded | Percentage changes | P value |
| | n=6 | n=6 | | |
| **Ct. BV ($mm^3$)** | 0.66±0.017 | 0.82±0.02 | 20.27 | ** |

| | Week 3 | | | |
|---|---|---|---|---|
| | Non-loaded | Loaded | Percentage changes | P value |
| | n=5 | n=5 | | |
| **Ct. BV ($mm^3$)** | 0.65±0.017 | 0.88±0.01 | 26.08 | *** |

Values are mean ± SEM

NS: Non-significant

Percentage changes = (Loaded mean – Non-loaded mean)/Non-loaded mean × 100

** $p < 0.01$ (Student's paired t-test)

***$p<0.001$ (Student's paired t-test)

### 3.2.2. Histomorphometry suggests redistribution of osteoblasts within the endocortical surface of the tibias subjected to mechanical loading

#### 3.2.2.1. Endocortical Surface

Histomorphological analysis of the tibias was performed to examine the cellular events that take place under mechanical loading treatment in immunocompromised naïve mice. The samples were processed and analysed as described in section 2.8. Firstly, on the lateral endocortical surface, the loaded tibias showed lower osteoblast number (N.Ob/B.Pm, ~45%) compared to non-loaded at the 3$^{rd}$ week of mechanical loading stimulus, figure 3.6 A-C ($p=0.005$). No significant differences were observed in the osteoclast number (N.Oc) and osteoclast perimeter (Oc.Pm) in the lateral endocortical side (figure 3.6 D-F). In the medial endocortical side there was no significant differences in the number and perimeter of osteoblast (figure 3.7 A-C) but there was an increased trend of N.Oc/B.Pm and Oc.Pm where the number of osteoclasts reached increased significance at week 2 of loading ($p=0.03$) compared to non-loaded controls, figure 3.7 D-F (~70% lower osteoclasts quantity).

#### 3.2.2.2. Trabecula region

Analysis of the trabecula region by histomorphometry revealed that an increased osteoblast number (N. Ob/B.Pm) was identified after one week of loading compared to controls, figure 3.8 A-C ($p=0.0499$). The number of osteoclasts and osteoclast perimeter was reduced at week 1 but it did not reached significance, figure 3.8 D-F. No significant differences were observed in the following weeks for these cells' parameters.

## Lateral endocortical side (Osteoblasts)

A)

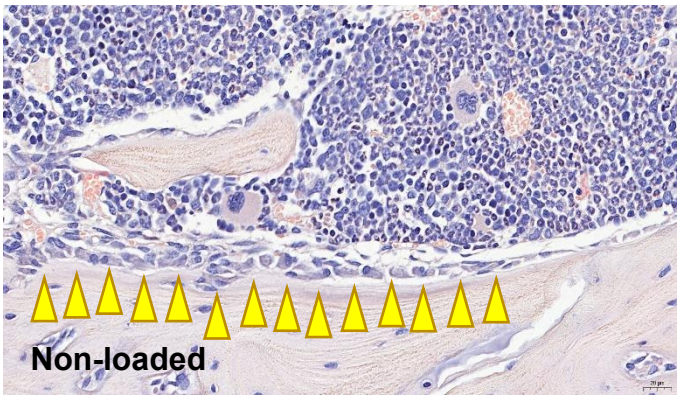


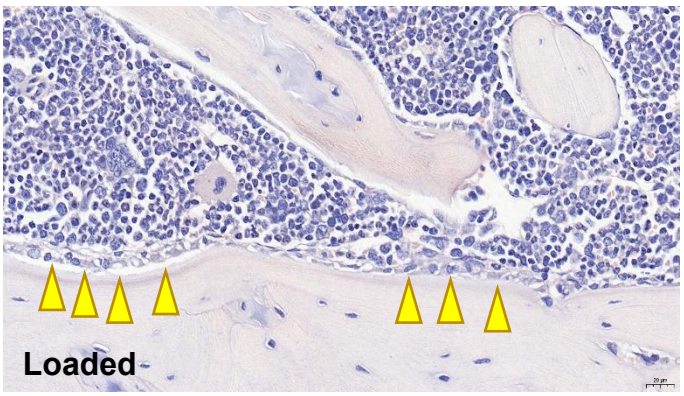


B)

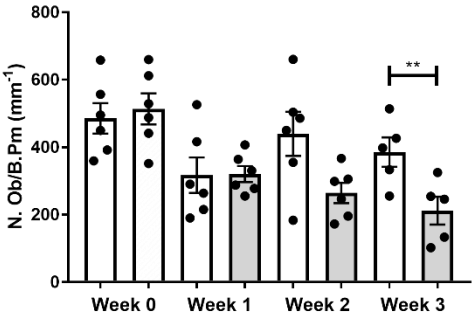


C)

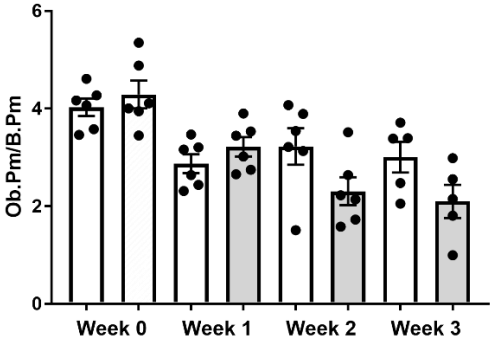


## Lateral endocortical side (Osteoclasts)

D)

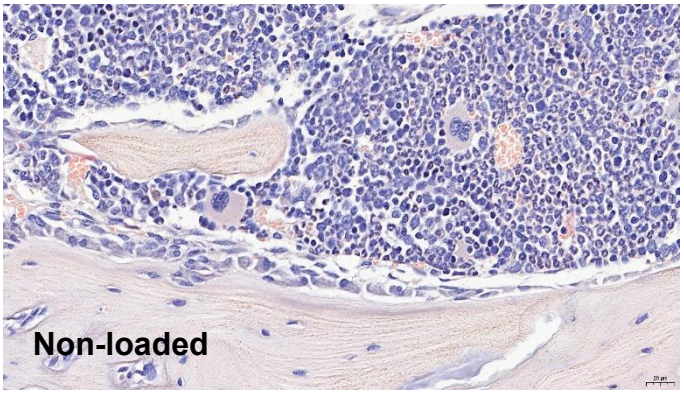


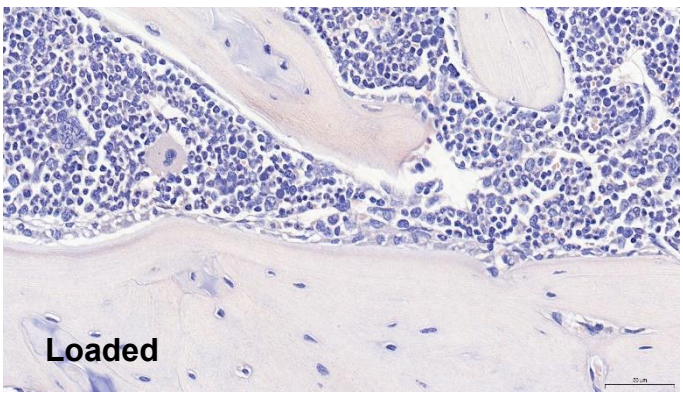


E)

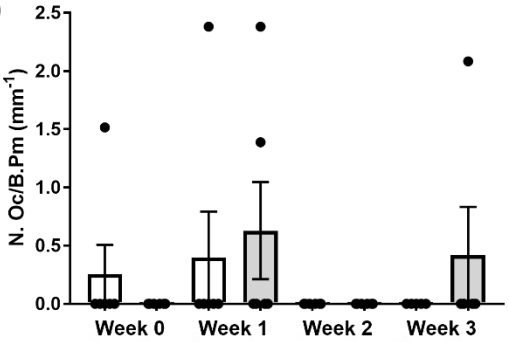


F)

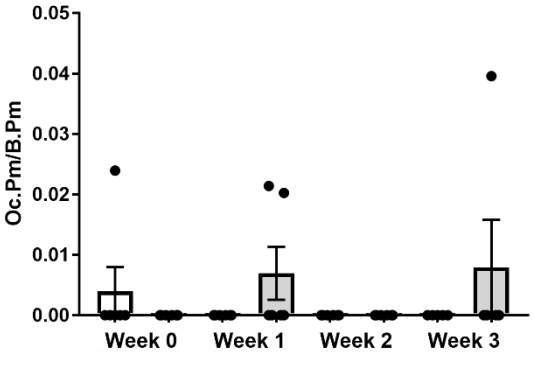

**Figure 3. 6. Histomorphometry showed reduced osteoblast number in the endocortical lateral surface of loaded tibias.** *The sections of loaded and non-loaded tibias of the 12-week-old BALB/c nude mice were TRAP stained to identify the osteoblasts and osteoclasts bone cells. Bone cells were quantified 0.15 mm away from the growth plate on the lateral region under a DMBR microscope using the Osteomeasure bone histomorphometry software. A) Yellow arrows indicate cobblestone like osteoblasts on the lateral endocortical surface. B) Quantification of the osteoblast number per mm in the lateral endocortical bone surface (N.Ob/B.Pm). C) Quantification of the percentage of surface occupied by osteoblasts (Ob.Pm/B.Pm). D) Red arrows indicate pink TRAP-stained osteoclasts on the lateral endocortical surface of loaded and non-loaded tibias. E) Quantification of the corresponding osteoclast number per mm in the lateral endocortical bone surface (N.Ob/B.Pm). F) Quantification of the percentage of surface occupied by osteoclasts (Ob.Pm/B.Pm). Scale bar= 20µm. All data is presented as mean±SEM. n≥5, **p<0.01, unpaired t-test.*

## Medial endocortical side (Osteoblasts)

A)

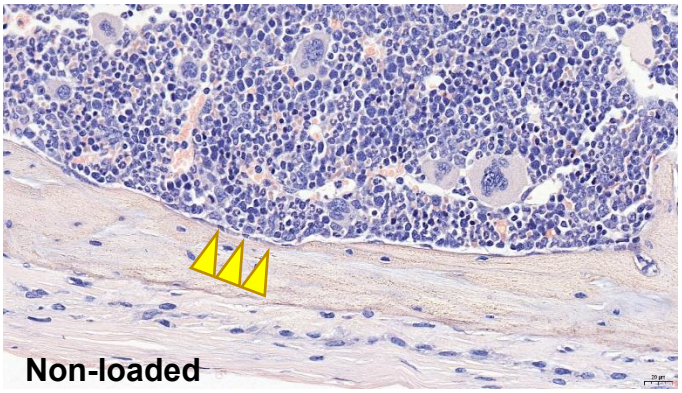


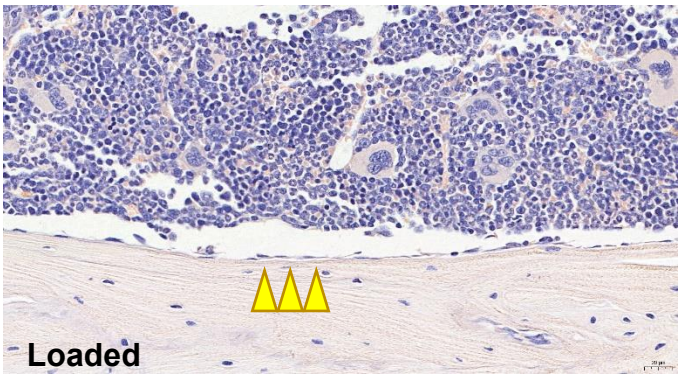


B)

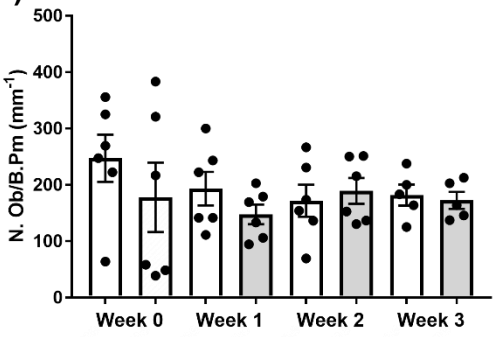


C)

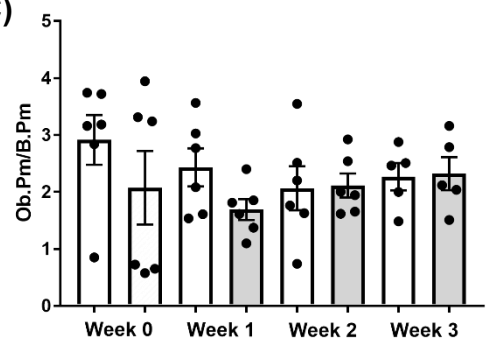


## Medial endocortical side (Osteoclasts)

D)

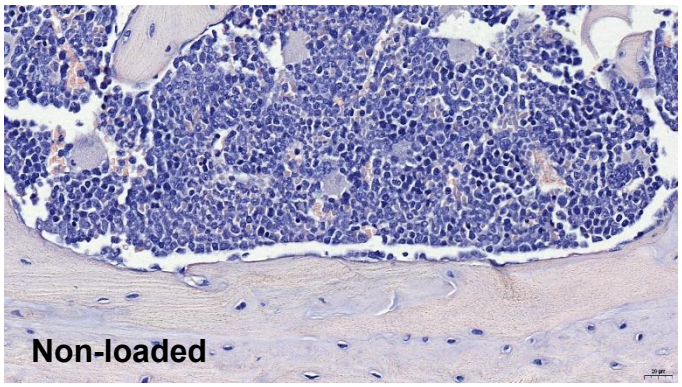


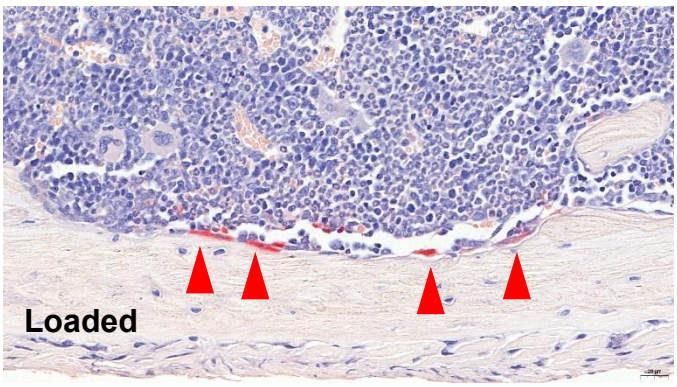


E)

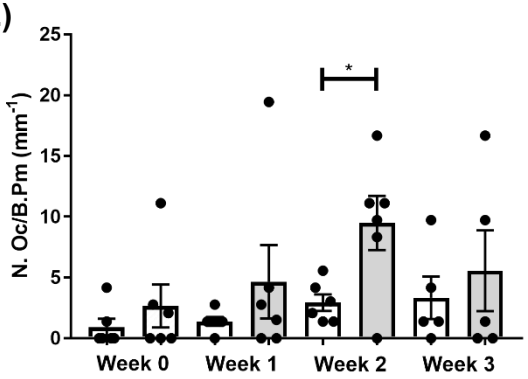


F)

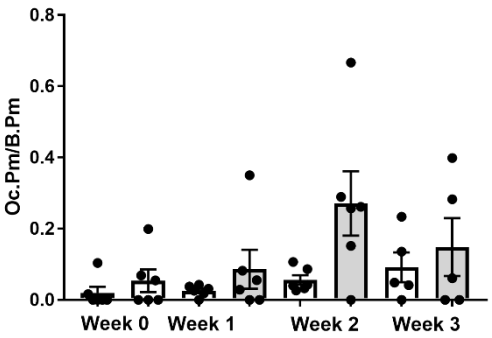

**Figure 3. 7. Histomorphometry showed increased osteoclast number in the medial endocortical surface of loaded tibias.** *The loaded and non-loaded tibias of the 12-week-old BALB/c nude mice were TRAP stained to identify the osteoblasts and osteoclasts bone cells. Bone cells were quantified 0.15 mm away from the growth plate on medial region under a DMBR microscope using the Osteomeasure bone histomorphometry software. A) Yellow arrows indicate pink-cuboidal osteoblasts cells on the medial endocortical surface. B) Quantification of the corresponding osteoblast number per mm in the medial endocortical bone surface (N.Ob/B.Pm). C) Quantification of the percentage of surface occupied by osteoblasts (Ob.Pm/B.Pm). D) Red arrows indicate red trap-stained osteoclasts cells in the medial endocortical surface of loaded and non-loaded tibias. E) Quantification of the corresponding osteoclast number per mm in the medial endocortical bone surface (N.Ob/B.Pm). F) Quantification of the percentage of surface occupied by osteoclasts (Ob.Pm/B.Pm). Scale bar= 20µm. All data is presented as mean±SEM. n≥5, *p<0.05, unpaired t-test.*

## Trabecula region (Osteoblasts)

A)

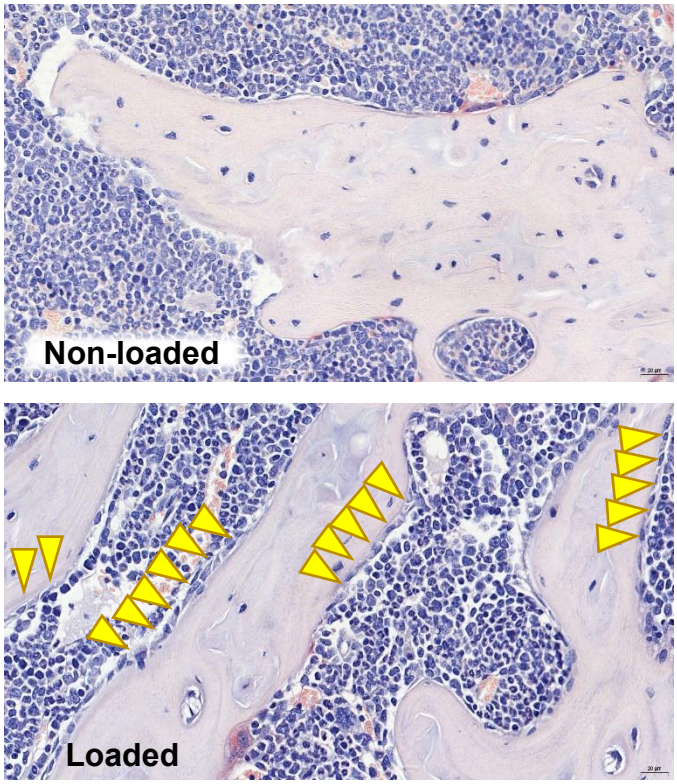


B)

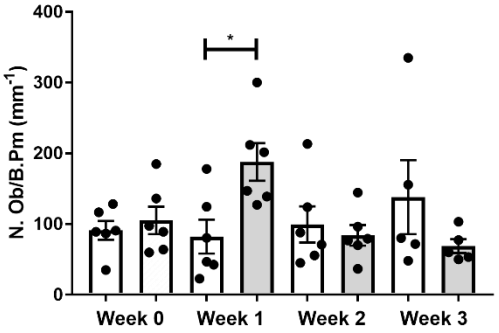


C)

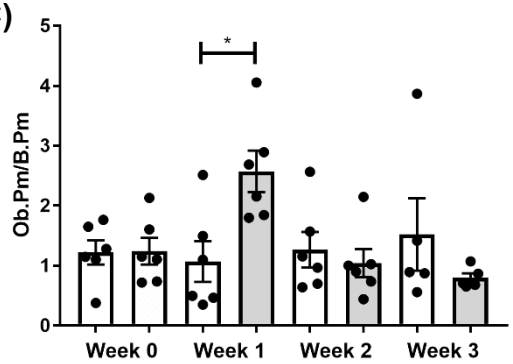


## Trabecula region (Osteoclasts)

D)

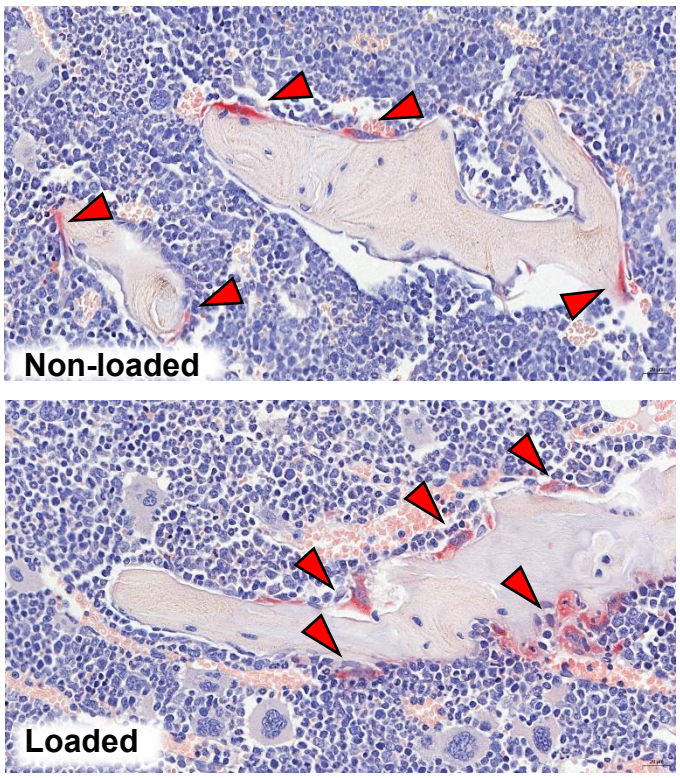


E)

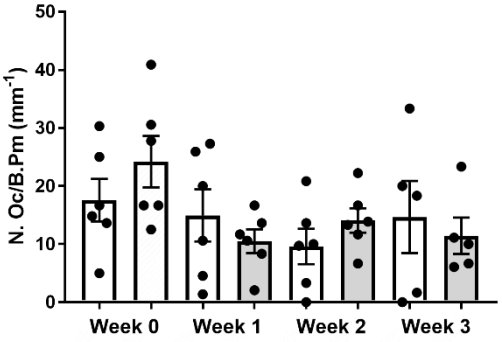


F)

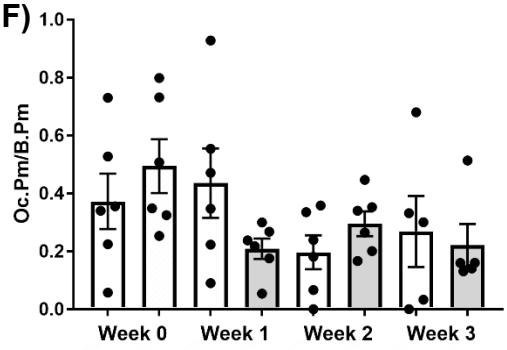

**Figure 3. 8. Histomorphometry showed increased osteoblast number in the trabecula region of loaded tibias.** *The loaded and non-loaded tibias of the 12-week-old BALB/c nude mice were TRAP stained to identify the osteoblasts and osteoclasts bone cells. Bone cells were quantified 0.15 mm away from the growth plate on the trabecula region under a DMBR microscope using the Osteomeasure bone histomorphometry software. A) Yellow arrows indicate pink-cuboidal osteoblasts cells in the trabecula region. B) Quantification of the osteoblast number per mm in the trabecula surface (N.Ob/B.Pm). C) Quantification of the percentage of surface occupied by osteoblasts (Ob.Pm/B.Pm). D) Red arrows indicate red trap-stained osteoclasts cells in the trabecula surface of loaded and non-loaded tibias. E) Quantification of the osteoclast number per mm in the trabecula surface (N.Ob/B.Pm). F) Quantification of the percentage of surface occupied by osteoclasts (Ob.Pm/B.Pm). Scale bar= 20µm. All data is presented as mean±SEM. n≥5, *p<0.05, unpaired t-test.*

### 3. 2.3. Redistribution of osteoblasts cells in loaded tibias

The reduced number of osteoblasts quantified in the lateral tibial surface could indicate a spatial redistribution of osteoblasts within the bone marrow over time. Therefore, we analyse the ratio of osteoblast number in the medial into the lateral endocortical side to clarify this matter. According to the results, there is a statistically significant increment in the ratio of the number of osteoblasts in the medial side into the lateral surface, figure 3.9, $n \geq 5$, $p=0.013$, linear regression test. Therefore, mechanical loading redistributes the number of osteoblasts in the endocortical surface of loaded tibias. The osteoclasts redistribution cannot be analysed as many of the media readings are zero.

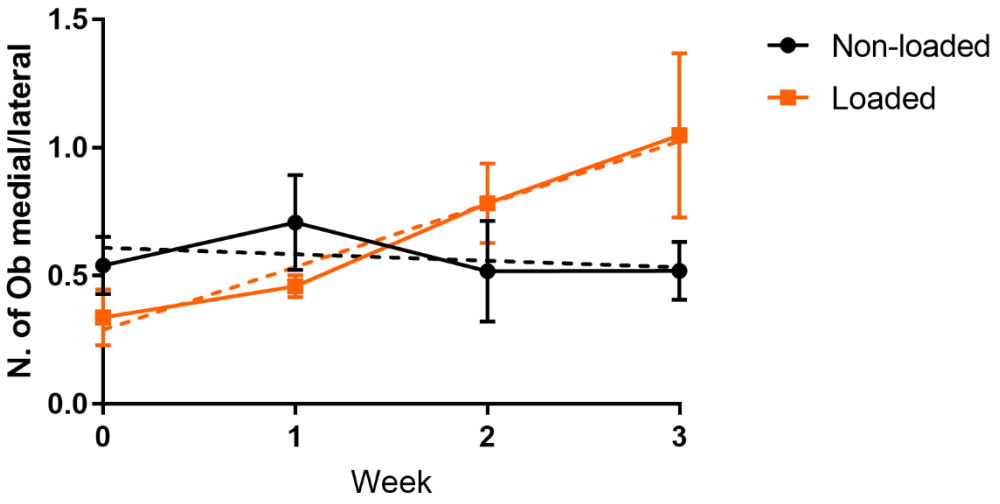


**Figure 3. 9. Redistribution of osteoblasts in the endocortical surface of loaded tibias.** *Ratio comparison of osteoblasts number in the medial endocortical surface into the lateral endocortical region of loaded and non-loaded tibias. All data is presented as mean±SEM, n≥5, p=0.013, linear regression test.*

### 3.2.4. Bone remodelling serum markers in naïve immunocompromised mice subjected to mechanical loading

The activity of osteoblasts and osteoclasts was measured according to the serum levels of P1NP, a marker for collagen 1 deposition and therefore bone formation, and the marker for bone resorption TRAP5b, released by active osteoclasts. The levels of P1NP showed no significant differences during the 3 weeks of mechanical stimulus, while the levels of TRAP5b decreased significantly ($p=0.001$) after 1 week of mechanical loading and were increased back again at week 2 ($p=0.003$) and 3 of loading stimulus, figure 3.10, $n \geq 5$, $^{**}p<0.01$, unpaired t-test.

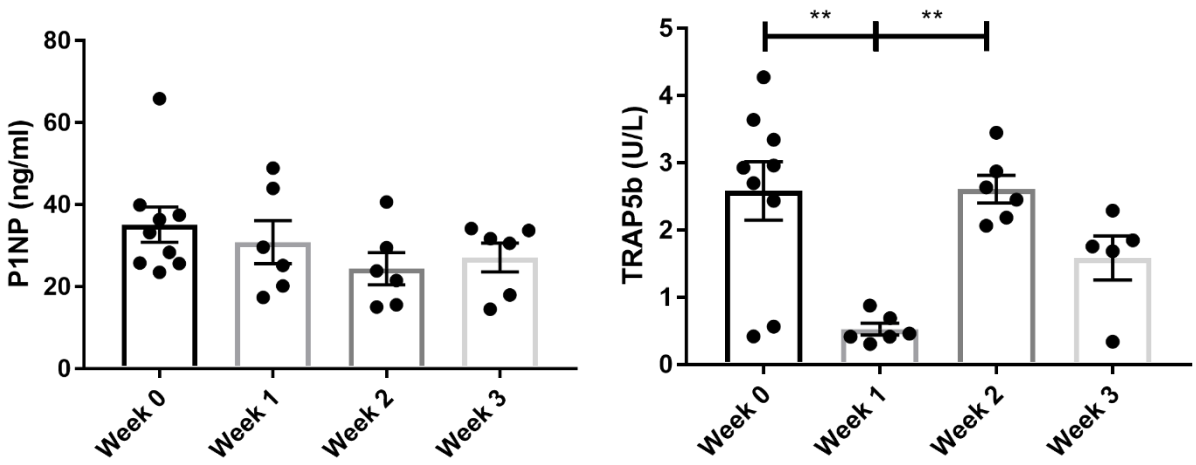


**Figure 3. 10. Serum levels of bone remodelling markers in naïve mice subjected to right-tibial mechanical loading.** *A) P1NP osteoblast bone marker levels and B) TRAP5b osteoclast bone serum marker levels along 3 weeks of mechanical loading stimulus. All data are presented in mean±SEM, n≥5, **p<0.01, unpaired t-test.*

## 3.6. Discussion

In this project, a non-invasive axial mechanical loading protocol was applied into immunocompromised naïve mice to mimic weight-bearing exercise and investigate the osteogenic response and bone formation (De Souza et al. 2005; Sugiyama et al. 2010). A loading force of 12 N was applied for 3 weeks into the mice right tibia using the contralateral limb as internal controls. The bone structure parameters were analysed by Micro-CT *ex vivo* and bone cellular changes by histomorphometry. The aim is to apply a mechanical stimulus that is sufficient to induce an osteogenic response and bone formation which will be later correlated with its impact in the progression of PCa bone metastasis in xenograft models.

### 3.6.1. Mechanical loading improves bone structure parameters within a week of loading stimulus (3 loading cycles)

According to Micro-CT analysis, bone remodelling parameters were significantly improved in the tibia subjected to loading compared to non-loaded controls. The trabecula bone volume fraction (BV/TV%), trabecula thickness (Tb.Th), trabecula number (Tb.N) and cortical bone volume (Ct.BV) were significantly improved. The Tb.S was significantly decrease in loaded tibias compared to non-loaded. A lower trabeculae space means that the trabecula tissue became thicker, therefore, reducing the space within the trabecula tissue. The Micro-CT analysis also indicates significantly lower Tb.Pf compared to controls. The Tb.Pf represents the connection among the whole trabecula architecture, taken as convex and concave structures (Hahn et al. 1992). A lower Tb.Pf indicates a concave surface associated with a well-connected trabecular structure suggesting a well-connected trabecular architecture due to mechanical loading.

The structure model index (SMI) was significantly increased in loaded tibias at the second week of loading stimulus. This parameter indicates whether the trabecula has a plate or a rod-like structure in a 3D model, and gives them values of 0 and 3 respectively (Hildebrand & Rüegsegger 1997). The SMI is usually used to analyse bone degradation in which the trabecula structure will change from a plate to a rod-

like form. In this study, the loaded tibias seemed to change its shape to rods, however, this does not mean there is bone degradation. It is more likely that the trabecula tissue undergoes first a rod-like structure and then a plate-like form. For instance, a mathematical model of trabeculae studied by Rucci & Angelucci (2014), found that the transition from rod to plate-like shape under loading takes approximately 10 days. In our model, it is likely that the osteoblast used the large flat surface of the trabecula to create new bone which will have firstly a rod-like structure to be later a plate-like structure. However, to test this we would need to apply the mechanical loading regimen for a longer period of time.

Overall, the Micro-CT data suggest an osteogenic response within 3 loading cycles applied in one week. This allowed the modification of the further experiments which originally were planned to be performed for 2 weeks in accordance with De Souza, et al. (2005), whose loading protocols were scheduled for 2 weeks to achieve osteogenic response.

In respect of mechanical loading protocols, it has been suggested that bone tissue will respond differently depending on the loading waveform used to achieve bone formation (Holguin et al. 2013). Therefore, when developing a loading protocol, six parameters should be used to describe the loading waveform, which are: waveform shape, peak strain, strain rate, number of cycles, frequency and rest period between each cycle.(Meakin et al. 2014). In regards of our loading protocol, we applied a trapezoidal waveform with 40 loading cycles and 10 seconds rest period between each cycle which is in accordance with previous loading protocols where they found increase in cortical and trabecular bone volume after mechanical stimulus (De Souza, et al. 2005). However, to provide a detailed protocol we need to corroborate the strain rate and frequency. Strain rate is the deformation of an object within a period of time ($\mu\varepsilon\ s^{-1}$) where increase strain rate has been associated with bone formation (O'Connor et al. 1982; Sugiyama et al. 2012). Regarding frequency, osteogenic response is achieved either by high frequency/low magnitude or low frequency/high magnitude (Snow-harter et al. 1992; Rubin et al. 2001; Shi et al. 2010). In order to predict the strain, and study the frequency we could use finite elements (FE) analysis, which are useful to study how a structure or material behaves when a stimulus is applied into it (Charoenphan & Polchai 2006; Oliviero et al. 2018). Although we are aware that the

strain is >1200 με, the application of FE could also reveal the strain induced into mice tibia in detail. Moreover, studies which have applied a similar 12N loading force in mice have predicted a 2400 με in mice models and others have applied FE elements to predict the strain in different regions of the mice tibia (Wener et al. 2014; Patel et al. 2014).

Another possible confounder has been the use of a contralateral non-loaded bone as internal control. Some authors suggest that mechanical loading applied in long bones of animal models stimulates bone formation of adjacent bones via neuronal signalling and release of neuropeptides such as calcitonin gene-related peptide (CGRP), substance P (SP) and vasoactive intestinal peptide (VIP), claiming that loading is not a local effect (Sample et al. 2008). To test the previous study, (Sugiyama et al. (2010) subjected 19-weeks old C57BL/6 mice into a pre-load (0.2 N), dynamic (11.5 N) and non-loaded mechanical loading regimens. Micro-CT technique and fluorochrome labelling suggested increased bone formation in bones stimulated with any form of mechanical loading compared to non-loaded bones, contradicting the study of Sample et al. (2008). In addition, other studies found that mechanical adaptation of bone occurs even in the absence or inhibition of the sympathetic nervous system, supporting the use of a contralateral limb as internal control (De Souza, Pitsillides, et al. 2005; Marenzana et al. 2007). Therefore, in this project we used the contralateral non-loaded tibia as internal control. This method also reduces the use of animals in experiments, which is in accordance with the three Rs principles (Sneddon et al. 2017).

### 3.6.2. Mechanical loading affects the osteoblasts and osteoclasts quantity and distribution within the endocortical and trabeculae surface

In addition to the bone parameters analysed, the cellular changes due to loading were also significantly different. Firstly, the quantity of osteoblasts was significantly lower in the loaded versus non-loaded tibias in the lateral endocortical surface. Since the bone parameters highly suggests bone formation, the lower osteoblast number could be related with enhanced individual osteoblast activity rather than their recruitment. This correlates with the increased osteoclasts number found in the medial endocortical

surface which would couple the enhanced osteoblast activity, as it is the physiological process which takes place in bone remodelling (Florencio-silva et al. 2015). Interestingly, an increased osteoblast number was found in the trabecula surface at the first week of loading which decreases in the following weeks. This result can be explained by means of the bone adaptative response due to loading. It has been suggested by FE analysis that the strain applied in bone differs among bone regions due to its geometry, which in consequence could affect the mechanical adaptation of particular regions (Verhelle et al. 2009). Willie et al. (2013) found an improvement in cortical tissue in young and old mice model subjected to mechanical loading approximately at the same time but not in trabecula, which needed more time to achieve an osteogenic response. Others have found that the peak and tensile strain is 10% and 34% lower in trabecula tissue compared to cortical (Yang et al. 2014). These studies suggest that cortical tissue withstands more force than trabecula under mechanical loading; therefore, osteoblast activity would be enhanced first in cortical region and later in trabecula tissue. In our results, the increased osteoblast number in trabecula could be an acute recruitment response which later became an enhance activity. In order to stablish a more detailed histomorphometry result comparing the osteoblast number in the cortical and trabecula tissue, we could perform a cohort study at different time points with days of difference (i.e., at day 1, 3 and 5) instead of weeks. This would provide more data regarding the osteoblast and osteoclast recruitment in different bone regions. Interestingly, a further analysis of the ratio of the osteoblasts number in the medial versus the lateral endocortical side, revealed a redistribution of osteoblasts due to decreased number of osteoblasts in the lateral side. Therefore, mechanical loading affects the localisation of osteoblasts cells within the endocortical surface. An elegant mathematical model suggested by Prasad & Goyal (2019), taking a number of axial mechanical loading examples, shows a site-specific response (medial versus lateral) in the bone and the consequent bone formation within that site. Therefore, mechanical loading affects the bone endocortical regions in different manner and redistributing the osteoblast quantity within.

### 3.6.3. Serum resorption but not formation marker can detect mechanical loading induced local osteogenic response

To further confirm the osteoblasts and osteoclasts activity, we measured the levels of the osteoblast's marker P1NP and the osteoclast's marker TRAP5b in the mice's serum. The levels of P1NP showed no significant difference among the three weeks of loading. This result could be explained by stability of the P1NP marker. It has been shown that the P1NP marker is presented in the circulation as a trimeric form (Samoszuk et al. 2008). However, it is unstable at body temperature and tends to be degraded into a dimeric or monomeric more stable forms. Such degradation can happen within ~10 hours since it is synthesized in the bone (Parfitt et al. 1987; Samoszuk et al. 2008; Skoumal et al. 2005). As the serum collection took place 72 hours after the last mechanical loading stimulus, the method used to analyse the P1NP marker could not be accurate, as it may identify the trimeric or the degraded P1NP forms. In regards of osteoclasts activity, the TRAP5b marker was significantly reduced after one week of mechanical loading and was restored at the second week of loading stimulus. According to several studies, mechanical loading applied either *in vitro* or *in vivo*, inhibits osteoclasts activity (Noble et al. 2003; You et al. 2009; Kulkarni et al. 2010; Kulkarni et al. 2012; Kameyama et al. 2013). For instance, Guo et al. (2015) showed that mechanical stimulation *in vitro* of osteoblasts and osteoclasts cells for 7 days, enhanced the osteoblasts activity and inhibited osteoclastogenesis and their resorption activity. However, during the bone remodelling bone process, the osteoclasts couple the osteoblasts activity, in order to maintain the bone homeostasis, which could explain the restored TRAPb5 levels at the second week as well as the increased osteoclasts quantity in the same week in line with the histomorphometry results (Florencio-silva et al. 2015).. Another explanation could be that the bone formation at the first week could be due to osteoclast inhibition rather than enhanced osteoblast activity, shifting the balance of bone remodelling (Florencio-silva et al. 2015).

## 3. 7. Conclusion

Non-invasive mechanical loading stimulus applied at 12 N achieves an osteogenic response and bone formation in 12-week-old immunocompromised BALB/c nude mice within 3 loading cycles. Bone structure parameters associated with trabecula and cortical tissue are significantly improved in loaded tibias compared to controls. Mechanical loading affects the distribution of osteoblasts within the endocortical surface by decreasing the number of osteoblasts located in the lateral endocortical surface but increase it in the trabecular surface of loaded tibia. Serum resorption but not formation marker can detect mechanical loading induced local osteogenic response.

# CHAPTER 4:

## Mechanical loading does not affect the arrival of prostate cancer cells into the bone marrow

## 4.1. Introduction

Exercise is a well-established factor associated with a healthy-life style and positive outcomes (Warburton et al. 2006). Therefore, it is highly prescribed as a complement treatment for patients to improve their quality of life. Patients with cancer are also encouraged to perform exercise to alleviate cancer-related symptoms. For instance, in PCa, some studies have assessed the role of exercise in which they suggest it improves the QoL, submaximal fitness, lower body strength, improves PCa survival and is safe and tolerable for the patients (L Bourke et al. 2018; Cormie et al. 2013; Kenfield et al. 2011). This is of importance as a manner to link exercise benefits with PCa; however, there is a lack of information regarding PCa patients with bone metastasis, the most common outcome due to the high predilection of PCa cells to nest bone tissue (Nørgaard et al. 2010).

One important aspect to consider is the role of exercise in bone remodelling, where it stimulates osteoclasts to resorb old bone tissue and importantly, enhances osteoblast activity to create new bone (Florencio-silva et al. 2015). However, recent evidence suggests that PCa cells target osteoblastic lineages in bone marrow to establish footholds (Wang et al. 2014; Wang, et al. 2015; Shiozawa et al. 2011). Consequently, exercise could be counterproductive in PCa by enhancing osteoblastic niche and attracting PCa cells into bone marrow, thus aggravating the disease outcome. Up to date, no studies have assessed the role of mechanical loading in PCa bone metastasis, particularly to study if PCa cells are attracted into BM due to mechanical stimulus.

In this chapter, we tested whether mechanical loading affects the arrival of PCa cells into the BM. Firstly, two exercise regimens were used a pre-injected and a pre-loaded regimen.

The pre-injected model will mimic patients who start exercise after disseminated PCa cells enter circulation. Briefly, 12-week-old immunocompromised BALB/c nude mice (n=10), C57BL/6J immunocompetent mice (n=10) and NOD SCID mice (n=7) were IC injected with the PC3/C4-2B4, RM1 and LAPC-9 PCa cells (~100,000 cells in ~100µl

PBS). The following day, the mice were subjected to mechanical loading for one week (3 loading cycles) and then sacrificed figure 4.1 A.

The pre-loaded model mimic patients who continuously perform exercise before and after disseminated PCa cells enter circulation. This was translated into the *in vivo* setting as follows: 12-week-old immunocompromised BALB/c nude mice (n=8) and C57BL/6J immunocompetent mice (n=9) were subjected to mechanical loading for 1 week (3 loading cycles) as described in section 2.4, figure 4.1 B. The immunocompromised and immunocompetent mice were then IC injected with the pre-stained PC3/C4-2B4 and RM1 cells, respectively (~100,000 cells in ~100µl PBS). Mechanical loading was then applied for another week and then sacrificed.

In the BALB/c nude mice we applied the osteolytic PCa cell line PC3 and the osteoblastic cell line C4-2B4 as PCa creates osteolytic and osteoblastic lesions. However, the main phenotype is osteoblastic (Keller & Brown 2004). In the C57BL/6 mice we applied the RM1 cell line as it is a murine PCa cell line, by this manner studying a syngeneic in an *in vivo* setting (Mccabe et al. 2010). Furthermore, we used a patient xenograft model by injecting the LAPC-9 (Y. P. Lee et al. 2002; Pompili et al. 2016)

At the end of the experiment, tibias were dissected and kept at -80°C to analyse the pre-stained PCa cells in BM *ex vivo* by means of multi-photon scanning as described in section 2.9. The picture obtained by multiphoton scanning was analysed using the Volocity software, which allowed the measurement of the following parameters of the pre-stained PCa cells: number of tumour cells in the bone marrow (No. of tumour cells/$mm^3$ bone marrow), DiD signal total volume in bone marrow ($mm^3$), size of target ($mm^3$), and minimal distance from DiD+ centroid to bone edge (µm).

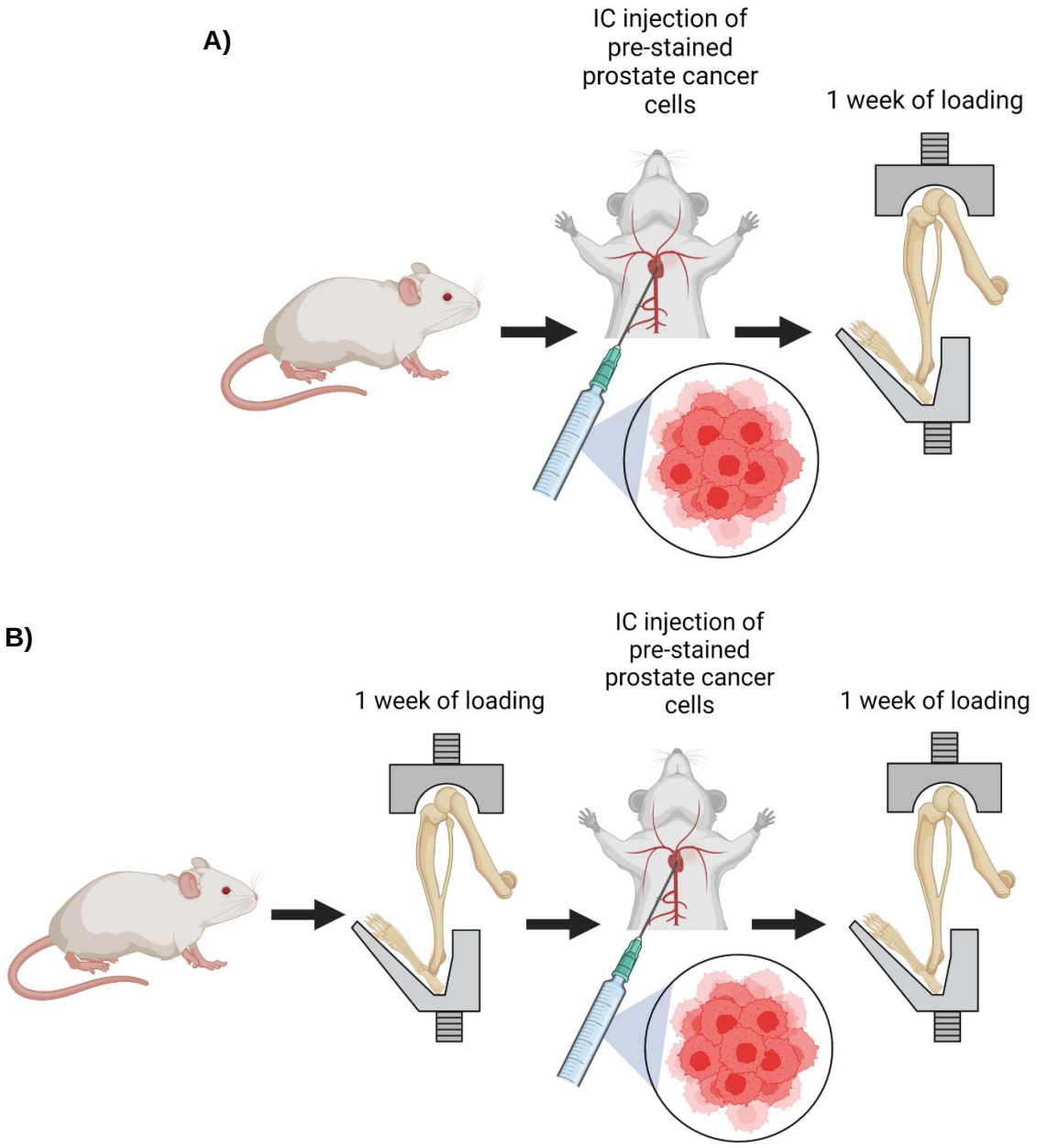


**Figure 4. 1. In vivo experiment design to test PCa cells arrival into bone marrow under mechanical loading treatment.** *A) The pre-injected mice were IC injected with pre-stained PCa cells and subjected to one week of mechanical loading the following day. B) The pre-loaded mice were subjected to mechanical loading for one-week prior IC injection of pre-stained PCa cells. Mechanical loading was then continued for a further week. Both groups were culled 7 days post injection and both tibias dissected to perform multi-photon microscopy analysis ex vivo*

## 4.2. Results

### 4.2.1. Mechanical loading does not affect the arrival of PCa cells into bone marrow in the pre-injected mice.

All Vibrant DiD pre-stained PCa cells were visualized in BM using multiphoton microscopy, including the PDX model LAPC-9, figure 4.2 A, 4.3 A, 4.4 A and 4.5 A. This allowed the analysis of the PCa cells arriving at the BM. The number of PCa cells were selected using the settings mentioned in 2.9.3 and normalised into the area delimited as bone marrow using the Volocity software. The C4-2B4 cell line showed significantly lower number of arrivals compared to controls, figure 4.6 B, p=0.03 as well as a tendency towards a lower cell size in loaded tibias compared to non-loaded (p=0.0627, figure 4.6 D). The cell size was found significantly lower in the LAPC-9 model (figure 4.8 D, p=0.0211). No additional significant differences were observed for the PCa cells parameters in the PC3, C4-2B4, RM1 and LAPC-9 cells, figure 4.2-4.5 B-E.

### 4.2.2. Mechanical loading does not affect the arrival of PCa cells into bone marrow in the pre-loaded mice.

The PCa cells pre-stained with the lipophilic dye Vibrant DiD were successfully visualised in the BM of mice tibias, 7 days after IC injection using multi-photon microscopy, figure 4.6A, 4.7A, 4.8A. We found a significant increase in size in the PC3 cells in the loaded tibia compared to those in the non-loaded tibia (figure 4.2 D, p=0.0146). No additional significant differences were observed for the PCa cells parameters in the PC3, C4-2B4 and RM1 cells figure 4.6-4.8 B-E. Interestingly in all models, PCa cells are in proximity of bone surface >40 µm away from bone edge. This result will be further discussed in section 4.3.

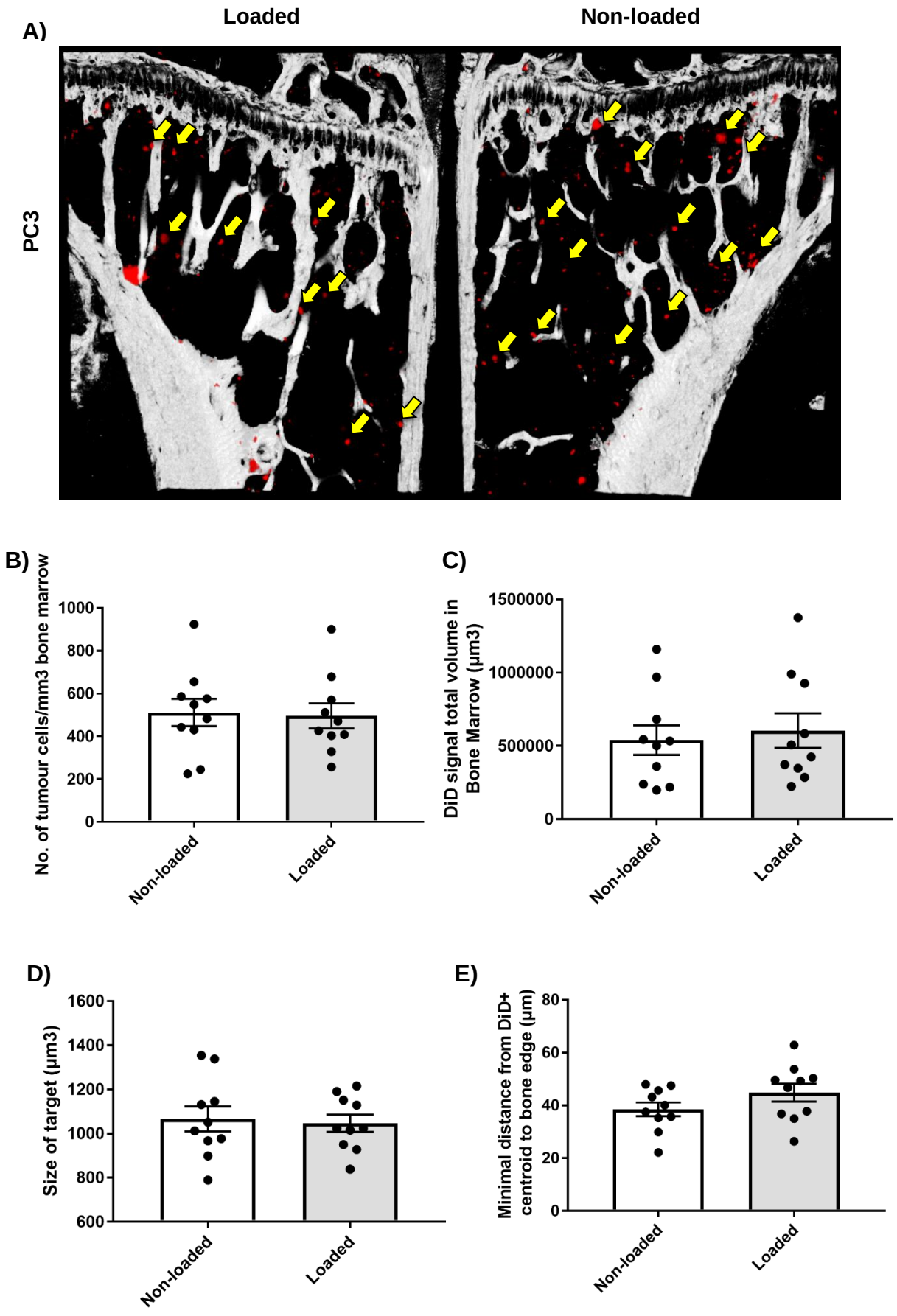
A)
Loaded
Non-loaded
PC3
B)
No. of tumour cells/mm3 bone marrow
1000
800
600
400
200
0
Non-loaded
Loaded
C)
DiD signal total volume in Bone Marrow (µm3)
1500000
1000000
500000
0
Non-loaded
Loaded
D)
Size of target (µm3)
1600
1400
1200
1000
800
600
Non-loaded
Loaded
E)
Minimal distance from DiD+ centroid to bone edge (µm)
80
60
40
20
0
Non-loaded
Loaded

**Figure 4. 2. The arrival of the PCa PC3 cell line into bone marrow during one week of mechanical loading.** *The PC3 cells pre-stained with Vibrant DiD dye were IC injected into 12-week-old immunocompromised BALB/c nude mice followed by mechanical loading for one week. A)The PC3 cells were successfully mapped (yellow arrows) in loaded and non-loaded mice tibias by multi-photon microscopy applying 633 nm wavelength stimulus 7 days post injection ex vivo. B) The PC3 cell number arriving at the loaded and non-loaded tibia bone marrow C) the whole volume of cancer cells arriving at bone marrow, measured as the total DiD signal emitted by these cells D) the median size PC3 cells value and E) the minimal distance among the PCa cells and bone surface was measured as the distance from the cancer cell centroid to bone edge surface using the Volocity software. Pre-injected group n= 10, paired-t test..*

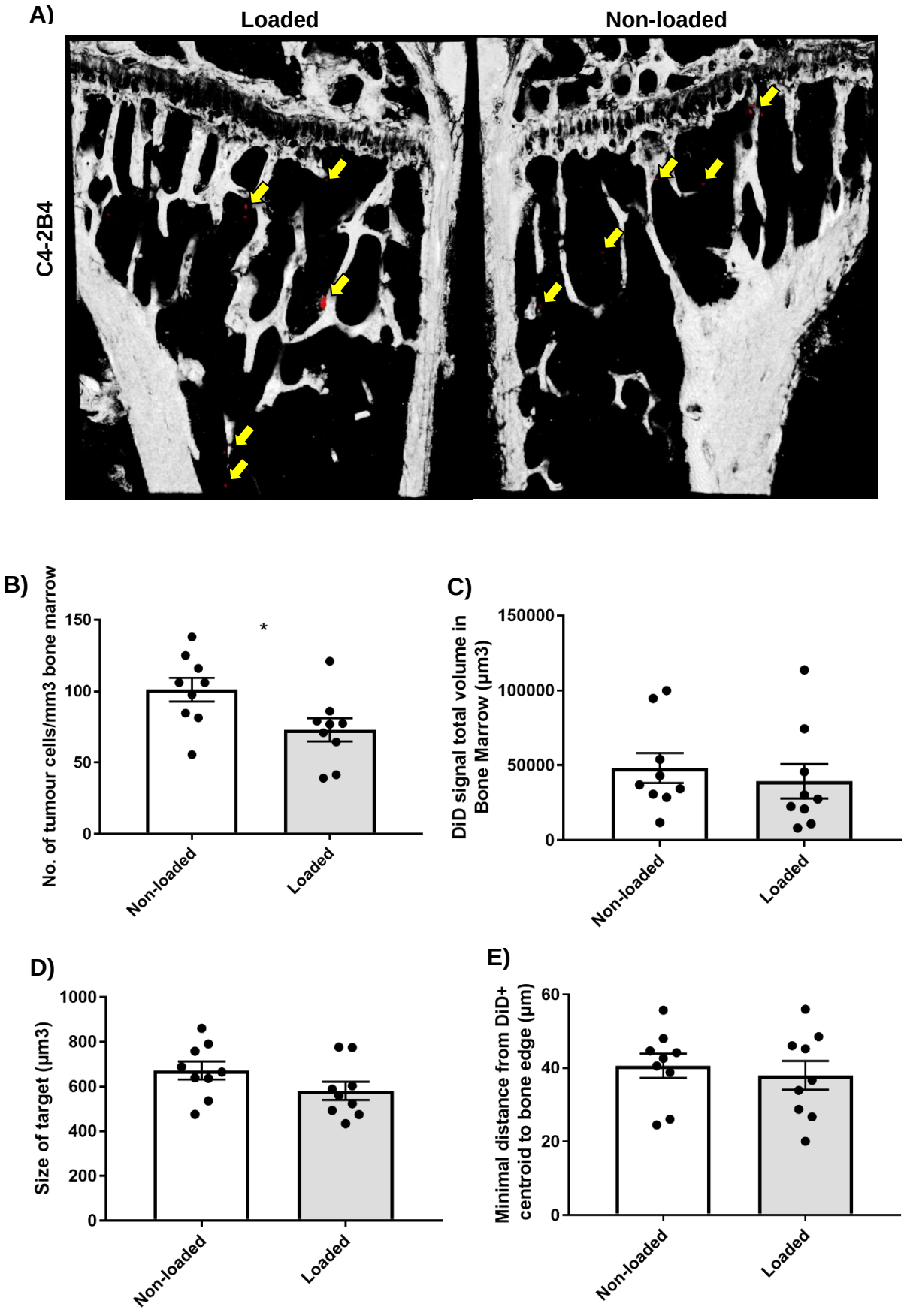
A)
Loaded
Non-loaded
C4-2B4
B)
No. of tumour cells/mm3 bone marrow
150
100
50
0
*
Non-loaded
Loaded
C)
DiD signal total volume in Bone Marrow (µm3)
150000
100000
50000
0
Non-loaded
Loaded
D)
Size of target (µm3)
1000
800
600
400
200
0
Non-loaded
Loaded
E)
Minimal distance from DiD+ centroid to bone edge (µm)
60
40
20
0
Non-loaded
Loaded

**Figure 4. 3. The arrival of the PCa C4-2B4 cell line into bone marrow during one week of mechanical loading.** *The C4-2B4 cells pre-stained with Vibrant DiD dye were IC injected into 12-week-old immunocompromised BALB/c nude mice followed by mechanical loading for one week. A)The C4-2B4 cells were successfully mapped (yellow arrows) in loaded and non-loaded mice tibias by multi-photon microscopy applying 633 nm wavelength stimulus 7 days post injection ex vivo. B) The C4-2B4 cell number arriving at the loaded and non-loaded tibia bone marrow C) the whole volume of cancer cells arriving at bone marrow, measured as the total DiD signal emitted by these cells D) the median size C4-2B4 cells value and E) the minimal distance among the PCa cells and bone surface was measured as the distance from the cancer cell centroid to bone edge surface using the Volocity software. Pre-injected group n= 10, paired-t test, *p=<0.05.*

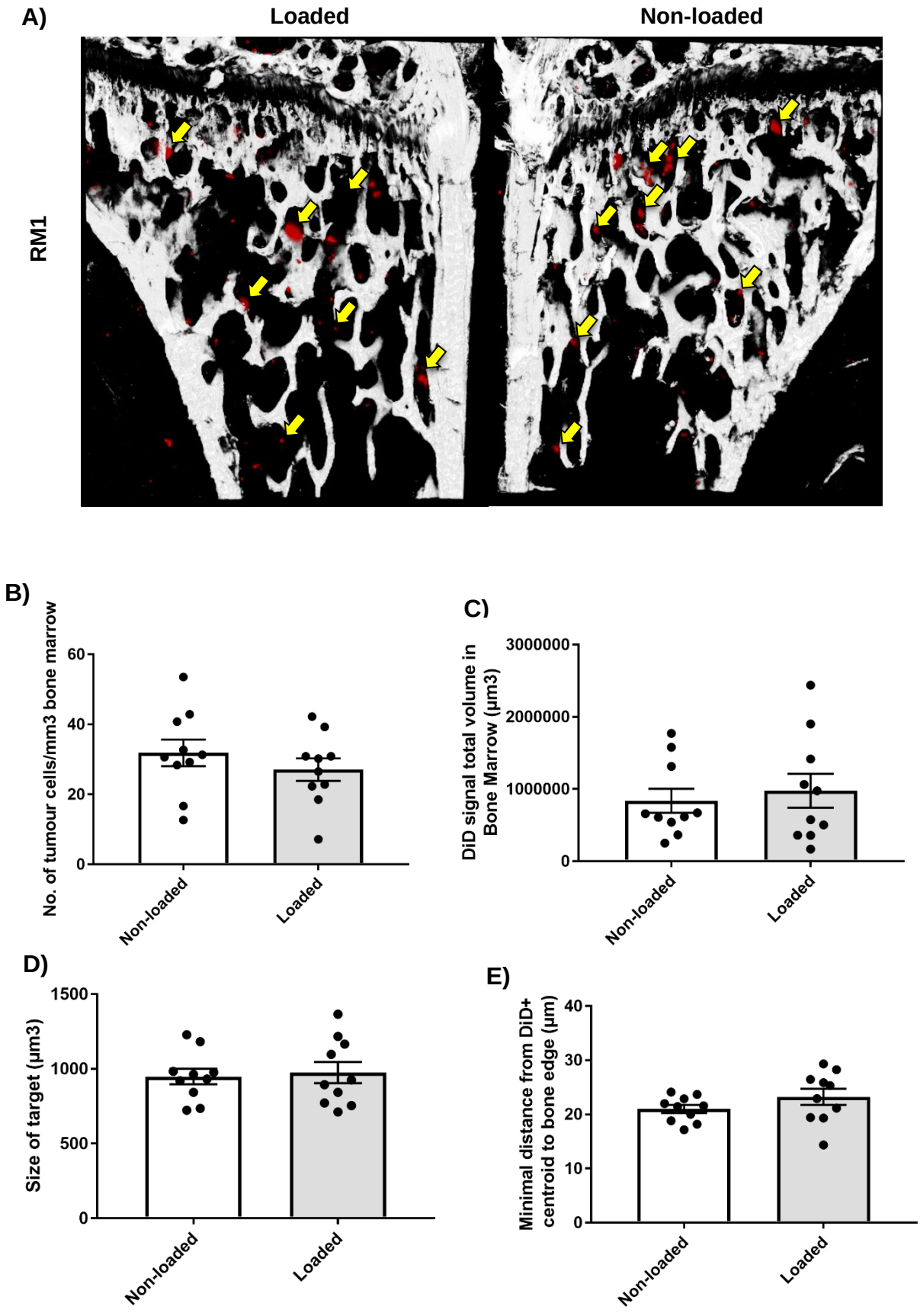
A)
Loaded
Non-loaded
RM1
B)
No. of tumour cells/mm3 bone marrow
60
40
20
0
Non-loaded
Loaded
C)
DiD signal total volume in Bone Marrow (µm3)
3000000
2000000
1000000
0
Non-loaded
Loaded
D)
Size of target (µm3)
1500
1000
500
0
Non-loaded
Loaded
E)
Minimal distance from DiD+ centroid to bone edge (µm)
40
30
20
10
0
Non-loaded
Loaded

**Figure 4. 4. The arrival of the PCa RM1 cell line into bone marrow during one week of mechanical loading.** *The RM1 cells pre-stained with Vibrant DiD dye were IC injected into 12-week-old immunocompetent C57BL/6J mice. A)The RM1 cells were successfully mapped (yellow arrows) in loaded and non-loaded mice tibias by multi-photon microscopy applying 633 nm wavelength stimulus 7 days post injection ex vivo. B) The RM1 cell number arriving at the loaded and non-loaded tibia bone marrow C) the whole volume of cancer cells arriving at bone marrow, measured as the total DiD signal emitted by these cells D) the median size of RM1 cells and E) the minimal distance among the PCa cells and bone surface was measured as the distance from the cancer cell centroid to bone edge surface using the Volocity software. Pre-injected group n= 10, paired-t test.*

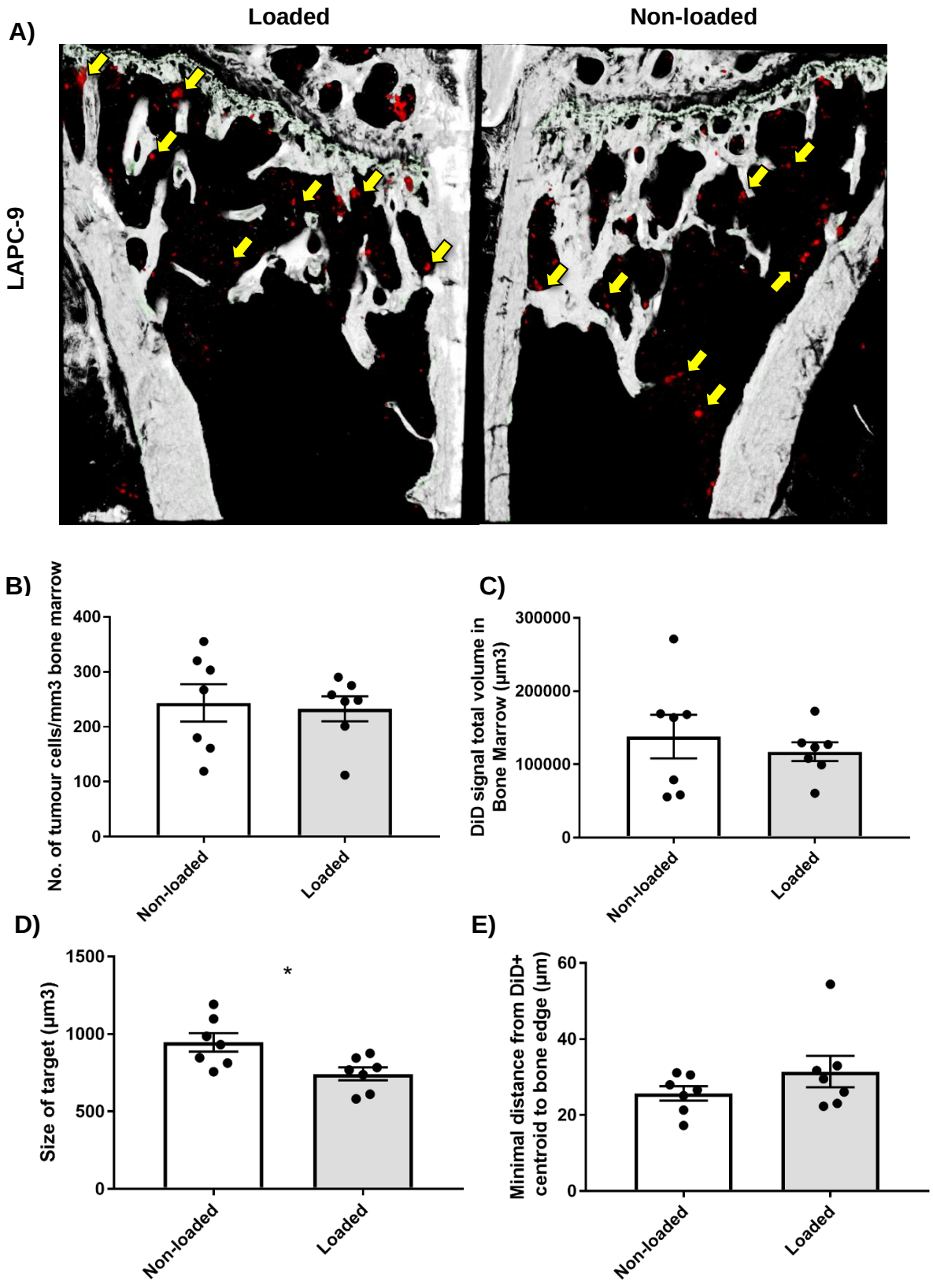
A)
Loaded
Non-loaded
LAPC-9
B)
No. of tumour cells/mm3 bone marrow
400
300
200
100
0
Non-loaded
Loaded
C)
DiD signal total volume in Bone Marrow (µm3)
300000
200000
100000
0
Non-loaded
Loaded
D)
Size of target (µm3)
1500
1000
500
0
*
Non-loaded
Loaded
E)
Minimal distance from DiD+ centroid to bone edge (µm)
60
40
20
0
Non-loaded
Loaded

**Figure 4. 5. The arrival of the xenograft LAPC-9 PCa tumour cells into bone marrow during one week of mechanical loading.** *A) The LAPC-9 cells pre-stained with Vibrant DiD dye were IC injected into 12-week-old immunocompromised NOD SCID mice. A) The LAPC-9 cells were successfully mapped (yellow arrows) in loaded and non-loaded mice tibias by multi-photon microscopy applying 633 nm wavelength stimulus 7 days post injection ex vivo. B) The LAPC-9 cell number arriving at the loaded and non-loaded tibia bone marrow C) the whole volume of cancer cells arriving at bone marrow, measured as the total DiD signal emitted by these cells D) the median size of LAPC-9 cells value and E) the minimal distance among the PCa cells and bone surface was measured as the distance from the cancer cell centroid to bone edge surface using the Volocity software. n= 10, paired-t test, *p=<0.05.*

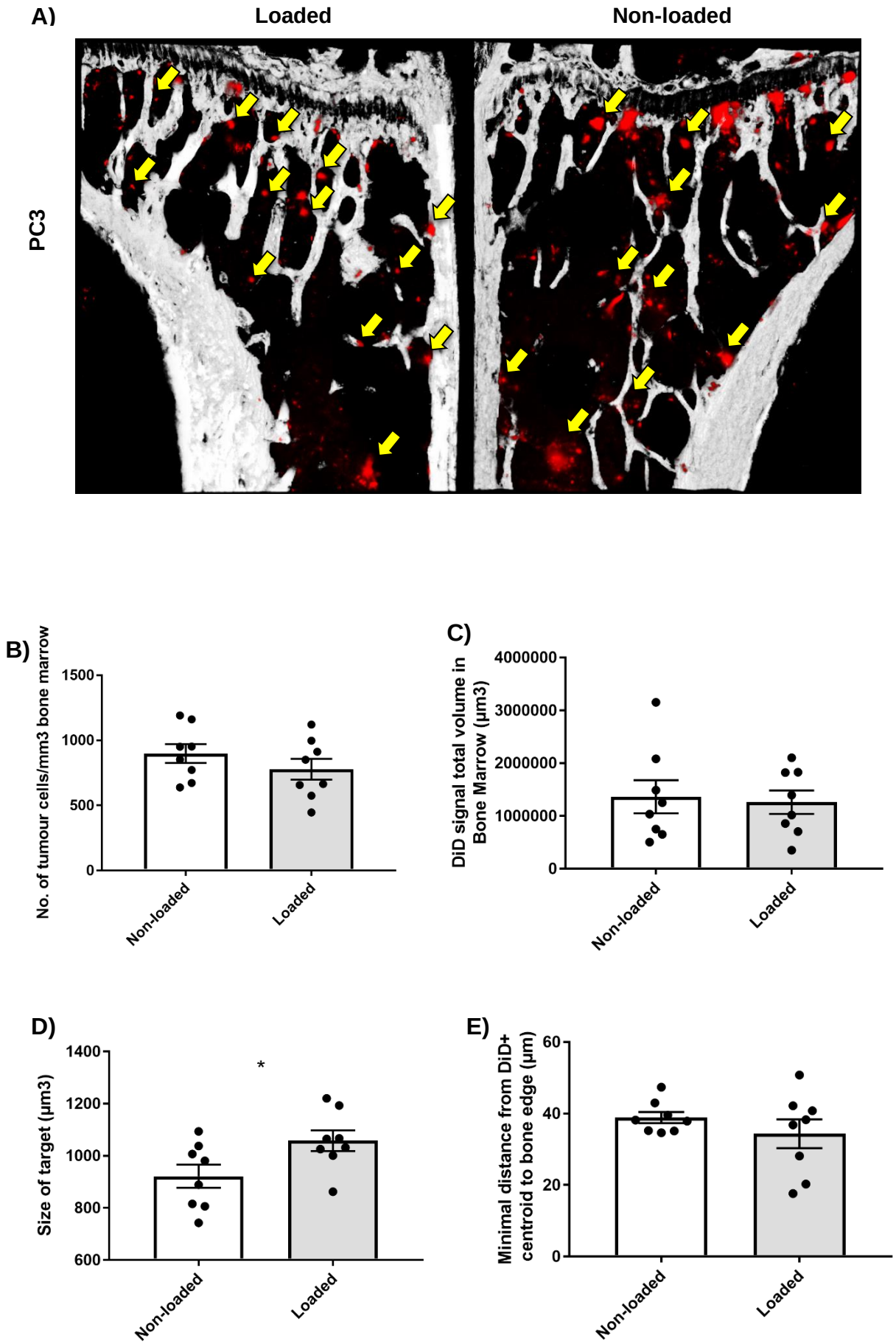
A)
Loaded
Non-loaded
PC3
B)
No. of tumour cells/mm3 bone marrow
1500
1000
500
0
Non-loaded
Loaded
C)
DiD signal total volume in Bone Marrow (µm3)
4000000
3000000
2000000
1000000
0
Non-loaded
Loaded
D)
Size of target (µm3)
1400
1200
1000
800
600
*
Non-loaded
Loaded
E)
Minimal distance from DiD+ centroid to bone edge (µm)
60
40
20
0
Non-loaded
Loaded

**Figure 4. 6. The arrival of the PCa PC3 cell line into bone marrow during two weeks of mechanical loading.** *The PC3 cells pre-stained with Vibrant DiD dye, were IC injected into a pre-mechanically loaded 12-week-old immunocompromised BALB/c nude mice model. Mechanical loading was performed for a further week post-injection. A)The PC3 cells were successfully mapped (yellow arrows) in loaded and non-loaded mice tibias by multi-photon microscopy applying 633 nm wavelength stimulus 7 days post injection ex vivo. B) The PC3 cell number arriving at the loaded and non-loaded tibia bone marrow C) the whole volume of cancer cells arriving at bone marrow, measured as the total DiD signal emitted by these cells D) the median size of identified signals and E) the minimal distance between the PCa cell centroids and bone surfaces were measured using the Volocity software. Pre-loaded group n= 8, paired-t test, *p=<0.05.*

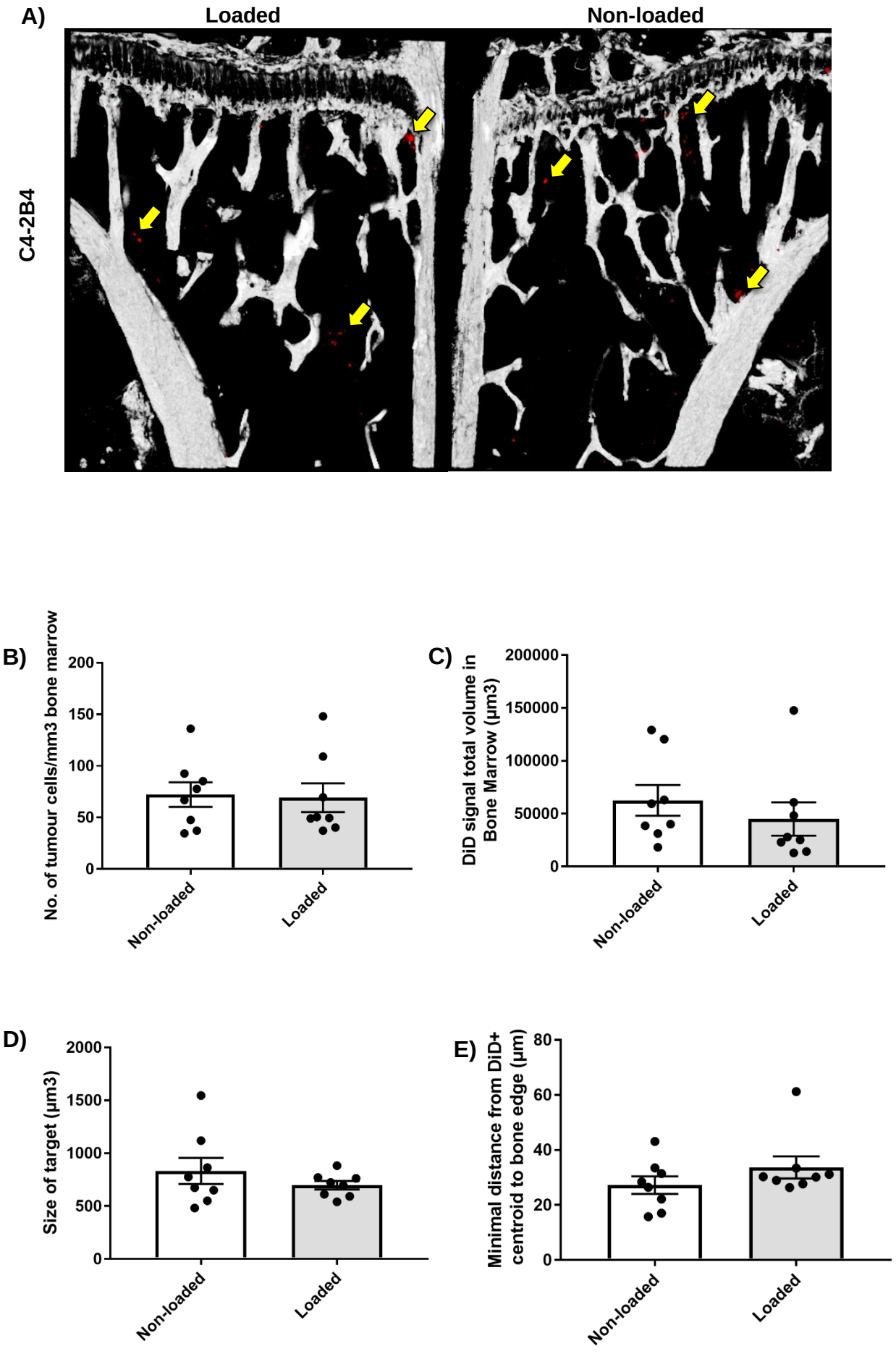
A)
Loaded
Non-loaded
C4-2B4
B)
No. of tumour cells/mm3 bone marrow
200
150
100
50
0
Non-loaded
Loaded
C)
DiD signal total volume in Bone Marrow (µm3)
200000
150000
100000
50000
0
Non-loaded
Loaded
D)
Size of target (µm3)
2000
1500
1000
500
0
Non-loaded
Loaded
E)
Minimal distance from DiD+ centroid to bone edge (µm)
80
60
40
20
0
Non-loaded
Loaded

**Figure 4. 7. The arrival of the PCa C4-2B4 cell line into bone marrow during two weeks of mechanical loading.** *The C4-2B4 cells pre-stained with Vibrant DiD dye, were IC injected into a pre-mechanically loaded 12-week-old immunocompromised BALB/c nude mice model. Mechanical loading was performed for a further week post-injection. A)The C4-2B4 cells were successfully mapped (yellow arrows) in loaded and non-loaded mice tibias by multi-photon microscopy applying 633 nm wavelength stimulus 7 days post injection ex vivo. B) The C4-2B4 cell number arriving at the loaded and non-loaded tibia bone marrow C) the whole volume of cancer cells arriving at bone marrow, measured as the total DiD signal emitted by these cells D) the median size C4-2B4 cells and E) the minimal distance among the PCa cells and bone surface was measured as the distance from the cancer cell centroid to bone edge surface using the Volocity software. Pre-loaded group n= 8, paired-t test..*

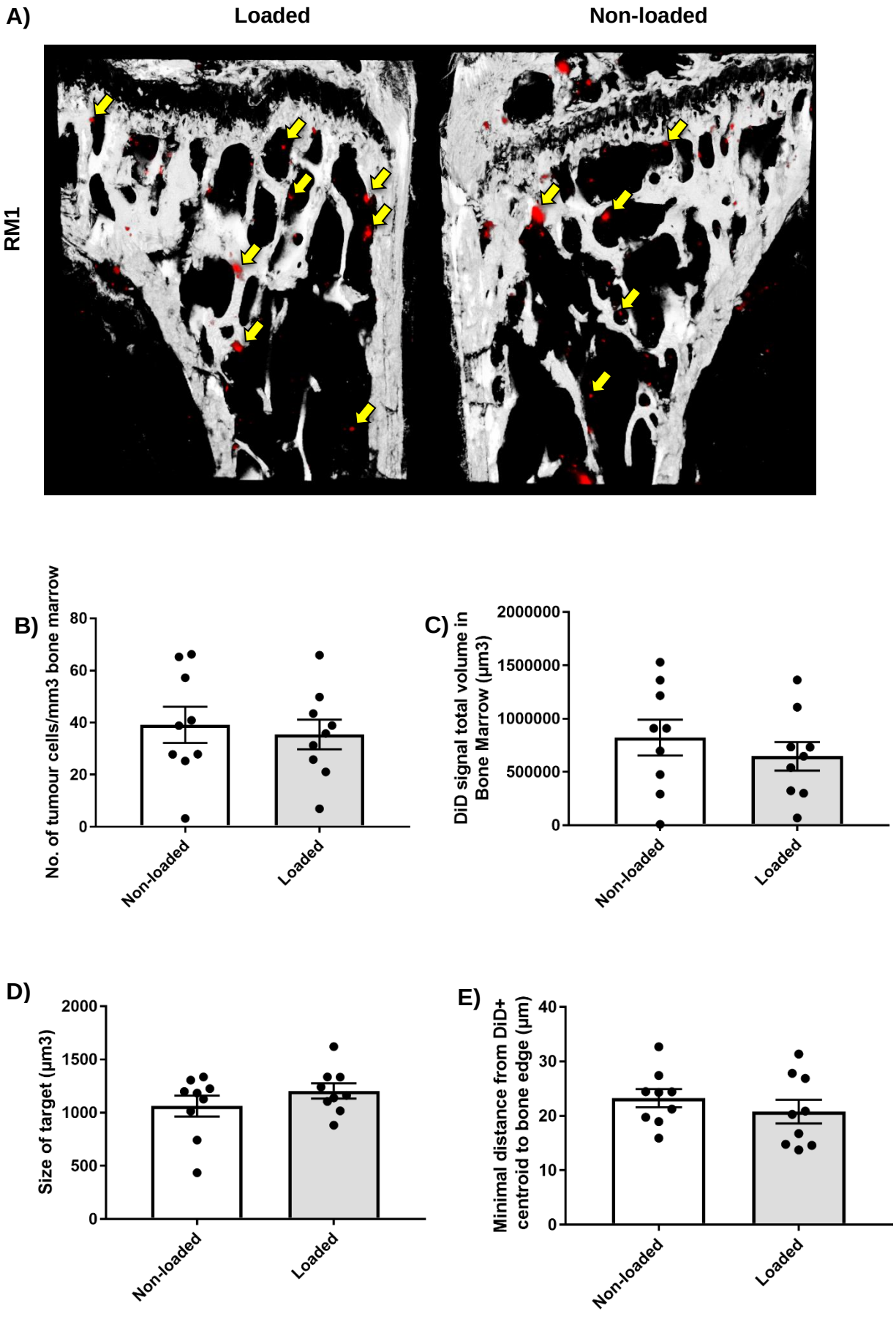
A)
Loaded
Non-loaded
RM1
B)
No. of tumour cells/mm3 bone marrow
80
60
40
20
0
Non-loaded
Loaded
C)
DiD signal total volume in Bone Marrow (µm3)
2000000
1500000
1000000
500000
0
Non-loaded
Loaded
D)
Size of target (µm3)
2000
1500
1000
500
0
Non-loaded
Loaded
E)
Minimal distance from DiD+ centroid to bone edge (µm)
40
30
20
10
0
Non-loaded
Loaded

**Figure 4. 8. The arrival of the PCa RM1 cell line into bone marrow during two weeks of mechanical loading.** *The RM1 cells pre-stained with Vibrant DiD dye were IC injected into a pre-mechanically loaded 12-week-old immunocompetent C57BL/6J mice model. Mechanical loading was performed for a further week post-injection. A)The RM1 cells were successfully mapped (yellow arrows) in loaded and non-loaded mice tibias by multi-photon microscopy applying 633 nm wavelength stimulus 7 days post injection ex vivo. B) The RM1 cell number arriving at the loaded and non-loaded tibia bone marrow C) the whole volume of cancer cells arriving at bone marrow, measured as the total DiD signal emitted by these cells D) the median size of RM1 cells and E) the minimal distance among the PCa cells and bone surface was measured as the distance from the cancer cell centroid to bone edge surface using the Volocity software. Pre-injected group n= 10, paired-t test.*

### 4.2.4. The spatial distribution of the pre-loaded PC3 and C4-2B4 is affected by mechanical loading.

The ratio of PCa cells homing into the medial vs the lateral endocortical side was analysed to understand whether mechanical loading affect the spatial distribution of PCa cells in BM. No significant differences were observed in the medial/lateral ratio for the RM1 and LAPC-9 cells. In the pre-injection, there were no significance difference in any model tested, figure 4.9 A-D. In the pre-loaded regimen, a significant difference towards a higher ratio of PCa cells in the medial vs lateral bone regions was found in the PC3 and C4-2B4 cells in the pre-loaded model (figure 4.10 A and B, $p=0.03$ and $p= 0.0088$, respectively). The ratio of medial/lateral PCa cells distance to bone edge did not show significant differences in any xenograft model (data not shown).

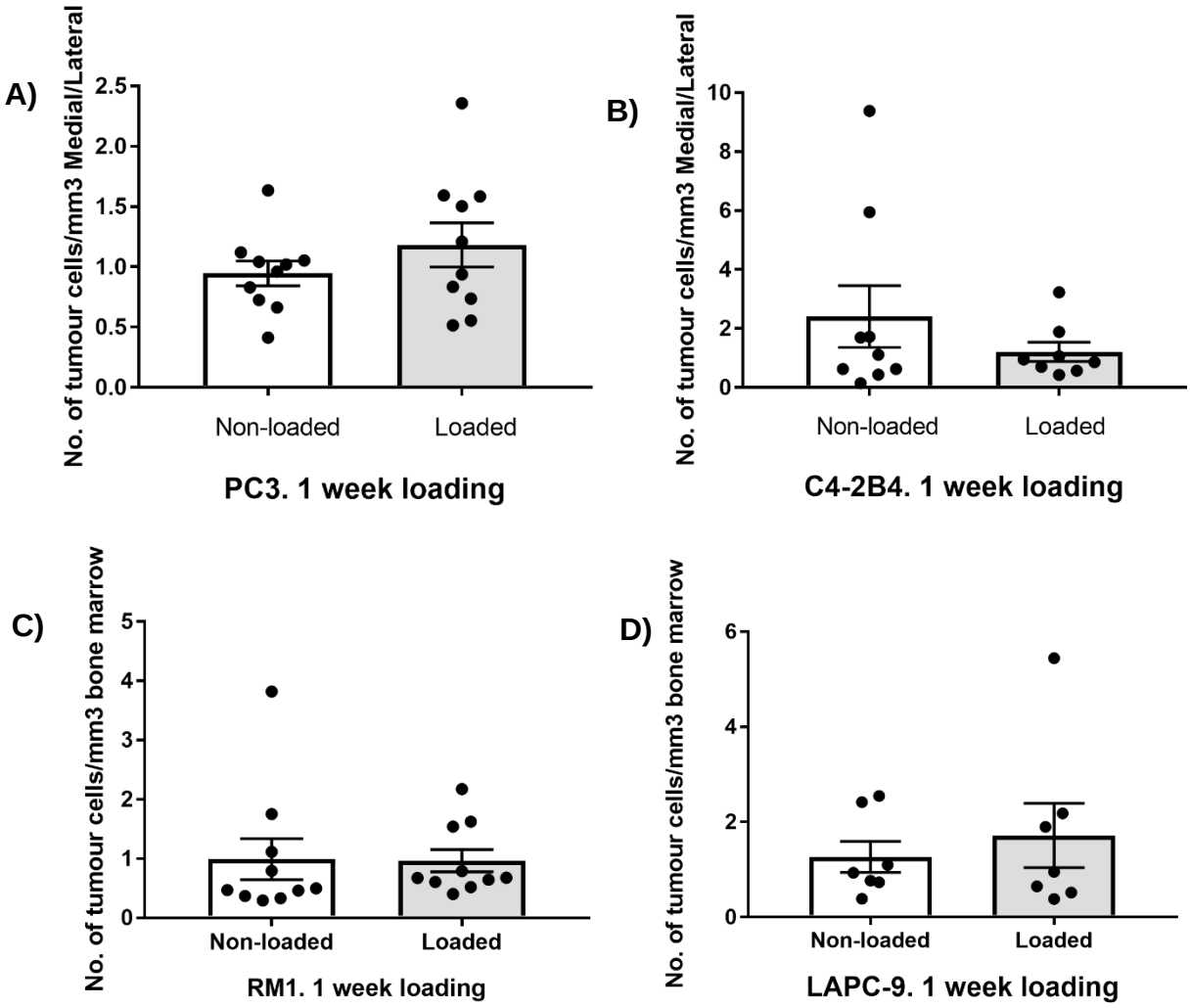


**Figure 4. 9. The spatial distribution pattern of the PCa cells under one week of mechanical loading stimulus in the pre-injected regimen.** *A) -D) The number of PCa cells in the medial endocortical side divided into the lateral endocortical side was analysed to observe the ratio distribution of the PCa cells when mechanical loading is applied at 1 week of mechanical loading stimulus. Pre-injected group n=10, paired-t test.*

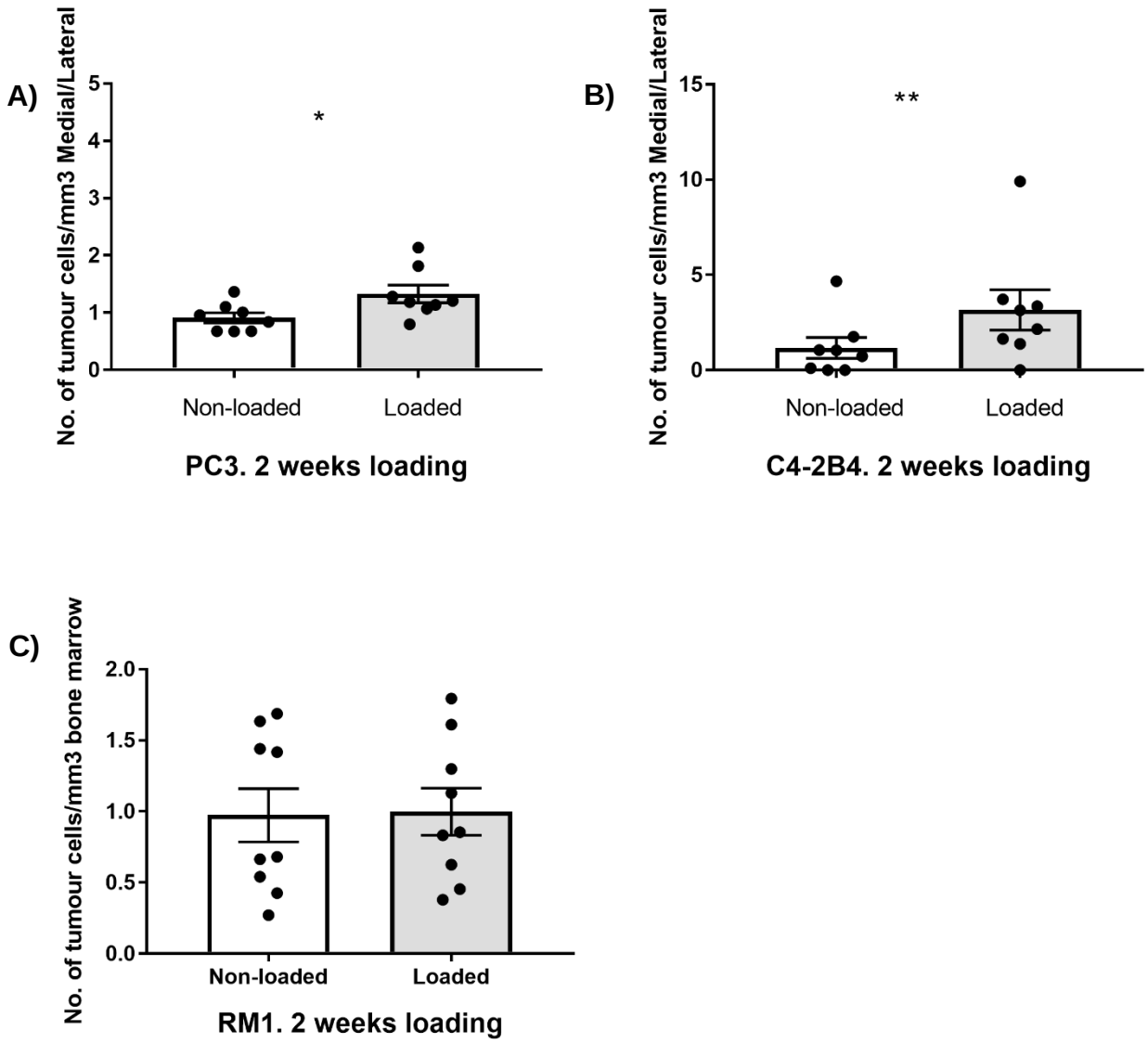


**Figure 4. 10. The spatial distribution pattern of the PCa cells under 2 weeks of mechanical loading stimulus.** *A) -C) The number of PCa cells in the medial endocortical side divided into the lateral endocortical side was analysed to observe the ratio distribution of the PCa cells when mechanical loading is applied at 2 weeks of mechanical loading stimulus. Pre-loaded group n= 8, paired-t test, *p=<0.05, **p=0.01.*

## 4.3. Discussion

Although positive outcomes have been found in patients with PCa who perform exercise, recent studies suggest that PCa cells target osteoblastic lineages to establish footholds (Wang et al. 2014; Shiozawa et al. 2011). Since exercise is an important anabolic stimulus in bone that enhances osteoblast niche, exercise could attract more PCa cells into bone and therefore present increased risk of developing overt bone metastases, in which the disease is considered to be incurable (Yuan et al. 2016; Nørgaard et al. 2010).

Statistics suggests that physical activity in men living in the UK varies among age. It is estimated that ~70% of men between 16-54 years old perform physical activity. A drop of physical activity was observed after 55 years old of age where 55% of men have an active lifestyle. This parameter further decreases to 36% in 75-year-old men or more (Townsend et al. 2015). Moreover, PCa incidence is detected in men aged between 40-44 and increases when they reach 70-74 years old (Leitzmann & Rohrmann 2012). To translate this clinical data into xenograft models we applied two models: a pre-loaded and a pre-injected group. The pre-loaded group will mimic patients who have an active lifestyle and then develop PCa. The pre-injected group will give insights of patients who decide to perform exercise regularly after PCa diagnosis, when most cases there are DTCs in bone.

According to our results, we successfully mapped the Vybrant DiD pre-stained PC3 and C4-2B4 cell lines by means of multiphoton microscopy as previously demonstrated in other studies (Wang et al. 2014; Wang et al. 2015; Price et al. 2016). Importantly, this is the first study known so far to successfully map the LAPC-9 and RM1 cells *ex-vivo* in BM after systemic inoculation of PCa cells using the IC injection. In regards of the LAPC-9 model, previous studies have used intratibial injection as a metastasis model applying this organoid; however, intratibial inoculation does not properly resembles the metastatic process since the cells are directly injected in skeletal tissue and are not allowed to circulate through blood/lymphatic vessels and colonise foreign tissues (Y. P. Lee et al. 2002; Campbell et al. 2012). In the IC injection, most of the metastatic process steps after intravasation are recapitulated, from which we observed LAPC-9 cells homing into BM. This provides evidence regarding PCa

cells tropism to bone tissue (Rucci & Angelucci 2014). Nonetheless, if the LAPC-9 cells would fully establish into BM and undergo metastatic tumour growth remains to be unveiled. Additionally, The number of PCa cells arriving at BM differs between each model used, where PC3 cells showed higher cells arrival compared to C4-2B4 and LAPC-9. The higher number of PC3 cell in bone could lead to increased metastatic growth (Hanahan & Weinberg 2011)

Another point for discussion is the distinction between the arrival of individual cancer cells into BM and tumour growth. According to previous studies, where they applied the PC3/C4-2B4 pre-stained PCa cell lines and metastasis model (IC injection), the DiD signal intensity in the PCa cells reaches a peak one-week post IC and after this period starts to decline, meaning that the lipophilic dye on their membrane starts to fade due to cellular proliferation and tumour development (Wang et al. 2014). Therefore, in the pre-injected and pre-model mice regimens, the mice were sacrificed one-week post IC injection. This will be in line with the previous mentioned studies to assure that we are analysing individual arrival of PCa cells before they undergo proliferation and create overt metastasis.

Regarding the number of PCa cells arriving at bone, no significant difference was seen in most models at different loading regimens. In the case of PC3 cells, this could be correlated with their osteolytic nature (further explained). Also, no difference in cell number arrival was observed in the LAPC-9 organoid. To date, there are no genetic studies regarding the LAPC-9 model; however, since this xenograft resembles more accurately the nature of PCa, it is unlikely that PCa cells will be attracted into bone due to loading or translated into the clinical side, due to exercise. An explanation of why the number of PCa cells was not increased due to loading could be linked to our results in chapter 3, where the osteoblast number was not increased, therefore, not enlarging the osteoblast niche. However, we lack evidence about the differentiation and proliferation of the osteoblasts during the week of loading (i.e., number of osteoblasts at day 1, 3 and 5) in histology settings. Possibly, the osteoblast number was increased at some time point during the first week of loading and after this time we observed a reduced number of osteoblasts as they may have undergone their osteogenic response and started to become bone lining cells. Indeed, the life spam of murine osteoblast is suggested to be ~10 days, a time period similar to our mechanical

loading regimen (McCulloch & Heersche 1988). The evidence suggests PCa cells have predilection to nest osteoblast-rich regions; however, there is lack of information regarding PCa cell tropism to the differentiation stage of osteoblasts, i.e., whether they prefer pre-osteoblasts, fully differentiated osteoblasts or even bone lining cells. Unveiling the differentiation stage of the osteoblasts in our loading model would reveal which osteoblast stage they have predilection to nest and possible clinical impacts.

Different from the mentioned PCa arrival models, the arrival of PCa cells into BM was significantly different in the C4-2B4 pre-injected group, observing a decreased cell number in the loaded tibia compared to controls. This result could be associated with the lower osteoblast number in loaded bones in the baseline study (chapter 3) in hand with the osteoblastic nature of C4-2B4 cells. To explain this, the osteomimicry theory could be applied. Osteomimicry is a process in which PCa cells express bone markers, acquiring an osteoblastic-like phenotype in order to adapt themselves into bone tissue (Jadaan et al. 2015). The genetic profile of C4-2B4 and PC3 was analysed by Hagberg et al. (2014). These authors found expression of osteoblast markers in C4-2B4 cells such as dentin sialophoshoprotein (DSPP), fibroblast growth factor receptor (FGFR), RUNX2, OCN and IGF while PC3 cells showed markers associated with inhibition of bone formation and osteoclast activity such as colony stimulating factor 2 (CSF2), twist homolog 2 (TWIST2) and BMP3. According to this theory, the C4-2B4 cells tried to adapt themselves into bone microenvironment by mimicking the lower number of osteoblasts that was taking place due to loading, compared to the pre-loaded group which probably already had lower osteoblast number, explaining why fewer C4-2B4 cells arrived in the pre-injected compared to the pre-loaded group.

In respect of the size of PCa cells, a greater size was detected in loaded tibias in the pre-loaded PC3 cells model while a reduced size was observed in the organoid cells LAPC-9 in the pre-injected model. Two theories could explain this result: the mechanical loading effect into blood vessels intercellular junctions and cancer cells clusters arrival into BM. Regarding the first proposition, mechanical stimulus has been associated with increased development of intercellular junctions such as GAP junctions in blood vessels (Salameh & Dhein 2013). PCa cells extravasate blood vessels using two mechanisms: paracellular extravasation by disrupting the endothelial intercellular junctions or by transcellular migration where they pass through

individual cell bodies. The paracellular extravasation being the most common (Schumacher et al. 2013; Leong et al. 2014; Khuon et al. 2010). In the case of PC3, the blood vessels in the pre-loaded tibia probably already had increased GAP junctions which these cells needed to disrupt in order to arrive into bone by increased the secretion of factors such as MMP2 and MMP9 (Gong et al. 2014). An augment in cancer cell size has been associated with increased protein synthesis, which could explain why these cells arrive with a bigger size compared to controls, or probably, they were undergoing proliferation already (Barna et al. 2008). The second proposition would be that these cells arrived as clusters instead of individual cells. According to Araujo et al. (2018), PCa cells arrive into bone as clusters which must be within an specific range (~100 cells), not too small to be able to colonise bone but not too large to avoid competition of resources (i.e. TGF-β) with others cells, resulting in a successful vicious cycle (Guise 2002). To add, another method applied to measure the arrival of PCa cells into bone marrow was to analyse the total DiD signal, which would represent all the cells as a group, since the cells could have arrived as clusters instead of individual cells (Vlaeminck-Guillem 2015). The result suggests no significant difference in the total volume of cells arriving at the BM in either model, which further supports the idea that mechanical loading does not affect the arrival of PCa cells into the BM. In contrast, the size of the LAPC-9 cells was reduced in loaded tibias compared to controls. In this scenario, as the GAP junction theory does not explain this result, there was possibly an expression of anti-tumour cytokines (i.e., IL-2, IFN-α and IL-27) and inhibition of pro-tumour cytokines (i.e., IL-1, IL-6, IL-8, IL-17, IFN-γ, and RANTES) which may reduce the PCa cells size (Mussbacher et al. 2019; Kourko et al. 2019). This should be tested using a cytokine profile assay in naïve models of NOD SCID mice.

Overall, our results suggest that the arrival of PCa cells into BM is not affected by mechanical loading. This is in line with other evidence, where they studied the arrival of PCa and BCa cells into BM using young mice models (6-weeks-old) with high bone turnover and mature mice (16-weeks-old) with a steady bone turnover (Wang et al. 2015). These authors found that the number of PCa cells that arrived at the BM was higher in mature than young mice, suggesting that PCa cell will prefer to arrive to a more inactivated osteoblast niche. This could further explain why there is no enhanced PCa arrival, probably there is a temporal increase in activated osteoblast but not

enhanced aged osteoblast. Again, we would need to study the differentiation status of the osteoblast cells to clarify this theory.

Of note, the spatial distribution pattern of the PCa cells changed towards a higher ratio on the medial versus the lateral endocortical side in the xenograft models treated with the PC3 and C4-2B4 human PCa cell lines. This is in line with previous experiments where we observed the redistribution of the osteoblasts (reduced osteoblast in the lateral side), after 2 weeks of mechanical loading in a naïve mice model. This result not only support osteoblasts as a homing link for PCa to stablish footholds in the BM but also that PCa cells obey the change of location of osteoblasts within the bone marrow under mechanical loading stimulus (Wang et al. 2014; Shiozawa et al. 2011). This is of importance as previous studies performed in naïve mice suggest that osteoblast's preferred location within the bone is the lateral endocortical side, as it is a rich-osteoblast region (Wang et al. 2014). However, under conditions of mechanical stimulus, the osteoblasts ratio favours the medial side and with that, the location of PCa cells. The location of cancer cells in the bone could affect their proliferation as suggested by Allocca et al. (2019). In this study, they found that BCa cells tend to be located in the trabeculae region in murine xenograft models, a region rich blood vessel. In addition to this, Ghajar et al. (2013) suggest that molecules like periostin and TGF-β1 produced during sprouting vasculature promotes the proliferation of cancer cells while thrombospondin (TSP-1) expressed in stable vasculature maintains the cancer cells in a dormant status. Additionally, the oxygen levels in the bone vary along the bone regions and affect the cancer proliferation as suggested by Devignes (et al. 2018). In this study they found higher proliferation of BCa cells in hypoxic areas like the trabecula region ($pO_2$=0.08%) compared to the cortical tissue ($pO_2$=4.2%) (Devignes et al. 2018; Zahm et al. 2010). The mentioned studies are examples on how the location of cancer cells within the diverse bone regions could affect their proliferation; however, how the precise location of PCa cells in the bone would affect their proliferative status remains to be elucidated. To complement this study, the oxygen levels within the lateral and medial endocortical bone side should be elucidates, providing more hallmarks of how cancer cells are affected by the bone microenvironment.

## 4.4. Conclusion

Multiphoton microscopy is a suitable technique to quantify PCa cells arriving in bone, including PDX models. Osteogenic response achieved through mechanical loading does not attracts the arrival of PCa cells into BM. This theory should be translated to clinical settings as a matter to study the risk of PCa cells arrival into bone due to loading-impact exercise.

# CHAPTER 5:

## Mechanical loading delays prostate cancer bone metastases onset and decreases cancer-osteolytic lesions

## 5.1. Introduction

PCa is the most common cancer diagnosed in men in the UK, accounting for 47,000 cases in 2014 (Bourke et al. 2018). The first line treatments consist of ADT, radical prostatectomy, chemotherapy and radiotherapy (Namiki et al. 2012). Although they seem to be effective in the initial stage of PCa, they have no effect on PCa bone metastasis, which is developed in ~70% of patients and is associated with a significant decrease in the survival rate (Svensson et al. 2017; Hensel & Thalmann 2016).

As an alternative therapy, exercise in PCa has been evaluated, finding improvement in health-parameters like upper and lower body strength, body lean mass, BMD, and significant fat mass decrease, among others (Keilani et al. 2017, Uth et al. 2018, Yunfeng et al. 2017). Particularly for PCa bone metastasis, the study of Cormie et al. (2013) found an improvement in muscle strength, submaximal AE capacity and ambulation. Although these clinical trials suggest benefits for patients with PCa with or without bone metastasis, studies that assess the possible effect of exercise in skeletal tumour initiation are scarce.

In the case of BCa, this question has been investigated by Lynch et al. (2013). The group applied axial mechanical loading into BCa xenograft mice models to mimic load-bearing exercise. They found a significant reduction in BCa bone metastasis in mice subjected to loading compared to controls. They hypothesised that mechanical loading induced an osteogenic response and bone formation which took place before the BCa osteolytic lesions, disrupting the cancer vicious cycle and delaying the BCa skeletal tumour onset.

Another important topic to consider are the SRE, which are pathological conditions in bone caused by PCa metastasis such as spinal cord compression and cancer-related fractures (So et al. 2012). According to Nørgaard et al. (2010), patients with no bone metastasis have a survival rate of 87% that decreases to 55% after 5 years of diagnosis. Patients with bone metastasis have a survival rate of 47% decreasing to 3% and 40% decreasing to 0.3% if the patient has had any SRE after 5 years of the initial diagnostic.

Therefore, the purpose of this study is to understand whether exercise (in form of mechanical loading) inhibits skeletal tumour growth as well as osteolytic lesions. To test this, mechanical loading was applied in the right tibia of xenograft models, using the left contra-lateral tibia (non-loaded) as internal control. First, human PC3 cells and murine RM1 PCa cells, successfully transfected with the luciferase gene, were injected IC (~100,000 cells in 100 µl PBS) into 8-week-old BALB/c nude (n=12), and C57BL/6 mice (n=11), respectively, figure 5.1 A). The following day, mice were subjected to the mechanical loading regimen for 3 weeks (3 loading cycles per week) as described in section 2.4. Tumour growth was assessed weekly by bioluminescence assay as described in section 2.10. The tibias were scanned *ex-vivo* using the Skyscan bunker machine as described in 2.7 and the bone parameters (Trabecula bone volume trabecula fraction, trabecula thickness, trabecula number, trabecula separation, trabecula pattern factor, structure model index, degree of anisotropy and cortical bone volume) were analysed using the CTan software as described in 2.7. A further histological analysis was carried out to measure the area of tumour developed in loaded versus non-loaded legs. More details in section 2.11.

Another PCa bone metastasis model was included, to test the effect of continuous mechanical loading in a xenograft model in which the PCa cells have already taken place in bone. To achieve this, the PC3 cells were injected in the tail artery of the mice (~$1x10^6$ cells in ~100 µl of PBS) under anaesthetic conditions, as mentioned in section 2.3, figure 5.1 B.

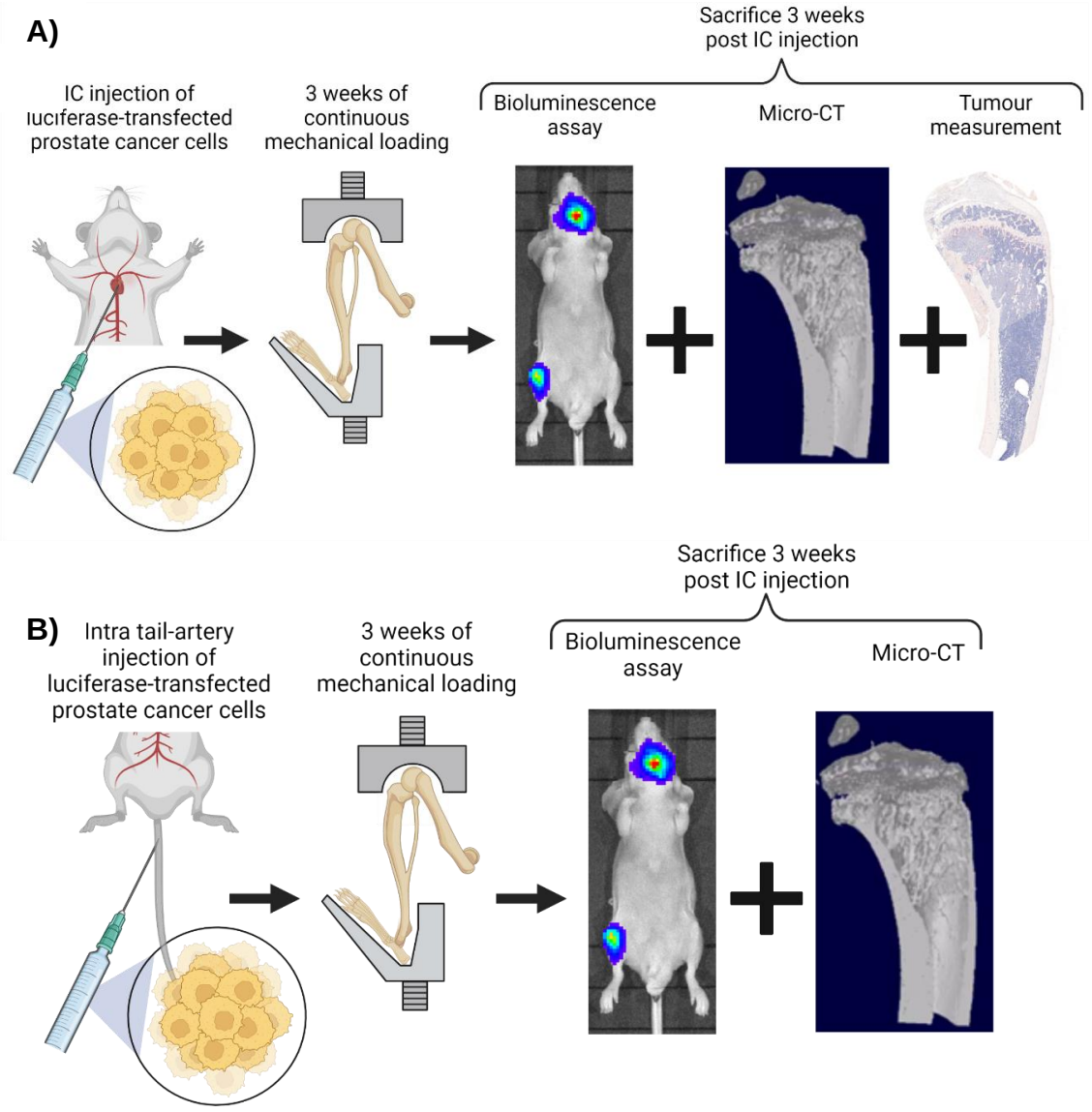


**Figure 5. 1. Experiment schematic to test whether mechanical loading inhibits tumour growth in xenograft models.** *A) Luciferase-transfected PCa cells (human PC3 and murine RM1) were IC injected into BALB/c nude and C57BL/6 mice. Mechanical loading (0.2 sec hold at 9 N) was applied the following day for 3 weeks. Bioluminescent assay was performed weekly to detect skeletal metastasis growth. Mice were euthanised 3 weeks post injection, their tibias dissected and analysed using Micro-CT technique. Tumour burden between loaded and non-loaded tibias was measured using the Living Image 4.3.1 software. Tumour area was measured using the QuPath software. B) Intra-tail artery injection model inoculated with luciferase transfected PC3 cells. In this metastasis model, the PCa cells travel through the iliac arteries (left and right), achieving bone metastasis in both legs. The same mechanical loading regimen was applied for 3 weeks one day after the PC3 cells injection.*

## 5.2. Results

### 5.2.1. Mechanical loading delays the onset and incidence of PCa bone metastasis in a PC3 intracardiacally injected xenograft model.

Forty loading cycles (0.2 sec hold at 9 N) with 10 seconds rest period between each cycle were applied 3 times a week for 3 weeks into the mice right tibia. Once per week, after 3 loading cycles, bioluminescent analysis was applied in mice *in vivo* to assess the tumour burden. According to the bioluminescent analysis, in the BALB/c nude mice model, the skeletal metastasis was identified in all of the 12 non-loaded left tibias (100%) figure 5.2 A. From the 12 mice, 8 showed skeletal metastasis in the loaded tibias (67%) and four out of these 12 mice had no detectable skeletal metastasis in the loaded tibia (33%). The tumour tibial incidence was analysed finding a significant lower tumour tibial incidence in the loaded tibia at week 3, suggesting that mechanical loading significantly delays the incidence of skeletal metastasis in this xenograft model. No tumour signals were identified at week 1. Tumour tibial incidence at week 2, figure 5.2 B, tumour tibial incidence at week 3, figure 5.2 C, n=12, chi-square, p=0.02.

### 5.2.2. The tumour burden is reduced in continuously mechanical loaded tibias in a PC3 intracardiacally injected xenograft model.

The tumour burden was measured as photons/second by creating a ROI surrounding the skeletal metastasis in each tibia using the Living Image 4.3.1 software. In the continuously loaded IC PC3 xenograft model, the tumour burden was ~45% lower in loaded tibias compared to controls, figure 5.2 D, Wilcoxon test, n=12, p=0.3804. To further corroborate the lower tumour burden in the loaded tibias, TRAP-stained bone sections were analysed by drawing a ROI in the tumour as well as the BM region. More details about the tumour area analysis in section 2.11. The histological analysis revealed an ~25% reduction in the tumour burden of the loaded tibias, figure 5.3. These results suggest that mechanical loading applied in the bone reduces the development of PCa bone metastasis.

### 5.2.3. Mechanical loading preserves the bone structure from PCa osteolytic lesions in a PC3 intracardiacally injected xenograft model

The Micro-CT technique was performed to examine the bone morphometry changes due to tumour growth by comparing the non-loaded and loaded tibias *ex vivo*. The bone parameters measured were the same as in 3.2.1.2 and 3.2.1.3 using the CTan software. In comparison to the non-loaded tibias, the BV/TV%, Tb.Th, Tb.N and Ct.BV of loaded tibias were significantly higher (paired t-test, n=12, $p=0.0009$, $p<0.0001$, $p=0.0093$, $p<0.0001$, respectively) whilst the Tb.Pf, Tb.Sp and SMI were significantly lower (paired t-test, n=12, $p=0.0004$, $p=0.0240$, $p=0.0005$, respectively). The differences in these bone parameters suggest that mechanical loading protected the bone from the osteolytic lesions caused by the PC3 cells, either by maintaining or improving the bone tissue. Quantitative data of the Micro-CT analysis is presented in table 5.1.

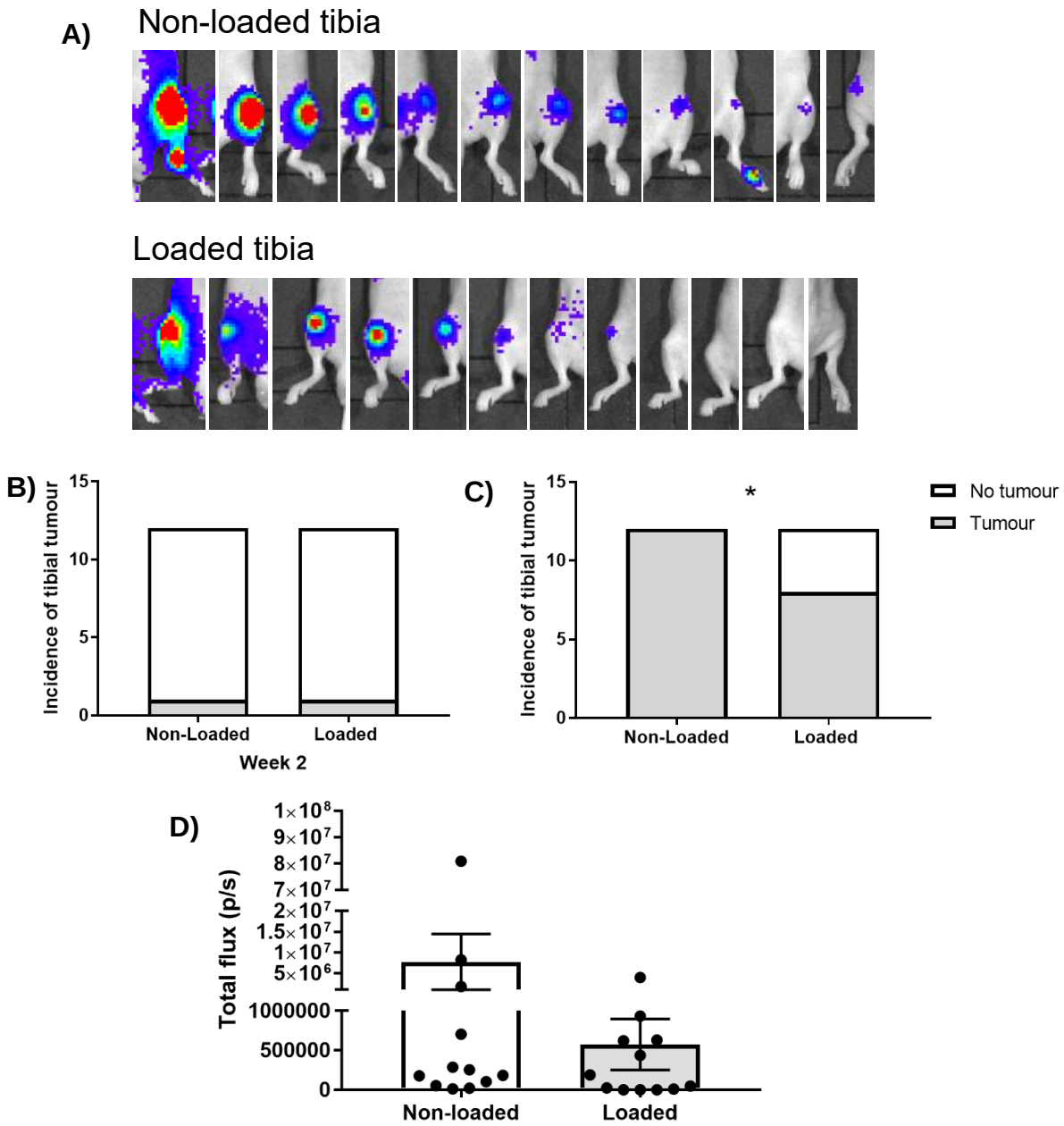


**Figure 5. 2. The effect of mechanical loading on the onset of PCa bone metastasis in an intracardiacally PC3 injected xenograft model.** *The human PCa cell line PC3 was intracardiacally injected in 8-week-old BALB/c nude mice followed by 3 weeks of continuous mechanical loading in the right tibia. A) Endpoint (3 weeks) IVIS pictures of loaded vs non-loaded tibia. The skeletal tumour growth was examined weekly by bioluminescence assay, comparing the loaded versus non-loaded tibias. B) and C) The tumour incidence was significantly lower in the loaded tibia compared to controls. chi-square test, n=12, *p=<0.05. D) The tumour burden, measured as photons/second, was ~45% lower in the loaded tibias. Data presented as mean±SEM, Wilcoxon test.*

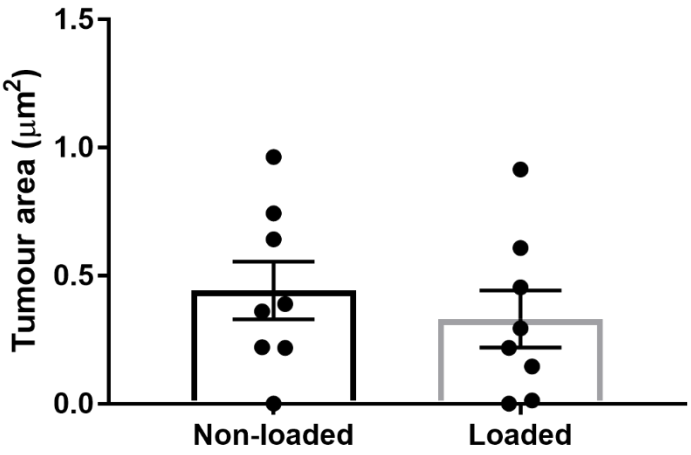


**Figure 5. 3. PCa bone metastasis tumour area measurement between non-loaded and loaded tibias**. *The tumour area developed in non-loaded and loaded tibias subjected to 3 weeks of loading stimulus were measured using the QuPath histology software as a matter to corroborate the effect of loading into PCa bone metastasis progression at a histologic level, finding an ~25% reduction of tumour area in the loaded tibias versus non-loaded contralateral controls.*

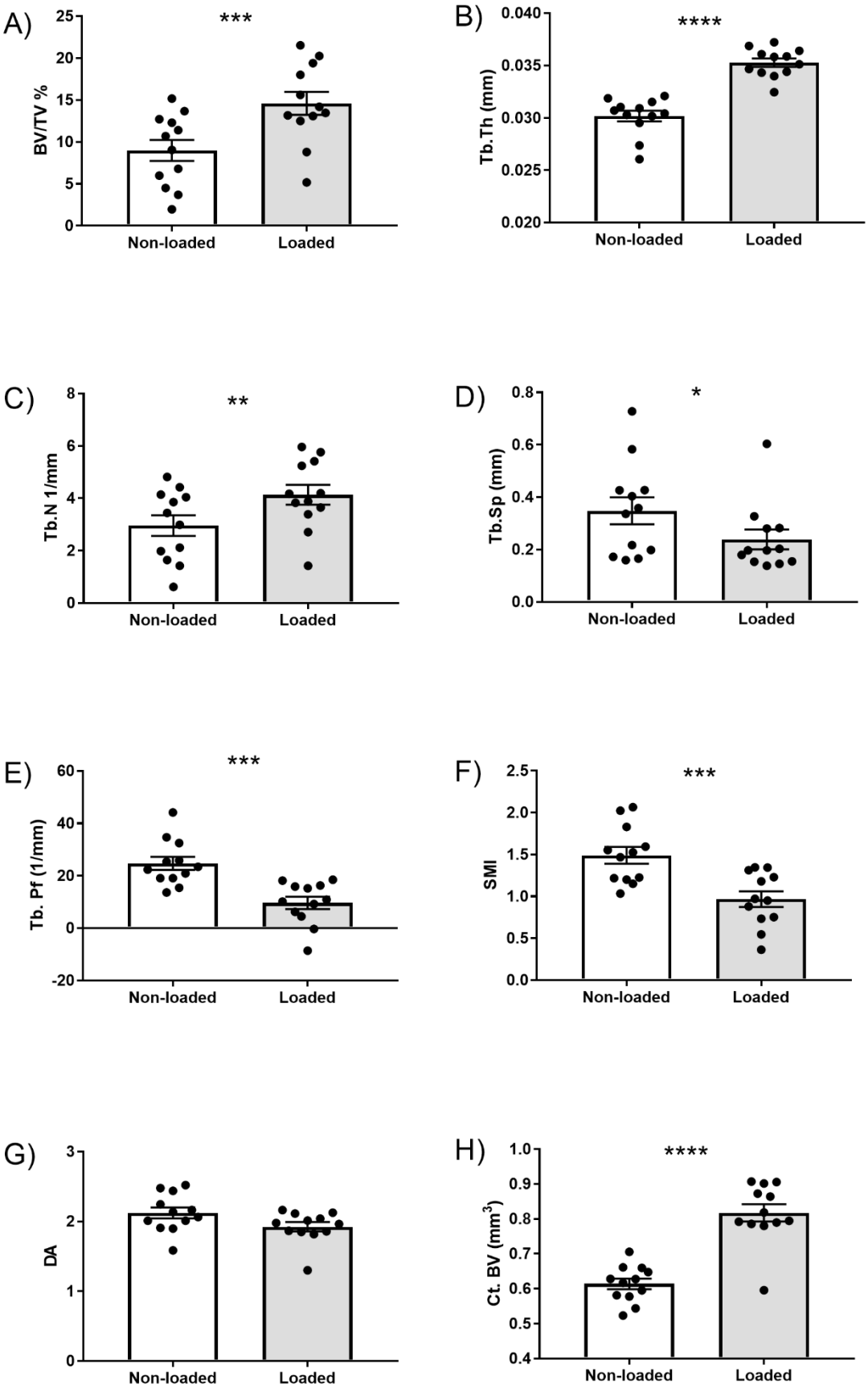
A)
***
BV/TV %
25
20
15
10
5
0
Non-loaded
Loaded
B)
****
Tb.Th (mm)
0.040
0.035
0.030
0.025
0.020
Non-loaded
Loaded
C)
**
Tb.N 1/mm
8
6
4
2
0
Non-loaded
Loaded
D)
*
Tb.Sp (mm)
0.8
0.6
0.4
0.2
0.0
Non-loaded
Loaded
E)
***
Tb. Pf (1/mm)
60
40
20
0
-20
Non-loaded
Loaded
F)
***
SMI
2.5
2.0
1.5
1.0
0.5
0.0
Non-loaded
Loaded
G)
DA
3
2
1
0
Non-loaded
Loaded
H)
****
Ct. BV (mm3)
1.0
0.9
0.8
0.7
0.6
0.5
0.4
Non-loaded
Loaded

**Figure 5. 4. The effect of mechanical loading in the bone morphometry of an intracardiacally PC3 injected xenograft model.** *The loaded and non-loaded tibias were scanned using micro-CT ex vivo to analyse the bone morphometric parameters. The A) trabecula bone volume percentage, B) trabecula number, C) trabecula thickness, D) trabecula separation, E) trabecula pattern factor, F) structure model index, G) degree of anisotropy, and H) cortical bone volume were analysed and compared between loaded and non-loaded tibias, finding significant results in most of the bone parameters A)-F) and H). This indicates that continuous mechanical loading improves/preserves the bone structure in PCa bone metastasis. All data is presented is mean±SEM, paired t-test, n=12, *p=<0.05, **p=<0.01, ***p=<0.001, ****p=<0.0001.*

**Table 5. 1. Quantitative bone morphometry analysis by Micro-CT in BALB/c nude mice subjected to I.C injection of PC3 cells and right tibial mechanical loading stimulus.**

| | Non-loaded | Loaded | Percentage change | P value |
|---|---|---|---|---|
| | **n=12** | **n=12** | | |
| **BV/TV %** | **8.99** | **14.6** | **62.29** | ******* |
| **Tb.Th (mm)** | **0.03** | **0.035** | **16.93** | ******** |
| **Tb.N (1/mm)** | **2.95** | **4.13** | **39.85** | ****** |
| **Tb.Sp (mm)** | **0.34** | **0.23** | **-31.43** | ***** |
| **Tb. Pf (1/mm)** | **24.71** | **9.69** | **-60.78** | ******* |
| **SMI** | **1.49** | **0.96** | **-35.07** | ******* |
| **DA** | 2.12 | 1.92 | -9.28 | NS |
| **Ct. BV** | **0.61** | **0.81** | **33.12** | ******** |

Values are mean ± SEM

Percentage changes = (Loaded mean – Non-loaded mean)/Non-loaded mean × 100

NS: Non-significant

* $p < 0.05$ (Student's paired t-test)

** $p < 0.01$ (Student's paired t-test)

*** $p < 0.001$ (Student's paired t-test)

**** $p < 0.0001$ (Student's paired t-test)

### 5.2.4. Mechanical loading delays the onset and incidence of PCa bone metastasis in a RM1 intracardiacally injected syngeneic model.

The RM1 IC mice model showed skeletal metastasis in 10 out of the 11 non-loaded tibias (~90%) while only 6 (~54%) of the 11 loaded tibias developed skeletal metastasis. Skeletal tumour was not detectable in 5 (~46%) of the 11 loaded tibias figure 5.5 A. The incidence of tibial tumour was analysed for the tree weeks of loading regimen, finding a tendency to significance at week 3 to lower tumour incidence in the loaded tibias. This is in line with the BALB/c mice model, where mechanical loading conferred protection against the development of PCa bone metastasis. Tumour tibial incidence at week 1, figure 5.5 B, tumour tibial incidence at week 2, figure 5.5 C, tumour tibial incidence at week 3, figure 5.2 D, chi-square, n=11, p=0.055.

### 5.2.5. Continuous mechanical loading does not alter the PCa tumour burden progression in the RM1 intracardiacally injected syngeneic model.

The tumour burden was measured as photons/second by creating a ROI surrounding the skeletal metastasis in each tibia using the Living Image 4.3.1 software as described in section 2.10. The PCa bone metastasis tumour burden was not significantly different when comparing the non-loaded and loaded tibias in the RM1 syngeneic model, figure 5.5 E, Wilcoxon test, n=11, p= 0.4648. To further corroborate the tumour burden in this syngeneic model, a histologic tumour area measurement should be provided.

### 5.2.6. Mechanical loading preserves the bone structure from PCa osteolytic lesions in a RM1 intracardiacally injected syngeneic model.

According to the Micro-CT analysis, in the syngeneic mice model, the BV/TV%, Tb.Th, Tb.N and Ct. BV were significantly higher (figure 5.6 A, B, C and H, paired t-test, n= 12, p= 0.0071, p= 0.0019, p= 0.0243, p= 0.0002, respectively). The Tb. Pf, and SMI were significantly lower in the loaded tibias compared to non-loaded tibias, figure 5.6 E and F, paired t-test, n=12, p= 0.0073, p= 0.0299, respectively. The Tb.Sp was reduced ~26% in the loaded tibias compared to non-loaded tibia. The results in the

bone parameters after mechanical loading treatment are suggestive of increased bone mass, even in the event of PCa bone metastasis, as in the case of the PC3 IC model. Quantitative data of Micro-CT analysis presented in table 5.2.

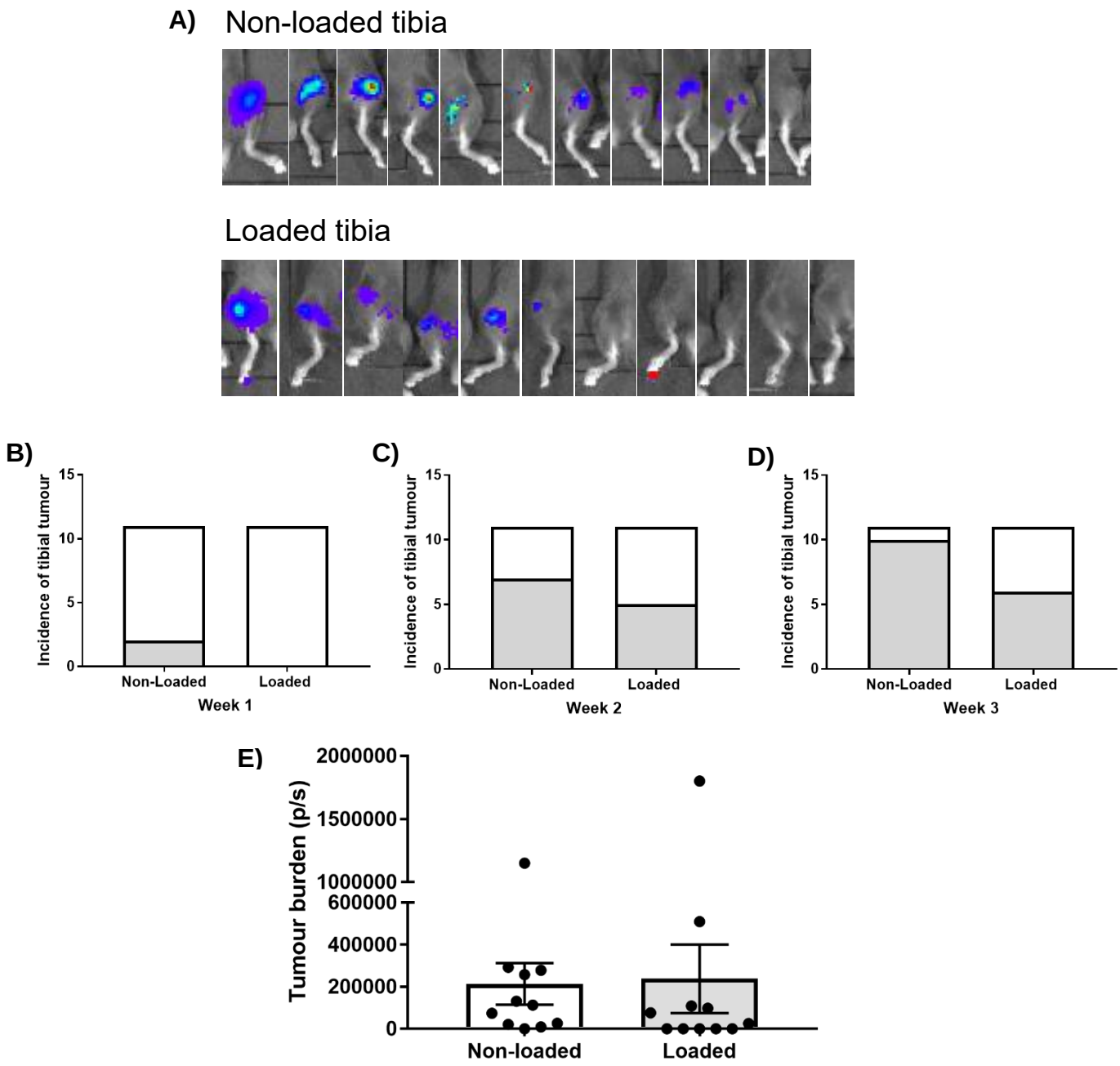


**Figure 5. 5. The effect of mechanical loading on the onset of PCa bone metastasis in a RM1 intracardiacally injected syngeneic model.** *The murine RM1 PCa cell line was intracardiacally injected in 8-week-old C57BL/6 mice followed by 3 weeks of continuous mechanical loading in the right tibia. A) Endpoint (3 weeks) IVIS pictures of loaded vs non-loaded tibia. The skeletal tumour growth was examined weekly by bioluminescence assay, comparing the loaded versus non-loaded tibias. B) The tumour incidence was nearly significant (p=0.055) lower in the loaded tibia compared to controls. chi-square. C) The tumour burden, measured as photons/second, was ~77% lower in the loaded tibias. Data presented as mean±SEM, Wilcoxon test, n=12.*

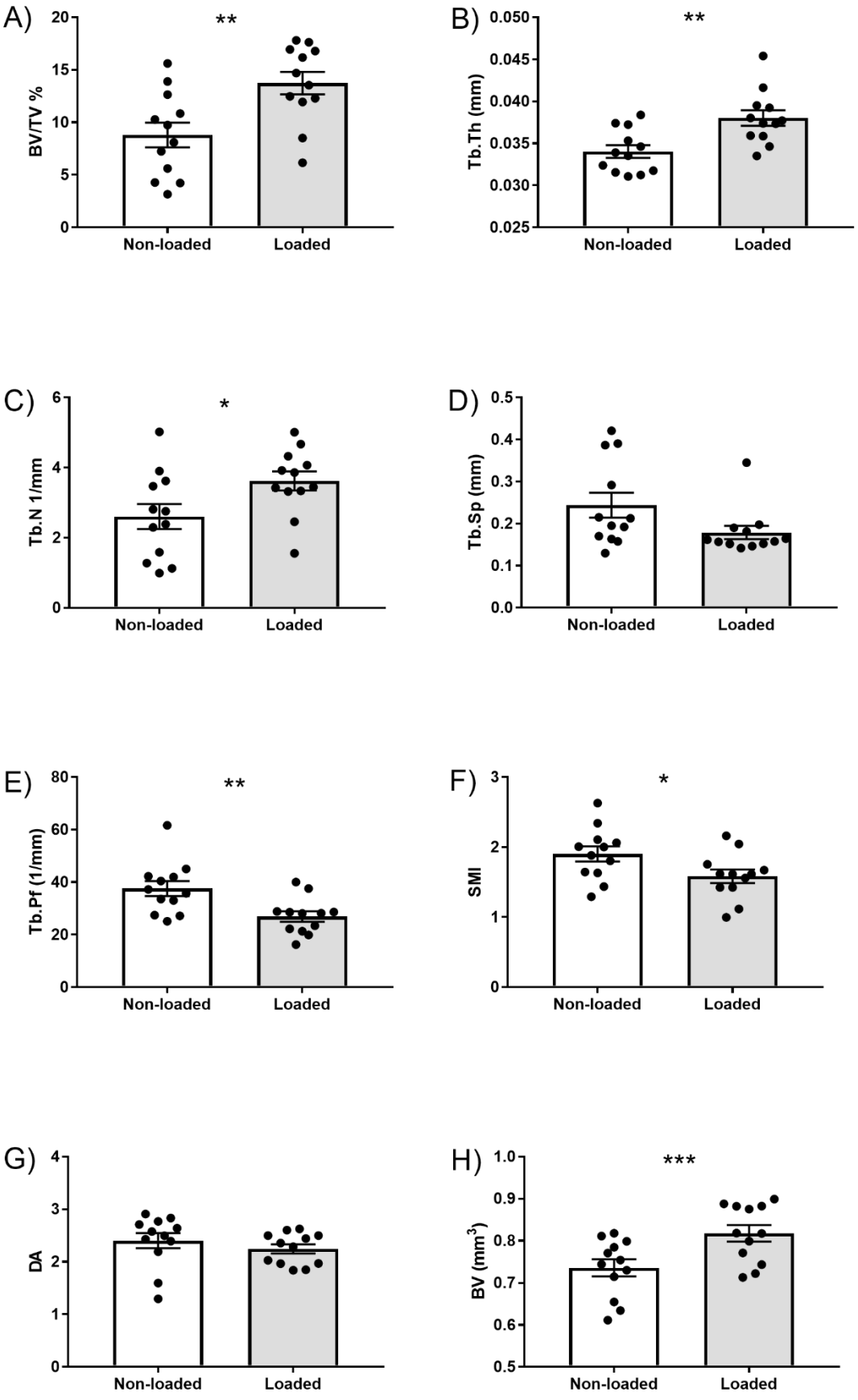
A)
BV/TV %
20
15
10
5
0
**
Non-loaded
Loaded
B)
Tb.Th (mm)
0.050
0.045
0.040
0.035
0.030
0.025
**
Non-loaded
Loaded
C)
Tb.N 1/mm
6
4
2
0
*
Non-loaded
Loaded
D)
Tb.Sp (mm)
0.5
0.4
0.3
0.2
0.1
0.0
Non-loaded
Loaded
E)
Tb.Pf (1/mm)
80
60
40
20
0
**
Non-loaded
Loaded
F)
SMI
3
2
1
0
*
Non-loaded
Loaded
G)
DA
4
3
2
1
0
Non-loaded
Loaded
H)
BV (mm3)
1.0
0.9
0.8
0.7
0.6
0.5
***
Non-loaded
Loaded

**Figure 5. 6. The effect of mechanical loading in the bone morphometry of a RM1 intracardiacally injected syngeneic model.** *The loaded and non-loaded tibias were scanned using micro-CT ex vivo to analyse the bone morphometric parameters. The A) trabecula bone volume percentage, B) trabecula number, C) trabecula thickness, D) trabecula separation, E) trabecula pattern factor, F) structure model index, G) degree of anisotropy, and H) cortical bone volume were analysed and compared between loaded and non-loaded tibias, finding significant results in most of the bone parameters A)-C), E), F) and H). This indicates that continuous mechanical loading improves/preserves the bone structure in PCa bone metastasis. All data is presented as mean±SEM, paired t-test, n=11, *p=<0.05, **p=<0.01, ***p=<0.001.*

**Table 5. 2. Quantitative bone morphometry analysis by Micro-CT in C57BL/6 mice subjected to I.C injection of RM1 cells and right tibial mechanical loading stimulus.**

| | Non-loaded | Loaded | Percentage change | P value |
|---|---|---|---|---|
| | **n=12** | **n=12** | | |
| **BV/TV %** | **8.8** | **13.75** | **56.25** | ** |
| **Tb.Th (mm)** | **0.03** | **0.03** | **11.69** | ** |
| **Tb.N (1/mm)** | **2.60** | **3.61** | **38.88** | * |
| **Tb.Sp (mm)** | 0.24 | 0.17 | -26.63 | NS |
| **Tb. Pf (1/mm)** | **37.56** | **26.91** | **-28.35** | ** |
| **SMI** | **1.90** | **1.58** | **-16.81** | * |
| **DA** | 2.40 | 2.24 | -6.49 | NS |
| **Ct. BV** | **0.73** | **0.817** | **11.16** | *** |

Values are mean ± SEM

Percentage changes = (Loaded mean – Non-loaded mean)/Non-loaded mean × 100

NS: Non-significant

* $p < 0.05$ (Student's paired t-test)

** $p < 0.01$ (Student's paired t-test)

*** $p < 0.001$ (Student's paired t-test)

### 5.2.7. Mechanical loading delays the onset and incidence of PCa bone metastasis in an intra-tail artery injected xenograft model.

To study the effect of mechanical loading in already stablished PCa cells in bone, we applied the intra-arterial tail injected model inoculated with PC3 cells. In this xenograft model, the skeletal metastasis was identified in all the 7 non-loaded tibias with 6 skeletal metastases developed in the loaded tibias which showed a lower tumour burden, which can be better appreciated in the following section. The tibial tumour incidence was analysed the three weeks of mechanical loading; however no significant difference was found at any time point, figure 5.7 B-D, chi-square, n=7.

### 5.2.8. The tumour burden is reduced in continuously mechanical loaded tibias in an intra-tail artery injected xenograft model.

The benefit of the continuously mechanical loading was observed in the intra-tail artery mice, in which the tumour burden was significantly reduced in the loaded tibias, figure 5.7 E, paired t-test, n=7, p= 0.0262. The positive impact of continuous mechanical loading suggests that a sufficient loading force in the bone to induce an osteogenic response delays the onset of PCa bone metastasis.

### 5.2.9. Mechanical loading treatment significantly reduces bone destruction in mice with PCa bone metastasis

The intra-caudal injected mice model showed significantly increased Tb. Sp, SMI and Ct. BV, figure 5.8 C, F and H, paired t-test, n= 7, p= 0.0080, p=0.0366 and p=0.0432, n=7, respectively. The BV/TV%, Tb.Th, Tb. N were found increased ~54%, ~15% and ~35%, respectively in the loaded tibias compared to non-loaded tibias. The improved bone parameters are suggestive of protection against the PCa osteolytic lesions as we observed in the IC xenograft and syngeneic model. Quantitative data of the Micro-CT analysis is presented in table 5.3.

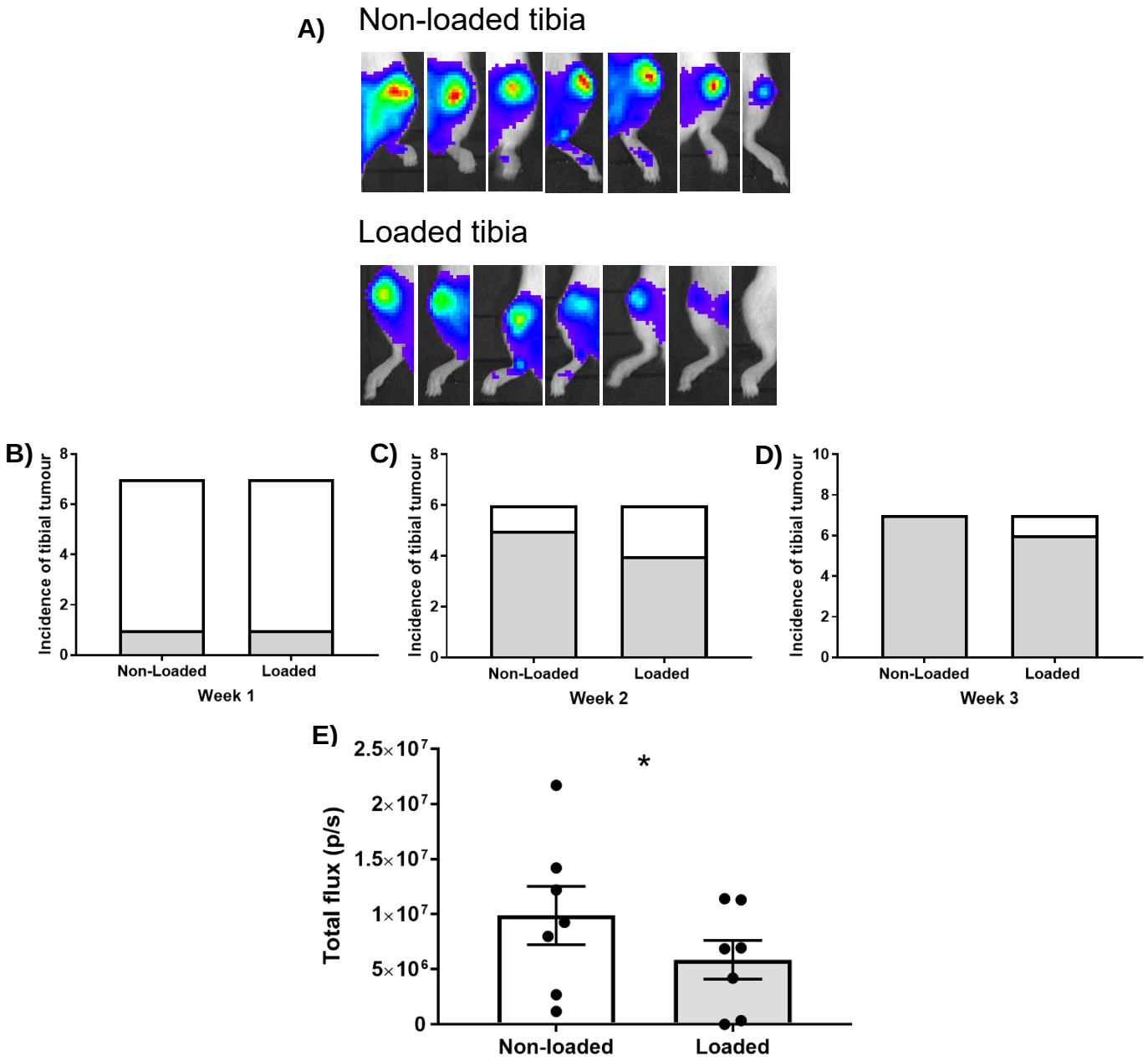


**Figure 5. 7. The effect of mechanical loading on the onset of PCa bone metastasis in an intra-tail artery PC3 injected xenograft model.** *The human PC3 PCa cell line was intra-tail arterial injected in 8-week-old BNDG mice followed by 3 weeks of continuous mechanical loading in the right tibia. A) Endpoint (3 weeks) IVIS pictures of loaded vs non-loaded tibia. The skeletal tumour growth was examined weekly by bioluminescence assay, comparing the loaded versus non-loaded tibias. B) The tumour incidence in the loaded tibia compared to controls was not significantly different. chi-square. C) The tumour burden, measured as photons/second, was significantly lower in the loaded tibias. Data presented as mean±SEM, paired t-test, n=7, *p=<0.05.*

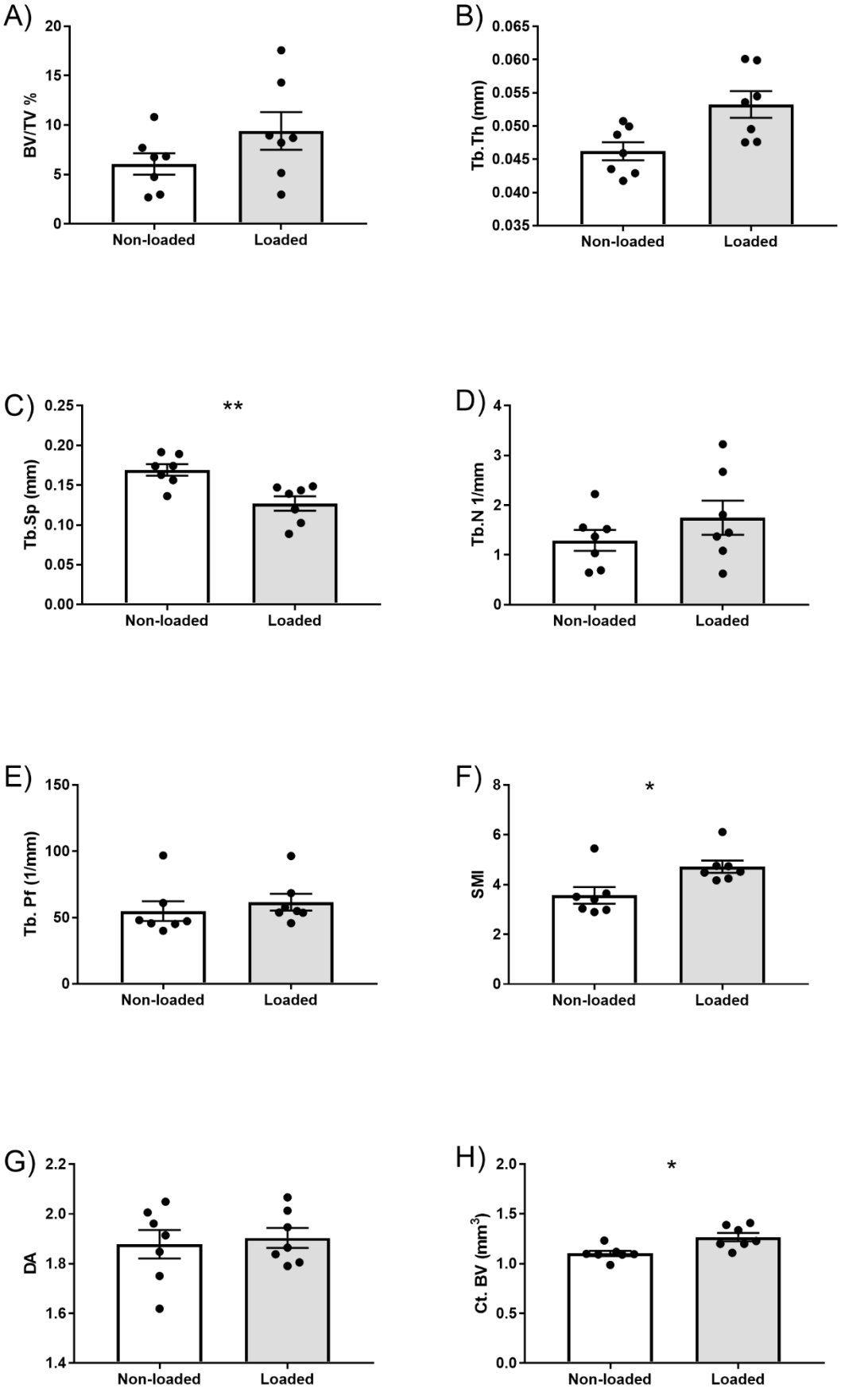
A)
BV/TV %
20
15
10
5
0
Non-loaded
Loaded
B)
Tb.Th (mm)
0.065
0.060
0.055
0.050
0.045
0.040
0.035
Non-loaded
Loaded
C)
**
Tb.Sp (mm)
0.25
0.20
0.15
0.10
0.05
0.00
Non-loaded
Loaded
D)
Tb.N 1/mm
4
3
2
1
0
Non-loaded
Loaded
E)
Tb. Pf (1/mm)
150
100
50
0
Non-loaded
Loaded
F)
*
SMI
8
6
4
2
0
Non-loaded
Loaded
G)
DA
2.2
2.0
1.8
1.6
1.4
Non-loaded
Loaded
H)
*
Ct. BV (mm3)
2.0
1.5
1.0
0.5
0.0
Non-loaded
Loaded

**Figure 5. 8. The effect of mechanical loading in the bone morphometry of an intra-tail artery PC3 injected xenograft model.** *The loaded and non-loaded tibias were scanned using micro-CT ex vivo to analyse the bone morphometric parameters. The A) trabecula bone volume percentage, B) trabecula number, C) trabecula thickness, D) trabecula separation, E) trabecula pattern factor, F) structure model index, G) degree of anisotropy, and H) cortical bone volume were analysed and compared between loaded versus non-loaded tibias, finding significant results in the C) Tb. Sp, F) SMI and H) Ct. BV. The A) BV/TV%, B) Tb. Th and Tb. N increased ~54%, ~15% and ~35% in the loaded tibias compared to non-loaded tibias, respectively. This indicates that continuous mechanical loading improves/preserves the bone structure in PCa bone metastasis. All data is presented as mean±SEM, paired t-test, n=7, *p=<0.05, **p=<0.01.*

**Table 5. 3. Quantitative bone morphometry analysis by Micro-CT in BNDG mice subjected to intra-tail artery injection of PC3 cells and right tibial mechanical loading stimulus.**

| | Non-loaded | Loaded | Percentage change | P value |
|---|---|---|---|---|
| | n=7 | n=7 | | |
| **BV/TV %** | 6.07 | 9.41 | 54.86 | NS |
| **Tb.Th (mm)** | 0.04 | 0.05 | 15.25 | NS |
| **Tb.N (1/mm)** | 1.29 | 1.74 | 35.39 | NS |
| **Tb.Sp (mm)** | **0.16** | **0.12** | **-24.92** | ** |
| **Tb. Pf (1/mm)** | 54.89 | 61.52 | 12.07 | NS |
| **SMI** | **3.56** | **4.71** | **32.39** | * |
| **DA** | 1.87 | 1.90 | 1.33 | NS |
| **Ct. BV** | **1.10** | **1.26** | **14.86** | * |

Values are mean ± SEM

Percentage changes = (Loaded mean – Non-loaded mean)/Non-loaded mean × 100

NS: Non-significant

* $p < 0.05$ (Student's paired t-test)

** $p < 0.01$ (Student's paired t-test)

### 5.2.10. The effect of short-term mechanical loading in a PC3 IC xenograft model.

Additionally, we tested the effect of short-term mechanical loading in a BALB/c nude xenograft model (n=6). This model mimic patients who decide to initiate load-bearing exercise at the moment of PCa development but then discontinue their exercise routine. The PC3 cells were injected following the same route as the continuously mechanically loaded mice, figure 5.1 A. However, the mechanical loading stimulus was applied for one week only post-IC injection, to be later withdrawn for 2 weeks (figure 5.9). The tumour growth and bone parameters were analysed in the same way as described in 2.10 and 2.7, respectively.

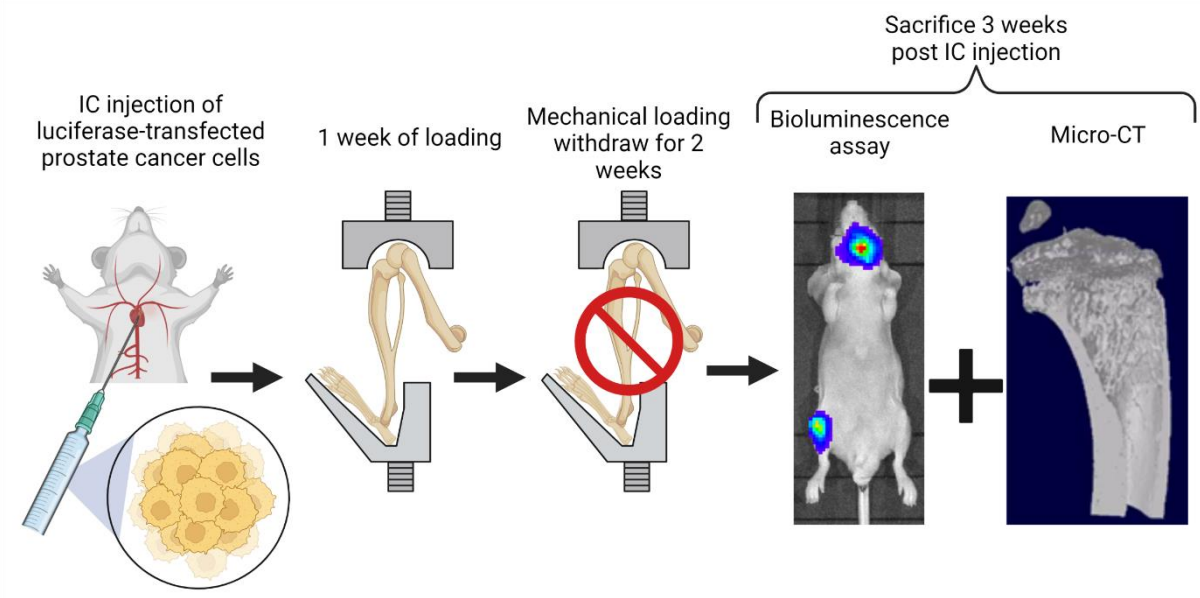


**Figure 5. 9. Experiment schematic to test whether short-term mechanical loading inhibits tumour growth in xenograft models.** *The BALB/c nude mice were IC injected with PC3 PCa cells (~100,000 cells in 100 µl PBS). The following day, mechanical loading was performed in the right tibia for one week to be later discontinued for 2 weeks, to study the effect of short-term mechanical loading in PCa bone metastasis.*

### 5.2.11. Short-term mechanical loading delays the incidence of PCa bone metastasis in a PC3 IC xenograft model.

In the short-term mechanically loaded model, all the mice developed skeletal tumour in the non-loaded tibia (100%). From the loaded tibias, 3 developed skeletal tumour while other 3 had no detectable skeletal tumour at the end of the experiment (figure 5.10 A). The incidence of tibial tumour was analysed finding a significant lower tumour tibial incidence in the loading withdraw tibia at the 3$^{rd}$ week of the study versus non-loaded tibias (figure 5.10 C, chi-square, n=6, p= 0.0455), suggesting that one week of mechanical loading stimulus, even when is discontinued, is still able to alter the development of PCa bone metastasis.

### 5.2.12. The tumour burden is reduced in the short-term mechanical loaded tibias in a PC3 IC xenograft model.

The short-term mechanically loaded model showed a ~66% reduction in tumour burden in the short-term loaded tibias compared to controls (figure 5.10 D, Wilcoxon test, n=6). This result indicates that the mechanical loading stimulus applied at the moment of PCa development, even when discontinued, is still able to reduce the PCa bone metastasis growth.

### 5.2.13. Short-term mechanical loading does not protect the bone structure from PCa osteolytic lesions in a PC3 IC injected xenograft model

The bone structure parameters were analysed using Micro-CT analysis to compare the structure of loading withdraw tibias and non-loaded controls. The Ct. BV showed increased significance in the loaded withdraw tibia compared to controls, figure 5.11 H, paired t-test, n=6, p= 0.0250. Additionally, the BV/TV% and Tb.N showed an increment of ~35% and ~33%, respectively. No significant differences were found in the remaining bone parameters among the non-loaded and loaded withdraw tibias. Although some bone parameters seem to be conserved in this 3-week period of time, the continuity of mechanical loading is important to preserve or maintain the bone

structure from the osteolytic lesions caused by PCa. Quantitative data of the Micro-CT analysis presented in table 5.4.

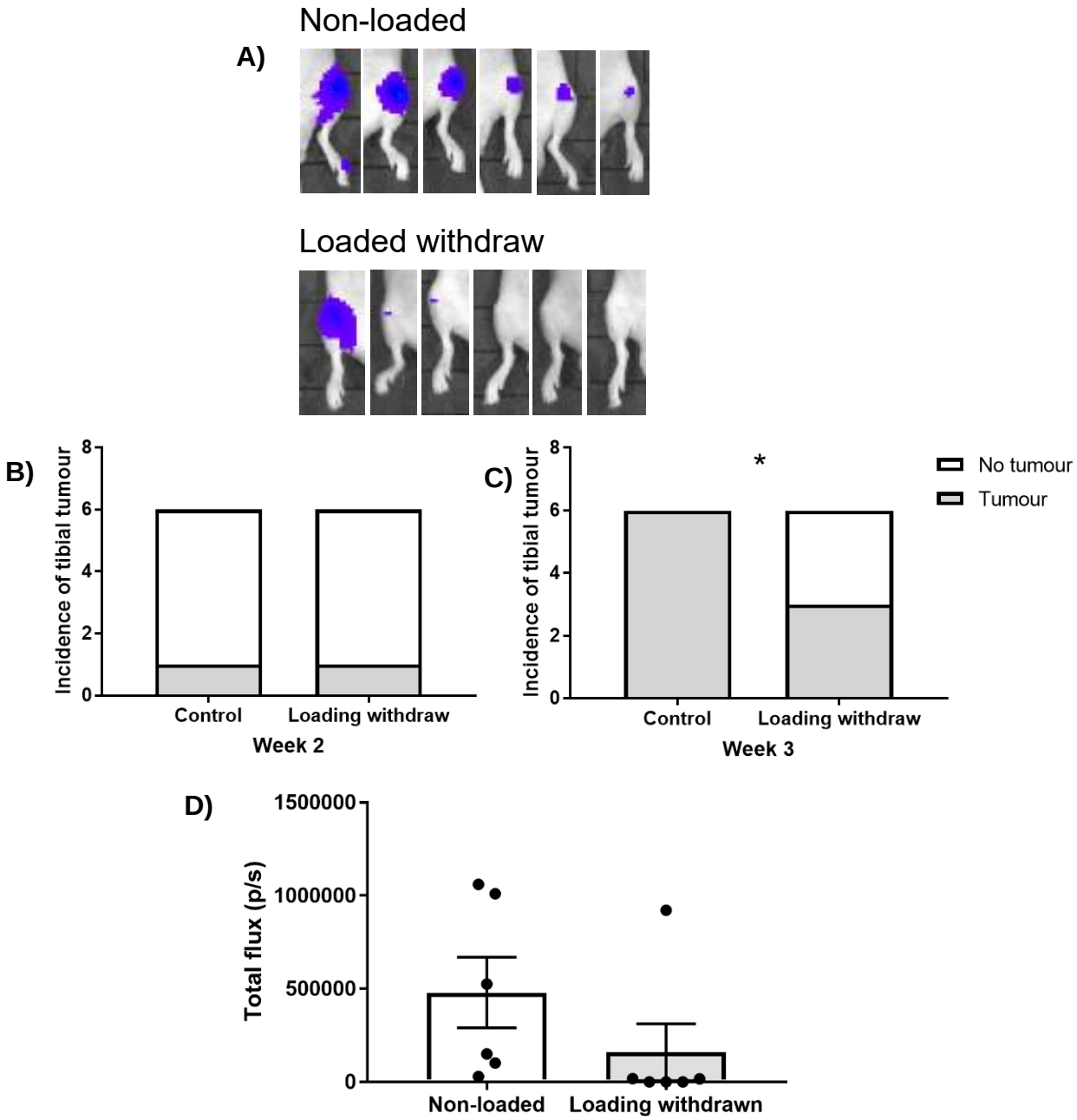


**Figure 5. 10. The effect of short-term mechanical loading on the onset of PCa bone metastasis in an intracardiacally PC3 injected xenograft model.** *The human PCa cell line PC3 was intracardiacally injected in 8-week-old BALB/c nude mice followed by 1-week mechanical loading in the right tibia. A) Endpoint (3 weeks) IVIS pictures of loaded withdraw vs non-loaded tibia. The skeletal tumour growth was examined weekly by bioluminescence assay, comparing the loaded versus non-loaded tibias. B) The tumour incidence was significantly lower in the loaded tibia compared to controls. C) The tumour burden, measured as photons/second, was ~66% lower in the loaded tibias. Incidence of tibial tumour: chi-square, tumour burden: presented as mean±SEM, Wilcoxon test, n=12, *p=<0.05.*

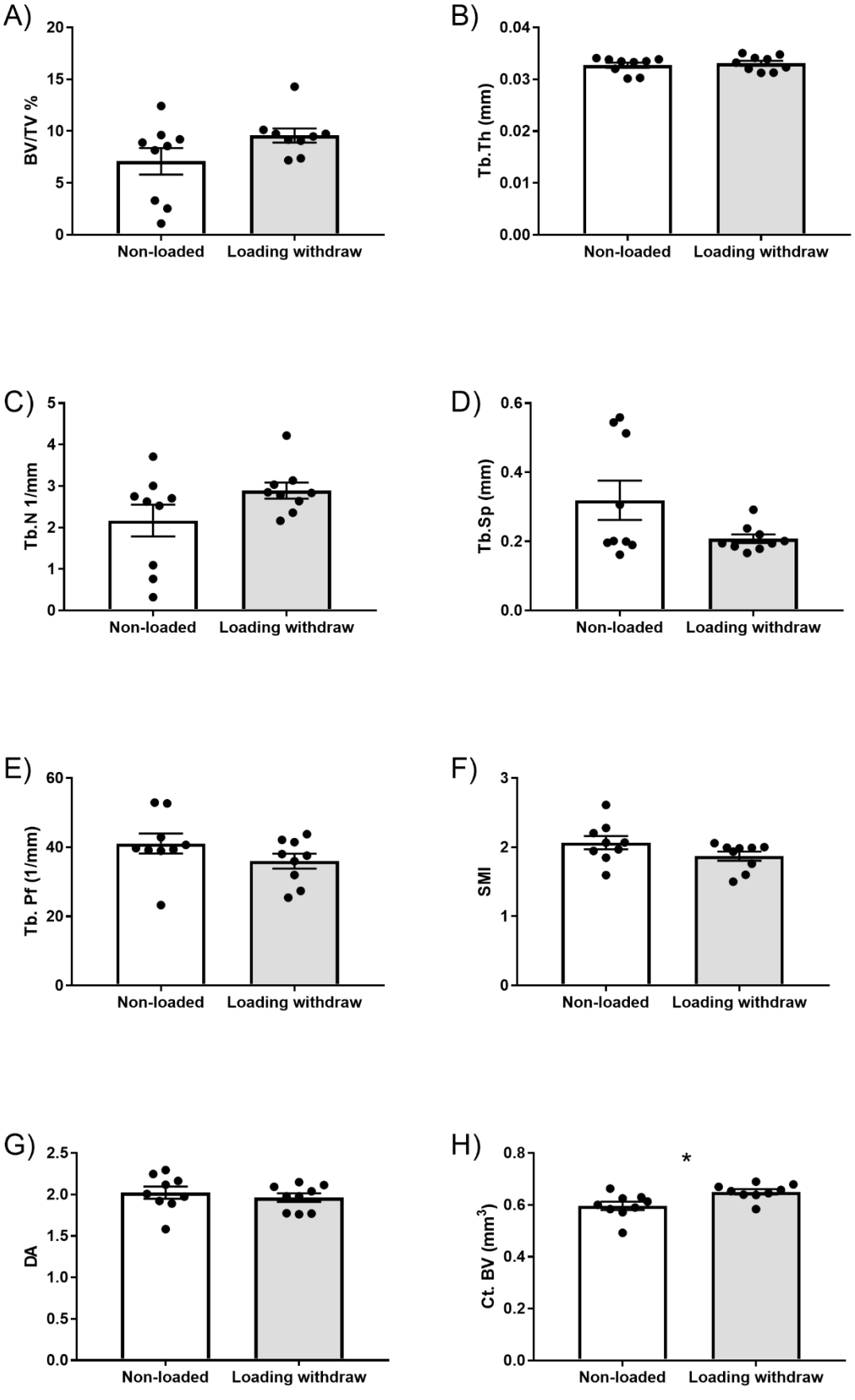
A)
BV/TV %
20
15
10
5
0
Non-loaded
Loading withdraw
B)
Tb.Th (mm)
0.04
0.03
0.02
0.01
0.00
Non-loaded
Loading withdraw
C)
Tb.N 1/mm
5
4
3
2
1
0
Non-loaded
Loading withdraw
D)
Tb.Sp (mm)
0.6
0.4
0.2
0.0
Non-loaded
Loading withdraw
E)
Tb. Pf (1/mm)
60
40
20
0
Non-loaded
Loading withdraw
F)
SMI
3
2
1
0
Non-loaded
Loading withdraw
G)
DA
2.5
2.0
1.5
1.0
0.5
0.0
Non-loaded
Loading withdraw
H)
Ct. BV (mm3)
0.8
0.6
0.4
0.2
0.0
*
Non-loaded
Loading withdraw

**Figure 5. 11. The effect of short-term mechanical loading in the bone morphometry of an intracardiacally PC3 injected xenograft model.** *The loading withdraw and non-loaded tibias were scanned using micro-CT ex vivo to analyse the bone morphometric parameters. The A) trabecula bone volume percentage, B) trabecula number, C) trabecula thickness, D) trabecula separation, E) trabecula pattern factor, F) structure model index, G) degree of anisotropy, and H) cortical bone volume were analysed and compared between loaded and non-loaded tibias. The Ct. BAll data is presented as mean±SEM, paired t-test, n=6.*

**Table 5. 4. Quantitative bone morphometry analysis by Micro-CT in Balb/C nude mice subjected to IC injection of PC3 cells and right tibial loading withdraw stimulus.**

| | Non-loaded | Loaded withdraw | Percentage change | P value |
|---|---|---|---|---|
| | **n=9** | **n=9** | | |
| **BV/TV %** | 7.08 | 9.57 | 35.12 | NS |
| **Tb.Th (mm)** | 0.03 | 0.03 | 1.16 | NS |
| **Tb.N (1/mm)** | 2.16 | 2.89 | 33.34 | NS |
| **Tb.Sp (mm)** | 0.31 | 0.20 | -34.85 | NS |
| **Tb. Pf (1/mm)** | 41.08 | 35.98 | -12.41 | NS |
| **SMI** | 2.06 | 1.87 | -9.44 | NS |
| **DA** | 2.02 | 1.96 | -2.96 | NS |
| **Ct. BV** | **0.59** | **0.65** | **9.06** | ***** |

Values are mean ± SEM

Percentage changes = (Loaded mean – Non-loaded mean)/Non-loaded mean × 100

NS: Non-significant

* *p<0.05* (Student's paired t-test)

## 5.3. Discussion

PCa is one of the most common cancers diagnosed in men of western countries, and in the UK. In this disease, the PCa bone metastasis represents the main issue as no current treatments are able to fully alleviate this diseases' stage and once stablished is associated with a significantly reduced survival rate (Nørgaard et al. 2010; Liam Bourke, Turner, Greasley, Sutton, Steed, Smith, Brown, Kelly, Hulme, Greenfield, Persad, Farrin, Hewison & Derek J. Rosario 2018) The benefits of exercise have been evaluated in many diseases, including PCa; however, most of the studies deliberated exclude patients with PCa bone metastasis as the exercise regimen may be counterproductive for the fragile skeleton of patients with bone metastasis, leading to a gap in knowledge regarding the effect of exercise in PCa bone metastasis (Courneya & Friedenreich 2011). To date, the effect of mechanical loading (which mimics weight-bearing exercise) in bone and tumour progression has been assessed, finding positive outcomes in reduced cancer progression (Lynch et al. 2013; Yang et al. 2019; M. Huang et al. 2021; Yokota 2021; Fan et al. 2021; Rummler et al. 2021). However, there still lack of evidence regarding the effect of exercise in PCa bone metastasis. To elucidate the effect of exercise in PCa bone metastasis progression, we applied axial mechanical loading (which mimics load-bearing exercise) in the right tibia of murine PCa pre-clinical models. We evaluated the tibial tumour incidence, tumour burden and bone structure parameters to observe the impact of loading in PCa bone progression.

Firstly, the incidence of skeletal tumours was reduced in the BALB/c nude mice (continuously loaded and loaded withdraw) and C57BL/6 while the tumour burden was lower in the BALB/c nude mice (both loading models) and in the BNDG mice. Overall, mechanical loading reduced the incidence and tumour burden *in vivo*. The reduced skeletal tumour incidence and burden in the loaded tibia could be explained by the osteogenic response caused by loading stimulus. As previously tested in chapter 4, IC injection of PC3 cells followed by mechanical loading applied for one week does not increases the arrival of PCa cell in the bone marrow, therefore, the lower skeletal tumour incidence and burden could have been consequence of inhibiting or delaying the overt growth of the individual PCa cells in bone. In line with this result, in chapter 3 we observed that at one week of loading stimulus there is an increase osteogenic response and bone formation. Regarding this theory, it takes approximately 3 weeks

to observe any skeletal tumour signal by bioluminescence technique post IC injection of PCa cells (Drake et al. 2005; Wang et al. 2015), while markers related to an osteogenic response are expressed 4 hours post mechanical loading and bone formation occurs in days, which is in line with our previous data (Mantila Roosa et al. 2011; Forwood et al. 1996; Chow et al. 1998). According to our loading protocol, bone formation is achieved after 1 week of loading stimulus, whereas skeletal tumours were only being detected after 2 weeks of PCa cells inoculation; being properly observed at 3 weeks. Moreover, mechanical loading is associated with osteoclasts inhibition, by this manner preventing the release of growth factors from bone tissue that could stimulate tumour growth (Kulkarni et al. 2010; Li et al. 2016). A decreased osteoclast activity in the first week of loading was indeed observed as described in chapter 3, supporting an inhibition of osteoclasts activity, at least during the first week of mechanical loading. According to the vicious cycle theory, PCa cells will interact with osteoblasts to promote their activity by secreting TGF-β and endothelin-1 and osteoclasts activity by means of RANKL (Guise 2002). Given the osteolytic nature of the PC3 cell line and the mixed nature of the RM1 cell line (osteolytic/osteoblastic) inoculated in our pre-clinical models, we speculate that loading interferes with the osteoclastic PCa growth support. This theory could be supported by our loading withdraw model, in which one week of loading led to a reduced incidence and tumour burden, even when loading was discontinued. Inhibition of osteoclast due to mechanical loading *in vitro* and *in vivo* has been shown by other studies, (Lynch et al. 2013; M. Huang et al. 2021; Yokota 2021; Rummler et al. 2021). Thus, osteogenic and bone formation response and osteoclast inhibition caused by mechanical loading could impair the progression and reduce the incidence of PCa cells, disrupting the cancer vicious cycle and decreasing overt-metastasis growth. The mentioned theory provides an explanation on how loading can affect the osteoclast activity and tumour progression. Therefore, what is the role the osteoblasts play in PCa progression? This can be discussed by the dormant factors released by osteoblasts and their impact in PCa proliferation.

The enhanced osteoblast activity and the release of pro-dormancy factors in response to mechanical loading is another potential contributor to alter the PCa growth. For instance, Kobayashi et al. (2011), found that the BMP7 released from bone cells leads to a quiescent status in PCa stem-like cells via p38 mitogen-activated protein kinase

(MAPK), increased expression of p21 which is related to cell cycle inhibition and N-myc downstream-regulated gene 1 (NDRG1), a metastasis suppressor gene. Indeed, mechanical loading induces increased expression of BMP7 by osteocytes as suggested by Santos et al. (2011). Additionally, Shiozawa et al. (2010), demonstrated that PCa cells interact with osteoblasts via annexin II, expressed by osteoblasts. Once they bind, PCa cells express AXL, a receptor for the growth factor growth arrest-specific 6 (GAS6), also produced by osteoblasts, which induces PCa cell quiescence. More recently, Yu et al. (2018) discovered a novel pathway associated with quiescence in PCa cells. These authors treated PCa cells with osteoblast-conditioned media, inducing cell-cycle arrest via TGFβ2 and GDF10. These osteoblast-derived factors activated the p38MAPK which phosphorylated the serine-249 and threonine-252 (S249/T252) N-terminus region of the tumour suppressor retinoblastoma protein, this in turn stimulated the cyclin dependent kinase (CDK) p27, a cell-cycle suppressor protein, resulting in quiescent PCa cells. The mentioned factors could be further released due to the anabolic stimulus of mechanical loading, promoting a slow-growing activity in the PCa cells, correlated with a lower skeletal tumour signal in loaded tibias (Damaraju et al. 2014; Guo et al. 2015). Therefore, mechanical loading could delay the onset of PCa skeletal tumour by disrupting the cancer vicious cycle and releasing of quiescent-related factors.

Mechanical loading can also affect the cytokines levels within the bone. An example of this is dickkopf-related protein 1 (DKK1), an inhibitor of the canonical Wnt pathway, important for osteoblastogenesis and bone formation (Pinzone et al. 2009; Colditz et al. 2018). Mechanical loading has been shown to inhibit DKK1 levels and promote bone formation *in vivo* (Robling et al. 2008b; Holguin et al. 2017; Morse et al. 2020). Possibly, our mechanical loading regimen affected the levels of DKK1 and other pro-tumour (i.e. CCL5, IL-12p40) or anti-tumour (i.e.IL-2, IL-12p70) cytokines, contributing to the increased bone structure observed in our naïve and pre-clinical models (Aldinucci & Colombatti 2014; Kundu et al. 2017; Jiang et al. 2016; Stanilov et al. 2010). A further discussion of the cytokines affected by mechanical loading can be found in chapter 8.

Moreover, recent evidence highlights the role of the bone ECM and cancer progression (Pickup et al. 2014; Winkler et al. 2020). For instance, mechanical loading

is linked to alterations in the bone ECM stiffness, possibly impacting the development of PCa bone metastasis (EB et al. 2003; Main et al. 2014a; Silder et al. 2015). As an example, Page et al. (2015). mimicked the cortical stifness in an *in vitro* model, finding that increased stiffness led to overexpression of GLI2 and PTHrP, two tumour-progression factors and osteolytic related genes, resulting in a PCa bone-destructive phenotype (Thiyagarajan et al. 2007; Li et al. 2011; Ruppender et al. 2010). Others have found that lower bone stiffness reduces cancer proliferation (Saatci et al. 2020). This hypothesis will be discussed in chapter 8.

Interestingly, bone morphometric parameters were maintained/enhanced in most of the loaded tibias compared to controls as analysed by Micro-CT analysis. The BV/TV%, Tb.Th, Tb.N and Ct.BV indicate increase bone mass in the trabecula and cortical tissue (Bouxsein et al. 2010). A lower Tb. Pf suggests a well-connected trabecula tissue while a lower Tb. Sp results from an increase trabecula bone mass (Hahn et al. 1992). A lower SMI correlates with a plate-like trabecula structure while an increased SMI is associated with a rod-like trabecula. A plate-like trabecula structure is able to wear more weight compared to a rod-like structure, further suggesting a stronger trabecula tissue in the loaded tibias (J. Wang et al. 2015). Overall, trabecular, and cortical tissue parameters were improved by mechanical loading. This can be explained by a possible inhibition and PCa prolfieration reduced osteolytic activity of the PCa cells. This is in line with experiments performed by Ziouti et al. (2017), who subjected a xenograft model of multiple myeloma into mechanical loading regimens, finding that loading stimulus could counteract the development of osteolytic lesions in mice with established skeletal tumour. Recent evidence suggests increased mortality in patients that in addition to PCa bone metastasis, also develop osteolytic lesions and SRE (pathological fractures, spinal cord compression, radiotherapy or surgery directed to heal bone lesions), compared to patients with PCa bone metastasis but not SRE (Nørgaard et al. 2010; Sathiakumar et al. 2011; Oefelein et al. 2002). This result suggests that mechanical loading is successfully useful to reduce cancer-related osteolysis, thereby preserving bone health and improving the quality of life in the patient.

There are limitations in this study. For instance, it would be of interest to achieve a longer loading withdraw model to assess whether the bone created during the first

week of mechanical stimulus would be reabsorbed by the osteoclasts and study its impact in PCa bone progression (i.e., the cancer vicious cycle). This is of interest as some patients who suffer from cancer tend to abandon exercise or other physical activities, resulting in a sedentary lifestyle, which is linked to loss of bone mass (Schoutens et al. 2012; Segal et al. 2017; Avancini et al. 2020).

Similar to us, Lynch et al. (2013) and Fan et al. (2020) applied mechanical loading one day or two after inoculation of cancer cells in xenograft models, respectively. Lynch et al. (2013) applied 4N loading force engendering a ~600 με, leading to reduced osteolysis and increase bone mass. Fan et al. (2020) applied 1N, 2N and 5N which resulted in 260, 480 and 1060 με, respectively. Reduced osteolysis was observed at 1N, no effect at 2N and bone microdamage when 5N were applied. Considering these studies, we should apply a method (i.e., finite elements or gauges inserted in the tibia of our *in vivo* models) to properly measure the strain caused by our loading stimulus and find exercises which could cause a similar strain in patients, promoting an osteogenic bone formation, avoiding damage in the skeleton, and evaluating its impact in clinical settings.

Finally, we must consider that mechanical loading is a local event, and we are not taking into consideration the fully physiological event of exercise (Sugiyama, Price, et al. 2010). To overcome this issue, we will apply a treadmill running exercise, which is an anaerobic exercise regimen with proven benefits in health and bone (Stacey A Kenfield et al. 2011; Richman et al. 2011; Esser et al. 2009; Wallace et al. 2007). Importantly, not all of the exercises routines can be performed by patients with PCa bone metastasis due to damaging of their skeleton (Courneya & Friedenreich 2011). Therefore, the whole body vibration platform (WBVP) seems a suitable stimulus, which is safe for the patient and also improves bone formation (Gómez-Cabello et al. 2012; Marín-Cascales et al. 2018). The effect of treadmill exercise and WVBP will be disscussed in chapter 6 and 7, respectively.

Overall, these results suggest that mechanical loading delays the incidence and reduces PCa skeletal tumour and preseves the bone structure frome PCa osteolytic lesions. Since current treatments fail to cure PCa bone metastasis and are associated with adverse effects, we are in need to look for more suitable, less aggressive

therapies that could be applied safely in most patients, in which exercise could be one promising answer (Rhee et al. 2015; Simoneau 2006; Michaelson et al. 2010). Our results suggest that exercise in the form of mechanical stimulus into bone, could impair the development of PCa bone metastasis, emphasising the role of exercise as an adjuvant therapy in patients with PCa.

## 5.4. Conclusion

Mechanical loading delays skeletal tumour onset and significantly preserves bone integrity by reducing cancer-related osteolysis. Translated to patients with PCa, this could be related with reduced SRE and a better life expectancy. Overall, appropriate exercise regimens, related to the patient stage and conditions, could delay the onset of PCa bone metastasis and decrease osteolytic bone lesions, suggesting exercise as a novel acceptable therapy.

# CHAPTER 6:

## Treadmill running affects the development of PCa bone metastasis in the presence of an intact immune system

## 6.1. Introduction

Running is one of the most popular weight-bearing exercises which is associated with a healthy lifestyle and longevity (Williams 2009; Schneider et al. 2009; Lee et al. 2017). It is a convenient exercise as it does not require special equipment, can be performed at open air, and even slow-jogging is considered to be vigorous-intensity physical activity, reaching the recommended levels of physical activity which is linked to commitment of the patient to this type of exercise and benefits in health (Ainsworth et al. 2011; Centers for Disease Control 2011).

Given the benefits of running exercise, some researchers have assessed the effect of running in patients with PCa. An example is the study carried out by Kenfield et al. (2011) where he compared the effect of vigorous vs non-vigorous exercise in patients with localised PCa (no evidence of metastasis). Within the vigorous exercises, running (10 min/mile or faster) was included while non-vigorous exercises consisted of walking to work and weightlifting. This group found 61% lower risk of death due to PCa in patients who performed ≥ 3 hours per week of vigorous exercise compared to those who performed less than 1 hour per week of vigorous exercise. In line with this study, Richman et al. (2011) identified a reduced PCa progression in patients who performed vigorous activity and walking at a brisk pace.

In respect of *in vivo* models, Esser et al. (2009) subjected TRAMP mice (which develop spontaneous PCa) to voluntary wheel running to assess its effect in PCa development. The mice which performed more than 5km/day of running displayed an ~83% prostate classified histologically as “within normal levels” while those which ran less than 5km/day presented the same type of histological benefit in only ~43% of the prostate. In another experiment, SCID male mice were subcutaneously injected with PC3 cells, one week post voluntary treadmill running (1.38±0.21 miles/day), finding 32% lower ratio of mitotic/apoptotic cells in the subcutaneous tumours versus controls (Zheng et al. 2008). Finally, another study involving voluntary treadmill running led to 60% reduction of tumour incidence among 5 xenograft models (Pedersen et al. 2016).

The mentioned evidence supports running exercise as a positive factor to counteract PCa development. However, there is a lack of knowledge regarding its effect into PCa

bone metastasis. To clarify such enigma, we adopted the mouse treadmill running regimen from the study of Wallace et al. (2007), as it was successful in achieving an osteogenic response perceived as: a greater cortical area, medial-lateral width in the mid-diaphysis, increased periosteal and endocortical perimeters and increased bone mineral density in 8-week-old male C57BL6/129 mice. The treadmill regimen consisted of 12 meters/minute speed, 5° incline for 30 minutes/day, 7 days/week for 21 consecutive days.

The same treadmill running protocol was applied into BALB/C nude and C57BL/6 mice for 5 days per week instead of 7 days per week as in Wallace's et al. (2007) protocol. The BALB/C nude mice were inoculated intracardiacally with human PC3 cells (~100,000 cells/injection in ~100µl PBS) and the C57BL/6 mice were inoculated with murine RM1 PCa cells at the same cells/injection concentration. The treadmill running regimen was performed for 3 weeks during which the tumour growth was tracked by bioluminescence assay weekly and the bone structure analysed *ex vivo* at the end of the experiment. Treadmill running design detailed in section 2.5.

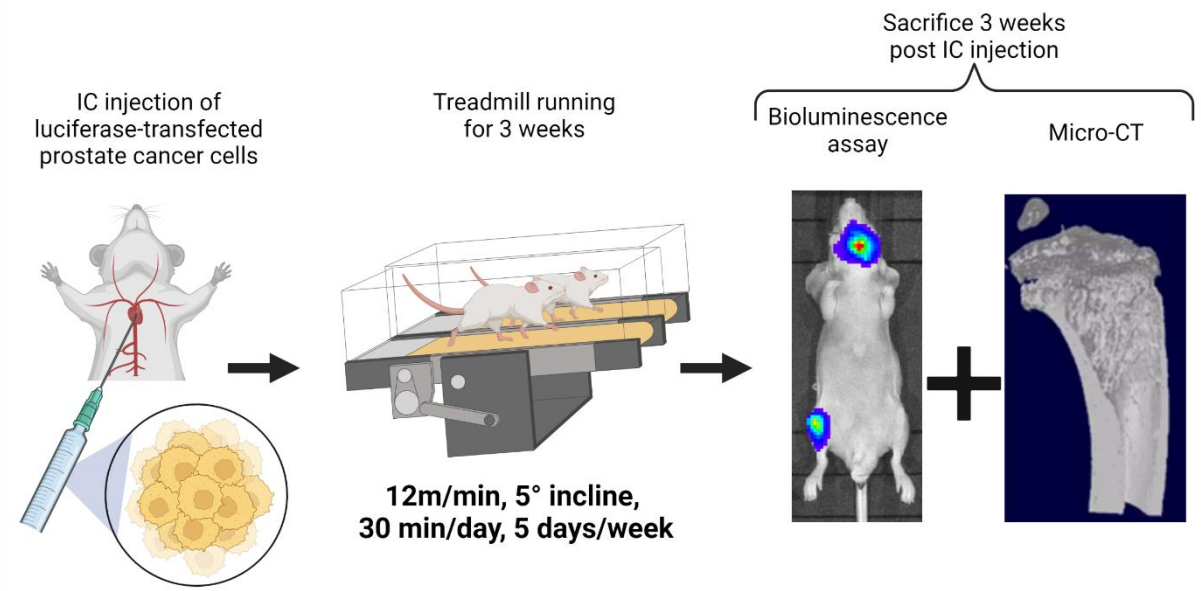


**Figure 6. 1. Schematic outline of mice xenograft model subjected to treadmill running exercise**. *The mice were inoculated intracardiacally with luciferase tagged PCa cells (human PC3 or murine RM1 PCa cells), followed by treadmill running exercise for 3 weeks. Tumour growth was monitored weekly by bioluminescence assay and bone structure analysed using Micro-CT technique.*

## 6.2. Results

### 6.2.1. Treadmill running increases the development of PCa bone metastasis in a PC3 IC xenograft model.

8-week-old BALB/c nude mice were IC injected with the PCa cell line PC3 and subjected to treadmill running as described in section 2.5. The tumour burden at the end of the experiment can be appreciated among the treadmill and sedentary groups, figure 6.2 A. The hindlimb tumour incidence was significantly higher in the treadmill group, reaching a significant lower incidence at week 2 and a tendency to significance at week 3, figure 6.2 B and C, chi-square, n=8, p= 0.0019 and p= 0.0547, respectively. The tumour burden was found significantly higher in the whole-body of the mice subjected to treadmill running compared to sedentary controls, figure 6.2 D, Mann-Whitney test, n=8, p= 0.0244.

### 6.2.2. Treadmill running does not protect cancer induced bone destruction in the PC3 xenograft model

The Micro-CT technique was performed into the left tibias of the mice subjected to treadmill running exercise and the sedentary controls *ex vivo* to study the bone morphometry changes. The bone parameters measured were introduced as in 3.2.1.2 and 3.2.1.3 using the CTan software. In the PC3 IC mice model no differences were observed between the exercised and sedentary controls (Table 6.1, n≥8, unpaired t-test). This result suggests that the treadmill running protocol we applied in this xenograft model is not sufficient to offer protection from the bone destruction caused by PCa bone metastases.

### 6.2.3. Three weeks treadmill exercise does not enhance bone mass in naïve BALB/c nude mice .

In order to study the effect of treadmill running at a baseline level in its possible effect in PCa development, we subjected naïve BALB/c nude mice (n=6) to our treadmill

protocol versus sedentary controls (n=7). The left tibia of both groups was analysed *ex vivo* by means of Micro-CT technique. According to the Micro-CT analysis, no significant results were obtained in the bone parameters analysed in the exercised mice and controls (table 6.2, n≥6, unpaired t-test). This suggests that the treadmill protocol applied in the naïve mice is not sufficient to increase bone mass at a tissue level. To complement the Micro-CT results, we performed histomorphometry in the left tibia of both groups as a mean to understand the changes at a cellular level. See next section.

### 6.2.4. Treadmill running causes a mild response at a bone cellular level in BALB/c nude naïve mice

In order to study the bone cellular changes at a baseline level, histomorphometry analysis was carried out using a DMRB microscope (Leica, Wetzlar, Germany) at 20x magnification with the Osteomeasure7 v4.2.0.1 (OsteoMetrics) software to quantify the osteoblasts and osteoclasts cells among the treadmill exercised naïve BALB/c nude mice (n=6) and sedentary controls (n=7), more details in section 2.8. The osteoblast quantity was significantly higher in the medial endocortical side versus controls (figure 6.3 A and B, p= 0.0160, n≥7, unpaired t-test) as well as the surface occupied (figure 6.3 A and C, p= 0.0125, n≥7, unpaired t-test). No significant changes were observed in other osteoblast and osteoclast paratmenters when comparing the exercised vs control mice, table 6.3, unpaired t-test. However, It is likely that this running regimen was starting to induce an osteogenic response in the bone areas subjected to more strain but it was not sufficient to promote an overall improved bone structure as suggested by the Micro-CT results.

### 6.2.5. Treadmill running does not cause a significant impact in the cytokine profile of BALB/c nude naïve mice.

To understand whether treadmill exercise induced changes in systemic cytokine landscape which have been shown to influence PCa bone metastasis, the cytokine profile of the treadmill exercised mice and the sedentary controls was studied by the Bio-Plex Pro Mouse Cytokine multiplex assays (23 cytokines), more details in section

2.12.3. The cytokine levels of the exercised and controls naïve mice were not significantly different. Only the cytokine Eotaxin was found significantly lower in the exercised mice (table 6.4, n=6, p= 0.0148, unpaired t-test). This cytokine is associated with the recruitment of eosinophils in sites of inflammation and will be later discussed (Lacy 2017a).

A)

Control

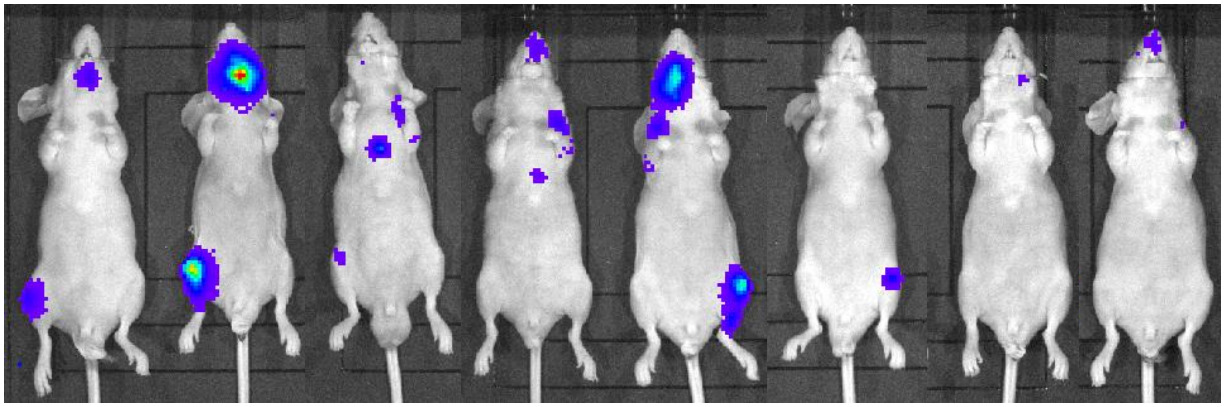

Treadmill group

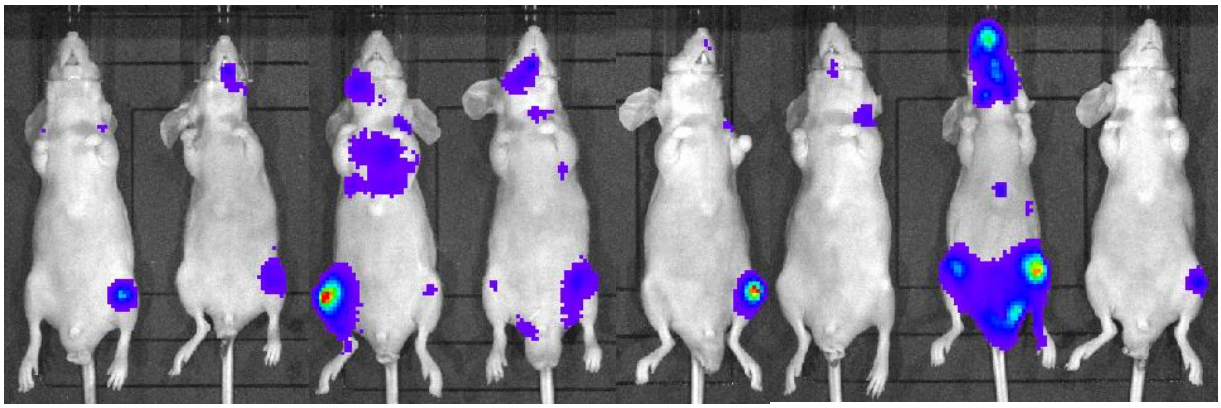

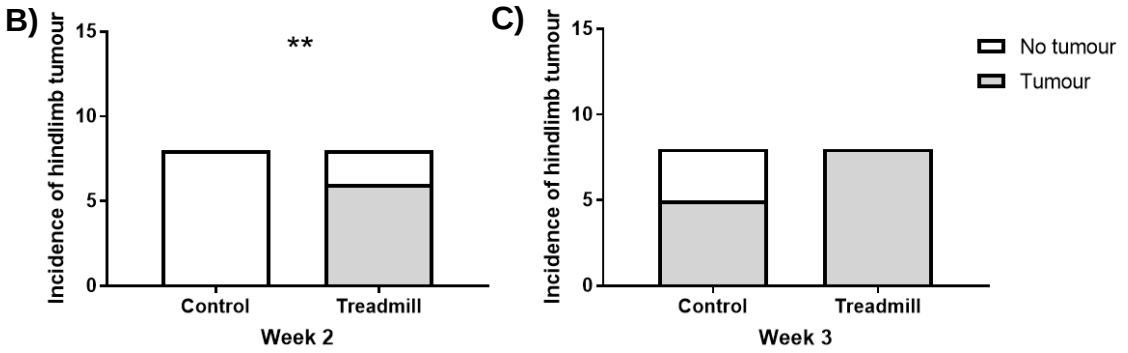


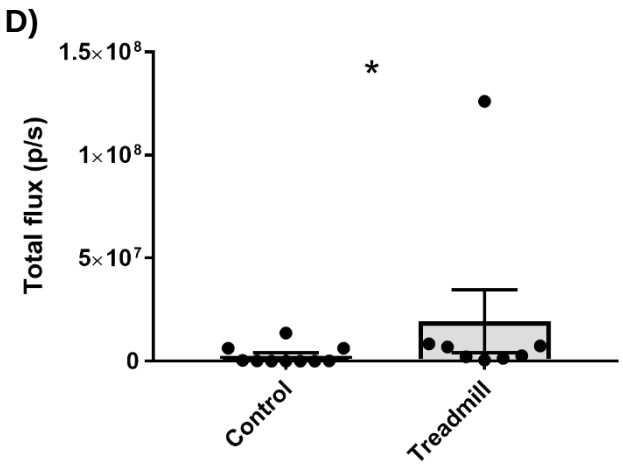

**Figure 6. 2. The effect of treadmill running on the development of PCa bone metastasis in an intracardiacally PC3 injected xenograft model.** *The human PCa cell line PC3 was intracardiacally injected in 8-week-old BALB/c nude mice followed by 3 weeks of treadmill running. A) Endpoint (3 weeks) IVIS pictures of mice subjected to treadmill exercise and control sedentary mice. The skeletal tumour growth was examined weekly by bioluminescence assay, comparing the treadmill exercised mice versus sedentary controls. B) and C) The hindlimb tumour incidence was increased in the treadmill exercise mice at week 2 and 3. The hindlimb tumour incidence was found significantly higher at week two in the mice subjected to treadmill exercise and a tendency to significance at week 3 (figure 6.2 B and C, chi-square, n=8, p= 0.0019 and p= 0.0547, respectively). D) The tumour burden, measured as total flux (photons/second), was significantly higher in the whole body of the exercised mice (Mann-Whitney test, n=8, p= 0.0244). Tumour burden: presented as mean±SEM.*

**Table 6. 1. Quantitative bone morphometry analysis in the left bone tibia of BALB/c nude mice subjected to I.C injection of PC3 cells and treadmill running exercise**

| | Control | Treadmill | Percentage change | P value |
|---|---|---|---|---|
| | n=10 | n=8 | | |
| **BV/TV %** | 7.10 ± 1.19 | 6.10 ± 1.2 | -14.10 | NS |
| **Tb.Th (mm)** | 0.029 ± 0.001 | 0.03 ± 0.001 | 7.44 | NS |
| **Tb.N (1/mm)** | 2.29± 0.37 | 1.94 ± 0.38 | -15.52 | NS |
| **Tb.Sp (mm)** | 0.21± 0.03 | 0.24 ± 0.03 | 12.36 | NS |
| **Tb. Pf (1/mm)** | 55.95 ± 17.83 | 39.67 ± 2.28 | -29.09 | NS |
| **SMI** | 2.13 ± 0.20 | 2.07 ± 0.07 | -2.89 | NS |
| **DA** | 9.19 ± 7.12 | 2.06 ± 0.08 | -77.50 | NS |
| **Ct. BV** | 0.68 ± 0.02 | 0.68 ± 0.02 | 0.14 | NS |

Values are mean ± SEM

Percentage changes = (Treadmill mean – Control mean)/Control mean × 100

NS= non-significant

**Table 6. 2. Quantitative bone morphometry analysis in the left tibia of a naïve BALB/c nude mice model subjected to treadmill running exercise**

| | Control | Treadmill | Percentage change | P value |
|---|---|---|---|---|
| | n=7 | n=6 | | |
| **BV/TV %** | 12.83 ± 0.53 | 11.75 ± 0.83 | -8.41 | NS |
| **Tb.Th (mm)** | 0.03 ± 0.001 | 0.03 ± 0.0006 | 4.88 | NS |
| **Tb.N (1/mm)** | 3.42 ± 0.14 | 2.97 ± 0.22 | -12.89 | NS |
| **Tb.Sp (mm)** | 0.15 ± 0.006 | 0.16 ± 0.006 | 6.81 | NS |
| **Tb. Pf (1/mm)** | 42.09 ± 3.79 | 43.44 ± 2.09 | 3.20 | NS |
| **SMI** | 2.32 ± 0.08 | 2.50 ± 0.08 | 7.61 | NS |
| **DA** | 2.36 ± 0.08 | 2.18 ± 0.04 | -7.76 | NS |
| **Ct. BV** | 0.71 ± 0.01 | 0.74 ± 0.01 | 4.33 | NS |

Values are mean ± SEM

Percentage changes = (Treadmill mean – Control mean)/Control mean × 100

NS= non-significant

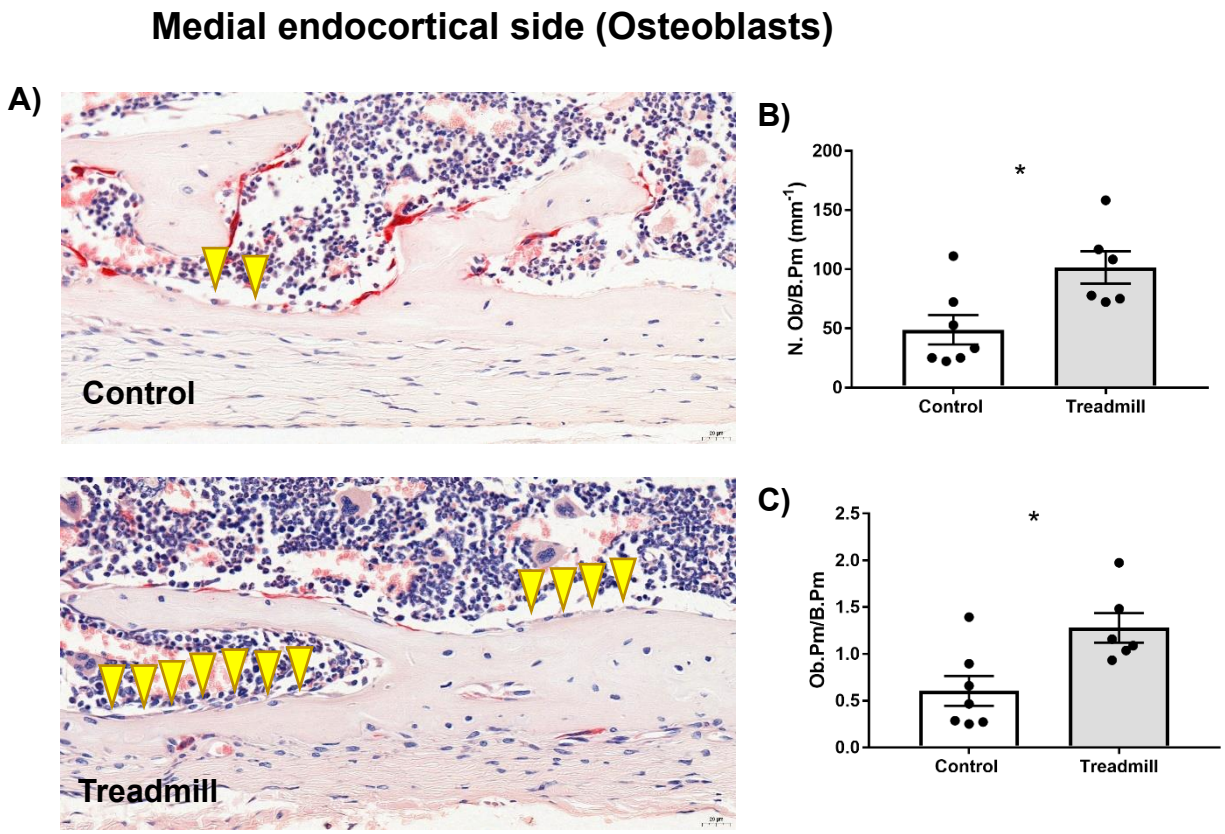


**Figure 6. 3. Treadmill running increases the quantity and surface occupied by osteoblasts in the medial endocortical region of naïve BALB/c nude mice**. *The left tibia bone sections of exercise and sedentary naïve BALB/c nude mice were TRAP-stained to identify the osteoblasts and osteoclasts bone cells. Bone cells were quantified 0.15 mm away from the growth plate on the medial endocortical region under a DMBR microscope using the Osteomeasure bone histomorphometry software. A) Yellow arrows indicate cobblestone like-cuboidal osteoblasts cells on the medial endocortical surface. B) Quantification of the osteoblast number per mm in the medial endocortical bone surface (N.Ob/B.Pm). C) Quantification of the percentage of surface occupied by osteoblasts (Ob.Pm/B.Pm) Scale bar= 20µm. All data is presented as mean±SEM. n≥6, *p<0.05, unpaired t-test.*

**Table 6. 3. Histomorphometry analysis in the left tibia of naïve BALB/c nude mice subjected to treadmill exercise**

| Bone region analysed | Cell type quantified | Number of cells | | | | Perimeter of cells/bone perimeter | | | |
|---|---|---|---|---|---|---|---|---|---|
| | | Control | Treadmill | Percentage change | P value | Control | Treadmill | Percentage change | P value |
| **Lateral endocortical** | Osteoblasts | 471.7±44.77 | 485.6±48.1 | 2.94 | NS | 3.33±0.25 | 3.50± 0.20 | 5.03 | NS |
| | Osteoclasts | 0 | 0 | - | NS | 0 | 0 | - | NS |
| **Medial endocortical** | **Osteoblasts** | **48.81±12.46** | **101.4±13.7** | **107.74** | ***** | **0.60±0.15** | **1.27±0.15** | **111.76** | ***** |
| | Osteoclasts | 2.77±1.21 | 6.01±2.90 | 116.66 | NS | 0.07±0.04 | 0.19±0.09 | 166.63 | NS |
| **Trabecula** | Osteoblasts | 103.2±12.27 | 155±28.54 | 50.19 | NS | **3.33±0.25** | **2.02±0.36** | **-39.37** | ***** |
| | Osteoclasts | 43.82±4.99 | 43.45±4.05 | -0.84 | NS | 0.98±0.12 | 1.43±0.24 | 45.57 | NS |

Values are mean ± SEM

Percentage changes = (Treadmill mean – Control mean)/Control mean × 100

**p=<0.05* (unpaired t-test)

**Table 6. 4. Quantitative analysis of a 23-cytokine profile panel of naïve BALB/c nude mice subjected to treadmill running exercise**

| | Control | Treadmill | Means difference | P value |
|---|---|---|---|---|
| | n=6 | n=6 | | |
| **IL-3** | 3.32 ± 0.51 | 3.77 ± 0.67 | 13.47 | NS |
| **IL-1b** | 10.19 ± 1.66 | 11.35 ± 2.17 | 11.38 | NS |
| **TNF-α** | 365.7 ± 33.71 | 319.1 ± 62.35 | -12.74 | NS |
| **IL-9** | 131.8 ± 15.19 | 115.1 ± 20.05 | -12.67 | NS |
| **IFN-γ** | 109.2 ± 13.31 | 99.35 ± 18.76 | -9.02 | NS |
| **IL-2** | 9.34 ± 1.74 | 10.62 ± 2.05 | 13.65 | NS |
| **IL-13** | 233.5 ± 33.28 | 215.3 ± 39.98 | -7.79 | NS |
| **IL-6** | 9.72 ± 0.73 | 9.30 ± 1.25 | -4.35 | NS |
| **IL-4** | 9.54 ± 1.22 | 9.16 ± 1.48 | -4.002 | NS |
| **MCP-1** | 490.5 ± 18.88 | 472.4 ± 49.16 | -3.69 | NS |
| **IL-5** | 25.61 ± 2.401 | 26.06 ± 4.36 | 1.75 | NS |
| **IL-1a** | 13.81 ± 1.61 | 14.1 ± 2.16 | 2.09 | NS |
| **G-CSF** | 145.9 ± 8.58 | 152.7 ± 11.1 | 4.66 | NS |
| **RANTES** | 204.6 ± 23.67 | 200.9 ± 32.38 | -1.80 | NS |
| **IL-10** | 119.8 ± 9.699 | 141.6 ± 64.16 | 18.19 | NS |
| **KC** | 75.21 ± 2.31 | 67.64 ± 4.187 | -10.06 | NS |
| **IL-17A** | 83.99 ± 6.96 | 103 ± 14.88 | 22.63 | NS |
| **GMCSF** | 142 ± 8.27 | 137.1 ± 16.87 | -3.45 | NS |
| **Eotaxin** | **3080 ± 262.8** | **1876 ± 314.7** | **-39.09** | ***** |
| **MIP-1b** | 248.8 ± 14.42 | 228.2 ± 16.57 | -8.27 | NS |
| **IL-12p40** | 1949 ± 213.6 | 1854 ± 141.6 | -4.87 | NS |
| **MIP-1a** | 10.98 ± 0.26 | 10.37 ± 0.81 | -5.55 | NS |
| **IL-12p70** | 207.2 ± 24.58 | 210.5 ± 37.63 | 1.59 | NS |

Values are mean ± SEM

Percentage changes = (Treadmill mean – Control mean)/Control mean × 100

NS: Non-significant

**p=<0.05* (unpaired t-test)

### 6.2.6. Treadmill running reduces the incidence and development of PCa bone metastasis in a RM1 syngeneic model.

8-week-old C57BL/6 mice were IC injected with the murine PCa cell line RM1 and subjected to treadmill running as described in section 2.5. The tumour burden at the end of the experiment can be appreciated among the treadmill and sedentary groups, ,figure 6.4 A. The hindlimb tumour incidence was delayed by treadmill running, reaching a significant lower incidence at week 3 of running exercise, figure 6.4 B-D, chi-square, n=12, p= 0.035. The tumour burden was found significantly lower at day 14 in the exercised mice compared to controls, figure 6.4 E, Mann-Whitney test, n=11, p= 0.0158. However, at day 18 the tumour burden was not significant different in both groups, figure 6.4 F, n=11, Mann-Whitney test.

### 6.2.7. Treadmill running does not protect cancer induced bone destruction in the RM1 syngeneic model

Bone morphometry changes in mice subjected to treadmill running exercise and RM1 cells IC injection were examined using the left tibia of the mice and micro-CT *ex vivo*. The bone parameters measured using the CTan software were listed in 3.2.1.2 and 3.2.1.3. In the RM1 IC mice model the trabecula thickness was found significantly increased compared to controls, table 6.5, n≥11, p=0.0005, unpaired t-test. Additionally, the trabecula bone volume fraction and trabecula number were increased ~28% and 12%, respectively, table 6.5. No significant differences were observed in the aditional bone structure parameters. To further confirm whether the bone structure changes were result of the treadmill running exercise, we subjected the same mice strain (n≥6) to the treadmill running protocol for 3 weeks. The results of the baseline experiment are described in the next section.

### 6.2.8. Treadmill running does not improve the bone structure parameters in naïve C57BL/6 mice

In order to study whether the changes in the bone structure of the syngeneic C57BL/6 mice model were consequence of the treadmill running protocol, naïve C57BL/6 mice

(n≥6) were subjected to the same running protocol for 3 weeks. The left tibia of the naïve mice was analysed *ex vivo*, comparing the exercised and control groups using micro-CT. According to the Micro-CT analysis, no differences were observed in the bone structure parameters of the left tibias between both groups (table 6.6, n≥6, unpaired t-test).

### 6.2.9. Treadmill running causes a mild response at a bone cellular level in C57BL/6 naïve mice

In order to study the bone cellular changes at a baseline level we used a group of 8-week-old naïve C57BL/6 mice running mice (n=6) as well as sedentary controls (n=7). Histomorphometry analysis was carried out in the left tibia section using a DMRB microscope (Leica, Wetzlar, Germany) at 20x magnification with the Osteomeasure7 v4.2.0.1 (OsteoMetrics) software to quantify the osteoblasts and osteoclasts cells. Histomorphometry is fully detailed in section 2.8. The osteoblast quantity was significantly lower in the trabecula region of exercised mice compared to controls, figure 6.5 A-C, unpaired t-test, n≥6, p= 0.0267. Additionally, the osteoblast quantity and surface occupied was ~69% and ~64% higher in the medial endocortical surface of the exercised mice when compared to controls (figure 6.5 D-F, n≥6). No significant differences were observed in the remaining histomorphometry parameters (table 6.7). As in the BALB/c nude mice, it is likely that this running protocol of 3-week has started to induce an osteogenic response which was not sufficient to reach the tissue levels and to be observed using techniques such as miccro-CT.

### 6.2.10. Treadmill running does not cause a significant impact in the cytokine profile of C57BL/6 naïve mice.

The cytokine profile of the treadmill exercised mice and the sedentary controls was studied by means of the multiplex assay which provides information regarding 23-mice cytokines, more details in section 2.12.3. The cytokine levels of the exercised and controls naïve mice were not significantly different (table 6.8). Only the cytokine IL-17A was found significantly lower in the exercised mice (table 6.8, n=7, p= 0.0398,

unpaired t-test).This cytokine is associated with the innate immune response and will be later discussed (Zenobia & Hajishengallis 2016).

**A)** Control

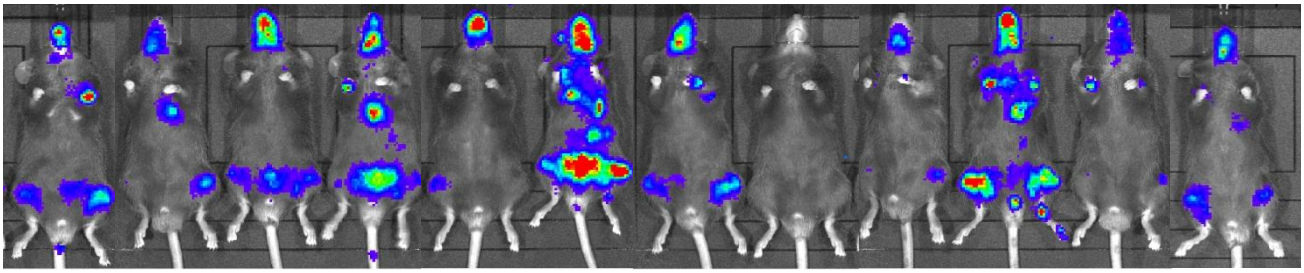

Treadmill group

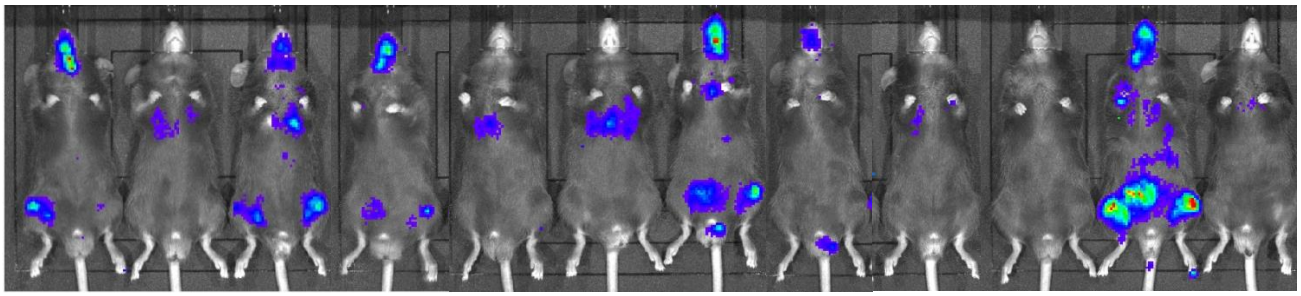


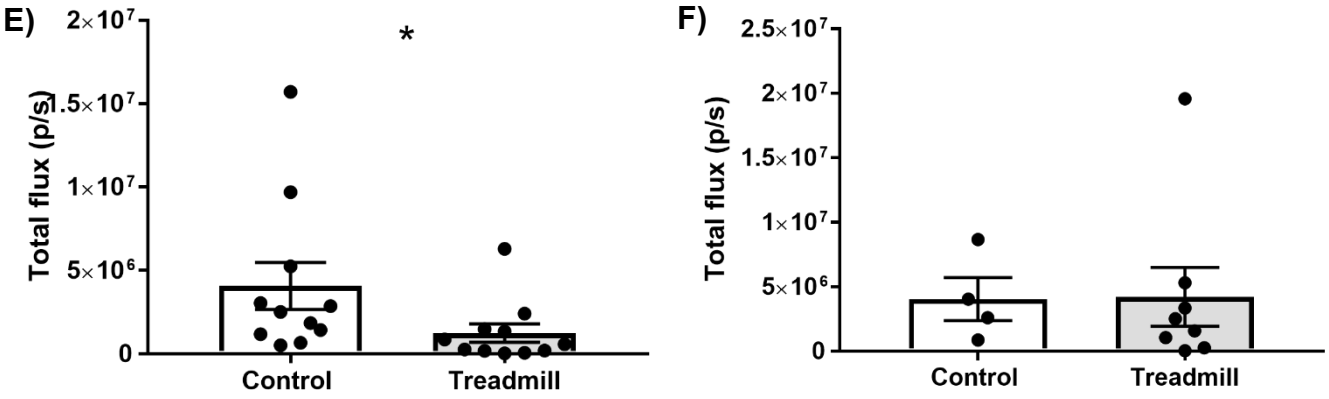

**Figure 6. 4. The effect of treadmill running on the development of PCa bone metastasis in an intracardiacally RM1 injected syngeneic model.** *The murine PCa cell line RM1 was intracardiacally injected in 8-week-old C57BL/6 mice followed by 3 weeks of treadmill running. A) Endpoint (3 weeks) IVIS pictures of mice subjected to treadmill exercise and control sedentary mice. The skeletal tumour growth was examined weekly by bioluminescence assay, comparing the treadmill exercised mice versus sedentary controls. B)- D) The hindlimb tumour incidence was delayed by treadmill exercise during the three weeks of running regimen. The hindlimb tumour incidence was found significant lower at week three in the mice subjected to treadmill exercise (chi-square, n=12, p=0.035). E) The whole-body tumour burden, measured as photons/second, was significantly lower in the exercised mice (Mann-Whitney test, n=11, p= 0.0158,).at day 14 of running. F) At the end of the experiment the tumour burden was not significantly different in both groups. Tumour burden: presented as mean±SEM.*

**Table 6. 5. Quantitative bone morphometry analysis in the left bone tibia of C57BL6 mice subjected to I.C injection of RM1 cells and treadmill running exercise**

| | Control | Treadmill | Percentage change | P value |
|---|---|---|---|---|
| | **n=6** | **n=7** | | |
| **BV/TV %** | 18.51±1.14 | 19.9±1.52 | 7.50 | NS |
| **Tb.Th (mm)** | **0.04±0.001** | **0.04±0.001** | **5.53** | ******* |
| **Tb.N (1/mm)** | 4.21±0.18 | 4.27±0.16 | 1.44 | NS |
| **Tb.Sp (mm)** | 0.12±0.004 | 0.13±0.005 | 6.08 | NS |
| **Tb. Pf (1/mm)** | 31.41±3.01 | 27.24±2.27 | -13.27 | NS |
| **SMI** | 2.08±0.12 | 1.93±0.12 | -7.37 | NS |
| **DA** | 2.55±0.07 | 2.49±0.05 | -2.27 | NS |
| **Ct. BV** | 0.98±0.05 | 0.90±0.05 | -7.90 | NS |

Values are mean ± SEM

Percentage changes = (Treadmill mean – Control mean)/Control mean × 100

NS=non-significant

****p=< 0.001* (unpaired t-test)

**Table 6. 6. Quantitative bone morphometry analysis in the left bone tibia of naïve C57BL6 mice subjected to treadmill running exercise**

| | Control | Treadmill | Percentage change | P value |
|---|---|---|---|---|
| | n=6 | n=7 | | |
| **BV/TV %** | 18.51±1.14 | 19.9±1.52 | 7.50 | NS |
| **Tb.Th (mm)** | 0.04±0.001 | 0.04±0.001 | 5.53 | NS |
| **Tb.N (1/mm)** | 4.21±0.18 | 4.27±0.16 | 1.44 | NS |
| **Tb.Sp (mm)** | 0.12±0.004 | 0.13±0.005 | 6.08 | NS |
| **Tb. Pf (1/mm)** | 31.41±3.01 | 27.24±2.27 | -13.27 | NS |
| **SMI** | 2.08±0.12 | 1.93±0.12 | -7.3 | NS |
| **DA** | 2.55±0.07 | 2.49±0.05 | -2.27 | NS |
| **Ct. BV** | 0.98±0.05 | 0.90±0.05 | -7.90 | NS |

Values are mean ± SEM

Percentage changes = (Treadmill mean – Control mean)/Control mean × 100

NS=non-significant

## Trabecula region (Osteoblasts)

A)

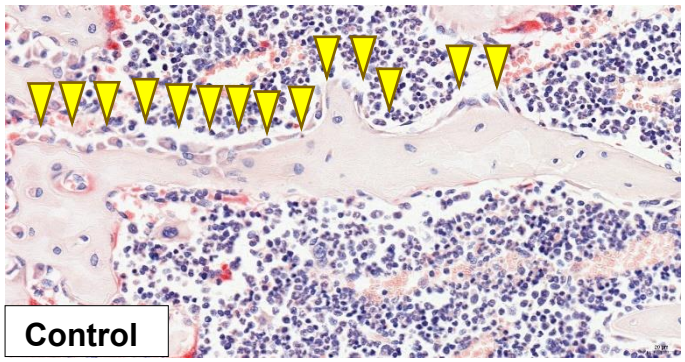


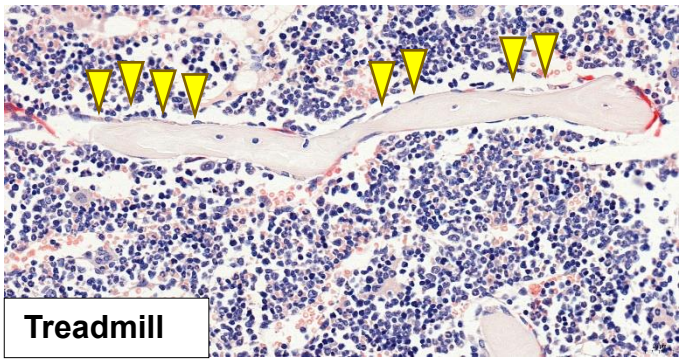


B)

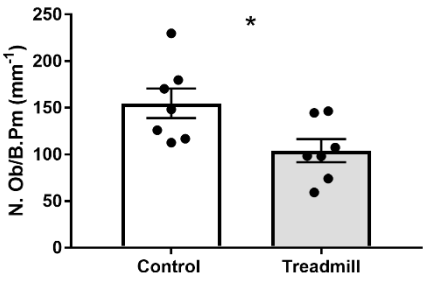


C)

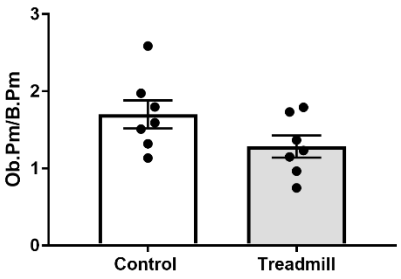


## Medial endocortical side (Osteoblasts)

D)

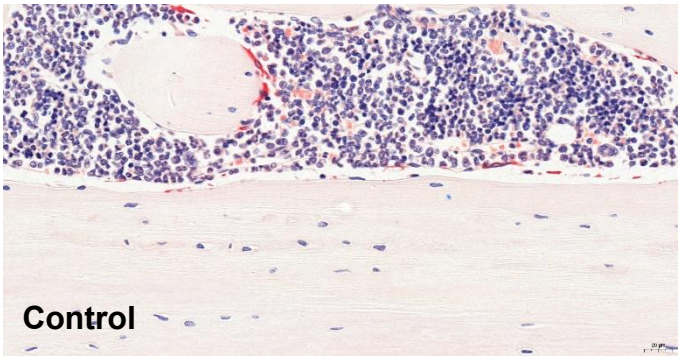


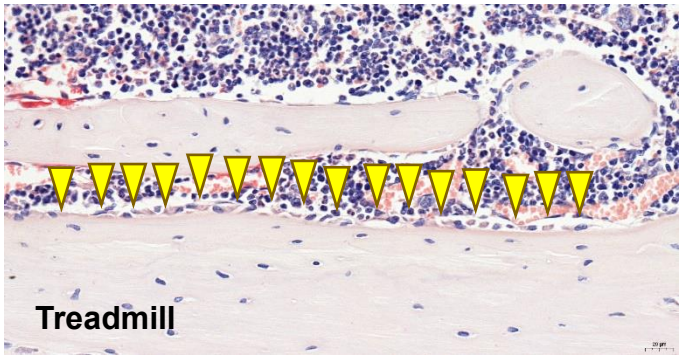


E)

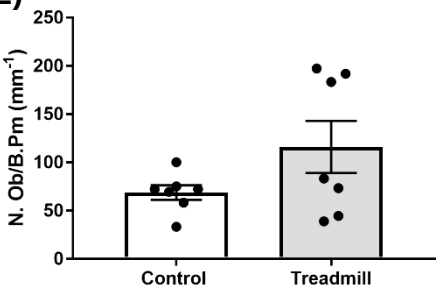


F)

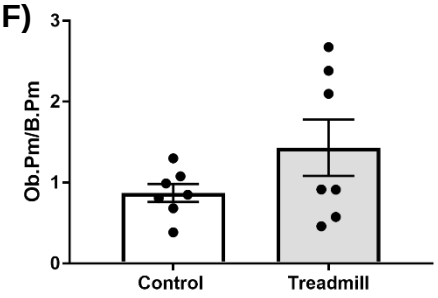

**Figure 6. 5. Treadmill running decreases the osteoblasts quantity in the trabecula region and increases the quantity and surface occupied by osteoblasts in the medial endocortical region of naïve C57BL/6 nude mice**. *The left tibia bone sections of exercise and sedentary naïve C57BL/6 mice were TRAP-stained to identify the osteoblasts and osteoclasts bone cells. Bone cells were quantified 0.15 mm away from the growth plate on the medial endocortical region under a DMBR microscope using the Osteomeasure bone histomorphometry software. A) Yellow arrows indicate cobblestone like-cuboidal osteoblasts cells on the trabecula endocortical surface and D) in the medial region. B) and E) Quantification of the osteoblast number per mm in the trabecula region and medial endocortical surface, respectively (N.Ob/B.Pm). C) and F) Quantification of the percentage of surface occupied by osteoblasts (Ob.Pm/B.Pm) Scale bar= 20µm. All data is presented as mean±SEM. n=7, *p<0.05, unpaired t-test.*

**Table 6. 7. Quantitative analysis of the number and surface occupied of bone cells (osteoblasts and osteoclasts ) in the left tibia of naïve C57BL/6 mice subjected to treadmill exercise.**

| Bone region analysed | Cell type quantified | Number of cells | | | | Perimeter of cells/bone perimeter | | | |
|---|---|---|---|---|---|---|---|---|---|
| | | Control | Treadmill | Percentage change | P value | Control | Treadmill | Percentage change | P value |
| **Lateral endocortical** | Osteoblasts | 431±47.81 | 371.8±47.72 | -13.73 | NS | 3.21±0.22 | 3.13±0.16 | -2.39 | NS |
| | Osteoclasts | 0.79±0.79 | 3.96±1.90 | 399.93 | NS | 0.01±0.01 | 0.08±0.05 | 430.17 | NS |
| **Medial endocortical** | Osteoblasts | 68.65±7.56 | 116±27.08 | 68.97 | NS | 0.86±0.11 | 1.43±0.34 | 64.51 | NS |
| | Osteoclasts | 16.11±3.22 | 12.78±6.86 | -20.67 | NS | 0.51±0.10 | 0.26±0.13 | -48.40 | NS |
| **Trabecula** | **Osteoblasts** | **154.7±15.8** | **103.9±12.35** | **-32.83** | * | 1.70±0.18 | 1.28±0.14 | -24.57 | NS |
| | Osteoclasts | 67.86±10.1 | 46.43±4.61 | -31.57 | NS | 1.59±0.25 | 1.13±0.13 | -28.84 | NS |

Values are mean ± SEM

Percentage changes = (Treadmill mean – Control mean)/Control mean × 100

NS: Non-significant

*$p=<0.05$ (unpaired t-test)

**Table 6. 8. Quantitative analysis of a 23-cytokine profile panel of naïve C57BL/6 mice subjected to treadmill running exercise**

| | Control | Treadmill | Percentage change | P value |
|---|---|---|---|---|
| | n=6 | n=7 | | |
| **IL-3** | 3.12±0.50 | 3.49±0.58 | 12.11 | NS |
| **IL-1b** | 9.74±2.52 | 5.63±0.83 | -42.15 | NS |
| **TNF-α** | 271.1±36.26 | 220.7±17.11 | -18.59 | NS |
| **IL-9** | 84.19±15.11 | 55.15±4.51 | -34.49 | NS |
| **IFN-γ** | 69.05±12.96 | 46.15±3.67 | -33.16 | NS |
| **IL-2** | 9.93±2.18 | 8.36±1.38 | -15.87 | NS |
| **IL-13** | 169.4±41.64 | 96.37±12.04 | -43.11 | NS |
| **IL-6** | 17.18±4.58 | 12.09±2.84 | -29.62 | NS |
| **IL-4** | 7.99±1.81 | 6.33±0.73 | -20.68 | NS |
| **MCP-1** | 465±48.55 | 393.5±17.9 | -15.37 | NS |
| **IL-5** | 23.31±4.29 | 16.46±2.02 | -29.38 | NS |
| **IL-1a** | 14.58±2.52 | 12.93±1.71 | -11.31 | NS |
| **G-CSF** | 483.6±136.7 | 336.3±85.01 | -30.45 | NS |
| **RANTES** | 200.7±23.98 | 176.9±13.46 | -11.85 | NS |
| **IL-10** | 116.9±11.61 | 90.33±9.108 | -22.72 | NS |
| **KC** | 84.7±10.9 | 91.82±7.39 | 8.40 | NS |
| **IL-17A** | **93.43±4.82** | **122.2±10.61** | **30.79** | ***** |
| **GMCSF** | 121.8±13.76 | 100.2±7.22 | -17.73 | NS |
| **Eotaxin** | 2598±330.2 | 2431±222.8 | -6.42 | NS |
| **MIP-1b** | 155.9±9.61 | 153.5±8.12 | -1.53 | NS |
| **IL-12p40** | 866.3±66.12 | 894±62.05 | 3.19 | NS |
| **MIP-1a** | 8.74±0.75 | 8.26±0.72 | -5.51 | NS |
| **IL-12p70** | 205.6±18.02 | 198.7±19.94 | -3.35 | NS |

Values are mean ± SEM

Percentage changes = (Treadmill mean – Control mean)/Control mean × 100

NS: Non-significant

**p=<0.05* (unpaired t-test)

## 6.3. Discussion

Running exercise is an attractive type of exercise due to its overall health benefits and because of the easy manner it can be performed. Several studies have assessed the effect of running exercise in patients with PCa, observing general benefits such as lower risk of death due to PCa and reduced PCa progression (Stacey A. Kenfield et al. 2011; Richman et al. 2011). Benefits of running exercise into lower PCa progression have been also observed in *in vivo* models as well as improvement in their bone structure. However, no studies have linked the benefit of running exercise and PCa bone metastasis (Esser et al. 2009; Zheng et al. 2008; Pedersen et al. 2016). To solve this question, we subjected PCa xenograft and syngeneic mice models to a 3-week treadmill running exercise regimen, which have been suggested to improve the bone structure of naïve mice models (Wallace et al. 2007).

In the immunocompromise mice model, we observed an increase tumour burden of the mice subjected to treadmill exercise. One explanation could be that the treadmill exercise we subjected the mice to initially was detrimental to the bone. During the early stage of the exercise, the metabolism of considered “non-life saving” organs (as the bone) is taken to a second plane as the energy expenditure will be used by organs required in “life-threaten” situations, such as the brain, liver, and skeletal muscle (Lombardi et al. 2016). Additionally, bone reabsorption is needed as a matter to release calcium and make it available for the skeletal muscle, neurotransmitters, and hormones during exercise (Barry et al. 2012; Guillemant et al. 2004; Scott et al. 2012). This means that at the beginning of exercise, the bone metabolism tends to be catabolic, leading to resorption and only the performance of continuous-chronic exercise will be effective in inducing bone formation, as the bone will be adapted to the loading forces applied within time but not when an individual is just starting to be adapted to a new exercise routine.

Another aspect to consider is the duration and pattern of our running protocol. In order to induce an anabolic response in the bone, rest periods between the loading cycles are needed, as enduring activities are suggested to be desensitized (Robling et al. 2000; Srinivasan et al. 2006). Possibly, our continuous running protocol lacked this “rest-period”, leading to the lack of osteogenic response and bone formation. This idea

is supported by recent data which suggest that intermittent running is feasible to improve the bone structure in mice models. Bourzac et al. (2020) subjected male Wistar rats to a continuous and intermittent running protocol. The continuous running consisted of 45 minutes at a moderate speed whilst the intermittent running regimen was performed for 5 min at moderate speed, then 2 min of intensive running and a final 1 min of passive recovery. Both running regimens lasted for 8 weeks, 5 days/week, 45 min/day and were compared with sedentary controls. These authors observed reduced mean cortical surface and osteocyte lacunae occupancy rates as well as increased TRAP-positive surface and apoptotic lacunae. The opposite was analysed in the intermittent exercised mice, where an increased lacunae occupancy and decreased apoptotic lacunae was obtained. They concluded that intermittent running was efficient in inducing cortical bone formation while continuous running drove the bone towards a catabolic status. Additionally, extenuating training lacking rest intervals is linked to impaired immunity (Walsh et al. 2011). Therefore, it is possible that our treadmill running protocol was too intense for these mice and led to an impaired immune response, even in these immunocompromised mice model. The cytokine profile of the naïve BALB/c nude mice showed a significant decrease in eotaxin, a cytokine associated with eosinophils recruitment (Lacy 2017b). BALB/c nude mice still express eosinophil cells, which are associated with anti-tumour activity in PCa (Kusama et al. 1995; Hogan et al. 2003; Furbert-harris et al. 2003; Wener et al. 2014). Therefore, the impaired immune response could have been an adjuvant in PCa tumour progression. This can be further testified by examining whether there are possible reduced eosinophils cells in the exercised mice.

Another reasoning of why the immunocompromised mice showed increased tumour burden could be the starting regimen of treadmill running, as it was performed the following day of IC injection of PCa cells. It has been suggested that voluntary treadmill exercise promotes lung metastasis in a orthotopically BCa mice model (Smeda et al. 2017). This group hypothesised that the voluntary running promoted the perfusion of the primary tumour's cells, leading to enhanced spreading of circulating tumour cells into the lungs. Although we did not utilise an orthotopic model with a PCa primary tumour, the IC injection to model metastasis plus the treadmill running exercise performed the following day, possibly promoted the circulation of the PCa cells throughout the body of the mice, resulting in increased seeding of cancer cells and

metastasis. Therefore, the seeding of the PCa cells into the bone due to treadmill running would complement this study.

As analysed in Chapter 3 and Chapter 4, the ratio of osteoblasts in the medial versus lateral side increased due to mechanical loading and this was linked to the distribution of the PCa cells as evidenced by multiphoton microscopy. Although we did not observe increased bone structure in both naïve mice models, a further Micro-CT analysis of the posterolateral and anteromedial tibia performed by our MSc student Yahui Ning (unpublished data), showed increased bone formation in the anteromedial side of the tibia (i.e., BV/TV, Tb. Th, Tb. N) of the tumour bearing mice subjected to our treadmill running protocol. This suggests that the response to treadmill exercise in tibias is spatially different. The antero-medial tibial region had achieved more bone formation (osteoblast activity) and possibly, lower osteoclast activity, which may be due to higher strain rate compared to the posterolateral region (Patel et al. 2014; Carriero et al. 2014). However, we would need to perform a more detailed histomorphometry analysis to elucidate this hypothesis, meaning, subject naïve mice models to running regimen and analyse the bone cellular changes weekly in order to observe the osteoblast and osteoclast quantity and occupied surface rather than relying only on the end point treadmill running bone cells response.

Interestingly, in the immunocompetent mice model subjected to treadmill running we observed a significant delayed tumour progression 2 weeks post-running training. As we did not observe significant changes in the bone structure in the naïve model, we hypothesise that the lower tumour burden was result of activation of the immune system. From the immune cells, the CD8+ cells are the ones considered to be the main with anti-tumour effects, as they recognize cancer-antigens and promote cancer apoptosis (Resegofetse et al. 2018; Tanaka et al. 1999; Lai et al. 2009). The antitumour effect of CD8+ cells in mice subjected to treadmill running has been assessed by some authors (Pedersen et al. 2016; Rundqvist et al. 2020). Rundqvist et al. (2020) applied a voluntary treadmill protocol into a BCa mice model, finding that the exercised mice had increased CD8+ cells in the BCa tumours, spleen and lymph nodes compared to sedentary controls. Of note, no differences were observed in the infiltration of other immune cells (i.e., CD4+, NK, macrophages nor neutrophils). Depletion of CD8+ cells using anti-CD8 antibodies led to increased tumour growth and

decreased survival. Also, transfusion of CD8+ cells from the exercised mice into the sedentary controls resulted in decreased tumour growth and increased survival in these mice, an effect not seen in non-transferred CD8+ mice. The increased expression of IL-17A in the exercised mice observed in our study could be related to enhanced mobilisation of CD8+ cells into the PCa tumour, as it has been shown to be produced by this type of immune cells, besides the classical expression of IL-17A by the CD4+ (th17 subset), further suggesting the recruitment of CD8+ cells (Kuen et al. 2020; Srenathan et al. 2016; He et al. 2006). Another study showed that voluntary running treadmill was linked to reduced tumour progression in 5 cancer models due to increase infiltration of IL-6 sensitive NK cells, mobilised to tumours linked to increased systemic epinephrine (Pedersen et al. 2016). During exercise, NK cells are the first immune cells to be recruited, followed by T and B cells (Idorn & Hojman 2016). Therefore, in this running protocol, the main effectors cells into reducing the tumour burden could have been the CD8+ and NK cells. However, at the endpoint experiment, the tumour burden was not significant among both groups. It is likely that this running protocol led to a depressive immune status, a consequence of intense training. Exhaustive training without recovery rest periods negatively affects the immune system and increases the risk of infection. It has been shown that endurance athletes such as runners and swimmers/cyclists have lower lymphocytes and NK cells counts, respectively (Baj et al. 1994; Gleeson et al. 2000; Pyne & Barnes 2010). To overcome this issue, a moderate-intensity training for a longer period would be a better approach, as it is linked to improvement of the immune system, better response to vaccines, viral infections, cancer and proliferation and activity of T and NK cells (Bourzac et al. 2020; Simpson et al. 2012; Woods et al. 2009; Lowder et al. 2005; Fairey et al. 2005; Hojman et al. 2011; Khandekar et al. 2011; Nieman et al. 1993; Shinkai et al. 1995; Woods et al. 1999).

Overall, a moderate-intensive running protocol would be a better approach to achieve an osteogenic response and bone formation as well as an enhanced immune surveillance against the PCa tumour. Translating this information to the clinical side, the intensity and duration of the running protocol should be properly adapted to the patient: should be sufficient to enhance bone formation and immune response but not too intensive as it could be detrimental for the bone tissue and the immune system.

## 6.4. Conclusion

The treadmill running regimen applied does not prevent the progression of PCa bone metastasis. The immune system could counteract the development of PCa bone metastasis. A moderate-intensive running regimen would be a better approach to achieve an osteogenic response as well as an effective immune response.

# CHAPTER 7:

## High-frequency low-magnitude vibration platform does not delay the progression of PCa bone metastasis

## 7.1. Introduction

The benefits of exercise in patients with localised PCa have been evaluated by some authors, finding improvement in the muscle strength, functional performance, balance and increased survival (Galvão et al. 2006; Stacey A. Kenfield et al. 2011; Newton et al. 2018) Despite this positive evidence, patients with PCa bone metastasis are deliberately excluded from clinical trials due to possible complications of the exercise routine into the bone, such as pathological fractures, SRE and increase risk of mortality (Courneya & Friedenreich 2011).

In light of this counterproductive effect of exercise into PCa bone metastasis, a safer modality to preserve the bone tissue is needed, in which the WBVP could be a suitable option. The WBVP creates a mechanical signal sensed by the osteocytes as a change in electrical charges which results in the activation of extracellular pathways (i.e., ERK, Runx2) and release of growth factors such as TGF-β and BMP, ultimately leading to osteoblasts differentiation, proliferation, activity and bone formation (Fukada & Yasuda 1957; Xu et al. 2009; Zayzafoon 2006).

One of the first studies which assessed the effect of WBVP found improved bone mass at the level of the femoral neck and spine in postmenopausal women (Rubin et al. 2004). The WBVP stimulus was applied for one year, where control patients had decreased BMD in the femoral neck and spine (2.1% and 1.6%, respectively) whereas the BMD in the same regions in patients on WBVP increased at 0.04% and 0.1%, respectively. Similarly, patients with beta thalassemia were treated with WBVP stimulus, as this disease results in bone loss and pathological fractures (Fung et al. 2012). After 6 months of WBVP treatment, the patients had increase BMC, BMD and increased bone turnover markers (osteocalcin and Ctx). Additionally, the WBVP stimulus has been shown to increase bone the hip bone density and preserved the spine BMD in cyclists compared to cyclist who did not undergo the WBVP stimulus and sedentary controls (Prioreschi et al. 2012). Since then, the effects of WBVP in bone have been reviewed by many authors, finding positive and negative outcomes (Gómez-Cabello et al. 2012; Marín-Cascales et al. 2018).

The introduction of WBVP in BCa survivors improved the muscle activation when frequencies of 20-30 Hz were applied and the perceived exertion also increased with increased frequency (Ruymbeke et al. 2014). In patients with lung cancer or mesothelioma undergoing radical treatment, WBVP increased the maximal workload (Salhi et al. 2015). Finally, Crevenna et al. (2017) evaluated a patient with urinary incontinence post-radical prostatectomy due to PCa. After WBVP treatment, the urinary incontinence ceased, the patient was able to return to work and attend social activities. Despite the positive evidence of WBVP in patients with cancer, no evidence is available regarding the effect of WBVP in patients with PCa bone metastasis.

To investigate the effect of WBVP in PCa bone metastasis, we evaluated a high-frequency low-magnitude vibration (HFVLM) WBVP regimen which has been shown to induce bone formation and major flexural rigidity in ovariectomised mice (Wehrle et al. 2015). The WBVP consisted of 20 minutes/day, 5 days/week for 3 weeks with 0.3 g peak-to-peak acceleration and a frequency of 45Hz, using the Juvent vibration platform. Briefly, eight-week-old male BALB/c nude and C57BL/6 mice (n=10) were intracardiacally injected with PC3 and RM1 cells (~$1x10^5$ cells/injection), respectively. The following day, the mice were placed onto the Juvent vibration platform and stimulated with the WBVP as previously described. The tumour growth and ex vivo Micro-CT analysis were performed in the same manner as the studies for mechanical loading and treadmill exercise. Full description of the WBVP design is explained in section 2.6.

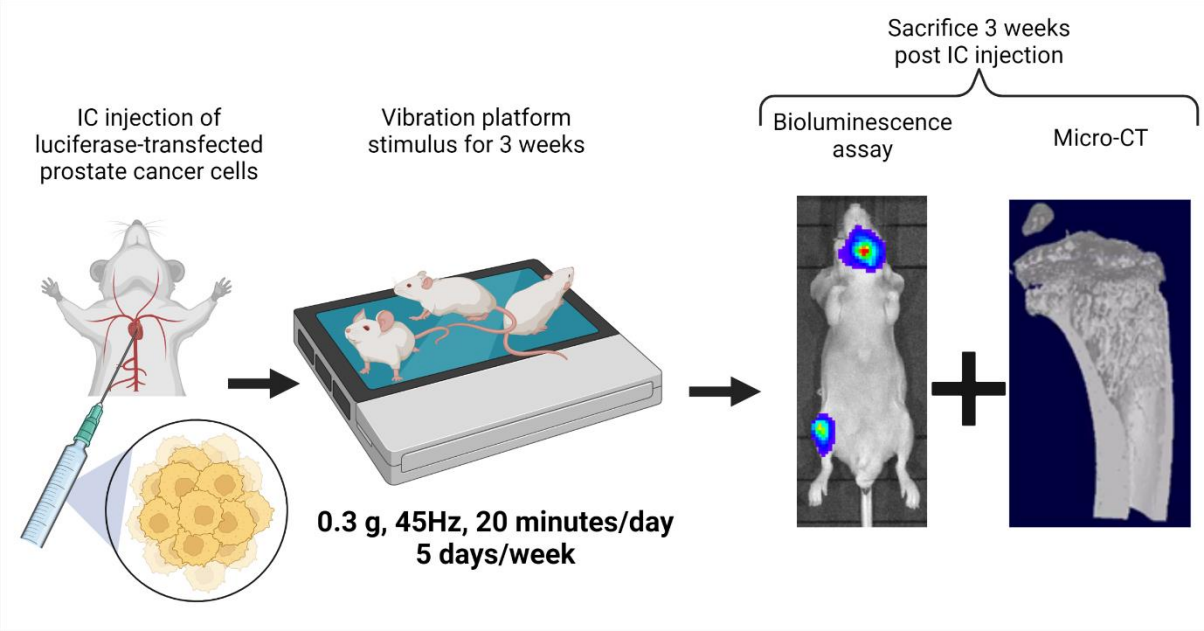


**Figure 7. 1. Schematic outline of mice xenograft model subjected to vibration platform stimulus.** *The mice were inoculated intracardiacally with luciferase tagged PCa cells (PC3), followed by vibration platform for 3 weeks. Tumour growth was monitored weekly by bioluminescence assay and bone structure using Micro-CT technique.*

## 7.2. Results

### 7.2.1. Vibration platform stimulus does not affect the development of PCa bone metastasis in a PC3 IC xenograft model.

8-week-old BALB/c nude mice were IC injected with the PCa cell line PC3 and subjected to vibration platform stimulus (section 2.6). The tumour was tracked by bioluminescence using IVIS and compared between the WBVP and sedentary groups (figure 7.2 A). The tumour burden was not significantly different among the mice subjected to WBVP versus controls (figure 7.2 B, Mann-Whitney test, n≥3).

### 7.2.2. Vibration platform does not affect the bone structure of a PC3 IC xenograft model

The Micro-CT technique was performed into the left tibia of the mice subjected to WBVP and the sedentary controls *ex vivo* to study the bone morphometry changes. The bone parameters measured were the same using the CTan software as described in 3.2.1.2 and 3.2.1.3. In the PC3 IC mice model, no differences were obtained between the tumour bearing tibias from the WBVP mice and sedentary controls (table 7.1, n≥3, unpaired t-test). This result suggests that the WBVP stimulus we applied in this xenograft model is not sufficient to compensate the tumour induced bone destructions detected by the Micro-CT technique.

### 7.2.3. The bone structure of naïve BALB/c nude mice is not affected by vibration platform stimulus

In order to study the effect of WVBP at a baseline level, we subjected naïve BALB/c nude mice (n=6) to our WBVP protocol versus sedentary controls (n=7). The left tibia of both groups was analysed *ex vivo* by means of Micro-CT technique. According to the Micro-CT analysis, no significant results were obtained in the bone parameters analysed in the exercised mice and controls (table 7.2, n≥6, unpaired t-test). Only the degree of anisotropy was found significantly lower in the WVBP mice compared to controls (table 7.2, n≥6, p=0.0056, unpaired t-test). This suggests that the WBVP protocol applied in the naïve mice is not sufficient to improve the bone structure at a

tissue level. To complement the Micro-CT results, we performed histomorphometry in the left tibia of both groups as a mean to understand the changes at a cellular level. See next section.

### 7.2.4. Vibration platform causes a mild response at a bone cellular level in BALB/c nude naïve mice

In order to study the bone cellular changes at a baseline level we used a group of 8-week-old naïve BALB/c nude mice subjected to WBVP (n=6) as well as sedentary controls (n=7). The mice tibias were TRAP-stained and histomorphometry analysis carried out using a DMRB microscope (Leica, Wetzlar, Germany) at 20x magnification with the Osteomeasure7 v4.2.0.1 (OsteoMetrics) software to quantify the osteoblasts and osteoclasts cells among the WBVP mice and sedentary controls, more details in section 2.8. The osteoblast quantity was significantly higher in the medial endocortical side versus controls (figure 7.3 A and B, $p= 0.0353$, $n\geq6$, unpaired t-test) as well as the surface occupied (figure 7.3 A and C, $p= 0.0296$, $n\geq6$, unpaired t-test). However, no significant changes were observed between the quantity and perimeter occupied by osteoblasts and osteoclasts in remaining histomorphometry parameters when comparing the WBVP vs control mice, table 7.3, unpaired t-test.

**A)** Control

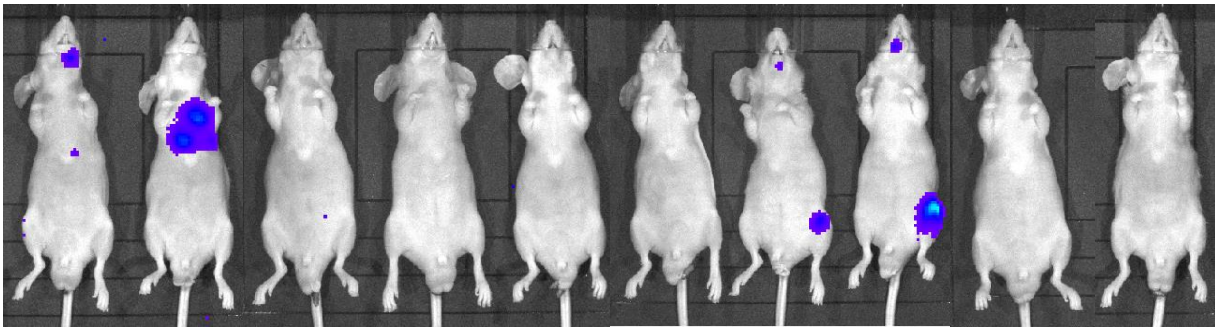

Vibration platform

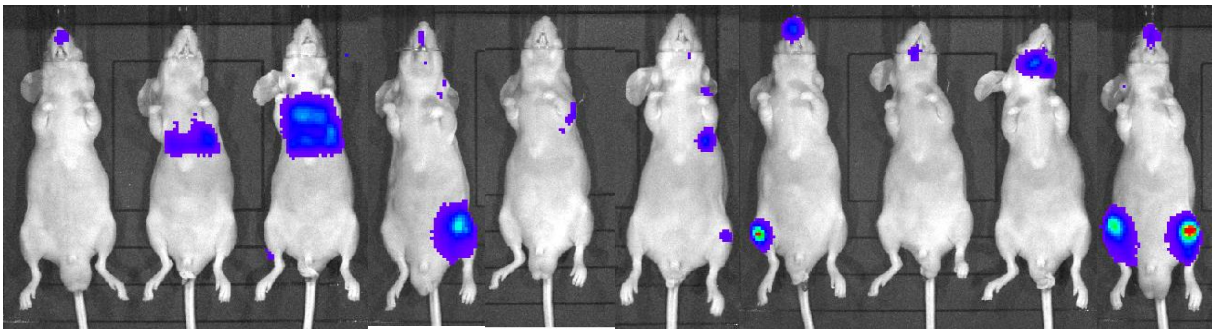

**B)**

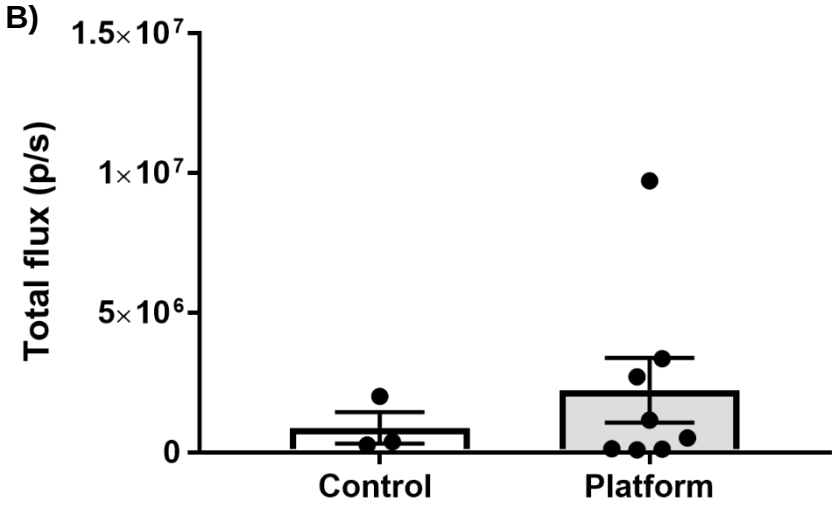

**Figure 7. 2. The effect of vibration platform on the development of PCa bone metastasis in an intracardiacally PC3 injected xenograft model.** *The human PCa cell line PC3 was intracardiacally injected in 8-week-old BALB/c nude mice followed by 3 weeks of vibration platform stimulus. A) Endpoint (3 weeks) IVIS pictures of mice subjected to whole-body vibration platform and control sedentary mice. The skeletal tumour growth was examined weekly by bioluminescence assay, comparing the vibration platform mice versus sedentary controls. B) The tumour burden, measured as total flux (photons/second), did not differ among both groups (Mann-Whitney test, n≥3). Tumour burden: presented as mean±SEM.*

**Table 7. 1. Quantitative bone morphometry analysis in the left bone tibia of BALB/c nude mice subjected to IC injection of PC3 cells and WBVP stimulus.**

| | Control | Vibration platform | Percentage change | P value |
|---|---|---|---|---|
| | n=3 | n=8 | | |
| **BV/TV %** | 6.68±2.17 | 8.87±1.01 | 32.81 | NS |
| **Tb.Th (mm)** | 0.02±0.001 | 0.02±0.0006 | 8.75 | NS |
| **Tb.N (1/mm)** | 2.46±0.73 | 3.06±0.30 | 24.31 | NS |
| **Tb.Sp (mm)** | 0.26±0.04 | 0.20±0.018 | -22.99 | NS |
| **Tb. Pf (1/mm)** | 11.65±6.63 | 12.94±2.55 | 11.07 | NS |
| **SMI** | 0.59±0.39 | 0.60±0.15 | 1.44 | NS |
| **DA** | 2.06±0.13 | 2.19±0.11 | 6.45 | NS |
| **Ct. BV** | 0.65±0.007 | 0.68±0.02 | 4.81 | NS |

Values are mean ± SEM

Percentage changes = (Vibration platform mean – Control mean)/Control mean × 100

NS= non-significant

**Table 7. 2. Quantitative bone morphometry analysis in the left tibia of a naïve BALB/c nude mice model subjected to WBVP**

| | Control | Vibration platform | Percentage change | P value |
|---|---|---|---|---|
| | **n=7** | **n=6** | | |
| **BV/TV %** | 12.83±0.53 | 13.07±0.81 | 1.87 | NS |
| **Tb.Th (mm)** | 0.03±0.001 | 0.03±0.0006 | 4.19 | NS |
| **Tb.N (1/mm)** | 3.42±0.14 | 3.33±0.23 | -2.36 | NS |
| **Tb.Sp (mm)** | 0.15±0.006 | 0.15±0.009 | -0.82 | NS |
| **Tb. Pf (1/mm)** | 42.09±3.79 | 44.04±2.31 | 4.63 | NS |
| **SMI** | 2.32±0.08 | 2.50±0.07 | 7.65 | NS |
| **DA** | **2.36±0.08** | **2.03±0.04** | **-14.30** | **** |
| **Ct. BV** | 0.71±0.01 | 0.72±0.01 | 1.85 | NS |

Values are mean ± SEM

Percentage changes = (Vibration platform mean – Control mean)/Control mean × 100

NS: Non-significant

***p=<0.01* (unpaired t-test)

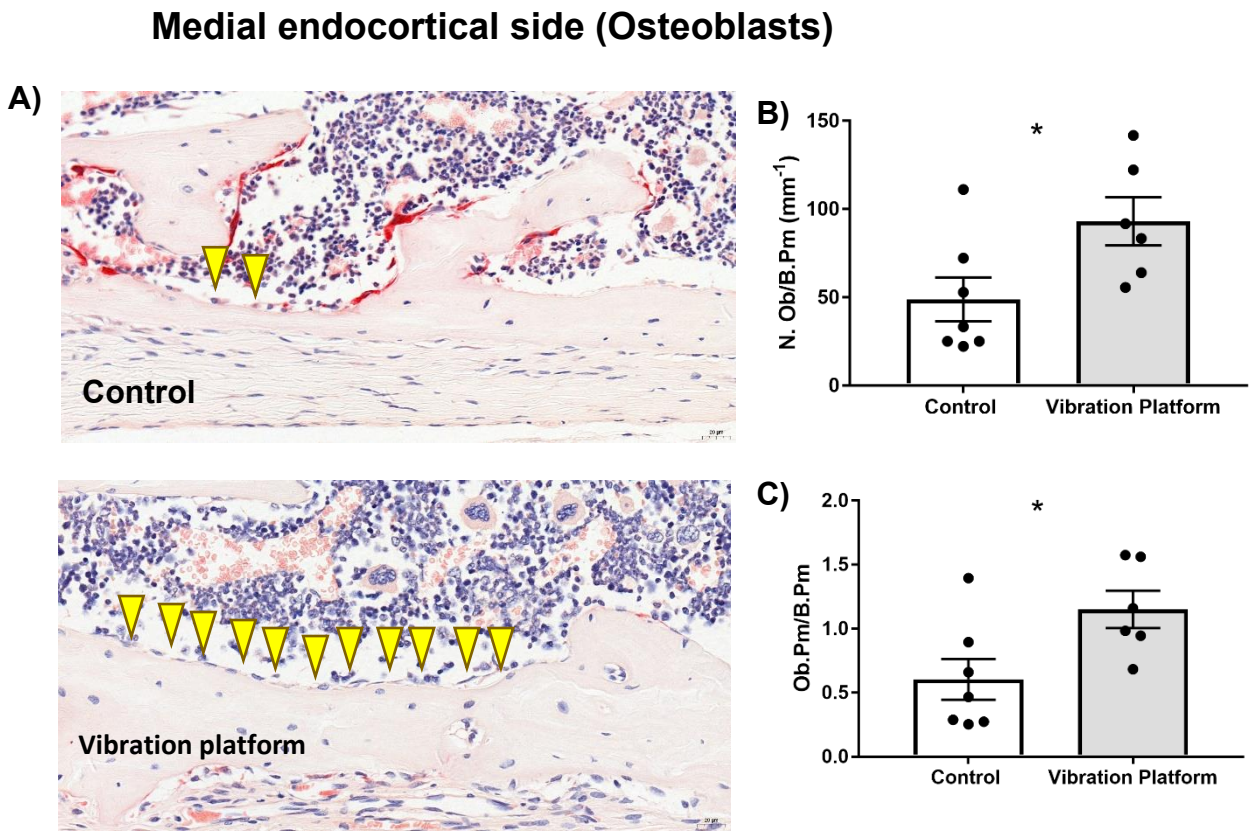


**Figure 7. 3. WBVP increases the quantity and surface occupied by osteoblasts in the medial endocortical region of naïve BALB/c nude mice.** *The left tibia bone sections of WBVP and sedentary naïve BALB/c nude mice were TRAP-stained to identify the osteoblasts and osteoclasts bone cells. Bone cells were quantified 0.15 mm away from the growth plate on the medial endocortical region under a DMBR microscope using the Osteomeasure bone histomorphometry software. A) Yellow arrows indicate cobblestone like-cuboidal osteoblasts cells on the medial endocortical surface, Scale bar= 20µm. B) Quantification of the osteoblast number per mm in the medial endocortical bone surface (N.Ob/B.Pm). C) Quantification of the percentage of surface occupied by osteoblasts (Ob.Pm/B.Pm). All data is presented as mean±SEM. n≥6, *p<0.05, unpaired t-test.*

**Table 7. 3. Histomorphometry analysis in the left tibia of naïve BALB/c nude mice subjected to WBVP**

| Bone region analysed | Cell type quantified | Number of cells | | | | Perimeter of cells/bone perimeter | | | |
|---|---|---|---|---|---|---|---|---|---|
| | | Control | Vibration platform | Percentage change | P value | Control | Vibration platform | Percentage change | P value |
| **Lateral endocortical** | Osteoblasts | 471.7±44.77 | 499.1±37.36 | 5.80 | NS | 3.33±0.25 | 3.87±0.20 | 16.09 | NS |
| | Osteoclasts | 0±0 | 0.46±0.46 | - | NS | 0 ± 0 | 0.01±0.01 | - | NS |
| **Medial endocortical** | **Osteoblasts** | **48.81±12.46** | **93.06±13.62** | **90.65** | ***** | **0.60±0.15** | **1.15±0.14** | **90.55** | ***** |
| | Osteoclasts | 2.77±1.21 | 5.09±1.32 | 83.33 | NS | 0.07±0.04 | 0.16±0.04 | 119.89 | NS |
| **Trabecula** | Osteoblasts | 103.2±12.27 | 136.6±25.22 | 32.36 | NS | 1.18±0.14 | 1.73±0.34 | 46.21 | NS |
| | Osteoclasts | 43.82±4.99 | 32.75±4.46 | -25.26 | NS | 0.98±0.12 | 0.89±0.16 | -9.02 | NS |

Values are mean ± SEM

Percentage changes = (Vibration platform mean – Control mean)/Control mean × 100

**p<0.05* (unpaired t-test)

### 7.2.5. Vibration platform does not affect the development of PCa bone metastasis in a RM1 syngeneic model.

8-week-old C57BL/6 mice were IC injected with the murine PCa cell line RM1 and subjected to WBVP as described in section 2.6. The tumour was tracked by bioluminescence using IVIS and compared between the WBVP and sedentary groups, figure 7.4 A. The hindlimb tumour incidence was not significantly different among the WBVP and sedentary controls during the three weeks of stimulus, figure 7.4 B-D, chi-square, n=12. There was not significant difference in the tumour burden among both groups, figure 7.4 E, Mann-Whitney test, n≥8,.

### 7.2.6. WBVP does not protect cancer induced bone destruction in the RM1 syngeneic model

Bone morphometry changes in mice subjected to WBVP stimulus and RM1 cells IC injection were examined using the left tibia of the mice and micro-CT *ex vivo*. The bone parameters measured using the CTan software were listed in 3.2.1.2 and 3.2.1.3. No differences were observed in any of the bone parameters analysed by the Micro-CT in tibias from the WBVP mice and sedentary controls, table 7.4, n=12, unpaired t-test. To further confirm whether the bone structure changes were result of the WBVP stimulus, we subjected the naïve mice of the same strain (n=6) to the identifical WBVP protocol for 3 weeks. The results of the baseline experiment are described in the next section.

### 7.2.7. WBVP does not improve the bone structure parameters in naïve C57BL/6 mice

In order to further study wether the applied WBVP stimulus does have an effect on the bone structure, naïve C57BL/6 mice (n=6) were subjected to the same WBVP protocol for 3 weeks. The left tibia of the naïve mice was analysed *ex vivo*, comparing the left tibias of WBVP mice and control groups using micro-CT. According to the Micro-CT analysis, the trabecula space was significantly higher in the WBVP tibia compared to

controls, table 7.5, n=6, p= 0.0370, unpaired t-test. No significant differences were found in the remaining bone structure parameters.

### 7.2.8. WVBP does not affect the bone cellular response in C57BL/6 naïve mice

In order to study the bone cellular changes at a baseline level we used a group of 8-week-old naïve C57BL/6 mice subjected to WBVP (n=6) as well as sedentary controls (n=6). The bone sections were TRAP-stained and histomorphometry analysis was carried out in the left tibia section using a DMRB microscope (Leica, Wetzlar, Germany) at 20x magnification with the Osteomeasure7 v4.2.0.1 (OsteoMetrics) software to quantify the osteoblasts and osteoclasts cells (more details in section 2.8). No significant differences were observed in any of the histomorphometry parameters (table 7.6, n≥5, unpaired t-test).

A) Control

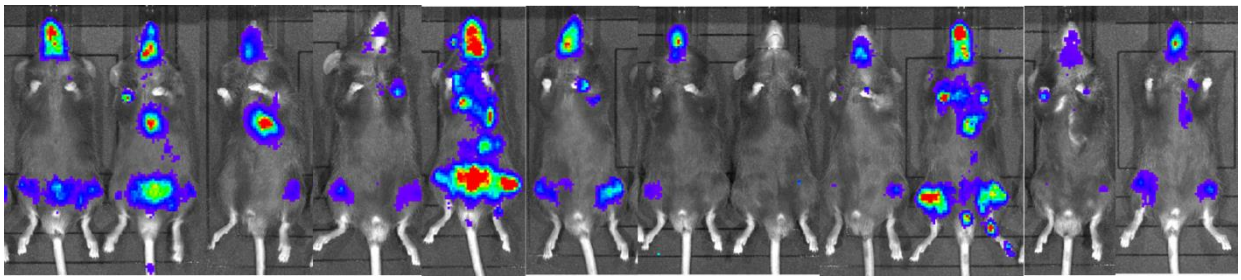

Vibration platform group

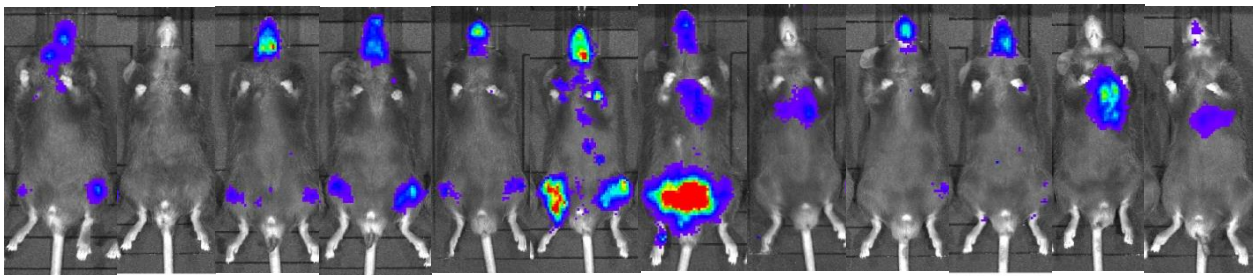

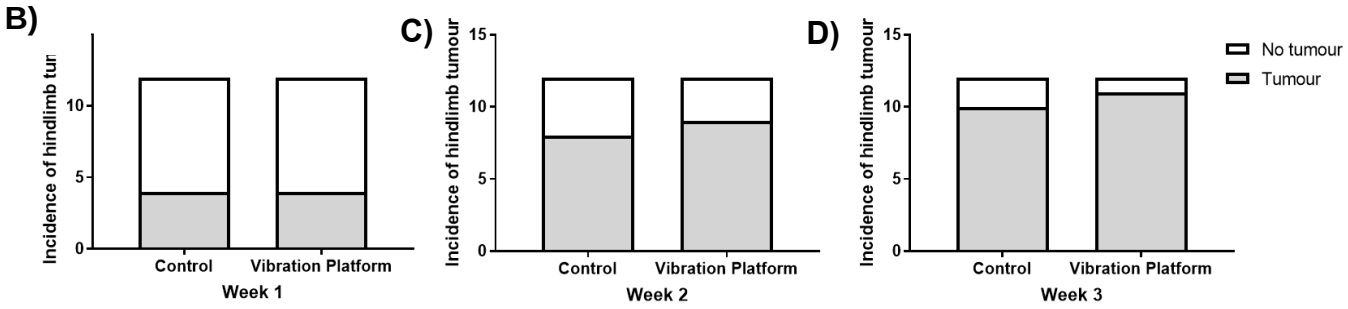


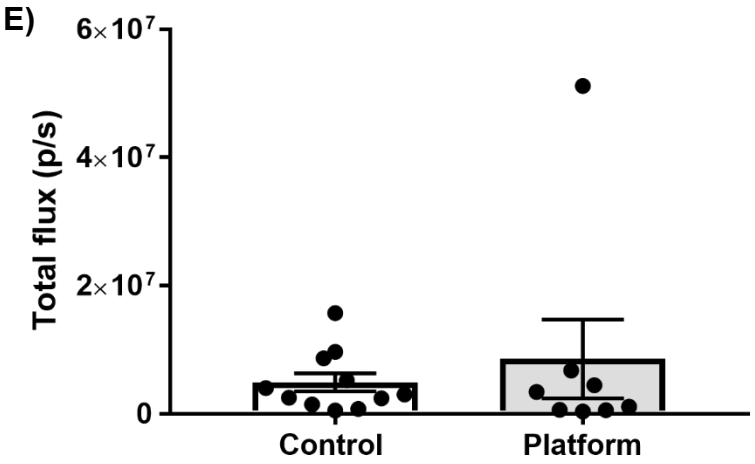

**Figure 7. 4. The effect of WBVP stimulus on the development of PCa bone metastasis in an intracardiacally RM1 injected syngeneic model.** *The murine PCa cell line RM1 was intracardiacally injected in 8-week-old C57BL/6 mice followed by 3 weeks of WBVP stimulus. A) Endpoint (3 weeks) IVIS pictures of mice subjected to whole-body vibration platform and control sedentary mice. The skeletal tumour growth was examined weekly by bioluminescence assay, comparing the WBVP mice versus sedentary controls. B)- D) The hindlimb tumour incidence did not differ among both groups during the three weeks of WVBP stimulus (chi-square, n=12). E) The whole-body tumour burden, measured as photons/second, did not differ among both groups (Mann-Whitney test, n≥8). Tumour burden: presented as mean±SEM.*

**Table 7. 4. Quantitative bone morphometry analysis in the left bone tibia of C57BL/6 mice subjected to I.C injection of RM1 cells and WBVP stimulus**

| | Control | Vibration platform | Percentage change | P value |
|---|---|---|---|---|
| | n=12 | n=12 | | |
| **BV/TV %** | 8.46±1.44 | 9.30±1.03 | 9.88 | NS |
| **Tb.Th (mm)** | 0.02±0.001 | 0.03±0.001 | 12.58 | NS |
| **Tb.N (1/mm)** | 2.71±0.41 | 2.77±0.29 | 2.50 | NS |
| **Tb.Sp (mm)** | 0.19±0.02 | 0.19±0.01 | -2.45 | NS |
| **Tb. Pf (1/mm)** | 35.45±5.65 | 28.63±2.53 | -19.23 | NS |
| **SMI** | 1.72±0.13 | 1.63±0.09 | -5.17 | NS |
| **DA** | 2.56±0.09 | 2.62±0.08 | 2.41 | NS |
| **Ct. BV** | 0.92±0.04 | 0.96±0.03 | 4.34 | NS |

Values are mean ± SEM

Percentage changes = (Vibration platform mean – Control mean)/Control mean × 100

NS: Non-significant

**Table 7. 5. Quantitative bone morphometry analysis in the left tibia of a naïve C57BL/6 mice model subjected to WBVP**

| | Control | Vibration platform | Percentage change | P value |
|---|---|---|---|---|
| | **n=6** | **n=6** | | |
| **BV/TV %** | 18.51±1.14 | 17.02±0.91 | -8.04 | NS |
| **Tb.Th (mm)** | 0.04±0.001 | 0.04±0.001 | -1.64 | NS |
| **Tb.N (1/mm)** | 4.21±0.18 | 3.95±0.12 | -6.30 | NS |
| **Tb.Sp (mm)** | **0.12±0.004** | **0.13±0.003** | **10.87** | ***** |
| **Tb. Pf (1/mm)** | 31.41±3.01 | 32.86±2.05 | 4.61 | NS |
| **SMI** | 2.08±0.12 | 2.11±0.06 | 1.24 | NS |
| **DA** | 2.55±0.07 | 2.63±0.11 | 3.05 | NS |
| **Ct. BV** | 0.98±0.05 | 0.86±0.031 | -12.20 | NS |

Values are mean ± SEM

Percentage changes = (Vibration platform mean – Control mean)/Control mean × 100

**p=<0.05* (unpaired t-test)

**Table 7. 6. Histomorphometry analysis in the left tibia of naïve C57BL/6 mice subjected to WBVP**

| Bone region analysed | Cell type quantified | Number of cells | | | | Perimeter of cells/bone perimeter | | | |
|---|---|---|---|---|---|---|---|---|---|
| | | Control | Vibration platform | Percentage changes | P value | Control | Vibration platform | Percentage changes | P value |
| **Lateral endocortical** | Osteoblasts | 431±47.81 | 448.9±66.33 | 4.15 | NS | 3.21±0.22 | 3.83±0.46 | 19.36 | NS |
| | Osteoclasts | 0.79±0.79 | 1.11±0.68 | 39.97 | NS | 0.01±0.01 | 0.03±0.02 | 127.81 | NS |
| **Medial endocortical** | Osteoblasts | 68.65±7.56 | 70.22±16.44 | 2.28 | NS | 0.86±0.11 | 0.94±0.21 | 8.67 | NS |
| | Osteoclasts | 16.11±3.22 | 24±4.67 | 48.97 | NS | 0.51±0.10 | 0.77±0.24 | 51.61 | NS |
| **Trabecula** | Osteoblasts | 154.7±15.87 | 163.9±20.09 | 5.94 | NS | 1.70±0.18 | 1.95 ±0.23 | 15.10 | NS |
| | Osteoclasts | 67.86±10.16 | 55.14±9.73 | -18.74 | NS | 1.59±0.25 | 1.40±0.25 | -11.95 | NS |

Values are mean ± SEM

Percentage changes = (Vibration platform mean – Control mean)/Control mean × 100

NS= non-significant

## 7.3. Discussion

In this chapter we subjected two different mice strains to WBVP stimulus to study whether whole body high-frequency, low magnitude vibration stimulus would affect the development of PCa bone metastasis.

Overall, the tumour burden was not affected in both mice strains as well as the bone structure parameters in the xenograft, syngeneic and naïve mice models. The same situation was observed for the histomorphometry analysis carried out in the syngeneic models. These results suggest that the WBVP stimulus we applied was not sufficient to either induce bone formation and an osteogenic response at a baseline level or delay the onset of PCa bone metastasis and protect the bone from PCa metastatic bone lesions. .

Although the positive effect of WBVP stimulus in patients has been documented by many, we did not achieved any positive outcome in our mice models (Rubin et al. 2004; Fung et al. 2012; Prioreschi et al. 2012; Gómez-Cabello et al. 2012; Marín-Cascales et al. 2018; Ruymbeke et al. 2014; Salhi et al. 2015; Crevenna et al. 2017). We must take into consideration the parameters stablished in the WBVP to deliver a proper stimulus which could benefit the patient. Rauch et al. (2010), elegantly explained the principles of WBVP to provide an appropriate methodology among the scientific consortiums. The principles are period duration, frequency, peak to peak displacement, amplitude, and peak acceleration (magnitude). Taking the frequency as an example, Baker et al. (2018) found that low-frequency low-magnitude WBVP stimulus (27-32 Hz, 0.3g, 20 minutes, 3 times per week for 12 weeks) was neither effective to reduce bone resorption markers nor improve bone formation markers, as well as not improving physical functions in BCa survivors treated with aromatase inhibitors. However, most of the positive effects of WBVP has been observed in high-frequency vibration platforms (Rubin et al. 2004; Fung et al. 2012; Prioreschi et al. 2012; Gómez-Cabello et al. 2012; Marín-Cascales et al. 2018; Ruymbeke et al. 2014; Salhi et al. 2015; Crevenna et al. 2017). Another example is the application of high magnitudes (>1g) as they are associated with negative outcomes such as haematuria, severe chest pain, gastrointestinal bleeding (Franchignoni et al. 2012; Griffin 1996; Ordan et al. 2005). As discussed, the WBVP parameters applied could have either a

positive or negative outcome. It is likely that the parameters we applied in our mice models were not appropriate for an *in vivo* model, either because of the parameters as well as the machinery used, as the vibration platform we used is meant to be for human usage.

The issue of translating the human WBVP to animal models has been addressed by Novotny et al. (2013). This group created a high-frequency low-magnitude vibration platform specifically for animal models. The platform delivers magnitudes of 0.2g-1g and frequencies of 25-90 Hz. The platform has a circular shape with an actuator placed in the middle to effectively deliver the vibration stimulus throughout the system regardless of the position and weight of the mice. The movement of weights in the platform could impair the vibration stimulus, an issue we possibly had in our model as the mice were free to move around the platform, giving more reasonability of why we did not achieve a positive outcome (Pel et al. 2009). In the WBVP model of Novotny et al. (2013), acceleration feedback was applied as a matter to verify that the vibration signal was constant during the stimulus and between vibration bouts, another limitation in our model as we did not verify any vibration stimulus bias during the WBVP study. Further limitations to our device are the square shape of the platform. It is suggested that squared or rectangular platform shapes could add or subtract vibration waves in the system, a limitation solved by using a circular platform as in the device created by Novotny et al. (2013) (Fritton et al. 1997; Christiansen & Silva 2006).

Interestingly, in the study of Wehrle et al. (2015), the mice model achieved bone formation and other positive parameters as flexural rigidity and callus properties using a very similar WBVP protocol. Possibly, the WBVP we translated from that group is sex and age dependant, as the bone improvement was observed in 41-week-old ovariectomised mice while we applied 8-week-old male mice (immunocompetent and immunocompromised).

## 7.4. Conclusion

High-frequency low-magnitude applied at 20 minutes/day, 5 days/week for 3 weeks with 0.3 g peak-to-peak acceleration and a frequency of 45Hz is not a suitable method to delay the onset of PCa bone metastasis as well as improve bone structure and induce an osteogenic response in immunocompetent and immunocompromised *in vivo* models. A suitable device or regimen should be applied to the *in vivo* model as a matter to deliver an appropriate vibration stimulus and study its effect in the PCa bone metastasis progression.

# Chapter 8:

## Mechanical loading negatively regulates DKK1 expression and affects the cytokine profile in bone

## 8.1. Introduction

The skeleton undergoes the process of remodelling to maintain its structure and strength, a process carried out by the coupled activity of osteoblasts and osteoclasts, to create new bone and reabsorb old bone tissue, respectively (Florencio-silva et al. 2015). During the PCa bone metastasis growth, the bone resorption has been identified as one hallmark which alters the balance of bone remodelling and plays an important part in the “vicious cycle” of bone cancer (Guise 2002). In fact, anti-resorptive drugs such as denosumab and zoledronic acid have been approved by the FDA in PCa as they have been shown to protect the bone structure, reduce pathological fractures and delay metastases (Wong et al. 2019). However, other factors such as exercise and molecules as DKK1 play an important role in bone remodelling.

DKK1 is a negative regulator of the canonical Wnt signalling an important pathway for osteoblast differentiation. Therefore, the expression of DKK1 is linked to inhibition of osteoblastogenesis; expression of DKK1 is also link to osteoclast differentiation and bone resorption (Baron & Rawadi 2007; Bodine & Komm 2006; Pinzone et al. 2009)). In an inactivated status, (i.e., absence of Wnt) β-catenin is degraded by a destruction complex comprised of the Axin/GSK3β/APC complex, figure 8.1 A. In an active status, Wnt binds Fzd and Lrp5/6, then, a downstream signalling activates Dishevelled, preventing the degradation of the destruction complex, leading to accumulation of β-catenin, its translocation into the nucleus and binding to Tcf/Lef family of transcription factors, ultimately regulating the expression of Wnt-target genes, figure 8.1 B) (Baron & Rawadi 2007; Bodine & Komm 2006). DKK1 is one molecule which can prevent the binding of the Wnt/Fzd/Lrp5/6 axis, leading to β-catenin inhibition.

In PCa, DKK1 has been linked to a poor prognosis in patients, promote PCa progression and lead to immunological evasion (Thudi et al. 2011; Rachner et al. 2014; Wise et al. 2020) In PCa bone metastasis, DKK1 has been found increased in osteolytic models of PCa but reduced in osteoblastic models. It was also shown to be highly expressed in PCa primary tumour and decreased in the bone metastasis stage with osteoblastic bone metastasis being the predominant type in PCa (Rachner et al. 2014; Wise et al. 2020; Thudi et al. 2011; Hall et al. 2008; Amelio et al. 2014; Clines

& Clines 2018). This indicates the role of DKK1 could be stage dependant. At an early stage, DKK1 could create an osteolytic environment, initiate the vicious cycle of cancer and start the metastatic growth, while at a late stage of PCa bone metastasis, DKK1 could be downregulated to allow the osteoblastic phenotype of PCa to take place

Interestingly, it has been evidenced that different types of exercises (i.e., treadmill running and resistance exercises) are able to downregulate the levels of DKK1 (Kim et al. 2017; Chen et al. 2020). In addition to DKK1, exercise has been shown to modulate a number of cytokines, according to the intensity of the exercise performed. For instance, when endurance exercise is performed for more than a couple of hours as in the case for marathons and triathlons, IL-1α, IL-1β, TNF-α IL-6, IL-8, and IL-10 are found increased (Nieman et al. 1997; Suzuki et al. 2002; Suzuki et al. 2003; Pedersen & Febbraio 2008; Goh et al. 2019). In contrast, when endurance exercise is performed for a short period of time, the levels of these cytokines does not increase significantly at the moment of the exercise or after recovery (Lombardi et al. 2019; Peake et al. 2004; Hayashida et al. 2015; Nieman et al. 1997; Suzuki et al. 2002; Suzuki et al. 2003; Pedersen & Febbraio 2008; Goh et al. 2019) Importantly for this project, some cytokines are suggested to carry anti-tumour or pro-tumour features (Dinarello 2006; Berraondo et al. 2019; Kartikasari et al. 2021; Lan et al. 2021). Thus, the intensity/duration of the exercise performed could impair the cytokines levels and promote either an anti-tumour or anti-tumour environment.

Therefore, to understand the potential mechanisms how exercise affects PCa bone metastasis, serum samples from naïve BALB/c nude mice were analysed to study the effect of mechanical loading and other exercise types on DKK1 serum levels as well as an additional panel of 23 cytokines. In addition, we subjected pre-osteoblasts and differentiated osteoblasts cells (MG-63 and SaOS2, respectively) to fluid flow assessment ($2.4\times10^{-4}$ L s−1 20 times in monolayer), to translate our mechanical model to an *in vitro* approach, figure 8.2 (Rumney et al. 2012). Briefly, the cells were seeded in a 12-well plate at a density of 50,000 cells per well. Once they reached an ~80% capacity, the cells were cultured with serum free media (SFM) for 24 hours. The following day, the cells were subjected to fluid flow technique, the condition media was collected, spined to avoid any cell debris and stored for further analysis. The

conditioned media generated was screened using the Proteome Profiler Human XL Cytokine Array as described in 2.12.1

In addition, exercise has been found to affect the bone ECM stiffness (Vlachopoulos et al. 2018). Jumping exercise increased the bone mass and stiffness in individuals who performed exercises known to have a lower osteogenic effect (i.e., swimming, cycling) (Vlachopoulos et al. 2018). In animal models, mechanical loading has been suggested to increase the tibia bone stiffness (6-11 week-old) but also to decrease the stiffness in old mice models (16-week-old) (Main et al. 2014b; Lambers et al. 2013). Interestingly, bone stiffness can affect the proliferative status of PCa. An in vitro model applied by Page et al. (2015) to mimic the stiffness of cortical bone tissue evidenced that increased stiffness modulated the expression of tumour progression factors (GLI2, PTHrP). Therefore, to understand how our mechanical loading regimen affect the bone ECM, the bone ECM stiffness was analysed in collaboration with Dr. Xinyue Chen (The University of Sheffield) using atomic force microscope (AFM) technique (JPK NanoWizard III microscope) by taking the mechanically loaded right leg (3 loading cycles, 9N) of one 8-week-old C57BL/6 mice and compared to its contralateral left tibia control.

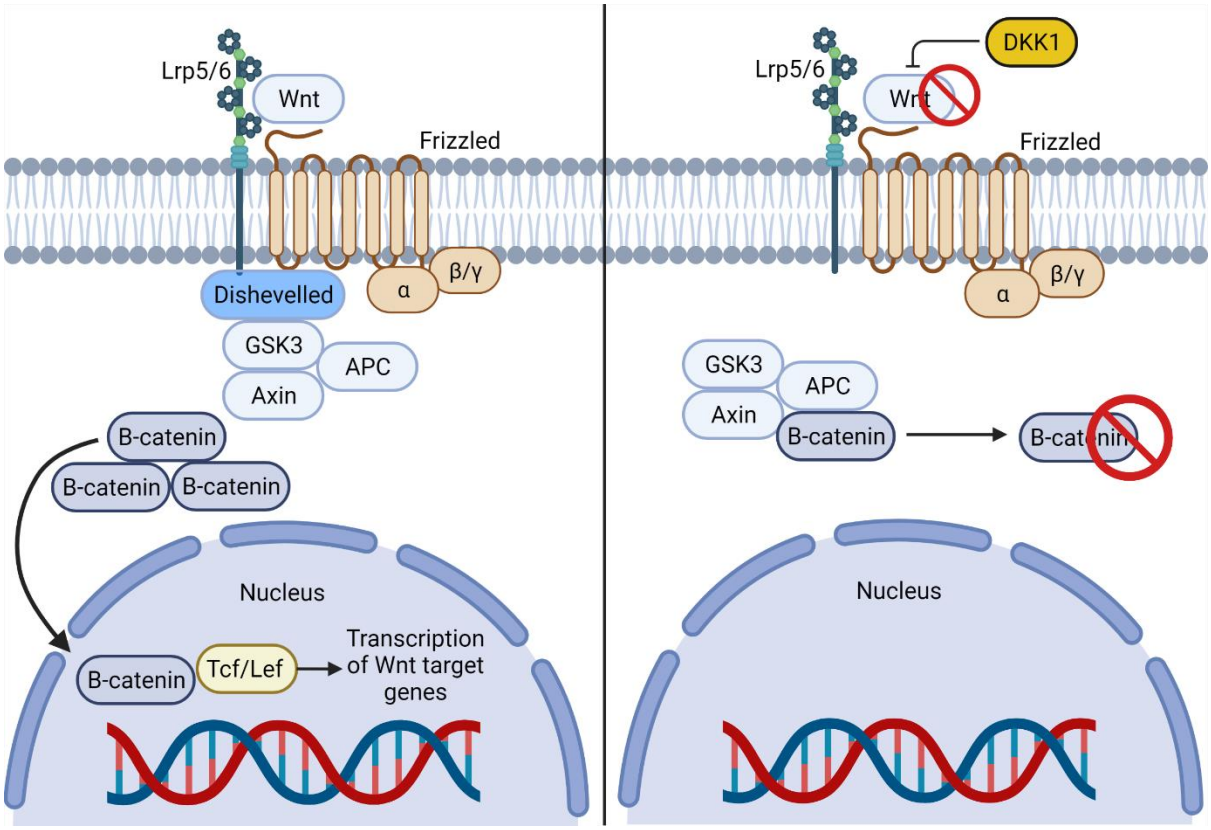


**Figure 8. 1. Schematics of Wnt signalling pathway.** *A) Upon Wnt binding to Lrp5/6 and Frizzled, Dishevelled inactivates the destruction complex comprised of GSK3/APC/Axin leading to β-catenin accumulation and translocation to the nucleus. Consequently, β-catenin forms a complex with Tcf/Lef resulting in the transcription of Wnt target genes. B) in the absence of Wnt ligand or inhibition of Wnt by DKK1, the destruction complex comprised of GSK3/APC/Axin phosphorylates β-catenin leading to its degradation, preventing β-catenin translocation to the nucleus and inhibiting the transcription of Wnt target genes.*

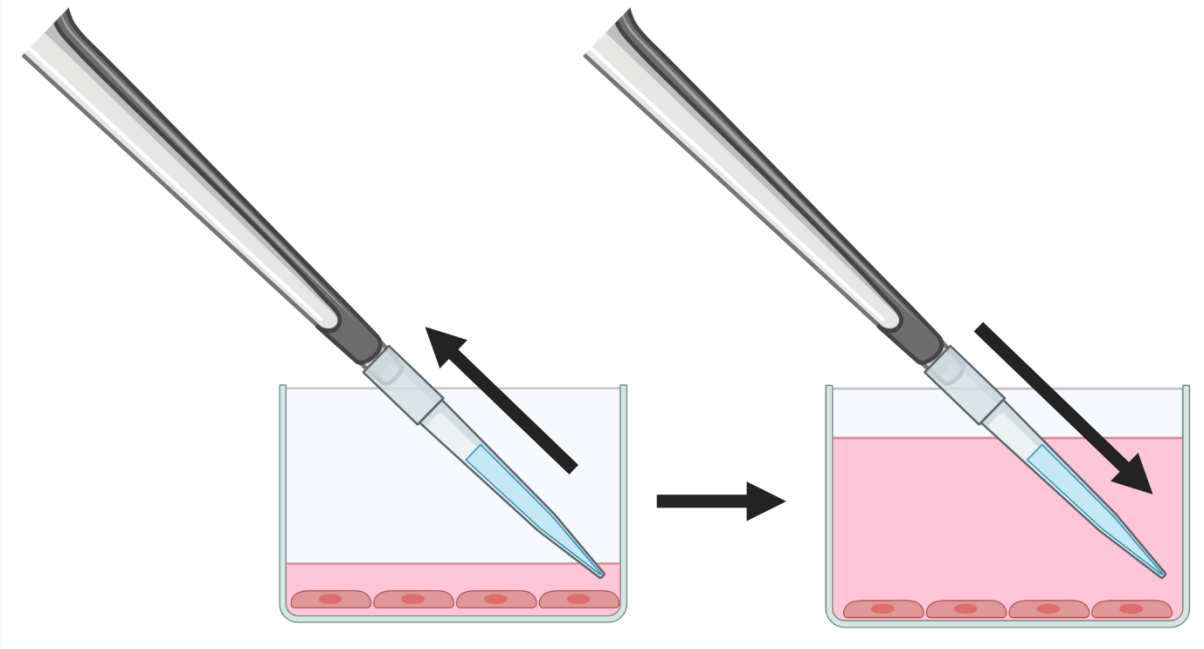

**Figure 8. 2. Fluid flow stimulation in vitro of MG-63 and SaOS2 cell lines.** *Mechanical loading was translated in vitro by applying fluid flow in monolayer cell lines. 80% of the media was displaced 20 times using a pipette as shown. Then, the media was spined to avoid cell debris and stored at -80°C to be further analysed by ELISA technique and determine its cytokine profile.*

## 8.2. Results

### 8.2.1. Fluid flow decreases the levels of DKK1 in condition media from MG-63 and SaOS2 cell lines.

The condition media of MG-63 and SaO2 cells was subjected to fluid flow induced by displacing 80% media for 20 times, as a matter to translate our mechanical loading technique *in vitro*. The conditioned media was then assessed using the Proteome Profiler Human XL Cytokine Array (105 cytokines). According to the membrane cytokine array, several cytokines were found expressed in the control condition media of the MG-63 and SaOS2 cells, figure 8.3 A and B, respectively. In the MG-63 condition media, the cytokines expressed were Chitinase 3-like 1, DKK1, Emmprin, FGF-19, HGF, IL-8, IL-17A, MCP-1, MIF, Pentraxin 3, Serpin E1, VEGF and Endoglin. The cytokines found significantly reduced after fluid flow (>2-fold changes) were Chitinase 3-like 1 (>2-fold), DKK1 (>4-fold), FGF-19 (>143-fold), HGF (>70-fold), IL-8 (>6-fold), MCP-1 (>9-fold) and VEGF (>6-fold), figure 8.3 C. In the SaOS2 control condition media, DKK1, MIF and uPAR were found expressed. From these cytokines, DKK1 and uPAR were found reduced >15-fold and >4-fold times, respectively, figure 8.3 D. Interestingly, DKK1 was the only cytokine uniformly expressed and reduced in both cell lines, figure 8.3 C and D.

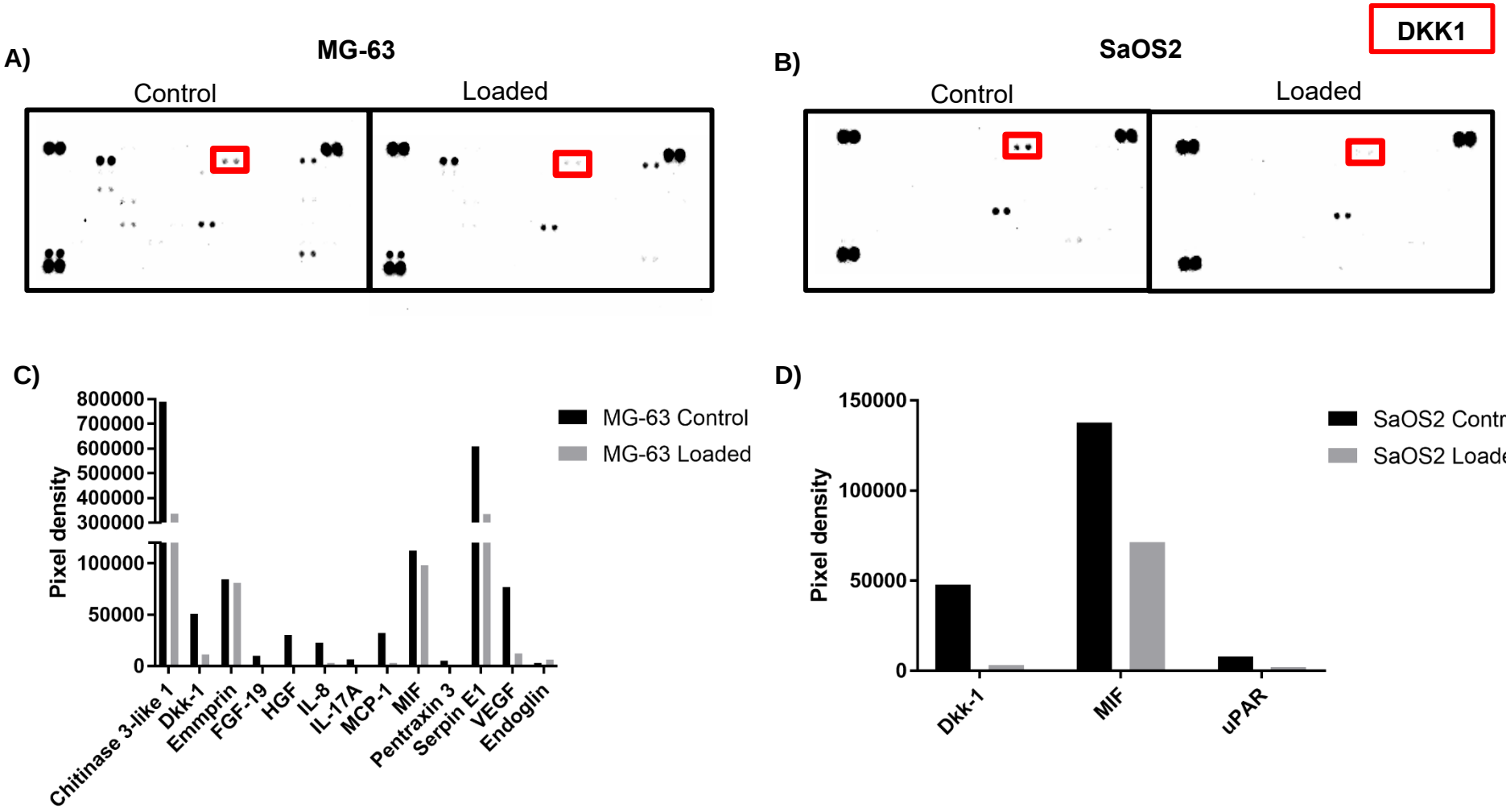
A)
MG-63
Control
Loaded
B)
SaOS2
DKK1
Control
Loaded
C)
Pixel density
800000
700000
600000
500000
400000
300000
100000
50000
0
MG-63 Control
MG-63 Loaded
Chitinase 3-like 1
Dkk-1
Emmprin
FGF-19
HGF
IL-8
IL-17A
MCP-1
MIF
Pentraxin 3
Serpin E1
VEGF
Endoglin
D)
Pixel density
150000
100000
50000
0
SaOS2 Control
SaOS2 Loaded
Dkk-1
MIF
uPAR

**Figure 8. 3. DKK1 is reduced in the MG-63 pre-osteoblast and SaOS2 differentiated osteoblast cell line after fluid flow stimulus.** *A) and B) A number of cytokines were found expressed in the control condition media of MG-63 and SaOS2 cell lines as shown in the cytokine membrane array. C) and D) the expression of these cytokines was affected after fluid flow stimulus. Only DKK1 was found expressed in both cell lines and reduced 4-fold and 15-fold after fluid flow in the MG-63 and SaOS2 cell lines, respectively (DKK1 circled in red). A)-D) combination of 3 biological repeats of the condition media subjected to mechanical loading in vitro, n=3*

### 8.2.2. Mechanical loading but not treadmill running exercise decreases the serum levels of DKK1 in naïve BALB/C nude mice.

The DKK1 serum levels of 12-week-old BALB/c nude mice subjected to 1, 2 and 3 weeks of mechanical loading (chapter 3) were analysed using ELISA technique as detailed in section 2.12.2. At the first week of mechanical loading, DKK1 was found reduced by ~69% compared to controls, figure 8.4 A. In the second week, DKK1 was significantly reduced, figure 8.4 A, one-way ANOVA, $n \geq 5$, $p = 0.0053$. At the third week of loading stimulus, DKK1 was reduced by ~73%, figure 8.4 A. To examine other models of exercise and its effect on DKK1, we assessed serum samples from the naïve treadmill running exercise models presented in chapter 6, finding that the serum levels of DKK1 were not affected by treadmill running either in the immunocompetent or immunocompromised mice models (figure 8.4 B and C).

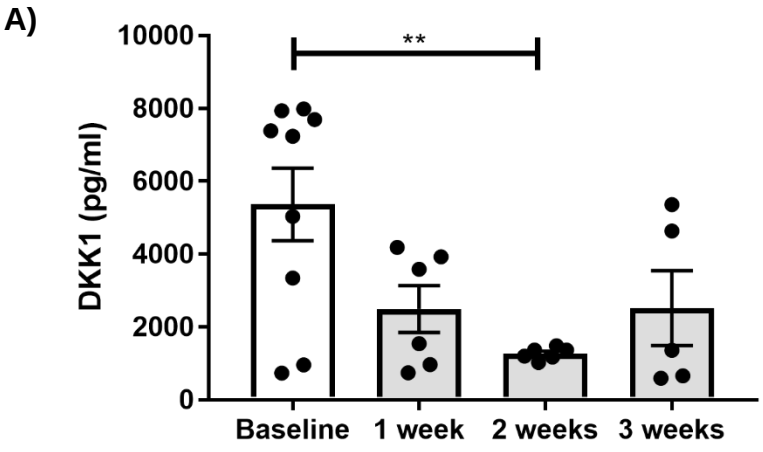
A)
10000
8000
6000
4000
2000
0
DKK1 (pg/ml)
**
Baseline
1 week
2 weeks
3 weeks

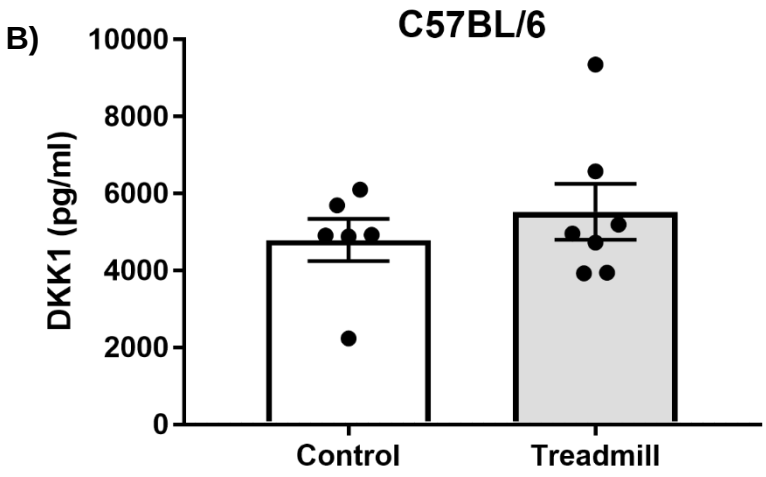
B)
C57BL/6
10000
8000
6000
4000
2000
0
DKK1 (pg/ml)
Control
Treadmill

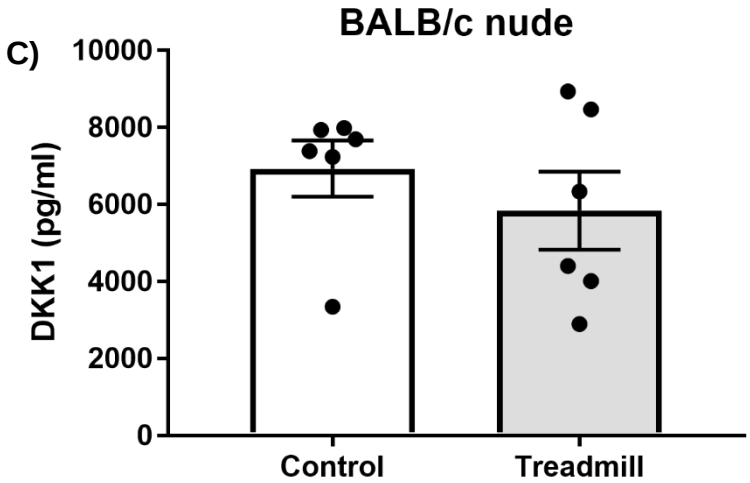
C)
BALB/c nude
10000
8000
6000
4000
2000
0
DKK1 (pg/ml)
Control
Treadmill

**Figure 8. 4. Mechanical loading but not treadmill running decreases DKK1 serum levels in mice.** *A) Mechanical loading applied in the right tibia of 12-week-old BALB/c nude mice significantly decreased the levels of DKK1 at the second week (one-way ANOVA, n≥5, p= 0.0053. At the first and third week, mechanical loading decreased the DKK1 serum levels at ~69% and ~73%, respectively. B) Three weeks of treadmill running applied to naïve immunocompetent and C) immunocompromised mice (chapter 6) did not affect the levels of DKK1 in serum. Values are mean ± SEM, unpaired t-test, n≤6.*

### 8.2.3. Bone parameters are negatively correlated with DKK1 serum levels.

To understand the correlation between trabecular bone mass and DKK1, we analysed the bone parameters and DKK1 serum levels of a cohort of 32 twelve-week-old male BALB/c nude mice. The DKK1 serum levels were examined by means of the Quantikine ELISA assay. According to the analysis, there is a negative correlation between DKK1 expression and BV/TV% ($r= -0.2222$, $p=0.2217$), Tb.Th ($r= -0.5445$, $p=0.0013$) and Ct.BV ($r= -0.3957$, $p= 0.0250$), figure 8.5, Pearson correlation test, $n=32$.

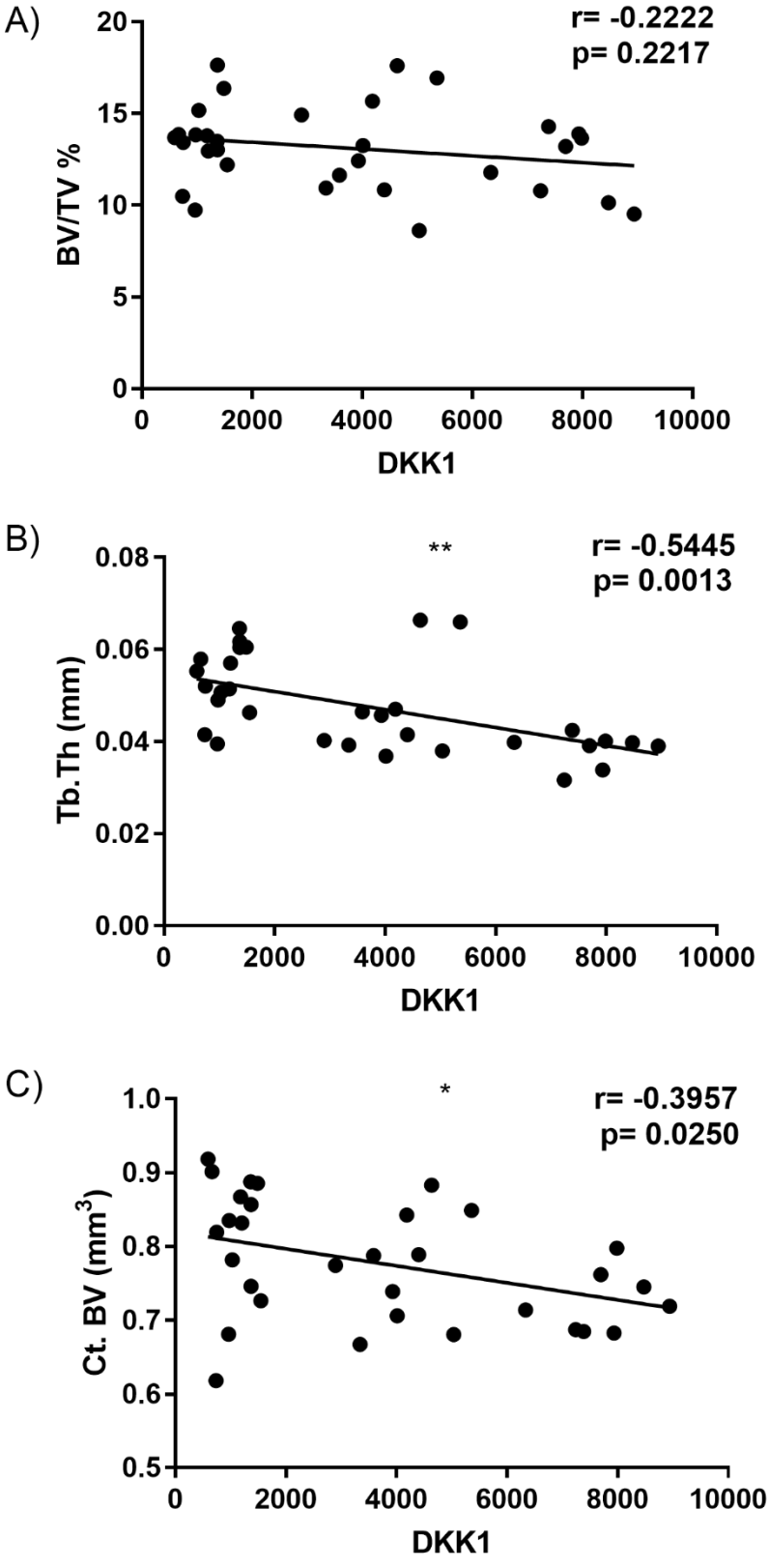
A)
r= -0.2222
p= 0.2217
BV/TV %
DKK1
B)
**
r= -0.5445
p= 0.0013
Tb.Th (mm)
DKK1
C)
*
r= -0.3957
p= 0.0250
Ct. BV (mm3)
DKK1

**Figure 8. 5. DKK1 expression is negatively correlated with bone structure parameters.** *The bone structure parameters of a cohort of 32 twelve-week-old BALB/c nude male mice were correlated against their corresponding DKK1 expression levels. The DKK1 serum levels were found negatively correlated with the (A) trabecula bone volume fraction (BV/TV%), (B) trabecula thickness (Tb.Th) and (C) Cortical Bone Volume (Ct. BV), suggesting that bone mass decreases DKK1 expression. Pearson correlation test, n=32, BV/TV% (r= -0.222, p=0.2217), Tb.Th (r= -0.5445, p= 0.0013) and Ct.BV (r= -0.3957, p= 0.0250).*

### 8.2.4. The expression of DKK1 is lower in patients with metastatic PCa versus patients with primary PCa.

To elucidate the transcriptomic expression level of *DKK1* in patients with PCa, a retrospective analysis of a clinical dataset was performed using the Gene Expression Omnibus database. Three final clinical databases were selected under the “Prostate cancer” term and human PCa samples analysed from primary and metastatic PCa cancer: GDS1439 and GDS3289, GDS2545 accession number (Varambally et al. 2005; Tomlins et al. 2006; Yu et al. 2004; Chandran et al. 2007) The transcriptomic profile of DKK1 was analysed using these databases comparing primary and metastatic PCa. More details of the retrospective analysis in section 2.13.

From the three clinical datasets, the GDS1439 and GDS2545 showed significantly lower expression of *DKK1* in the metastatic PCa samples versus primary PCa samples. GDS1439: figure 8.6 A, primary PCa samples: n=7; metastatic PCa samples: n=6, unpaired t-test, p= 0.0012. GDS2545: figure 8.6 B, primary PCa samples: n=65, metastatic PCa samples: 25, Mann-Whitney test, p<0.0001. No significant differences were observed in the *DKK1* expression in the GDS3289 dataset among both groups, figure 8.6 C, primary PCa samples: n=31, metastatic PCa samples: 18, unpaired t-test.

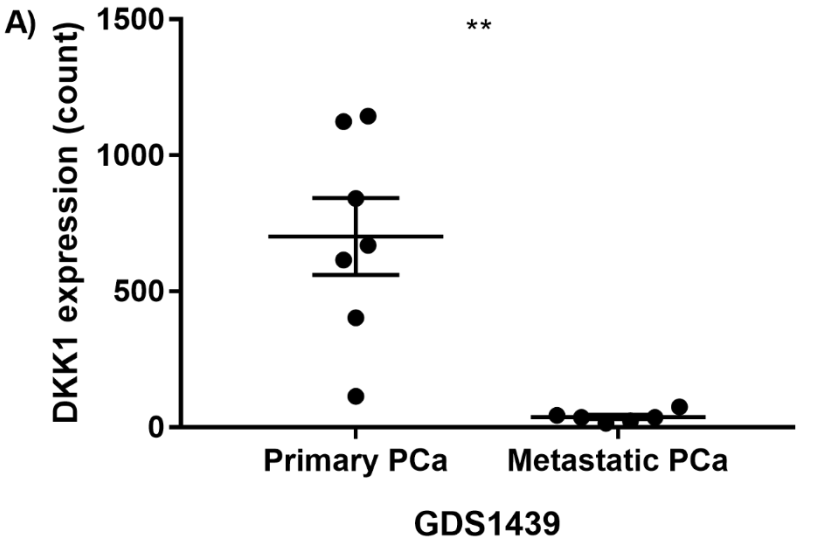
A)
1500
1000
500
0
DKK1 expression (count)
**
Primary PCa
Metastatic PCa
GDS1439

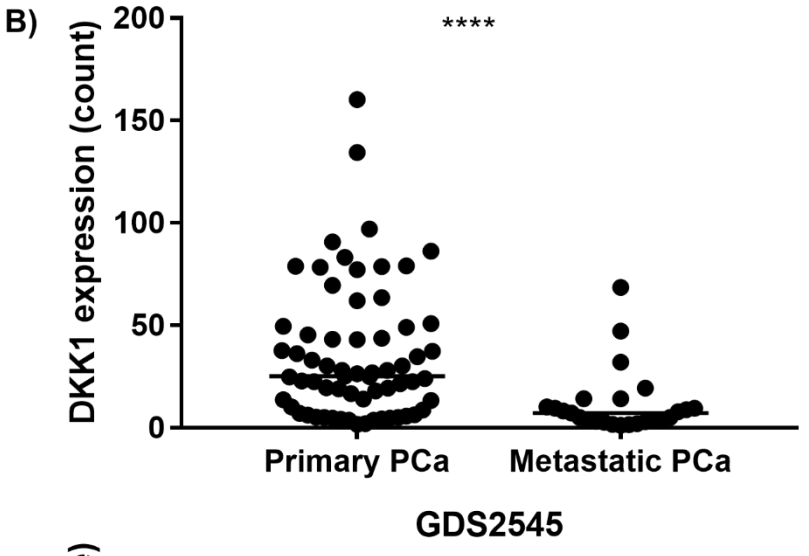
B)
200
150
100
50
0
DKK1 expression (count)
****
Primary PCa
Metastatic PCa
GDS2545

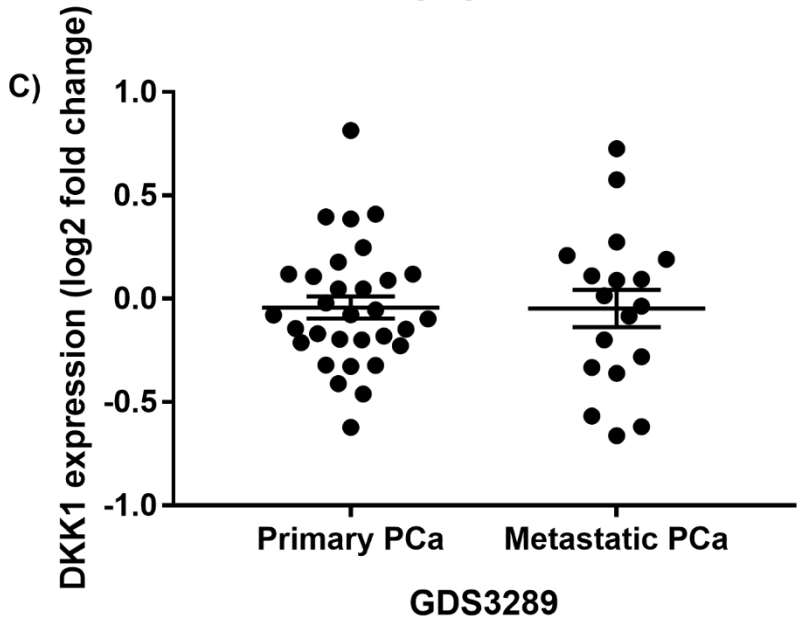
C)
1.0
0.5
0.0
-0.5
-1.0
DKK1 expression (log2 fold change)
Primary PCa
Metastatic PCa
GDS3289

**Figure 8. 6. DKK1 gene expression is downregulated in metastatic PCa compared to primary PCa patient samples**. *An analysis using the Genome Expression Omnibus database was performed to compare the genomic expression of DKK1 in three clinical data sets of primary and metastatic PCa. A and B) The analysis revealed a significantly lower gene expression of DKK1 in patients with metastatic PCa versus samples of patients with primary PCa in the clinical data set GDS 1439 and GDS 2545. C) No significant differences among both sample sets were analysed in the GDS3289 clinical data set. Values are mean ± SEM A) GDS1439: Primary PCa samples: n=7; metastatic PCa samples: n=6, unpaired t-test, p= 0.0012. B) GDS2545: Primary PCa samples: n=65, metastatic PCa samples: 25, Mann-Whitney test, p<0.0001. C) GDS3289: Primary PCa samples: n=31, metastatic PCa samples: 18, unpaired t-test.*

### 8.2.5. Mechanical loading affects the cytokine profile of naïve BALB/c nude mice

To further understand the impact of mechanical loading in PCa bone metastasis progression, we analysed the cytokine profile of 12-week-old naïve BALB/c nude mice subjected to right-tibial mechanical loading (presented in chapter 3). The serum samples of baseline, 1-week and 3-week loading were analysed using the multiplex Bio-Plex Pro Mouse Cytokine multiplex assay (Bio-Rad), manufactured to identify and analyse 23-cytokines, section 2.12.3. The results suggest that 10 cytokines were affected by mechanical loading stimulus. The cytokines found significantly increased were IL-3 (at 1$^{st,}$ week, 0.0342 and 3$^{rd}$ week, p=0.0403), TNF-α (at 1$^{st,}$ week, p=0.0371 and 3$^{rd}$ week, p= 0.0064), IL-6 (at 1$^{st}$ week, p=0.0296, and 3$^{rd}$ week, p=0.0250), IL-4 (at 1$^{st}$ week, p= 0.0309, and 3$^{rd}$ week, p= 0.0295), MCP-1 (at 1$^{st}$ week, p= 0.0087, and 3$^{rd}$ week, p= 0.0015), IL-5 (at 1$^{st}$ week, p=0.0340, and 3$^{rd}$ week, p=0.0265), KC (at 1$^{st}$ week, p= 0.0050 and 3$^{rd}$ week, p= 0.0005), GMCSF (at 1$^{st}$ week, p=0.0155, and 3$^{rd}$ week, p= 0.0141), MIP-1α (at 1$^{st}$ week, p=0.0026, and 3$^{rd}$ week, p<0.0001), IL-12p70 (at the 3$^{rd}$ week, p=0.0104), figure 8.7 A-J, One-way ANOVA, n≥5. The cytokine RANTES was found significantly lower in loaded groups compared to controls at the 1$^{st}$ week of loading stimulus, p=0.0275, figure 8.8 A, one-way ANOVA, n≥5. The quantitative data of all the cytokines analysed is presented in table 8.1.

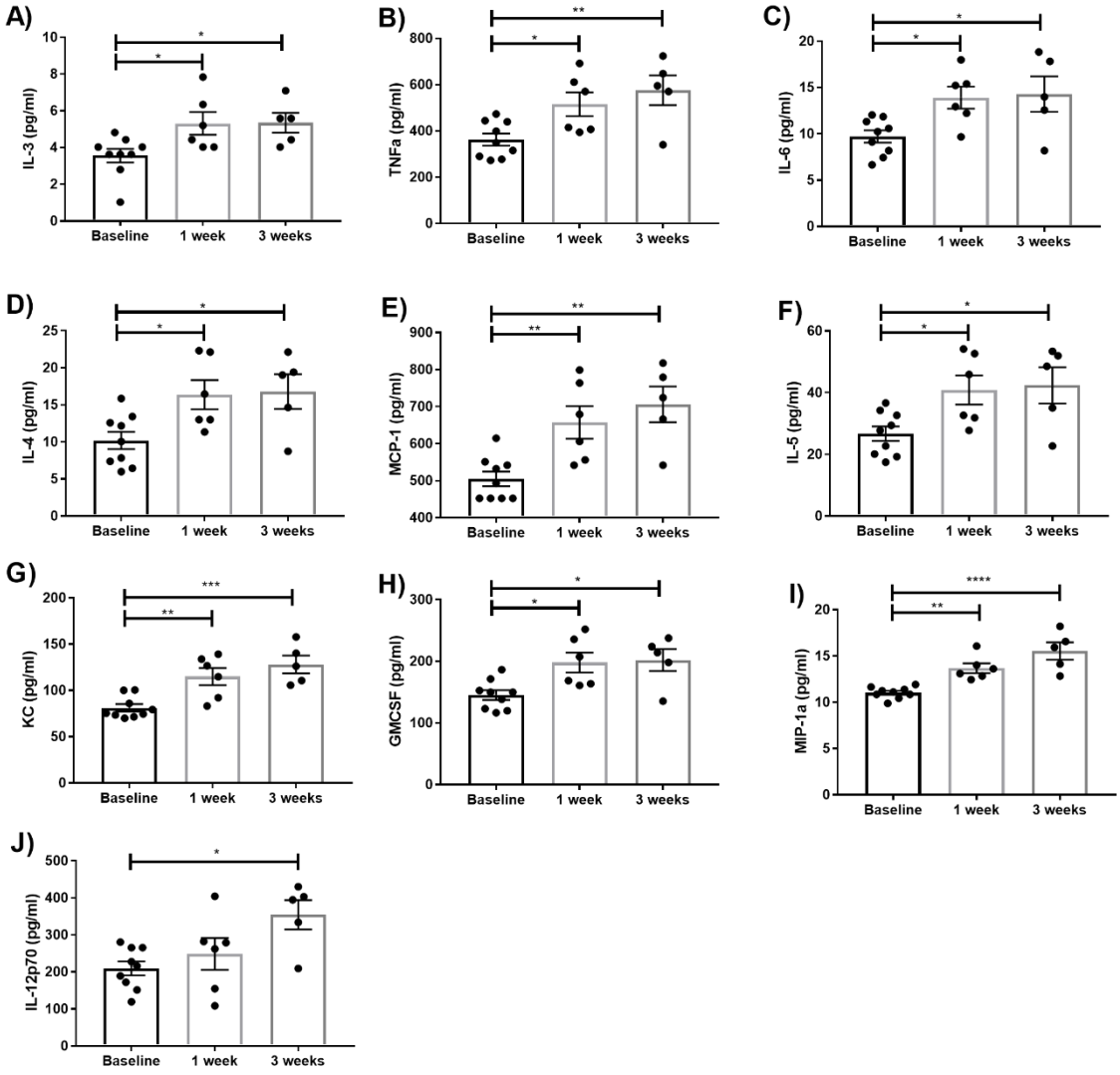


**Figure 8. 7. Mechanical loading affects the cytokine profile of naïve BALB/c nude mice.** *A panel of 23 cytokines of 12-week-old BALB/c nude mice subjected to right tibial mechanical loading was analysed by means of BioRad Mouse Cytokine multiplex assay. From the 23 cytokines analysed, 10 cytokines were found significantly upregulated either at the 3rd or 1st and 3rd weeks of mechanical loading stimulus: IL-3, TNF-α, IL-6, IL-4, MCP-1, IL-5, KC, GMCSF, MIP-1α and IL-12p70. Values are mean ± SEM, One-way ANOVA, n≥5, *p<0.05, **p < 0.01, ***p < 0.001, ****p < 0.0001.*

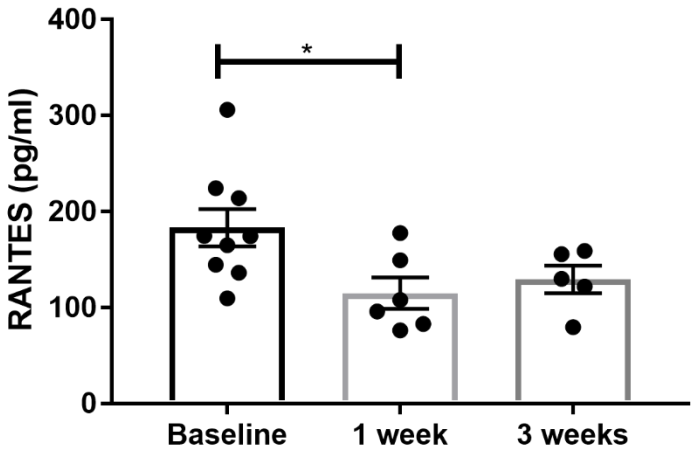


**Figure 8. 8. Mechanical loading affects the cytokine profile of naïve BALB/c nude mice.** *A panel of 23 cytokines of 12-week-old BALB/c nude mice subjected to right tibial mechanical loading was analysed by means of BioRad Mouse Cytokine multiplex assay. From the 23 cytokines analysed, RANTES was found significantly decreased compared to controls at the 1st week of loading stimulus. Values are mean ± SEM, One-way ANOVA, n≥5, *p<0.05.*

**Table 8. 1. Quantitative analysis of a 23-cytokine profile panel of naïve BALB/c nude mice subjected to right tibial mechanical loading stimulus.**

| | Non-loaded | 1 week loading | 3 weeks loading | P value Non-loaded vs 1 week of loading | P value Non-loaded vs 3 weeks of loading |
|---|---|---|---|---|---|
| | n=9 | n=6 | n=5 | | |
| **IL-3** | **3.55±0.36** | **5.31±0.62** | **5.34±0.53** | * | * |
| **TNF-α** | **362.3±26.08** | **515±51.53** | **575.4±64.32** | * | ** |
| **IL-6** | **9.72±0.65** | **13.91±1.187** | **14.29±1.91** | * | * |
| **IL-4** | **10.2±1.16** | **16.38±1.97** | **16.79±2.34** | * | * |
| **MCP-1** | **504.7±19.55** | **657.6±44.02** | **706±48.34** | ** | ** |
| **IL-5** | **26.72±2.35** | **40.86±4.698** | **42.36±5.88** | * | * |
| **KC** | **81.27±3.93** | **115.1±9.345** | **128.2±9.57** | ** | *** |
| **RANTES** | **183.1±19.46** | **114.9±16.35** | **129.1±14.32** | * | |
| **GMCSF** | **145.3±7.88** | **198±16.14** | **201.8±17.8** | * | * |
| **MIP-1α** | **11.04±0.20** | **13.69±0.52** | **15.54±0.93** | ** | **** |
| **IL-12p70** | **209.8±18.65** | **248.6±42.81** | **354.3±39.48** | **NS** | **NS *** |
| **IL-9** | 130.4±13.37 | 173.3±21.63 | 181.9±23.88 | NS | NS |
| **IFN-γ** | 105.3±10.38 | 123.2±12.76 | 130±13.82 | NS | NS |
| **G-CSF** | 141.9±6.12 | 154.1±23.89 | 158.5±8.49 | NS | NS |
| **IL-10** | 113.4±7.40 | 118.6±16.91 | 148.3±26.67 | NS | NS |
| **IL-17A** | 68.06±9.28 | 73.1±16.64 | 113.8±43.48 | NS | NS |
| **Eotaxin** | 3680±384.4 | 3887±517.3 | 4290±976.2 | NS | NS |
| **MIP-1b** | 246.8±10.75 | 253.2±21.74 | 267.3±12.28 | NS | NS |
| **IL-1α** | 14.03±1.56 | 17.51±3.09 | 22.06±3.056 | NS | NS |
| **IL-1β** | 11.33±1.63 | 20.33±2.79 | 18.88±5.49 | NS | NS |
| **IL-2** | 11.24±1.55 | 34.67±17.37 | 23.52±4.92 | NS | NS |

| | | | | | |
|---|---|---|---|---|---|
| **IL-13** | 228.2±24.53 | 342.6±37.99 | 344.6±52.01 | NS | NS |
| **IL-12p40** | 1913 ± 16 | 1443 ± 96.71 | 1396 ± 172 | NS | NS |

Values are mean ± SEM

**p<0.05* (One-way ANOVA)

***p<0.01* (One-way ANOVA)

****p< 0.001* (One-way ANOVA)

*****p< 0.0001* (One-way ANOVA)

### 8.2.6. Mechanical loading reduces the bone matrix stiffness in a homogeneous pattern

According to previous evidence, the ECM stiffness plays a role in the progression of cancer cells (Page et al. 2015; Grandhi et al. 2014; Senthebane et al. 2018; Walker et al. 2018; Lu et al. 2012). To test whether mechanical loading has altered the bone stiffness and thereby subsequently affected PCa bone metastasis progression, we analysed the mechanical properties of tibias from one 8-week-old C57BL/6 male mouse subjected to mechanical loading using AFM. Three measurements of 1mm, 1.5mm and 2mm were performed from the growth plate with a force map size and resolution of 30 µm × 30 µm and 30 pixels × 30 pixels, respectively. The ECM stiffness is represented as heat maps according to the Young's modulus from the Hertz-Sneddon fitting. The colour bar is in a log scale ranging from 1 to $10^6$, using Pascals (Pa) as measurement unit. The lower the Young's modulus is, the less stiffed the measured material is. According to the AFM analysis, the loaded tibia exhibits a less stiffed homogenous structure, specifically at 1.5mm and 2mm distance from the growth plate when compared to the non-loaded contra lateral tibia.

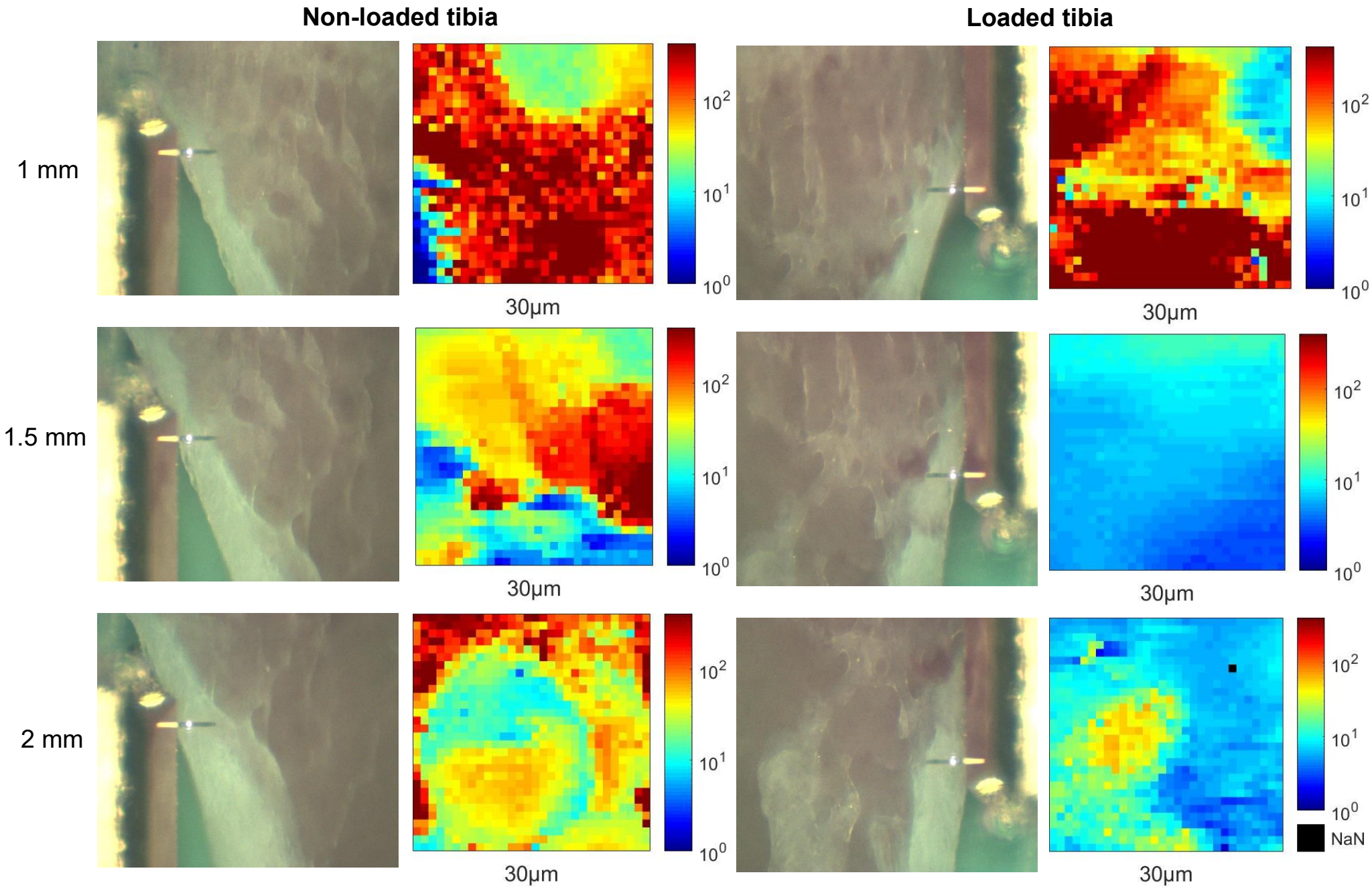
Non-loaded tibia
Loaded tibia
1 mm
1.5 mm
2 mm
30µm
30µm
30µm
30µm
30µm
30µm
$10^2$
$10^1$
$10^0$
NaN

**Figure 8. 9. Mechanical loading decreases the bone ECM stiffness.** *The bone ECM stiffness of a right tibia subjected to mechanical loading obtained from a single 8-week-old C57BL/6 mouse was analysed by means of atomic force microscopy (AFM). The non-loaded left tibia was used as internal control. Three measurements of 1 mm, 1.5 mm and 2 mm were performed taking the growth plate as starting reference. The stiffness is shown as heat maps corresponding to Young's modulus. The colour bar is in log scale (1-$10^6$ Pascals), presenting in dark red the regions with increased stiffness while those in blue represent less stiff bone regions. A decreased bone ECM stiffness is appreciated in the loaded tibia, particularly at 1.5 mm and 2 mm distance from the growth plate in a homogenous pattern.*

## 8.3. Discussion

In addition to the enhanced osteogenic response induced by mechanical loading and subsequent inhibition of the vicious cycle being the primary possibility of exercise inhibiting PCa bone metastasis as we suggested in previous chapters, other potential mechanisms are explored in this chapter. Firstly, the cytokine profile of patients is influenced by the type of exercise performed, either resulting in a pro-inflammatory or anti-inflammatory response. At the same time, the cytokine storm could promote or inhibit the progression of cancer, therefore we hypothesise that exercise may affect the cytokine expression in patients with PCa and alter its progression. To test this, we subjected osteoblasts cell lines to fluid flow media displacement and analysed their cytokine expression as well as a panel of 23 cytokines in the serum of pre-clinical models subjected to tibial mechanical loading or treadmill exercise to further understand the cytokine changes due to different exercise regimens. Moreover, the bone ECM stiffness plays a role in the development and progression of cancer. To test whether mechanical loading would affect the bone ECM stiffness, a naïve bone sample subjected to mechanical loading was analysed by AFM using the contra-lateral non-loaded bone as internal control.

The fluid flow media displacement revealed a greater number of cytokines expressed in the MG-63 OB cell line compared to the SaOS2 cells. This can be explained by the cell differentiation status of the SaOS2 and MG-63 cells. The SaOS2 osteoblasts cells display in a higher degree of mature osteoblast-cell like biology. SaOS2 cells express a similar ALP activity when compared to human primary osteoblasts (Czekanska et al. 2012; Clover & Gowenf 1994; Pautke et al. 2004; Saldaña et al. 2011). The core binding factor alpha1 (Cbfa1), Osterix (SP7), osteocalcin, bone sialoprotein (BSP), decorin, collagen I and III, are further osteoblasts markers highly expressed in SaOS2 cells which also have a consistent mineralisation activity compared to primary osteoblasts. The mentioned osteoblast features are missing or expressed in a lower degree in MG-63 cells, and they are considered to be in a pre-osteoblast status; therefore, they still carry a mesenchymal undifferentiated phenotype which explains the increase degree of expressed cytokines. For instance, MG-63 have been suggested to express stem-cell like markers such as ALDH, Oct4 and Nanog and stem-cell like features like chemoresistance (Honoki et al. 2010; Siclari & Qin 2010).

Other have shown the different gene cytokine expression status in mesenchymal cells versus differentiated bone-marrow cells, finding increased expression of cytokines in the mesenchymal cells when compared to osteoblasts, adipocytes and endothelial cells (Hyun et al. 2005).

From the cytokines found in these osteoblasts cell lines, DKK1 was consistently expressed in controls and reduced in fluid flow-treated cells. DKK1 is an inhibitor of the Wnt/β-catenin pathway, a downstream signalling important for osteoblasts differentiation and proliferation. According to the mechanical loading stimulus applied in the naïve BALB/c nude mice, DKK1 was reduced during the three weeks of loading stimulus, a phenomenon not observed in the immunocompromised and immunocompetent mice subjected to treadmill running. The previous results suggest that DKK1 was inhibited in models where a sufficient loading force to induce an osteogenic response and bone formation was applied. The bone parameters of immunocompromised mice further support the hypothesis that DKK1 is negatively correlated to bone mass. Indeed, our results are consistent with previous evidence that mechanical loading has been linked to reduced DKK1 levels whilst increasing bone formation in animal models (Robinson et al. 2006; Robling et al. 2008a; Agholme et al. 2011). Therefore, it is plausible to hypothesise that, in bone with PCa tumour cells already taking residence, exercise could reduce the secretion of DKK1, shift the balance of bone remodelling towards osteoblast bone formation, thereby negatively affect the initiation of vicious cycle and delay the bone metastasis process, as we observed in our mechanical loading experiments. To complement this hypothesis, osteocyte cell lines should be tested in the same manner, as they are suggested to be the mechanosensors cells within the bone and orchestrate the bone remodelling through influencing the osteoblasts and osteoclasts activity . Although the osteoblasts and BMSCs are the main sources of DKK1 within the bone, osteocytes also demonstrate increase DKK1 expression, where mechanical loading has been suggested to decrease its expression *in vivo* (Robling et al. 2008a; Terpos et al. 2019; Schaffler et al. 2014) To add, the quantitative levels of DKK1 should be analysed and verified by means of ELISA assay, as the membrane-based cytokine array is a semi-quantitative assay.

More recently, it has been suggested that DKK1 is secreted by a group of latency competent cancer cells, also known as dormant metastasis-initiating cells (Malladi et al. 2016). These cells are hypothesised to enter dormancy by growth inhibitory signals or factors by the host tissue stroma while initiate metastasis once they undergo pro-proliferative signals (Massagué & Obenauf 2016). In the model of Malladi et al. (2016), BCa and LCa latency competent cells underwent dormancy by SOX2/9 expression and autocrine secretion of DKK1 leading to inhibition of Wnt and its downstream proliferative signals. These cells also showed immune evasion by downregulation of ULBP ligands for NK cells. In line with this evidence, Wang et al. (2015) showed that PCa initiating cancer cells with a dormant phenotype have increase capacity to create bone metastasis once they are inoculated in *in vivo* models. To complement this data, we performed a clinical setting analysis using the Gene Expression Omnibus database, observing a significantly higher expression of DKK1 in primary PCa tumours compared to metastatic PCa samples, which showed lower DKK1 gene expression. Additional studies have found increased DKK1 expression in patients with PCa bone metastasis (Amelio et al. 2014). Given this information, we hypothesise that the role of DKK1 in PCa is stage dependant. The PCa metastasis-initiating cells will secrete DKK1 as a matter to create a pre-metastatic niche in the bone by stimulating osteoclast differentiation and bone resorption, an important step in the genesis of bone metastasis (Cox et al. 2015). Once the dormant metastasis-initiating cells nest the bone tissue, DKK1 would be downregulated to allow the formation of the osteoblastic phenotype of PCa bone metastasis, which is the main phenotype of this type of metastasis (Keller & Brown 2004). This hypothesis is supported by a recent work performed by Yue et al. (2022). In this study, BCa cells recruited osteoclastic progenitors via RSPO2/RANKL-LGR4 pathway, leading to pre-metastatic bone niche formation and increase bone metastasis. The RSPO2/RANKL-LGR4 pathway increased DKK1 levels, leading to *Rnasek* increased expression, a transmembrane V-ATPase–associated factor related to migration of a number of cells, including osteoclastic progenitors.

Inhibitors of DKK1 have been tested in multiple myeloma models as shown by Fulciniti et al. (2009). This group used a humanised IgG anti-DKK1 antibody named BHQ880 in *in vitro* and *in vivo* models. This agent inhibited DKK1 and achieved osteoblast differentiation and activity, resulting in increased trabecula thickness. The DKK1

inhibitor BHQ880 has also been used in combination with zoledronic acid and an anti-myeloma therapy, observing a delay in SRE and bone density increment (Lyer et al. 2014). Additionally, the group of Xu et al. (2015) used the micro-RNA152 to target DKK1 in mice models injected with MM cells. Inoculation of mi-RNA152 inhibited DKK1, leading to decreased bone resorption and increased bone mineralisation. In PCa, Wise et al. (2020) suggests DKK1 as an immunosuppressive agent in double-negative prostate cancer (DNPC). Blockage of DKK1 reduced the growth of PCa in a xenograft model in an NK-Cell dependent manner. This study provided the basis for a clinical trial to target DKK1 in PCa (NCT03837353). The mentioned studies further support the targeting of DKK1 to inhibit osteoclast activity and promote osteoblast activity. It would be of interest to test the mentioned agents, either antibodies or miRNA against DKK1 and or in combination with bisphosphonates, providing more evidence on the role of DKK1 in PCa bone metastasis.

The cytokine profile was also affected by mechanical loading. As most of cytokines show pro-inflammatory and pro-tumorigenic features, it is very intriguing to observe that RANTES was significantly reduced due to loading. RANTES, also known as CCL5, plays a pro-tumour activity in PCa. RANTES is found expressed in PCa cell lines, PCa primary cultures and PCa tissue samples (Vaday et al. 2005). RANTES promotes the proliferation and invasion of PCa, which can be inhibited by treatment of TAK-779, an antagonist of the RANTES receptor CCR5 (Maeda et al. 2012). Also, the proliferation of PCa is increased due to RANTES and IL-6 activity via RAS/RAC1/MAPK pathway, a phenomenon caused by the prostate specific membrane antigen (PSMA) (Colombatti et al. 2009). Additionally, tumour associated fibroblasts (TAMs) may secrete RANTES and promote prostate cancer stem cells (PCSCs) bone metastasis via β-catenin/STAT3 pathway according to Huang et al. (2020). The mentioned evidence may indicate a crosstalk pathway between RANTES and DKK1 worth of studying. Thus, RANTES could be of interest for further studies to assess its therapeutic potential. In addition, among all those up-regulated cytokines after mechanical loading, most of the evidence support that cytokines such as IL-3, IL-9, IFN-γ, IL-6, IL-5 have pro-osteoblastogenic roles or contribute in osteoclasts inhibition (Barhanpurkar et al. 2012; Soysa & Alles 2018; Srivastava et al. 2010; Macias et al. 2001; Noelle & Nowak 2010; Smith 2016; Xiao et al. 2017; Rauber et al. 2017; Tang et al. 2018). This is of importance as osteoblast activity has been linked

to release of pro-dormant factors such as TGFβ2, GDF10, BMP7, GAS6 and Wnt5a (Yumoto et al. 2016; Yu et al. 2019; Taichman et al. 2013; Shiozawa et al. 2010; Ren et al. 2019). As mentioned in chapter 5, these pro-dormant factors could have affected the proliferation of the PCa cells in the bone by delaying its onset. However, the upregulation of osteoclastogenic cytokines such as TNF-α, MCP-1, GM-CSF and MIP-1α was also observed. This could be explained by the time the serum samples were taken, which was after the 3$^{rd}$ week of loading stimulus. It is likely that at this time point, the osteoclast activity was enhanced to couple with the osteoblast activity as it happens in the bone remodelling process (Florencio-silva et al. 2015). As mentioned, the osteoclast activity is a key factor for the development of PCa bone metastasis; however, the PCa bone metastasis was found delayed as described in chapter 5, even with the suggestion of osteoclast activity. Possibly, other factors (i.e., the dormant factors and inhibition of DKK1) displayed an anti-tumour progression effect in the PCa bone metastasis which counteracted the osteoclast activity. The application of mechanical loading for a longer period of time would provide information on how the osteoclast activity, DKK1 and possibly osteoblast-released dormant factor influences PCa bone metastasis progression.

Another factor which could affect the progression of early PCa bone metastasis is the bone ECM stiffness. We observed a decreased stiffness in the loaded tibia compared to the non-loaded internal control. Particularly for cancers with predilection to metastasize the bone tissue, Page et al. (2015) tested the effect of matrix stiffness into BCa, LCa and PCa proliferation *in vitro*. This group applied a 2D polyurethane films with a stiffness of 70 MPa to 3800 MPa as a matter to mimic the stiffness in the basement membrane of cortical bone. In conditions of greater stiffness, the expression of the integrin β3 (ITGβ3) increased in hand with GLI2 and PTHrP, possibly via the TGF-β receptor type II (TGF-β RII). GLI2 and PTHrP are two factors associated with tumour progression, cancer-related osteolysis and have been found to be positively correlated with ECM stiffness (Thiyagarajan et al. 2007; Li et al. 2011; Ruppender et al. 2010). Inhibition of ITGβ3 in cancer cells, led to downregulation of GLI2 and PTHrP, decreased tumour growth and osteolysis *in vivo*. In a different study, it was tested that once PCa cells undergo cell-stroma contact by expressing integrin β1, there is downregulation of Cdc42 and TGFβ2, the latter being related to slow-cycling cancer cells (Ruppender et al. 2015; Yumoto et al. 2016). Downregulation of the mentioned

molecules led to MLCK activation, downregulation of the tumour suppressor E2F4 and upregulation of the pro-proliferative regulator CDK6, promoting the proliferation of PCa. As a less stiff bone ECM displays decreased integrin expression, this feature may inhibit the proliferation of PCa in the bone by reducing the cancer cell-bone ECM adhesion. Therefore, less bone ECM may confer an anti-proliferative PCa environment. Overall, a stiffened ECM tissue creates a pro-tumour environment due to increased expression of integrins, growth factors and genes, whilst this feature is not observed in a tissue with decreased stiffness, as the interaction between cancerous cells and ECM components will be decreased (Winkler et al. 2020; Pickup et al. 2014).

An important aspect to consider is the timing of mice subjected to mechanical loading. The tibia analysed by AFM was stimulated with mechanical loading for one week only (3 loading cycles). It is likely at this stage that the lower stiffness observed by AFM was due to presence of newly formed large area of woven bone, which displays a decreased stiffness and will be calcified later to lamellar bone (Turner et al. 1994; Moreira et al. 2019; Winkler et al. 2020). Therefore, an extended study of the bone ECM stiffness during a longer period of mechanical loading is needed, as the bone ECM stiffness could increase and affect PCa bone metastasis progression.

## 8.4. Conclusion

Mechanical loading inhibits the expression of DKK1, affecting the progression of PCa bone metastasis. Further cytokines such as RANTES (CCL5) are downregulated by mechanical loading with potential to reduce PCa progression. The ECM bone stiffness decreased by mechanical loading could affect the proliferation of PCa in bone.

# Chapter 9:

## General discussion

PCa is one of the most commons cancers diagnosed in men of western countries with an incidence of 52,300 new cases each year, representing 140 cases per day (2016-2018) (Cancer Research, UK). In 2018, the UK was ranked 7$^{th}$ amongst 31 European countries for PCa incidence, meaning that the incidence of PCa in the UK was higher compared to the European average (ABPI n.d.). It is estimated that 70% of patients with PCa will develop skeletal metastasis. Once PCa bone metastasis is diagnosed, the condition is considered to be incurable as current treatments available for PCa are inefficient to cure the bone metastasis. The survival rate is considered to have a significant decrease in the condition of skeletal metastasis. For instance, patients with diagnostic of primary PCa have a survival rate of 87% that decreases to 55% after 5 years of diagnosis while patients with skeletal metastasis have a survival rate of 47% which drops to 3% (Nørgaard et al. 2010). The inefficiency of currents treatments to cure PCa bone metastasis and its impact in the patient's survival rate, makes the targeting of better treatments against skeletal metastasis mandatory.

The benefits of exercise have been proved in patients with PCa. Either weight-bearing or running exercise led to improvement in body strength, body lean mass, cancer-related fatigue, quality of life and decreased PCa development and mortality (Keilani et al. 2017; Uth et al. 2018; Yunfeng et al. 2017; L Bourke et al. 2018). Additionally, exercise induces an anabolic response in the bone tissue towards bone formation and its benefits have also been shown in patients with PCa, such as increased or preventive loss of BMD (Westcott 2012; Newton et al. 2019; Yuan et al. 2016). Up to date, only one clinical trial has assessed the effect of exercise in patients with PCa bone metastasis, as patients at this stage may develop pathological fractures or bone lesions (Cormie et al. 2013).

Different exercise modalities, including tibial mechanical loading (to mimic load-bearing exercise), treadmill exercise and WBVP, have been applied in pre-clinical models of other cancer induced bone diseases, particular in osteolytic diseases such as breast cancer and multiple myeloma, resulting in improved bone mass and decreased cancer growth. One hypothesis states that the osteogenic response towards the osteoblast activation and inhibition of osteoclasts breaks the cancer vicious cycle, as in these models the cancer cells tend to drive osteolytic lesions and promote bone destruction (Lynch et al. 2013; Rummler et al. 2021; Guise 2002).

However, PCa is suggested to have a predilection to target osteoblasts and remain dormant until the cancerous cells reawaken and create overt metastasis. Therefore, the osteogenic response induced by exercise may be counterproductive in PCa as the seeding of PCa cells in bone may be increased due to the enhanced osteoblast activity and increase the risk of developing PCa bone metastasis.

In this project, pre-clinical models of PCa bone metastasis were subjected to three different exercise regimens as a matter to study the effect of exercise in the development of PCa bone metastasis. The chosen exercise modalities were tibial mechanical loading to mimic load-bearing exercise, treadmill running and WBVP (low-magnitude high-frequency), as they are exercise regimens suggested to improve the bone mass.

Firstly, we were able to induce and osteogenic response in 12-week-old immunocompromised mice with a mechanical loading protocol appropriate for this model regarding their age and sex as shown in chapter 3 (De Souza, Matsuura, et al. 2005). Up to date, this is the first study to assess male immunocompromised mice to mechanical loading stimulus, as most evidence has assessed immunocompetent models (Lynch et al. 2013; Rummler et al. 2021; Fan et al. 2021; Yang et al. 2019; M. Huang et al. 2021). This will provide important preliminary data and technical information for future other studies involving mechanical loading and xenografts or PDX models (Pompili et al. 2016). The osteogenic response achieved by loading may have been a result of osteoclast inhibition within the first week of stimulus (3 loads within a week) as demonstrated by the Quantikine TRAP5b ELISA analysis. Therefore, in the consecutive experiments, we chose one week loading stimulus as a set up point to study osteogenic response and PCa bone metastasis. In chapter 4, we study the arrival of PCa cell into bone as it is suggested that PCa target osteoblastic niches to establish footholds (Shiozawa et al. 2011; Wang et al. 2014). The number of PCa cells arriving at the BM was not increased under mechanical loading stimulus, suggesting that the enhanced osteogenic activity may not be a factor which attracts PCa cells into the BM.

Sequentially, we investigated whether continuous mechanical loading would affect the growth of PCa in bone in chapter 5. The mechanical loading stimulus applied

continuously for 3 weeks delayed the incidence of tibial tumour, reduced PCa tumour growth, and preserved bone tissue microarchitecture in several *in vivo* models. One theory, is that the decreased tumour burden and incidence might be consequence of breakage of the vicious cycle by inhibiting the osteoclast activity as observed in chapter 3 (Guise 2002; Lynch et al. 2013). Currently, anti-resorptive agents, such as bisphosphonates and the RANKL inhibitor Denosumab, have been used clinically for preventing skeletal related events in patients with bone metastases from solid tumours (Perry & Figgitt 2004; Zekri et al. 2014; Gül et al. 2016; Groot et al. 2018; Wang et al. 2020). Therefore, it would be interesting to compare or combine the effects of these anti-resorptive agents and mechanical loading in preventing the PCa bone metastasis. *In vivo* models of axial mechanical loading and zoledronic acid treatment have been evaluated, demonstrating a negative or null interaction of both modalities (Feher et al. 2010; Stadelmann et al. 2011). Although Denosumab is suggested to have a better effect in reducing SRE in patients with PCa compared to zoledronic acid, the higher cost of Denosumab and the fact that is not being recommended for PCa patients by NICE makes the combination of zoledronic acid with our mechanical loading regimen a more feasible option to test the combined effect of an osteogenic and osteoclastic-inhibiting treatment (NICE 2012; Fizazi et al. 2011)

In chapter 6, the effect of treadmill on PCa bone metastasis was better appreciated in the immunocompetent model which showed lower tumour burden and incidence at the earlier stage of the experiment. This has not been observed in the immunocompromised model, which enlighten the importance of the intact immune system during this process. However, the tumour burden at the end of the experiment did not differ among the exercised and sedentary groups. This should be emphasised as the treadmill regimen used for this model may have been detrimental and possibly led to immunosuppression at later stage. A recent meta-analysis focused on aerobic exercise (running, cycling) evidenced, in the case of high intensity training (HIT) exercises, that single HIT sessions may impair the immune system towards a negative but not clinically relevant response, while HIT performed for at least 3 sessions in alternate or consecutive days may lead to immune system improvement (Souza et al. 2021). In contrast, when HIT is performed until exhaustion for consecutive days may lead to immunosuppression. As discussed in chapter 6, the rest periods and longitudinal duration in treadmill running are important to achieve an osteogenic

response and boost the immune system (Bourzac et al. 2020; Walsh et al. 2011). Therefore, applying an appropriate exercise regimen in patients which does not lead to immunosuppression is essential. In addition, the benefit on PCa bone metastasis was not observed in the WBVP study in chapter 7. This further highlights the importance of applying appropriate exercise regimens not only in murine models but also can be later translated to clinical approaches, in order to achieve positive outcomes in patients.

The possible mechanisms leading to reduced PCa incidence and growth were tested in chapter 8, where several cytokines were evidenced to be modulated by mechanical loading. Among these altered cytokines by mechanical loading, DKK1 has been shown to play an important role in the formation of pre-metastasis niche in bone when secreted by primary PCa cells, whilst its expression will be downregulated once PCa bone metastasis have taken place to enable the osteosclerotic growth (Yue et al. 2022). This indicates the possibility of DKK1 being the major mediator for exercise preventing or delaying the onset of PCa bone metastasis, via regulating the bone pre-metastatic niche. To test this hypothesis, several future studies could be carried out. For example, orthotopic models of DKK1-WT, KO and overexpression PCa cells could represent better the clinical reality and help us pinpoint the role of DKK1 at the early stage of the PCa bone metastasis, particular under mechanical loading stimulus. Furthermore, DKK1 KO animal models have been used to test the effect of mechanical loading in the bone anabolic response before and could be applied to test the role of DKK1 in mediating the host bone microenvironment during PCa bone metastasis and exercise (Morse et al. 2020). RANTES was another cytokine downregulated by mechanical loading and it has been proposed to have a role in PCa progression and bone metastasis via β-catenin/STAT3 pathway (Huang et al. 2020; R. Huang et al. 2021). Studies assessing the combined role of DKK1 and RANTES in PCa bone metastasis are of interest as these two molecules might be regulated by weight-bearing exercise in the bone environment and affect PCa bone metastasis. The bone ECM was another element modified by mechanical loading, as its stiffness was found reduced after one week of loading. Cancer cells show decreased proliferation in lower ECM stiffness (J. Huang et al. 2021). Therefore, studies performed for a longer period of time on assessing how mechanical loading modifies the bone ECM and its potential impact in PCa proliferation would complement this project.

Studying the pro-dormancy factors (i.e., BMP7, GAS6, TGFβ2, Wnt5a) released by osteoblasts would expand the potential benefit of load-bearing stimulus in PCa bone metastasis (Shiozawa et al. 2010; Kobayashi et al. 2011; Yu et al. 2018; Ren et al. 2019). Targeting dormant markers could be a novel therapy approach as several authors suggest that maintaining the cancer cells in a dormant status could be a more feasible treatment strategy rather than reawakening the cancer cells and initiate aggressive (Recasens & Munoz 2019; Phan & Croucher 2020). Dormancy has already been induced as shown in models of ER+ BCa metastasis where tamoxifen (ER antagonist) or the aromatase inhibitor letrozole inhibit the proliferation of BCa cells and maintain BCa dormant for up to 10 years after diagnosis (Davies et al. 2013; Abderrahman & Jordan 2018). Inhibitors of CDK4/6 induce dormancy in several cancer models and the CDK4/6 inhibitor Palbociclib has been approved by the FDA in ER+ BCa (Wiedemeyer et al. 2010; Davies et al. 2013; Leary et al. 2016; Bollard et al. 2017; Chou et al. 2018). To examine whether exercise induce PCa cells dormancy or maintain them in dormant status longer, we could perform further in vivo experiments

Of notice, PCa mainly affects patients above 50 years old and is most commonly diagnosed between 65 and 69 years of age (Prostate Cancer UK 2022). In this project we used 8-week-old murine models to test the development of PCa bone metastasis in chapter 5-8, which age translated to humans resembles patients younger than 20 years old (Flurkey et al. 2007). This age was deliberately selected due to the feasibility of experimental model as young mice have higher tumour take rate compared to older models (N. Wang, Reeves, et al. 2015). However, this is not reflecting the clinical reality. In order to apply a murine model which mimics the age of PCa diagnosis, 18-24-months-old murine models (mirroring 56-69 human years) could be used for future verification studies. To overcome the low tumour take rate issue, the older mice can be subjected to castration which was shown to increase tumour take rate in aged mice (Flurkey et al. 2007; Ottewell et al. 2014).

The other obvious issue is the appropriate and effective magnitude or intensity of exercise to be adopted by PCa patients, which is particular important considering the generally older age of this patient cohorts. To achieve this goal, we need firstly translate our animal-based results into clinically applicable exercise regimens. As exercise settings optimized in mouse models (e.g., loading force in N) cannot be

applied to patients directly, we can use strain (strain: a measure of deformation in response to an applied force) as a cross-species common parameter to translate the pre-clinical data. In our mechanical load model, we observed an osteogenic response and bone formation when 9-12 N were applied in the mice's tibia. This is consistent with previous evidence which suggested that bone formation happens when strain is above 1200 με-1500 με, therefore exercises which produce a similar bone strain should be translated from murine models to patients (Frost 1987; De Souza, Matsuura, et al. 2005). Exercises which induces similar strains in human are zigzag uphill or downhill running which result in 1966 με and 1872 με respectively or 26 cm jump height (1905 με) (Burr et al. 1996; Milgrom et al. 2000). Several approaches could be adopted to further accurately measure the exact strain induced by various exercise regimens in our murine models. For example, the need to apply strain gauges in the murine models would highly complement this project. The strain gages have been widely used in animal and human to quantify the strain generated when the loading force is applied in the bone. We could also use innovative subject-specific computational models (finite element approach) to calculate the strain distribution in the bone subjected to exercise. Cross-species computational or *in silico* models can even be used to optimise meaningful exercise intensity in patients.

Furthermore, we must take into consideration that the loading stimulus in bone is local and does not influence contralateral limbs (Sugiyama, Price, et al. 2010). This has been assessed by hopping exercises in patients where jumping exercise improves the BMD femoral neck and the BMC of the femur at the trabecula and cortical compartments in the exercised leg only (Bailey & Brooke-wavell 2010; Allison et al. 2015). This is of importance as PCa tends to metastasize the hips, spine, and ribs while metastasis to the femur and humerus is not common and even rarer below the knee (Barkow et al. 1994; Bagi 2003). Therefore, the selected exercise should have a sufficient impact to induce an osteogenic response in bones where PCa has tropism to metastasize. Examples of these type of exercises are deadlifts or squats, as they induce load forces in the spine and hips (Granhed et al. 1987; Cappozzo et al. 1985). For instance, a recent study conducted by Watson et al. (2018) determined that High-Intensity Resistance and Impact Training (HiRIT) improved the BMD of the lumbar spine and femoral neck in post-menopausal women with clinically diagnosed low bone mass. The HiRIT combined deadlift, overhead press, and back squat exercises which

were safe and tolerable for the women as no adverse effects in the bone were reported. Another high intensity exercise modality training in patients with lung transplantation (associated with osteoporosis and sarcopenia) led to increased trabecular bone score in the spine of exercised patients. The exercised performed were uphill interval walking on a treadmill followed by muscular strength training which included leg press, arm press, back extension, and seated row in stationary machines (Ulvestad et al. 2021). These exercises modalities have provided important insights in designing effective and tolerable exercise regimens for men with PCa bone metastasis, not only to test the hypothesis of this project but also to be applied in future clinical trials.

## 9.1 General conclusion

Collectively, the results of the present study support our original hypothesis and demonstrate that load-bearing exercise plays a significant role in decreasing PCa bone metastasis by inducing osteogenic response and negatively modulating DKK1. Patients in risk of developing or with already stablished PCa bone metastasis may benefit from appropriate exercises regimens sufficient to induce an osteogenic response and boost the immune system towards an anti-tumour environment.

# APPENDIX A:

## Reagents & materials

**Table A.1.1 Reagents and material applied in tissue culture**

| **Reagent** | **Source** |
|---|---|
| Dulbecco's modified Eagle's medium (DMEM) | Thermo Fisher Scientific |
| Foetal calf serum (FCS) | Sigma-Aldrich |
| Penicillin-Streptomycin (Pen-Strep) | Thermo Fisher Scientific |
| Phosphate-buffered saline (PBS) | Thermo Fisher Scientific |
| Advanced DMEM/F12 | Thermo Fisher Scientific |
| GlutaMAX (100x) | Thermo Fisher Scientific |
| HEPES | Thermo Fisher Scientific |
| Collagenase type 2 | Abnova |
| DNAse | Thermo Fisher Scientific |
| Y-27632 | LKT Laboratories, Inc. |
| Ammonium chloride (NH4Cl) | Sigma-Aldrich |
| Potassium bicarbonate (KHCO3) | Sigma-Aldrich |
| EDTA | Thermo Fisher Scientific |
| Trypsin-EDTA | Thermo Fisher Scientific |
| Vibrant DiD | Thermo Fisher Scientific |
| **Material** | |
| Tissue culture 75cm$^2$ flasks | Thermo Fisher Scientific |
| 100 µm Cell strainer | Thermo Fisher Scientific |
| Disposable pipettes | Thermo Fisher Scientific |
| Tips | STARLAB |
| Haemocytometer | Thermo Fisher Scientific |
| Olympus inverted CK2 microscope | Olympus |

**Table A.1.2 Reagents and material applied in mechanical loading technique**

| **Reagent** | **Source** |
|---|---|
| Isoflurane | Zoetis Inc. |
| **Material** | |
| Bose ElectroForce 5500 Test | TA instruments |
| Anaesthetic machine | Burtons |

**Table A.1.3 Materials used in treadmill running exercise**

| **Material** | **Source** |
|---|---|
| LE8708 mouse treadmill | Stoelting |

**Table A.1.4 Reagents and material used in whole-body vibration platform stimulus**

| **Material** | **Source** |
|---|---|
| Juvent 1000 low intensity full body vibration platform | Juvent |

**Table A.1.5 Reagents and material used in histomorphometry**

| **Reagent** | **Source** |
|---|---|
| Neutral buffered formalin | In-house |
| Ethanol | In-house |
| EDTA | In-house |
| Paraffin wax | In-house |
| Sodium tartrate | Sigma-Aldrich |
| Sodium acetate trihydrate | Sigma-Aldrich |
| Naphthol AS-BI phosphate | Sigma-Aldrich |
| Dimethylformamide | Fisher |
| Pararosaniline | Sigma-Aldrich |
| Sodium nitrite | Sigma-Aldrich |
| Gill's II haematoxylin and blue | Sigma-Aldrich |
| Xylene | Sigma-Aldrich |
| DPX | Sigma-Aldrich |

**Table A.1.6 Materials used in multi-photon confocal microscopy**

| **Reagent** | **Source** |
|---|---|
| Bright Cryo-M-Bed | Bright Instrument Co Ltd |
| Liquid nitrogen | In-house |
| **Material** | |
| Zeiss LSM510 NLO Upright two-photon microscope | Carl Zeiss |
| Bright OTF Cryostat with a 3020 microtome | Bright Instrument Co Ltd |
| Nunc™ Glass Base Dish | Thermo Fisher Scientific |
| 22x22 mm Coverslips | Menzel-Gläser |
| Blu-tack | Bostik |
| Chameleon laser | Coherent |
| HeNe laser | Coherent |

**Table A.1.7 Materials used in bioluminescence assay**

| **Reagent** | **Source** |
|---|---|
| D-Luciferin | Thermo Fisher Scientific |
| **Material** | |
| IVIS Lumina II | PerkinElmer |

**Table A.1.8 Reagents and material used in Proteome Profiler Human XL Cytokine Array**

| **Reagent** | **Source** |
|---|---|
| Array buffer 4 | R & D systems |
| Array buffer 6 | R & D systems |
| Chemi reagent 1 | R & D systems |
| Chemi reagent 2 | R & D systems |
| Detection antibody cocktail, Human XL Cytokine Array | R & D systems |
| Streptavidin-HRP | R & D systems |
| Wash Buffer concentrate (25X) | R & D systems |

| **Material** | |
|---|---|
| Rectangular 4-well multi-dish | R & D systems |
| 4 Human XL Cytokine Array nitrocellulose membranes spotted with 105 different antibodies to human cytokines | R & D systems |
| Transparency overlay template | R & D systems |
| Rocking platform shaker | Antylia Scientific |
| Plastic transparent sheet protector | In-house |
| ChemiDoc MP imaging system | Bio-Rad Laboratories |

**Table A.1.9 Reagents and material used in Mouse DKK1 Quantikine ELISA**

| **Reagent** | **Source** |
|---|---|
| Mouse DKK1 standard | R & D systems |
| Mouse DKK1 control | R & D systems |
| Mouse DKK1 conjugate | R & D systems |
| Assay Diluent RD1-21 | R & D systems |
| Calibrator diluent RD5-26 concentrate | R & D systems |
| Wash Buffer concentrate | R & D systems |
| Colour reagent A and B | R & D systems |
| Stop solution | R & D systems |
| **Material** | |
| Mouse DKK1 microplate | R & D systems |
| Plate sealers | R & D systems |

**Table A.1.10 Reagents and material used in Magnetic multiplex immunoassay**

| **Reagent** | **Source** |
|---|---|
| Bio-Plex assay buffer | Bio-Rad Laboratories |
| Bio-Plex wash buffer | Bio-Rad Laboratories |
| Bio-Plex sample diluent | Bio-Rad Laboratories |
| 10x couple beads | Bio-Rad Laboratories |
| 10x detection antibodies | Bio-Rad Laboratories |
| 100x SA-PE | Bio-Rad Laboratories |

| Material | |
|---|---|
| 1-96 well assay plate | Bio-Rad Laboratories |
| Rocking platform shaker | Antylia Scientific |
| Sealing tape | Bio-Rad Laboratories |
| Magnetic 96-Well Separator | Thermo Fisher Scientific |
| Luminex 200 Multiplex Assay Instrument | Luminex Corporation |

**Table A.1.11 Reagents and material used in Atomic Force Microscopy analysis**

| Material | Source |
|---|---|
| JPK NanoWizard III AFM | JPK Instruments |

# References


Abderrahman, B. & Craig Jordan, 2018. Rethinking Extended Adjuvant Antiestrogen Therapy to Increase Survivorship in Breast Cancer. *JAMA Oncology*, 4(1), pp.15–16.

ABPI, No Title. Available at: https://www.abpi.org.uk/facts-figures-and-industry-data/cancer-in-the-uk-digital-data-toolkit/prostate-cancer/ [Accessed March 10, 2022].

Agholme, F. et al., 2011. The effects of Dickkopf-1 antibody on metaphyseal bone and implant fixation under different loading conditions. *Bone*, 48(5), pp.988–996. Available at: http://dx.doi.org/10.1016/j.bone.2011.02.008.

Ainsworth, B.E. et al., 2011. 2011 Compendium of physical activities. *Medicine and Science in Sports and Exercise*, 43(39), pp.1575–1581.

Alavanja, M.C.R. et al., 2003. Use of Agricultural Pesticides and Prostate Cancer Risk in the Agricultural Health Study Cohort. *American Journal of Epidemiology*, 157(9), pp.800–814.

Aldinucci, D. & Colombatti, A., 2014. The Inflammatory Chemokine CCL5 and Cancer Progression. *Mediators of inflammation*.

Allison, S.J. et al., 2015. The Influence of High-Impact Exercise on Cortical and Trabecular Bone Mineral Content and 3D Distribution Controlled Unilateral Intervention. *Journal of Bone and Mineral Research*, 30(9), pp.1709–1716.

Allocca, G. et al., 2019. The bone metastasis niche in breast cancer: potential overlap with the haematopoietic stem cell niche in vivo. *Journal of Bone Oncology*, 17, p.100244. Available at: https://doi.org/10.1016/j.jbo.2019.100244.

Amelio, P.D. et al., 2014. DKK-1 in prostate cancer diagnosis and follow up. *BMC Clinical Pathology*, 14(1), pp.1–6. Available at: BMC Clinical Pathology.

Anane, L.H. et al., 2009. Mobilization of cd T lymphocytes in response to psychological stress, exercise, and b-agonist infusion. *Brain Behavior and Immunity*, 23(6), pp.823–829. Available at: http://dx.doi.org/10.1016/j.bbi.2009.03.003.

Araujo, A. et al., 2018. Size Matters: Metastatic Cluster Size and Stromal Recruitment in the Establishment of Successful Prostate Cancer to Bone Metastases. *Bulletin of Mathematical Biology*, 80(5), pp.1046–1058. Available at: https://doi.org/10.1007/s11538-018-0416-4.

Avancini, A. et al., 2020. Exercise Levels and Preferences in Cancer Patients : A Cross-Sectional Study. *International Journal of Environmental Research and Public Health*, 17(15), p.5351.

Avrameas, S., T, T. & Guesdon, J., 1978. Coupling of Enzymes to Antibodies and Antigens. *Scandinavian Journal of Immunology*, 8, pp.7–23.

Bagi, C.M., 2003. Skeletal implications of prostate cancer. *Journal of Musculoskeletal and Neuronal Interactions*, 3(2), pp.112–117.

Bailey, C.A. & Brooke-wavell, K., 2010. Optimum frequency of exercise for bone health: Randomised controlled trial of a high-impact unilateral intervention. *Bone*, 46(4), pp.1043–1049. Available at: http://dx.doi.org/10.1016/j.bone.2009.12.001.

Baj, Z. et al., 1994. Immunological Status of Competitive Cyclists Before and After the Training Season. *International Journal of Sports Medicine*, 15(6), pp.319–324.

Baker, M.K. et al., 2018. Whole Body Vibration Exposure on Markers of Bone Turnover , Body Composition , and Physical Functioning in Breast Cancer Patients Receiving Aromatase Inhibitor Therapy : A Randomized Controlled Trial. *Integrative Cancer Therapies*, 17(3), pp.968–978.

Balemans, W. et al., 2001. Increased bone density in sclerosteosis is due to the deficiency of a novel secreted protein ( SOST ). *Human Molecular Genetics*, 10(5), pp.537–544.

Bankhead, P. et al., 2017. QuPath: Open source software for digital pathology image analysis. *Scientific Reports*, 7(1), p.16878.

Barhanpurkar, A.P. et al., 2012. IL-3 promotes osteoblast differentiation and bone formation in human mesenchymal stem cells. *Biochemical and Biophysical Research Communications*, 418(4), pp.669–675. Available at: http://dx.doi.org/10.1016/j.bbrc.2012.01.074.

Barkow, U. et al., 1994. Solitary metastasis of prostate cancer in the tibia. *Aktuelle Radiologie*, 4(5), p.274–6.

Barna, M. et al., 2008. Suppression of Myc oncogenic activity by ribosomal protein haploinsufficiency. *Nature*, 456(7224), pp.971–5. Available at: https://www.ncbi.nlm.nih.gov/pmc/articles/PMC4485391/.

Baron, R. et al., 1985. Cell-mediated Extracellular Acidification and Bone Resorption: Evidence for a Low pH in Resorbing Lacunae and Localization of a 100-kD Lysosomal Membrane Protein at the Osteoclast Ruffled Border. *The Journal of Cell Biology*, 101(6), pp.2210–2222.

Baron, R. & Rawadi, G., 2007. Targeting the Wnt/Catenin Pathway to Regulate Bone Formation in the Adult Skeleton. *Endocrinology*, 148(6), pp.2635–2643.

Barry, D.W. et al., 2012. Acute Calcium Ingestion Attenuates Exercise-induced Disruption of Calcium Homeostasis. *Medicine and Science in Sports and Exercise*, 43(4), pp.617–623.

Berraondo, P. et al., 2019. Cytokines in clinical cancer immunotherapy. *British Journal of Cancer*, 120, pp.6–15. Available at: http://dx.doi.org/10.1038/s41416-018-0328-y.

Bodine, P.V.N. & Komm, B.S., 2006. Wnt signaling and osteoblastogenesis. *Reviews in Endocrine and Metabolic Disorders*, 7, pp.33–39.

Bollard, J. et al., 2017. Palbociclib ( PD-0332991 ), a selective CDK4 / 6 inhibitor , restricts tumour growth in preclinical models of hepatocellular carcinoma. *Gut*, 66(7), pp.1286–1296.

Bourke, L., Turner, R., Greasley, R., Sutton, E., Steed, L., Smith, D., Brown, J., Kelly, B., Hulme, C., Greenfield, D., Persad, R., Farrin, A., Hewison, J. & Rosario, D.J., 2018. A multi-centre investigation of delivering national guidelines on exercise training for men with advanced prostate cancer undergoing androgen deprivation therapy in the UK NHS. *PLoS ONE*, 13(7), pp.1–14.

Bourke, L., Turner, R., Greasley, R., Sutton, E., Steed, L., Smith, D., Brown, J., Kelly, B., Hulme, C., Greenfield, D., Persad, R., Farrin, A., Hewison, J. & Rosario, D.J., 2018. A multi-centre investigation of delivering national guidelines on exercise training for men with advanced prostate cancer undergoing androgen deprivation therapy in the UK NHS. *PLoS ONE*, 13(7), pp.1–14.

Bourke, L. et al., 2018. Exercise training as a novel primary treatment for localised prostate cancer : a multi-site randomised controlled phase II study. *Scientific Reports*, 8(8374), pp.1–10.

Bourzac, C. et al., 2020. Effects of running exercise on bone histological parameters in Wistar rats: Comparison between continuous and intermittent running. *Bone Reports*, 13, p.5. Available at: https://doi.org/10.1016/j.bonr.2020.100313.

Bouxsein, M.L. et al., 2010. Guidelines for assessment of bone microstructure in rodents using micro-computed tomography. *Journal of Bone and Mineral Research*, 25(7), pp.1468–1486.

Burr, D.B. et al., 1996. In Vivo Measurement of Human Tibial Strains During Vigorous Activity. *Bone*, 18(5), pp.405–410.

Burr, D.B. & Allen, M.R., 2013. *Basic and Applied Bone Biology* 1st ed. D. B. Burr & M. R. Allen, eds., Academic Press.

Campbell, J.P. et al., 2012. Models of Bone Metastasis. *Journal of Visualized Experiments*, 67, pp.1–7. Available at: http://www.jove.com/video/4260/models-of-bone-metastasis.

Cancer Research, U., No Title. Available at: https://www.cancerresearchuk.org/health-professional/cancer-statistics/statistics-by-cancer-type/prostate-cancer#heading-Zero [Accessed March 10, 2022].

Cappella, B. & Dietler, G., 1999. Force-distance curves by atomic force microscopy. *Surface Science Reports*, 34(1–3), pp.1–3, 5–104.

CAPPOZZO, A. et al., 1985. Lumbar spine loading during half squat exercises. *Medicine and Science in Sports and Exercise*, 17(5), pp.613–620.

Carriero, A. et al., 2014. Ex vivo determination of bone tissue strains for an in vivo mouse tibial loading model. *Journal of Biomechanics*, 47(10), pp.2490–2497.

Cavendish, M., 2010. *Mammal Anatomy* Illustrate., Marshall Cavendish.

Centers for Disease Control, 2011. Overcoming barriers to physical activity. Available at: https://www.cdc.gov/physicalactivity/basics/adding-pa/barriers.html.

Chandran, U.R. et al., 2007. Gene expression profiles of prostate cancer reveal involvement of multiple molecular pathways in the metastatic process. *BMC Cancer*, 7(64), pp.1–21.

Charoenphan, S. & Polchai, A., 2006. Finite Element Modeling for Strain Rate Dependency of Fracture Resistance in Compact Bone. *Journal of Biomechanical Engineering*, 129(1), pp.20–25.

Chen, D. et al., 2020. Exercise Attenuates Brain Aging by Rescuing Down-Regulated Wnt / β -Catenin Signaling in Aged Rats. *Frontiers in Aging Neuroscience*, 12(April), pp.1–12.

Chodzko-Zajko, W.J. et al., 2009. Exercise and Physical Activity for Older Adults. *Medicine and Science in Sports and Exercise*, 41(7), pp.1510–1530.

Chou, A. et al., 2018. Tailored first-line and second-line CDK4-targeting treatment combinations in mouse models of pancreatic cancer. *Pancreas*, 67(12), pp.2142–2155.

Chow, J.W.M. et al., 1998. Mechanical loading stimulates bone formation by reactivation of bone lining cells in 13-week-old rats. *Journal of Bone and Mineral Research*, 13(11), pp.1760–1767.

Christiansen, B.A. & Silva, M.J., 2006. The Effect of Varying Magnitudes of Whole-Body Vibration on Several Skeletal Sites in Mice. *Annals of biomedical engineering*, 34(7), pp.1149–1156.

Clark, D.P. & Badea, C.T., 2014. Micro-CT of rodents: State-of-the-art and future perspectives. *Physica Medica*, 30(6), pp.619–634.

Clarke, B., 2008. Normal Bone Anatomy and Physiology. *Clinical Journal of the American Society of Nephrology*, 3(3), pp.131–139.

Clines, K.L. & Clines, G.A., 2018. DKK1 and Kremen Expression Predicts the Osteoblastic Response to Bone. *Translational Oncology*, 11(4), pp.873–882. Available at: https://doi.org/10.1016/j.tranon.2018.04.013.

Close, D.M. et al., 2011. In vivo bioluminescent imaging (BLI): Noninvasive visualization and interrogation of biological processes in living animals. *Sensors*, 11(1), pp.180–206.

Clover, J. & Gowenf, M., 1994. Are MG-63 and HOS TE85 Human Osteosarcoma Cell Lines Representative Models of the Osteoblastic Phenotype ? *Bone*, 15(6), pp.585–591.

Colditz, J. et al., 2018. Postnatal Skeletal Deletion of Dickkopf-1 Increases Bone Formation and Bone Volume in Male and Female Mice, Despite Increased Sclerostin Expression. *Journal of Bone and Mineral Research*, 33(9), pp.1698–1707.

Colombatti, M. et al., 2009. The Prostate Specific Membrane Antigen Regulates the Expression of IL-6 and CCL5 in Prostate Tumour Cells by Activating the MAPK Pathways. *PLoS ONE*, 4(2).

Cormie, P. et al., 2013. Safety and efficacy of resistance exercise in prostate cancer patients with bone metastases. *Prostate Cancer and Prostatic Diseases*, 16(4), pp.328–335.

Courneya, K.S. & Friedenreich, C., 2011. *Physical Activity and Cancer* 1st ed. K. S. Courneya & C. Friedenreich, eds., Springer-Verlag Berlin Heidelberg.

Cox, T.R. et al., 2015. The hypoxic cancer secretome induces pre-metastatic bone lesions through lysyl oxidase. *Nature*, 522, pp.106–110.

Craft, N. et al., 1999. Evidence for Clonal Outgrowth of Androgen-independent Prostate Cancer Cells from Androgen-dependent Tumors through a Two-Step Process. *Cancer Research*, 59(19), pp.5030–5036.

Craven, G., Steers, E. & Anfinsen, C., 1965. Purification , and Molecular Weight p-G1 a ac t osi d ase of Escherichia coli K12 of the. *Journal of Biological Chemistry*, 240(6), pp.2468–2477.

Crevenna, R. et al., 2017. Whole body vibration therapy on a treatment bed as additional means to treat postprostatectomy urinary incontinence. *Wiener Medizinische Wochenschrift*, 167(5–6), pp.139–141.

Crowther, J.R., 2009. *The ELISA Guidebook* 2nd ed., Humana Press.

Czekanska, E.M. et al., 2012. IN SEARCH OF AN OSTEOBLAST CELL MODEL FOR IN VITRO RESEARCH. *European Cells and Materials*, 24, pp.1–17.

Damaraju, S. et al., 2014. The Effect of Mechanical Stimulation on Mineralization in Differentiating Osteoblasts in Collagen-I Scaffolds. *Tissue Engineering*, 20(23–24), pp.3142–3153.

Davies, C. et al., 2013. Long-term effects of continuing adjuvant tamoxifen to 10 years versus stopping at 5 years after diagnosis of oestrogen receptor-positive breast cancer: ATLAS, a randomised trial. *Lancet*, 381(9869), pp.805–816.

Day, R.N. & Davidson, M.W., 2009. The fluorescent protein palette: tools for cellular imaging. *Chemical Society Reviews*, 38(10), pp.2887–2921.

Devignes, C. et al., 2018. HIF signaling in osteoblast-lineage cells promotes systemic breast cancer growth and metastasis in mice. *Proceedings of the National Academy of Sciences of the United States of America*, 115(5).

Dinarello, C.A., 2006. The paradox of pro-inflammatory cytokines in cancer. *Cancer and Metastasis Reviews*, 25, pp.307–313.

Discacciati, A., Orsini, N. & Wolk, A., 2012. Body mass index and incidence of localized and advanced prostate cancer—a dose–response metaanalysis of prospective studies. *Annals of Oncology*, 23(7), pp.1665–1671.

Drake, J.M., Gabriel, C.L. & Henry, M.D., 2005. Assessing tumor growth and distribution in a model of prostate cancer metastasis using bioluminescence imaging. *Clinical and Experimental Metastasis*, 22(8), pp.674–684.

Dudley, R. & Spiro, D., 1961. The Fine Structure of Bone Cells. *The Journal of Biophysical and Biochemical Cytology*, 11(3), pp.627–649.

EB, G. et al., 2003. Reduced mechanical load decreases the density , stiffness , and strength of cancellous bone of the mandibular condyle. *Clinical Biomechanics*, 18(4), pp.358–363.

Elliott, J.C. & Dover, S.D., 1982. X-ray microtomography. *Journal of Microscopy*, 126(2), pp.211–213.

Engvall, E., 2010. The ELISA , Enzyme-Linked Immunosorbent Assay. *Clinical*

*Chemistry*, 56(2), pp.319–320.

Engvall, E. & Perlmann, P., 1971. Enzyme-linked immunosorbent assay (ELISA) Quantitative assay of immunoglobulin G. *Immunochemistry*, 8(9), pp.4–7.

Enzymes, O.F., Proteins, T.O. & Avrameas, S., 1969. Immunoelectrophoretic analysis Electrophoresis in acrylamide-agarose gels Molecular sieving chromatography U ltracentrifugation analysis Immunofluorescence microscopy. *Immunochemistry*, 6(1), pp.43–48.

Esser, K.A. et al., 2009. Physical Activity Reduces Prostate Carcinogenesis in a Transgenic Model. *Prostate*, 69(13), pp.1372–1377.

Everts, V. et al., 2002. The Bone Lining Cell: Its Role in Cleaning Howship ' s Lacunae and Initiating Bone Formation. *Journal of Bone and Mineral Research*, 17(1), pp.77–90.

Fairey, A.S. et al., 2005. Randomized controlled trial of exercise and blood immune function in postmenopausal breast cancer survivors. *Journal of Applied Physiology*, 98(4), pp.1534–1540.

Fan, Y. et al., 2021. Mechanical tibial loading remotely suppresses brain tumors by dopamine-mediated downregulation of CCN4. *Bone Research*, 9(26).

Fan, Y. et al., 2020. Skeletal loading regulates breast cancer-associated osteolysis in a loading intensity-dependent fashion. *Bone Research*, 8(9), pp.1–11. Available at: http://dx.doi.org/10.1038/s41413-020-0083-6.

Feher, A. et al., 2010. Bisphosphonates do not inhibit periosteal bone formation in estrogen de fi cient animals and allow enhanced bone modeling in response to mechanical loading. *Bone*, 46(1), pp.203–207. Available at: http://dx.doi.org/10.1016/j.bone.2009.10.023.

Feng, J.Q. et al., 2007. Loss of DMP1 causes rickets and osteomalacia and identifies a role for osteocytes in mineral metabolism. *Nature Genetics*, 38(11), pp.1310–1315.

Fizazi, K. et al., 2011. Denosumab versus zoledronic acid for treatment of bone metastases in men with castration-resistant prostate cancer: a randomised , double-blind study. *The Lancet*, 377(9768), pp.813–822. Available at: http://dx.doi.org/10.1016/S0140-6736(10)62344-6.

Florencio-silva, R. et al., 2015. Biology of Bone Tissue: Structure , Function , and Factors That Influence Bone Cells. *BioMed Research International*, 2015(421746), pp.1–17.

Flurkey, K., Currer, J.M. & Harrison, D.E., 2007. Mouse Models in Aging Research. In *The Mouse in Biomedical Research (Second Edition)*. pp. 637–672.

Fornera, S. & Walde, P., 2010. Spectrophotometric quantification of horseradish peroxidase with o -phenylenediamine. *Analytical Biochemistry*, 407(2), pp.293–295. Available at: http://dx.doi.org/10.1016/j.ab.2010.07.034.

Forwood, M.R. et al., 1996. Increased bone formation in rat tibiae after a single short period of dynamic loading in vivo. *The American journal of physiology*, 270(3), pp.419–23. Available at: http://www.ncbi.nlm.nih.gov/pubmed/8638687.

Fotiadis, D. et al., 2002. Imaging and manipulation of biological structures with the AFM. *Micron*, 33(4), pp.385–397.

Franchignoni, F., Vercelli, S. & Özçakar, L., 2012. Hematuria in a runner after treatment with whole body vibration : A case report. *Scandinavian Journal of Medicine and Science in sports*, 23(3), pp.383–385.

Franz-Odendaal, T.A., Hall, B.K. & Witten, P.E., 2006. Buried Alive : How Osteoblasts Become Osteocytes. *Developmental Dynamics*, 235(1), pp.176–190.

Fritton, J.C. et al., 1997. Whole-body vibration in the skeleton: development of a resonance-based testing device. *Annals of Biomedical Engineering*, 25(5), pp.831–9.

Frost, H.M., 1987. Bone “Mass” and the “Mechanostat ”: A Proposal. *The Anatomical Record*, 219(1), pp.1–9.

Frost, H.M., 2001a. From Wolff’s Law to the Utah Paradigm: Insights About Bone Physiology and Its Clinical Applications. *The Anatomical Record*, 262(4), pp.398–419.

Frost, H.M., 2001b. From Wolff ’ s Law to the Utah Paradigm: Insights About Bone Physiology and Its Clinical Applications. *The Anatomical Record*, 262(4), pp.398–419.

Fukada, E. & Yasuda, I., 1957. On the Piezoelectric Effect of Bone. *Journal of The Physical Society of Japan*, 12, pp.1158–1162.

Fulciniti, M. et al., 2009. Anti-DKK1 mAb (BHQ880) as a potential therapeutic agent for multiple myeloma. *Blood*, 114(2), p.371–379.

Fung, E.B. et al., 2012. The effect of whole body vibration therapy on bone density in patients with thalassemia: A pilot study. *American Journal of Hematology*, 87(10), pp.E76–E79.

Furbert-harris, P. et al., 2003. Inhibition of Prostate Cancer Cell Growth by Activated Eosinophils. *The Prostate*, 57(2), pp.165–175.

Galão, M.J. et al., 2011. Optimization of the tartrate-resistant acid hosphatase detection by histochemical method. *European Journal of Histochemistry*, 55(1), pp.1–4.

Galvão, D. et al., 2006. Resistance Training and Reduction of Treatment Side Effects in Prostate Cancer Patients. *Medicine and Science in Sports and Exercise*, 38(12), pp.2045–2052.

Galvão, D.A. et al., 2008. Changes in muscle, fat and bone mass after 36 weeks of maximal androgen blockade for prostate cancer. *BJU International*, 102(1), pp.44–47.

Gann, P.H., 2002. Risk Factors for Prostate Cancer. *Reviews in Urology*, 4(5), pp.3–10.

Ghajar, C.M. et al., 2013. The perivascular niche regulates breast tumour dormancy. *Nature Cell Biology*, 15(7), pp.807–817.

Gleeson, M. et al., 2000. Immune status and respiratory illness for elite swimmers during a 12-week training cycle. *International Journal of Sports Medicine*, 21(4), pp.302–307.

Goh, J., Lim, C.L. & Suzuki, K., 2019. Effects of Endurance-, Strength-, and Concurrent Training on Cytokines and Inflammation. In R. B. Schumann M., ed. *Concurrent Aerobic and Strength Training*. pp. 125–138. Available at: https://doi.org/10.1007/978-3-319-75547-2_9.

Gómez-Cabello, A. et al., 2012. Effects of Training on Bone Mass in Older Adults. *Sports Medicine*, 42(4), pp.301–325.

Gong, Y., Chippada-Venkata, U.D. & Oh, W.K., 2014. Roles of matrix metalloproteinases and their natural inhibitors in prostate cancer progression. *Cancers*, 6(3), pp.1298–1327.

Goodship, A., Lanyon, L. & McFie, H., 1979. Functional Adaptation of Bone to Increased Stress. *The Journal of Bone and Joint Surgery*, 61(4), pp.539–546.

Graham, H., Chandler, D.J. & Dunbar, S.A., 2019. The genesis and evolution of bead-based multiplexing. *Methods*, 158, pp.2–11. Available at: https://doi.org/10.1016/j.ymeth.2019.01.007.

Grandhi, T.S.P. et al., 2014. Design of Bone Microenvironment Mimicking Antibiotic-based Hydrogels for Generation of Three Dimensional Tumor Models of Dormancy and Relapse. *Society for Biomaterials*.

GRANHED, H., JONSON, R. & HANSSON, T., 1987. The Loads on the Lumbar Spine During Extreme.pdf. *Spine*, 12(2), pp.146–149.

Griffin, M., 1996. *Handbook of Human Vibration*,

Groot, A.F. De et al., 2018. The anti-tumor effect of RANKL inhibition in malignant solid tumors – A systematic review. *Cancer Treatment Reviews*, 62, pp.18–28. Available at: https://doi.org/10.1016/j.ctrv.2017.10.010.

Gross, T. et al., 2002. Noninvasive Loading of the Murine Tibia: An In Vivo Model for the Study of Mechanotransduction. *Journal of Bone and Mineral Research*, 17(3), pp.493–501.

Guadalupe-Grau, A. et al., 2009. Exercise and bone mass in adults. *Sports Medicine*, 39(6), pp.439–468. Available at: http://www.springerlink.com/content/9x334157g700u405/?p=a61c45c139434bb2801de27c80c11d10&pi=34.

Gueritat, J. et al., 2014. Free Radical Biology and Medicine Exercise training combined with antioxidant supplementation prevents the antiproliferative activity of their single treatment in prostate cancer through inhibition of redox adaptation. *Free Radical Biology and Medicine*, 77, pp.95–105.

Guillemant, J. et al., 2004. Acute Effects of an Oral Calcium Load on Markers of Bone Metabolism During Endurance Cycling Exercise in Male Athletes. *Calcified Tissue International*, 74, pp.407–414.

Guise, T.A., 2002. The vicious cycle of bone metastases. *Journal of Musculoskeletal and Neuronal Interactions*, 2(6), pp.570–572.

Gül, G. et al., 2016. A comprehensive review of denosumab for bone metastasis in patients with solid tumors Review A comprehensive review of denosumab for bone metastasis in patients with solid tumors. *Current Medical Research and Opinion*, 32(1), pp.133–145.

Guo, D. et al., 2010. Identification of Osteocyte-Selective Proteins. *Proteomics*, 10(20), pp.3688–3698.

Guo, Y. et al., 2015. Effect of the same mechanical loading on osteogenesis and osteoclastogenesis in vitro. *Chinese Journal of Traumatology*, 18(3), pp.150–156. Available at: http://dx.doi.org/10.1016/j.cjtee.2014.09.004.

Hagberg, M. et al., 2014. Osteoblasts stimulate the osteogenic and metastatic progression of castration-resistant prostate cancer in a novel model for in vitro and in vivo studies. *Clinical and Experimental Metastasis*, 31(3), pp.269–283.

Hahn, M. et al., 1992. Trabecular bone pattern factor-a new parameter for simple quantification of bone microarchitecture. *Bone*, 13(4), pp.327–330.

Hall, C.L. et al., 2008. Dickkopf-1 expression increases early in prostate cancer development and decreases during progression from primary tumor to metastasis. *Prostate*, 68(13), pp.1396–1404.

Hamdy, F.C. et al., 2016. 10-Year Outcomes after Monitoring, Surgery, or Radiotherapy for Localized Prostate Cancer. *The New England Journal of Medicine*, 375(15), pp.1415–1424.

Han, R. & Chen, J., 2021. A modified Sneddon model for the contact between conical indenters and spherical samples. *Journal of Materials Research*, 36(8), pp.1762–1771. Available at: https://doi.org/10.1557/s43578-021-00206-5.

Hanahan, D. & Weinberg, R.A., 2011. Hallmarks of Cancer: The Next Generation. *Cell*, 144(5), pp.646–74. Available at: http://dx.doi.org/10.1016/j.cell.2011.02.013.

Hardell, L. et al., 2006. Adipose Tissue Concentrations of Persistent Organic Pollutants and the Risk of Prostate Cancer. *Journal of Occupational and Enviromental Medicine*, 48(7), pp.10–12.

Hayashida, H. et al., 2015. Effects of the Menstrual Cycle and Acute Aerobic Exercise on Cytokine Levels. *Journal of Sports Medicine & Doping Studies*, 6(1), pp.6–10.

He, D. et al., 2006. CD8+ IL-17 producing T cells are important in effector functions for the elicitation of contact hypersensitivity responses. *Journal of Immunology*, 177(10), pp.6852–6858.

Hensel, J. & Thalmann, G.N., 2016. Biology of Bone Metastases in Prostate Cancer. *Urology*, 92, pp.6–13. Available at: http://dx.doi.org/10.1016/j.urology.2015.12.039.

Hert, J., Lisková, M. & Landa, J., 1971. Reaction of bone to mechanical stimuli. 1. Continuous and intermittent loading of tibia in rabbit. *Folia Morphologica*, 19(3), pp.290–300.

Hert, J., Sklenská, A. & Lisková, M., 1971. Reaction of bone to mechanical stimuli. 5.

Effect of intermittent stress on the rabbit tibia after resection of the peripheral nerves. *Folia Morphologica*, 19(4), pp.378–387.

Hildebrand, T. & Rüegsegger, P., 1997. Quantification of bone microarchitecture with the structure model index. *Computer Methods in Biomechanics and Biomedical Engineering*, 1(1), pp.15–23.

Hoffman, W., Lakkis, F.G. & Chalasani, G., 2016. B Cells , Antibodies , and More. *Clinical Journal of the American Society of Nephrology*, 11(1), pp.137–154.

Hogan, M.B. et al., 2003. Regulation of Eosinophilopoiesis in a Murine Model of Asthma. *The Journal of Immunology*, 171(5), pp.2644–2651.

Hojman, P. et al., 2011. Exercise-induced muscle-derived cytokines inhibit mammary cancer cell growth. *American Journal of Physiology. Endocrinology and Metabolism*, 301(3), pp.504–510.

Holguin, N. et al., 2013. Adaptation of tibial structure and strength to axial compression depends on loading history in Both C57BL/6 and BALB/c mice. *Calcified Tissue International*, 93(3), pp.211–221.

Holguin, N., Brodt, M.D. & Silva, M.J., 2017. Activation of Wnt Signaling by Mechanical Loading Is Impaired in the Bone of Old Mice. *Journal of Bone and Mineral Research*, 31(12), pp.2215–2226.

Honoki, K. et al., 2010. Possible involvement of stem-like populations with elevated ALDH1 in sarcomas for chemotherapeutic drug resistance. *Oncology Reports*, 24, pp.501–505.

Hough, J. et al., 2013. Salivary cortisol and testosterone responses to high-intensity cycling before and after an 11-day intensified training period. *Journal of Sports Sciences*, 31(14), pp.1614–23.

Houser, B., 2012. Bio-Rad ' s Bio-Plex ® suspension array system , xMAP technology overview. *Archives of Physiology and Biochemistry*, 118(4), pp.192–196.

Howden, E.J. et al., 2019. Exercise as a diagnostic and therapeutic tool for the prevention of cardiovascular dysfunction in breast cancer patients. *European Journal of Preventive Cardiology*, 26(3), pp.305–315.

Huang, J. et al., 2021. Extracellular matrix and its therapeutic potential for cancer treatment. *Signal Transduction and Targeted Therapy*, 6(153), pp.1–24. Available at: http://dx.doi.org/10.1038/s41392-021-00544-0.

Huang, M. et al., 2021. Mechanical loading attenuates breast cancer - associated bone metastasis in obese mice by regulating the bone marrow microenvironment. *Journal of Cellular Physiology*, 236(9), pp.6391–6406.

Huang, R. et al., 2020. CCL5 derived from tumor-associated macrophages promotes prostate cancer stem cells and metastasis via activating β -catenin / STAT3 signaling. *Cell Death and Disease*, 11(4), p.234. Available at: http://dx.doi.org/10.1038/s41419-020-2435-y.

Huang, R. et al., 2021. Research Trends and Regulation of CCL5 in Prostate Cancer. *OncoTarget and Therapies*, 14, pp.1417–1427.

Humphries, B. et al., 2009. Whole-body vibration effects on bone mineral density in women with or without resistance training. *Aviation, Space, and Environmental Medicine*, 80(12), pp.1025–31.

Hurst, R. et al., 2004. Actin-Related Protein 2/3 Complex Is Required for Actin Ring Formation. *Journal of Bone and Mineral Research*, 19(3), pp.499–506.

Hyun, D. et al., 2005. Gene expression profile of cytokine and growth factor during differentiation of bone marrow-derived mesenchymal stem cell. *Cytokine*, 31(2), pp.119–126.

Idorn, M. & Hojman, P., 2016. Exercise-Dependent Regulation of NK Cells in Cancer Protection. *Trends in Molecular Medicine*, 22(7), pp.565–577. Available at: http://dx.doi.org/10.1016/j.molmed.2016.05.007.

Iyer, S.P. et al., 2014. A Phase IB multicentre dose-determination study of BHQ880 in combination with anti-myeloma therapy and zoledronic acid in patients with relapsed or refractory multiple myeloma and prior skeletal-related events. *British Journal of Haemathology*, 167(3), pp.366–375.

Jacome-galarza, C.E. et al., 2019. Developmental origin, functional maintenance and genetic rescue of osteoclasts. *Nature*, 568, pp.541–545. Available at: http://dx.doi.org/10.1038/s41586-019-1105-7.

Jadaan, D.Y., Jadaan, M.M. & McCabe, J.P., 2015. Cellular plasticity in prostate cancer bone metastasis. *Prostate Cancer*.

Jaivika Govindbhai Patel and Anjali R Bhise, 2017. Effect of Aerobic Exercise on Cancer-related Fatigue. *Indian Journal of Palliative Care*, 23(4), pp.355–361.

Jakobsson, K., Mikoczy, Z. & Skerfving, S., 1997. Deaths and tumours among workers grinding stainless steel : a follow up. *Journal of Occupational and Enviromental Medicine*, 54(11), pp.825–829.

Janckila, A.J. et al., 2001. Naphthol-ASBI phosphate as a preferred substrate for tartrate-resistant acid phosphatase isoform 5b. *Journal of Bone and Mineral Research*, 16(4), pp.788–793.

Jiang, T., Zhou, C. & Ren, S., 2016. Role of IL-2 in cancer immunotherapy. *OncoImmunology*, 5(6), pp.1–10. Available at: http://dx.doi.org/10.1080/2162402X.2016.1163462.

Jones, L.W. et al., 2012. Exercise modulation of the host-tumor interaction in an orthotopic model of murine prostate cancer. *Journal of Applied Physiology*, 113(2), pp.263–272. Available at: http://jap.physiology.org/cgi/doi/10.1152/japplphysiol.01575.2011.

Jones, L.W. et al., 2012. Exercise modulation of the host-tumor interaction in an orthotopic model of murine prostate cancer. *Journal of Applied Physiology*, 113(2), pp.263–272.

Jones, M.K. et al., 2014. Prostate Cancer and Occupational Exposure to Whole-Body Vibration in a National Population-Based Cohort Study. *AMERICAN JOURNAL OF INDUSTRIAL MEDICINE*, 57(8), pp.896–905.

Kaighn, M. et al., 1979. Establishment and characterization of a human prostatic

carcinoma cell line (PC-3). *Investigative Urology*, 17(1), pp.16–23.

Kameyama, S. et al., 2013. Short-term mechanical stress inhibits osteoclastogenesis via suppression of DC-STAMP in RAW264 . 7 cells. *International Journal of Molecular Medicine*, 31, pp.292–298.

Karst, M. et al., 2015. Roles of Stromal Cell RANKL, OPG, and M-CSF Expression in Biphasic TGF-β Regulation of Osteoclast Differentiation. *Journal of Cellular Physiology*, 200(1), pp.99–106.

Kartikasari, A.E.R. et al., 2021. Tumor-Induced Inflammatory Cytokines and the Emerging Diagnostic Devices for Cancer Detection and Prognosis. *Frontiers in Oncology*, 11(692142), pp.1–16.

Keilani, M. et al., 2017. Effects of resistance exercise in prostate cancer patients : a meta-analysis. *Supportive Care in Cancer*, 25(9), pp.2953–2968.

Keller, E.T. & Brown, J., 2004. Prostate Cancer Bone Metastases Promote Both Osteolytic and Osteoblastic Activity. *Journal of Cellular Biochemistry*, 91, pp.718–729.

Kenfield, S.A. et al., 2011. Physical activity and survival after prostate cancer diagnosis in the health professionals follow-up study. *Journal of Clinical Oncology*, 29(6), pp.726–732.

Kenfield, S.A. et al., 2011. Physical Activity and Survival After Prostate Cancer Diagnosis in the Health Professionals Follow-Up Study. *Journal of Clinical Oncology*, 29(6), pp.726–732.

Khandekar, M.J., Cohen, P. & Spiegelman, B.M., 2011. Molecular mechanisms of cancer development in obesity. *Nature Reviews Cancer*, 11(12), pp.886–95.

Khuon, S. et al., 2010. Myosin light chain kinase mediates transcellular intravasation of breast cancer cells through the underlying endothelial cells: a three-dimensional FRET study. *Journal of Cell Science*, 123(3), pp.431–440. Available at: http://jcs.biologists.org/cgi/doi/10.1242/jcs.053793.

Kim, T.H. et al., 2017. Effects of exercise training on circulating levels of Dickkpof-1 and secreted frizzled- related protein-1 in breast cancer survivors : A pilot single-blind randomized controlled trial. *PLoS ONE*, 12(2), pp.1–13. Available at: http://dx.doi.org/10.1371/journal.pone.0171771.

Kobayashi, A. et al., 2011. Bone morphogenetic protein 7 in dormancy and metastasis of prostate cancer stem-like cells in bone. *The Journal of Experimental Medicine*, 208(13), pp.2641–2655. Available at: http://www.jem.org/lookup/doi/10.1084/jem.20110840.

Kohl, T.O. & Ascoli, C.A., 2017a. Direct Competitive Enzyme-Linked Immunosorbent Assay (ELISA). *Cold Spring Harbor Protocols*, 7, pp.564–569.

Kohl, T.O. & Ascoli, C.A., 2017b. Immunometric Double-Antibody Sandwich Enzyme-Linked Immunosorbent Assay. *Cold Spring Harbor Protocols*, pp.458–463.

Kohl, T.O. & Ascoli, C.A., 2017c. Indirect Immunometric ELISA. *Cold Spring Harbor Protocols*, 5, pp.396–402.

Kourko, O. et al., 2019. IL-27, IL-30, and IL-35: A Cytokine Triumvirate in Cancer. *Frontiers in Oncology*, 9, pp.1–15.

Krstev, S. & Knutsson, A., 2019. Occupational Risk Factors for Prostate Cancer : A Meta-analysis. *Journal of Cancer Prevention*, 24(2), pp.91–111.

Kuchimaru, T. et al., 2018. A reliable murine model of bone metastasis by injecting cancer cells through caudal arteries. *Nature Communications*, 9, p.2981. Available at: http://dx.doi.org/10.1038/s41467-018-05366-3.

Kuen, D., Kim, B. & Kim, B., 2020. IL-17-Producing Cells in Tumor Immunity : Friends or Foes ? *Immune Network*, 20(1), pp.1–20.

Kulkarni, R.N. et al., 2010. Inhibition of osteoclastogenesis by mechanically loaded osteocytes: Involvement of MEPE. *Calcified Tissue International*, 87(5), pp.461–468.

Kulkarni, R.N. et al., 2012. Mechanical loading prevents the stimulating effect of IL-1 b on osteocyte-modulated osteoclastogenesis. *Biochemical and Biophysical Research Communications*, 420(1), pp.11–16. Available at: http://dx.doi.org/10.1016/j.bbrc.2012.02.099.

Kundu, M., Roy, A. & Pahan, K., 2017. Selective neutralization of IL-12 p40 monomer induces death in prostate cancer cells via IL-12 – IFN- γ. *Proceedings of the National Academy of Sciences of the United States of America*, 114(43).

Kuo, Z. et al., 2016. Osteogenic differentiation of preosteoblasts on a hemostatic gelatin sponge. *Scientific reports*, 6(32884), pp.1–12.

Kusama, Y. et al., 1995. Mechanisms of eosinophilia in BALB/c-nu/+ and congenitally athymic BALB/c-nu/nu mice infected with Toxocara canis. *Immunology*, 84, pp.461–468.

Lacy, P., 2017a. *Eosinophil Cytokines in Allergy*, Elsevier Inc. Available at: http://dx.doi.org/10.1016/B978-0-12-804214-4.00011-7.

Lacy, P., 2017b. Eosinophil Cytokines in Allergy. In *Cytokine Effector Functions in Tissues*. pp. 173–218.

Lai, Y. et al., 2009. CD4 + T Cell-Derived IL-2 Signals during Early Priming Advances Primary CD8 + T Cell Responses. *PLoS ONE*, 4(11), pp.1–14.

Lambers, F.M. et al., 2013. Trabecular bone adapts to long-term cyclic loading by increasing stiffness and normalization of dynamic morphometric rates. *Bone*, 55(2), pp.325–334. Available at: http://dx.doi.org/10.1016/j.bone.2013.04.016.

Lan, T., Chen, L. & Wei, X., 2021. Inflammatory Cytokines in Cancer: Comprehensive Understanding and Clinical Progress in Gene Therapy. *Cells*, 10(100), pp.1–16.

Lanyon, L. & Rubin, C., 1984. Static vs dynamic loads as an influence on bone remodelling. *Journal of Biomechanics*, 17(12), pp.897–905. Available at: http://www.ncbi.nlm.nih.gov/pubmed/4077869.

Lanyon, L. & Smith, R., 1969. Measurements of bone strain in the walking animal. *Research in Veterinary Science*, 10(1), pp.93–94.

Leary, B.O., Finn, R.S. & Turner, N.C., 2016. Treating cancer with selective CDK4/6 inhibitors. *Nature Reviews Clinical Oncology*, 13(7), pp.417–430.

Lee, D. et al., 2017. Running as a Key Lifestyle Medicine for Longevity. *Progress in Cardiovascular Diseases*, 60(1), pp.45–55. Available at: http://dx.doi.org/10.1016/j.pcad.2017.03.005.

Lee, K.C.L., Maxwell, A. & Lanyon, L.E., 2002. Validation of a technique for studying functional adaptation of the mouse ulna in response to mechanical loading. *Bone*, 31(3), pp.407–412.

Lee, Y.P. et al., 2002. Use of zoledronate to treat osteoblastic versus osteolytic lesions in a severe-combined-immunodeficient mouse model. *Cancer Research*, 62(19), pp.5564–5570.

Leitzmann, M.F. & Rohrmann, S., 2012. Risk factors for the onset of prostatic cancer: Age, location, and behavioral correlates. *Clinical Epidemiology*, 4(1), pp.1–11.

Leong, H.S. et al., 2014. Invadopodia Are Required for Cancer Cell Extravasation and Are a Therapeutic Target for Metastasis. *Cell Reports*, 8(5), pp.1558–1570. Available at: http://dx.doi.org/10.1016/j.celrep.2014.07.050.

Li, J. et al., 2011. PTHrP drives breast tumor initiation , progression , and metastasis in mice and is a potential therapy target. *The Journal of Clinical Investigation*, 121(12), pp.4655–4669.

Li, X. et al., 2016. Knee loading inhibits osteoclast lineage in a mouse model of osteoarthritis. *Scientific Reports*, 6(April), pp.1–13. Available at: http://dx.doi.org/10.1038/srep24668.

Lisková, M. & Hert, J., 1971. Reaction of bone to mechanical stimuli. 2. Periosteal and endosteal reaction of tibial diaphysis in rabbit to intermittent loading. *Folia Morphologica*, 19(3), pp.301–317.

Liu, Y. et al., 2011. Does Physical Activity Reduce the Risk of Prostate Cancer ? A Systematic Review and Meta-analysis. *European Urology*, 60(5), pp.1029–1044.

Lombardi, G. et al., 2016. Implications of exercise-induced adipo-myokines in bone metabolism. *Endocrine*, 54(2), pp.284–305.

Lombardi, G., Ziemann, E. & Banfi, G., 2019. Physical Activity and Bone Health : What Is the Role of Immune System ? A Narrative Review of the Third Way. *Frontiers in Endocrinology*, 10(60), pp.1–21.

Lowder, T. et al., 2005. Moderate exercise protects mice from death due to influenza virus. *Brain, Behavior, and Immunity*, 19(5), pp.377–380.

Lu, P., Weaver, V.M. & Werb, Z., 2012. The extracellular matrix: A dynamic niche in cancer progression. *Journal of Cancer Prevention*, 196(4), pp.395–406.

Lynch, M. et al., 2013. In Vivo Tibial Compression Decreases Osteolysis and Tumor Formation in a Human Metastatic Breast Cancer Model. *Journal of Bone and Mineral Research*, 28(11), pp.2357–2367.

Lynch, M. et al., 1995. The influence of type I collagen on the development and

maintenance of the osteoblast phenotype in primary and passaged rat calvarial osteoblasts modification of expression of genes supporting. *Experimental Cell Research*, 216(1), pp.35–45.

Macias, M.P. et al., 2001. Expression of IL-5 alters bone metabolism and induces ossification of the spleen in transgenic mice. *The Journal of Clinical Investigation*, 107(8), pp.949–959.

Maeda, K. et al., 2012. CCR5 inhibitors: emergence, success, and challenges. *Expert Opinion on Emerging Drugs*, 17(2), pp.135–145.

Main, R.P., Lynch, M.E. & Meulen, M.C.H. van der, 2014a. Load-induced changes in bone stiffness and cancellous and cortical bone mass following tibial compression diminish with age in female mice. *The Journal of Experimental Biology*, 217(10), pp.1775–1783.

Main, R.P., Lynch, M.E. & Meulen, M.C.H. van der, 2014b. Load-induced changes in bone stiffness and cancellous and cortical bone mass following tibial compression diminish with age in female mice. *Journal of Experimental Biology*, 217(10), pp.1775–1783.

Malladi, S. et al., 2016. Metastatic Latency and Immune Evasion through Autocrine Inhibition of WNT. *Cell*, 165, pp.45–60.

Mantila Roosa, S.M., Liu, Y. & Turner, C.H., 2011. Gene expression patterns in bone following mechanical loading. *Journal of Bone and Mineral Research*, 26(1), pp.100–112.

Marenzana, M., De Souza, R.L. & Chenu, C., 2007. Blockade of beta-adrenergic signaling does not influence the bone mechano-adaptive response in mice. *Bone*, 41(2), pp.206–215.

Marín-Cascales, E. et al., 2018. Whole-body vibration training and bone health in postmenopausal women. *Medicine*, 97(34).

Massagué, J. & Obenauf, A.C., 2016. Metastatic colonization by circulating tumour cells. *Nature*, 529(7586), pp.298–306.

Matic, I. et al., 2017. Quiescent Bone Lining Cells Are a Major Source of Osteoblasts During Adulthood. *Stem cells*, 34(12), pp.2930–2942.

Matsumoto, M. et al., 2004. Essential Role of p38 Mitogen-activated Protein Kinase in Cathepsin K Gene Expression during Osteoclastogenesis through Association of NFATc1 and PU . 1. *The Journal of biological chemistry*, 279(44), pp.45969–45979.

Mccabe, N.P. et al., 2010. Intraosseous injection of RM1 murine prostate cancer cells promotes rapid osteolysis and periosteal bone deposition. *Clinical and Experimental Metastasis*, 25(5), pp.581–590.

McCulloch, C.A.G. & Heersche, J.N.M., 1988. Lifetime of the Osteoblast in Mouse Periodontium. *The Anatomical Record*, 222(2), pp.128–135.

McCullough, D.J. et al., 2013. Effects of exercise training on tumor hypoxia and vascular function in the rodent preclinical orthotopic prostate cancer model. *Journal of Applied Physiology*, 115(12), pp.1846–1854.

Mcdonald, M.M. et al., 2021. Osteoclasts recycle via osteomorphs during RANKL-stimulated bone resorption. *Cell*, 184(5), pp.1330–1347.

Meakin, L.B., Price, J.S. & Lanyon, L.E., 2014. The contribution of experimental in vivo models to understanding the mechanisms of adaptation to mechanical loading in bone. *Frontiers in Endocrinology*, 5(154), pp.1–13.

Michaelson, M.D. et al., 2010. Management of Complications of Prostate Cancer Treatment. *A Cancer Journal for Clinicians*, 58(4), pp.196–213.

Midura, R.J., Evanko, S.P. & Hascall, V.C., 1994. Parathyroid Hormone Stimulates Hyaluronan Synthesis in an Osteoblast-like cell line. *The Journal of biological chemistry*, (18), pp.13200–13206.

Milgrom, C. et al., 2000. Do high impact exercises produce higher tibial strains than running ? *British Journal of Sports Medicine*, 34, pp.195–199.

Miller, S. et al., 1980. Characterization of endosteal bone-lining cells from fatty marrow bone sites in adult beagles. *The Anatomical Record*, 198(2), pp.163–173.

Minsky, M., 1988. Memoir on inventing the confocal scanning microscope. *Scanning*, 10(4), pp.128–138.

Moreira, C.A., Dempster, D.W. & Baron, R., 2019. *Anatomy and Ultrastructure of Bone – Histogenesis, Growth and Remodeling* E. [Internet], ed., Available at: https://www.ncbi.nlm.nih.gov/books/NBK279149/.

Morse, A. et al., 2020. Increased anabolic bone response in Dkk1 KO mice following tibial compressive loading. *Bone*, 131, p.115054. Available at: https://doi.org/10.1016/j.bone.2019.115054.

Mulari, M.T.K. et al., 2003. Osteoclast Ruffled Border Has Distinct Subdomains for Secretion and Degraded Matrix Uptake. *Traffic*, 4(2), pp.113–125.

Murphya, E.A. et al., 2012. Benefits of exercise training on breast cancer progression and inflammation in C3(1)SV40Tag mice. *Cytokine*, 55(2), pp.274–279.

Mussbacher, M. et al., 2019. Cell Type-Specific Roles of NF-κ B Linking Inflammation and Thrombosis. *Frontiers in Immunology*, 10(85), pp.1–31.

Nakane, K. & Kawaoi, A., 1974. PEROXIDASE-LABELED A NEW ANTIBODY METHOD CONJUGATION. *The Journal of Histochemistry and Cytochemistry*, 22(12), pp.1084–1091.

Namiki, M., Ueno, S. & Kitagawa, Y., 2012. Role of hormonal therapy for prostate cancer : perspective from Japanese experiences. *Translational Andrology and Urology*, 1(3), pp.160–172.

Newton, R.U. et al., 2019. Exercise Mode Specificity for Preserving Spine and Hip Bone Mineral Density in Prostate Cancer Patients. *Medicine and Science in Sports and Exercise*, 51(4), pp.607–614.

Newton, R.U. et al., 2018. Intense Exercise for Survival among Men with Metastatic Castrate-Resistant Prostate Cancer ( INTERVAL-GAP4 ): a multicentre ,

randomised , controlled phase III study protocol. *British Medical Journal*, 8(5).

Nguyen, V.T., Morange, M. & Bensaude, O., 1988. Firefly luciferase luminescence assays using scintillation counters for quantitation in transfected mammalian cells. *Analytical Biochemistry*, 171(2), pp.404–408.

NICE, 2012. Denosumab for the prevention of skeletal-related events in adults with bone metastases from solid tumours. Available at: https://www.nice.org.uk/guidance/ta265.

NIEMAN, D.C. et al., 1993. Effects of high- vs moderate-intensity exercise on natural killer cell activity.pdf. *Medicine and Science in Sports and Exercise*, 25(10), pp.1126–1134.

Nieman, D.C., Carolina, N. & Immune, D.C., 1997. Immune response to heavy exertion. *Journal of Applied Physiology*, 82(5), pp.1385–1394.

Noble, B.S. et al., 2003. Mechanical loading : biphasic osteocyte survival and targeting of osteoclasts for bone destruction in rat cortical bone. *American Journal of Physiology. Cell Physiology*, 248(4), pp.934–943.

Noelle, R.J. & Nowak, E.C., 2010. Cellular sources and immune functions of interleukin-9. *Nature Reviews. Immunology*, 10, pp.683–687.

Nørgaard, M. et al., 2010. Skeletal Related Events , Bone Metastasis and Survival of Prostate Cancer : A Population Based Cohort Study in Denmark ( 1999 to 2007 ). *The Journal f Urology*, 184(1), pp.162–167.

Novotny, S.A. et al., 2013. Vibration platform for mice to deliver precise , low intensity mechanical signals to the musculoskeleton. *Journal of Musculoskeletal and Neuronal Interactions*, 13(4), pp.412–417.

O'Connor, J.A., Lanyon, L.E. & MacFie, H., 1982. The influence of strain rate on adaptive bone remodelling. *Journal of Biomechanics*, 15(10), pp.767–781.

Oefelein, M.G. et al., 2002. SKELETAL FRACTURES NEGATIVELY CORRELATE WITH OVERALL SURVIVAL IN MEN WITH PROSTATE CANCER . *The Journal f Urology*, 168(3), pp.1005–1007.

Oliviero, S., Giorgi, M. & Ara, E.D., 2018. Validation of finite element models of the mouse tibia using digital volume correlation. *Journal of the Mechanical Behavior of Biomedical Materials*, 86(March), pp.172–184. Available at: https://doi.org/10.1016/j.jmbbm.2018.06.022.

Ordan, M.A.J.J. et al., 2005. VIBRATION TRAINING: AN OVERVIEW OF THE AREA, TRAINING CONSEQUENCES, AND FUTURE CONSIDERATIONS. *Journal of Strength and Conditioning Research*, 19(2), pp.459–466.

Oshiro, T. et al., 2001. Immunolocalization of Vacuolar-Type H+-ATPase, Cathepsin K , Matrix Metalloproteinase-9 , and Receptor Activator of NFkB Ligand in Odontoclasts During Physiological Root Resorption of Human Deciduous Teeth. *The Anatomical Record*, 264(3), pp.305–311.

Ottewell, P.D. et al., 2014. Castration-induced bone loss triggers growth of disseminated prostate cancer cells in bone. *Endocrine-Related Cancer*, 21(5), pp.769–781.

Ozcivici, E., Garman, R. & Ã, S.J., 2007. High-frequency oscillatory motions enhance the simulated mechanical properties of non-weight bearing trabecular bone. *Journal of Biomechanics*, 40, pp.3404–3411.

Paddock, S.W., 2000. Principles and practices of laser scanning confocal microscopy. *Molecular biotechnology*, 16(2), pp.127–149.

Page, J.M. et al., 2015. Matrix rigidity regulates the transition of tumor cells to a bone- destructive phenotype through integrin b 3 and TGF- b receptor type II. *Biomaterials*, 64, pp.33–44. Available at: http://dx.doi.org/10.1016/j.biomaterials.2015.06.026.

Paget, S., 1889. THE DISTRIBUTION OF SECONDARY GROWTHS IN CANCER OF THE BREAST. *The Lancet*, 133(3421), pp.571–573.

Pahl, A. et al., 2018. Feasibility of whole body vibration during intensive chemotherapy in patients with hematological malignancies – a randomized controlled pilot study. *BMC Cancer*, 18(1), pp.1–12.

Pandya, P.H. et al., 2016. The Immune System in Cancer Pathogenesis : Potential Therapeutic Approaches. *Journal of immunology research*, 2016.

Parfitt, A.M. et al., 1987. Bone Histomorphometry:Standardization of Nomenclature, Symbols, and Units. *Journal of Bone and Mineral Research*, 2(6), pp.595–610.

Patel, H. et al., 2017. Aerobic vs anaerobic exercise training effects on the cardiovascular system. *World Journal of Cardiology*, 9(2), pp.134–138.

Patel, T.K., Brodt, M.D. & Silva, M.J., 2014. Experimental and finite element analysis of strains induced by axial tibial compression in young-adult and old female C57Bl/6 mice. *Journal of Biomechanics*, 47(2), pp.451–457.

Pautke, C. et al., 2004. Characterization of Osteosarcoma Cell Lines MG-63 , Saos-2 and U-2 OS in Comparison to Human Osteoblasts. *Anticaner Research*, 24, pp.3743–3748.

Peake, J. et al., 2004. Changes in neutrophil surface receptor expression , degranulation , and respiratory burst activity after moderate- and high-intensity exercise. *Journal of Applied Physiology*, 97, pp.612–618.

Pedersen, B.K. & Febbraio, M.A., 2008. Muscle as an Endocrine Organ : Focus on Muscle-Derived Interleukin-6. *Physiological Reviews*, 88(4), pp.1379–1406.

Pedersen, L. et al., 2016. Voluntary running suppresses tumor growth through epinephrine- and IL-6-dependent NK cell mobilization and redistribution. *Cell Metabolism*, 23(3), pp.554–562.

Peel, J.B. et al., 2009. A prospective study of cardiorespiratory fitness and breast cancer mortality. *Medicine and Science in Sports and Exercise*, 41(4), pp.742–748.

Pel, J.J.M. et al., 2009. Platform accelerations of three different whole-body vibration devices and the transmission of vertical vibrations to the lower limbs. *Medical Engineering & Physics*, 31, pp.937–944.

Perry, C.M. & Figgitt, D.P., 2004. Zoledronic Acid: A Review of its Use in Patients

with Advanced Cancer. *Adis Review*, 64(11), pp.1197–1211.

Pettersson, U., Nordstro, P. & Alfredson, H., 2000. Effect of High Impact Activity on Bone Mass and Size in Adolescent Females: A Comparative Study Between Two Different Types of Sports. *Calcified Tissue International*, 67, pp.207–214.

Phan, T.G. & Croucher, P.I., 2020. The dormant cancer cell life cycle. *Nature Reviews Cancer*, 20(7), pp.398–411. Available at: http://dx.doi.org/10.1038/s41568-020-0263-0.

Pickup, M.W., Mouw, J.K. & Weaver, V.M., 2014. The extracellular matrix modulates the hallmarks of cancer. *EMBO Reports*, 15(12), pp.1243–1253.

Pinzone, J.J. et al., 2009. The role of Dickkopf-1 in bone development, homeostasis, and disease. *Blood*, 113(3), pp.517–525.

Pohanka, M., 2018. Overview of Piezoelectric Biosensors, Immunosensors and DNA Sensors and Their Applications. *Materials*, 11(3), p.448.

Pompili, L. et al., 2016. Patient-derived xenografts : a relevant preclinical model for drug development. *Journal of Experimental & Clinical Cancer Research*, 35(189), pp.1–8. Available at: http://dx.doi.org/10.1186/s13046-016-0462-4.

Power, C.A. et al., 2009. A Novel Model of Bone-Metastatic Prostate Cancer in Immunocompetent Mice. *The Prostate*, 69, pp.1613–1623.

Prasad, J. & Goyal, A., 2019. An Invertible Mathematical Model of Cortical Bone ' s Adaptation to Mechanical Loading. *Scientific Reports*, 9(5890), pp.1–14. Available at: http://dx.doi.org/10.1038/s41598-019-42378-5.

Price, T.T. et al., 2016. Dormant breast cancer micrometastases reside in specific bone marrow niches that regulate their transit to and from bone. *Science Translational Medicine*, 8(340), pp.1–12.

Prioreschi, A. et al., 2012. Whole Body Vibration Increases Hip Bone Mineral Density in Road Cyclists. *International Journal of Sports Medicine*, 33(8), pp.593–9.

Prostate Cancer UK, 2022. Prostate Cancer UK. Available at: https://prostatecanceruk.org/prostate-information/are-you-at-risk [Accessed March 12, 2022].

Pyne, P.L.H.D.B. & Barnes, W.G.H.C.J., 2010. Lower white blood cell counts in elite athletes training for highly aerobic sports. *European Journal of Applied Physiology*, 10, pp.925–932.

Rachner, T.D. et al., 2014. High serum levels of Dickkopf-1 are associated with a poor prognosis in prostate cancer patients. *BMC Cancer*, 14(649), pp.1–6.

Rauber, S. et al., 2017. Resolution of inflammation by interleukin-9-producing type 2 innate lymphoid cells. *Nature Medicine*, 23(8), pp.938–944.

Rauch, F. et al., 2010. Reporting whole-body vibration intervention studies: Recommendations of the International Society of Musculoskeletal and Neuronal Interactions. *Journal of Musculoskeletal and Neuronal Interactions*, 10(3), pp.193–198.

Recasens, A. & Munoz, L., 2019. Targeting Cancer Cell Dormancy. *Trends in*

*Pharmacological Sciences*, 40(2), pp.128–141. Available at: https://doi.org/10.1016/j.tips.2018.12.004.

Ren, D. et al., 2019. Wnt5a induces and maintains prostate cancer cells dormancy in bone. *Journal of Experimental Medicine*, 216(2), pp.428–449.

Resegofetse, N., Liu, S. & Zhang, Y., 2018. Fates of CD8 + T cells in Tumor Microenvironment. *Computational and Structural Biotechnology Journal*, 17, pp.1–13. Available at: https://doi.org/10.1016/j.csbj.2018.11.004.

Rhee, H. et al., 2015. Adverse effects of androgen-deprivation therapy in prostate cancer and their management. *BJU International*, 115(5), pp.3–13.

Richman, E.L. et al., 2011. Physical activity after diagnosis and risk of prostate cancer progression: data from the Cancer of the Prostate Strategic Urologic Research Endeavor. *Cancer Research*, 71(11), pp.3889–3895.

Rigby, P.J. & Goldie, R.G., 1999. Confocal microscopy in biomedical research. *Croatian medical journal*, 40(3), pp.346–352.

Robinson, J.A. et al., 2006. Wnt/β-Catenin Signaling Is a Normal Physiological Response to Mechanical Loading in Bone. *Journal of Biological Chemistry*, 281(42), pp.31720–31728. Available at: http://dx.doi.org/10.1016/S0021-9258(19)84086-3.

Robling, A.G. et al., 2008a. Mechanical Stimulation of Bone in Vivo Reduces Osteocyte Expression of Sost/Sclerostin. *Journal of Biological Chemistry*, 283(9), pp.5866–5875. Available at: http://dx.doi.org/10.1074/jbc.M705092200.

Robling, A.G. et al., 2008b. Mechanical Stimulation of Bone in Vivo Reduces Osteocyte Expression of Sost / Sclerostin. *Journal of Biological Chemistry*, 283(9), pp.5866–5875. Available at: http://dx.doi.org/10.1074/jbc.M705092200.

Robling, A.G., Burr, D.B. & Turner, C.H., 2000. Partitioning a Daily Mechanical Stimulus into Discrete Loading Bouts Improves the Osteogenic Response to Loading. *Journal of Bone and Mineral Research*, 15(8), pp.1596–1602.

Rochefort, G.Y., Pallu, S. & Benhamou, C.L., 2010. Osteocyte: the unrecognized side of bone tissue. *Osteoporos Int*, 1(21), pp.1457–1469.

Rowe, P.S.N. et al., 2005. Surface plasmon resonance (SPR) confirms that MEPE binds to PHEX via the MEPE–ASARM motif: a model for impaired mineralization in X-linked rickets (HYP). *Bone*, 36(1), pp.33–46.

Ruan, X.-Y. et al., 2008. Effects of vibration therapy on bone mineral density in postmenopausal women with osteoporosis. *Chinese Medical Journal*, 121(13), pp.1155–1158.

Rubin, C. et al., 2001. Low mechanical signals strengthen long bones. *Nature*, 412, pp.603–604.

Rubin, C. et al., 2004. Prevention of Postmenopausal Bone Loss by a Low-Magnitude, High- Frequency Mechanical Stimuli: A Clinical Trial Assessing Compliance, Efficacy, and Safety. *Journal of Bone and Mineral Research*, 19(3).

Rubin, C. et al., 2003. Transmissibility of 15-Hertz to 35-Hertz Vibrations to the

Human Hip and Lumbar Spine: Determining the Physiologic Feasibility of Delivering Low-Level Anabolic Mechanical Stimuli to Skeletal Regions at Greatest Risk of Fracture Because of Osteoporosis. *Spine*, 28(23), pp.2621–2627.

Rubin, C. & Lanyon, L., 1984. Regulation of bone formation by applied dynamic loads. *Journal of Bone and Joint Surgery*, 66(3), pp.397–402.

Rubin, C.T. et al., 2001. Inhibition of osteopenia by low magnitude , high-frequency mechanical stimuli. *Drug Discovery Today*, 6(16), pp.848–858.

Rucci, N. & Angelucci, A., 2014. Prostate cancer and bone: The elective affinities. *BioMed Research International*, 2014, p.167035.

Rummler, M. et al., 2021. Mechanical loading prevents bone destruction and exerts anti-tumor effects in the MOPC315 . BM . Luc model of myeloma bone disease. *Acta Biomaterialia*, 119, pp.247–258. Available at: https://doi.org/10.1016/j.actbio.2020.10.041.

Rumney, R.M.H. et al., 2012. Application of multiple forms of mechanical loading to human osteoblasts reveals increased ATP release in response to fluid flow in 3D cultures and differential regulation of immediate early genes. *Journal of Biomechanics*, 45(3), pp.549–554.

Rundqvist, H. et al., 2020. Cytotoxic T-cells mediate exercise- induced reductions in tumor growth. *eLife*, 9, pp.1–25.

Rundqvist, H. et al., 2013. Effect of Acute Exercise on Prostate Cancer Cell Growth. *PLoS ONE*, 8(7), p.e67579.

Ruppender, N. et al., 2015. Cellular Adhesion Promotes Prostate Cancer Cells Escape from Dormancy. *PLoS ONE*, 10(6), pp.1–16.

Ruppender, N.S. et al., 2010. Matrix Rigidity Induces Osteolytic Gene Expression of Metastatic Breast Cancer Cells. *PLoS ONE*, 5(11), pp.1–10.

Ruymbeke, B. Van et al., 2014. Whole-body vibration in breast cancer survivors : a pilot study exploring its effects on muscle activity and subjectively perceived exertion. *Internationl Journal of Rehabilitation Research*, 37(4), pp.371–374.

Sá-caputo, D.C. et al., 2014. Whole Body Vibration Exercises and the Improvement of the Flexibility in Patient with Metabolic Syndrome. *Rehabilitation Research and Practice*.

Saatci, O. et al., 2020. Targeting lysyl oxidase (LOX) overcomes chemotherapy resistance in triple negative breast cancer. *Nature Communications*, 11(1), pp.1–17. Available at: http://dx.doi.org/10.1038/s41467-020-16199-4.

Sadikot, R.T. & Blackwell, T.S., 2005. Bioluminescence Imaging. *Proceedings of the American Thoracic Society*, 2(6), pp.537–540. Available at: http://pats.atsjournals.org/cgi/doi/10.1513/pats.200507-067DS.

Saeidifard, F. et al., 2019. The association of resistance training with mortality : A systematic review and meta-analysis. *European Journal of Preventive Cardiology*, 26(15), pp.1647–1665.

Salameh, A. & Dhein, S., 2013. Effects of mechanical forces and stretch on intercellular gap junction coupling. *Biochimica et Biophysica Acta - Biomembranes*, 1828(1), pp.147–156. Available at: http://dx.doi.org/10.1016/j.bbamem.2011.12.030.

Saldaña, L. et al., 2011. In search of representative models of human bone-forming cells for cytocompatibility studies. *Acta Biomaterialia*, 7, pp.4210–4221.

Salhi, B. et al., 2015. Rehabilitation in patients with radically treated respiratory cancer: A randomised controlled trial comparing two training modalities. *Lung Cancer*, 89(2), pp.167–174. Available at: http://dx.doi.org/10.1016/j.lungcan.2015.05.013.

Samoszuk, M., Leuther, M. & Hoyle, N., 2008. Role of serum P1NP measurement for monitoring treatment response in osteoporosis. *Biomarkers in Medicine*, 2(5), pp.495–508.

Sample, S.J. et al., 2008. Functional adaptation to loading of a single bone is neuronally regulated and involves multiple bones. *Journal of Bone and Mineral Research*, 23(9), pp.1372–1381.

Santos, A. et al., 2011. Mechanical loading stimulates BMP7, but not BMP2, production by osteocytes. *Calcified Tissue International*, 89(4), pp.318–326.

Sathiakumar, N. et al., 2011. Mortality following bone metastasis and skeletal-related events among men with prostate cancer: a population-based analysis of US Medicare beneficiaries, 1999–2006. *Prostate Cancer and Prostatic Diseases*, 14(1), pp.177–183. Available at: http://dx.doi.org/10.1038/pcan.2011.7.

Schaffler, M.B. et al., 2014. Osteocytes: Master Orchestrators of Bone. *Calcified Tissue International*, 94(1), pp.5–24.

Schneider, S. et al., 2009. EEG activity and mood in health orientated runners after different exercise intensities. *Physiology & Behavior*, 96(4–5), pp.709–716. Available at: http://dx.doi.org/10.1016/j.physbeh.2009.01.007.

Schoutens, A., Laurent, E. & Poortmans, J.R., 2012. Effects of Inactivity and Exercise on Bone. *Sports Medicine*, 7, pp.71–81.

Schumacher, D. et al., 2013. Platelet-Derived Nucleotides Promote Tumor-Cell Transendothelial Migration and Metastasis via P2Y2 Receptor. *Cancer Cell*, 24(1), pp.130–137. Available at: http://dx.doi.org/10.1016/j.ccr.2013.05.008.

Scott, J.P.R. et al., 2012. Effect of fasting versus feeding on the bone metabolic response to running. *Bone*, 51(6), pp.990–999. Available at: http://dx.doi.org/10.1016/j.bone.2012.08.128.

Segal, R. et al., 2017. Exercise for people with cancer : a systematic review. *Current Oncology*, 24(4), p.e290–e315.

Senthebane, D.A. et al., 2018. The Role of Tumor Microenvironment in Chemoresistance : 3D Extracellular Matrices as Accomplices. *International Journal of Molecular Sciences*, 19, p.2861.

Shah, K. & Maghsoudlou, P., 2016. Enzyme-linked immunosorbent assay (ELISA): the basics. *British Journal of Hospital Medicine*, 77(7), pp.98–101.

Shanb, A.A. & Youssef, E.F., 2014. The impact of adding weight - bearing exercise versus nonweight bearing programs to the medical treatment of elderly patients with osteoporosis. *Journal of Family and Community Medicine*, 21(3), pp.176–181.

Shi, H.F. et al., 2010. Low-magnitude high-frequency vibration treatment augments fracture healing in ovariectomy-induced osteoporotic bone. *Bone*, 46(5), pp.1299–1305. Available at: http://dx.doi.org/10.1016/j.bone.2009.11.028.

SHINKAI, S. et al., 1995. Physical activity and immune senescence in men.pdf. *Medicine and Science in Sports and Exercise*, 27(11), pp.1516–1526.

Shiozawa, Y. et al., 2010. GAS6/AXL Axis Regulates Prostate Cancer Invasion, Proliferation, and Survival in the Bone Marrow Niche. *Neoplasia*, 12(2), pp.116–127. Available at: http://linkinghub.elsevier.com/retrieve/pii/S1476558610800910.

Shiozawa, Y. et al., 2011. Human prostate cancer metastases target the hematopoietic stem cell niche to establish footholds in mouse bone marrow. *The Journal of Clinical Investigation*, 121(4), pp.1298–1312. Available at: http://www.ncbi.nlm.nih.gov/pubmed/7891183.

Siclari, V.A. & Qin, L., 2010. Targeting the osteosarcoma cancer stem cell. *Journal of Orthopaedic Surgery and Research*, 5(78), pp.1–10.

Silder, A. et al., 2015. Running with a load increases leg stiffness. *Journal of Biomechanics*, 48(6), pp.1003–1008.

Simoneau, A.R., 2006. Treatment- and disease-related complications of prostate cancer. *Reviews in Urology*, 8(2), pp.56–67. Available at: http://www.ncbi.nlm.nih.gov/pubmed/17021643.

Simpson, R.J. et al., 2012. Exercise and the aging immune system. *Ageing Research Reviews*, 11(3), pp.404–420. Available at: http://dx.doi.org/10.1016/j.arr.2012.03.003.

Simpson, R.J. et al., 2015. Exercise and the Regulation of Immune Functions. In *Molecular and Cellular Regulation of Adaptation to Exercise*. Elsevier Inc., pp. 355–380. Available at: http://dx.doi.org/10.1016/bs.pmbts.2015.08.001.

Skerry, T.M., 1997. Mechanical loading and bone: What sort of exercise is beneficial to the skeleton? *Bone*, 20(3), pp.179–181.

Skoumal, M. et al., 2005. Serum cathepsin K levels of patients with longstanding rheumatoid arthritis: correlation with radiological destruction. *Arthritis Research and Therapy*, 7(1), pp.65–70.

Smeda, M. et al., 2017. Breast cancer pulmonary metastasis is increased in mice undertaking spontaneous physical training in the running wheel ; a call for revising beneficial effects of exercise on cancer progression. *American Journal of Cancer Research*, 7(9), pp.1926–1936.

Smith, J.K., 2016. Exercise , interleukins and bone homeostasis. *Integrative Molecular Medicine*, 3(5), pp.802–804.

Smith, M.R. et al., 2002. Changes in Body Composition during Androgen Deprivation

Therapy for Prostate Cancer. *The Journal of Clinical Endocrinology & Metabolism*, 87(2), pp.599–603.

Sneddon, L.U., Halsey, L.G. & Bury, N.R., 2017. Considering aspects of the 3Rs principles within experimental animal biology. *The Company of Biologists*, 220, pp.3007–3016.

Snow-harter, C. et al., 1992. Effects of Resistance and Endurance Exercise on Bone Mineral Status of Young Women : A Randomized Exercise Intervention Trial. *Journal of Bone and Mineral Research*, 7(7), pp.761–769.

So, A. et al., 2012. Management of skeletal-related events in patients with advanced prostate cancer and bone metastases: Incorporating new agents into clinical practice. *Journal of the Canadian Urological Association*, 6(6), pp.465–470.

Sobel, R. & Sadar, M., 2005. Cell Lines Used in Prostate Cancer Research: a Compendium of Old and New Lines—Part 1. *The Journal of Urology*, 173(2), pp.342–359. Available at: http://linkinghub.elsevier.com/retrieve/pii/S0022534705604685.

Søe, K. & Delaissé, J., 2017. Time-lapse reveals that osteoclasts can move across the bone surface while resorbing Journal of Cell Science • Advance article. *Journal of Cell Science*, 130(12), pp.2026–2035.

Song, J. et al., 2010. An in vivo model to study and manipulate the hematopoietic stem cell niche. *Blood*, 115(13), pp.2592–2601.

Souza, D. et al., 2021. Acute and Chronic Effects of Interval Training on the Immune System: A Systematic Review with Meta-Analysis. *Biology*, 10(9), p.868.

De Souza, R.L., Matsuura, M., et al., 2005. Non-invasive axial loading of mouse tibiae increases cortical bone formation and modifies trabecular organization: A new model to study cortical and cancellous compartments in a single loaded element. *Bone*, 37(6), pp.810–818.

De Souza, R.L., Pitsillides, A.A., et al., 2005. Sympathetic nervous system does not mediate the load-induced cortical new bone formation. *Journal of Bone and Mineral Research*, 20(12), pp.2159–2168.

Soysa, N.S. & Alles, N., 2018. The role of IL - 3 in bone. *Journal of Cellular Biochemistry*, 120(5), pp.6851–6859.

Srenathan, U., Steel, K. & Taams, L.S., 2016. IL-17+ CD8+ T cells: Differentiation, phenotype and role in inflammatory disease. *Immunology Letters*, 178, pp.20–26.

Srinivasan, S. et al., 2006. Low-magnitude mechanical loading becomes osteogenic when rest is inserted between each load cycle. *Journal of Bone and Mineral Research*, 17(9), pp.1613–1620.

Srivastava, R.K. et al., 2010. IL-3 Inhibits Human Osteoclastogenesis and Bone Resorption through Downregulation of c-Fms and Diverts the Cells to Dendritic Cell Lineage. *The Journal of Immunology*, 185(4), pp.2261–2272.

Stadelmann, V.A., Bonnet, N. & Pioletti, D.P., 2011. Combined effects of zoledronate and mechanical stimulation on bone adaptation in an axially loaded mouse tibia.

*Clinical Biomechanics*, 26(1), pp.101–105. Available at: http://dx.doi.org/10.1016/j.clinbiomech.2010.08.014.

Stamatakis, E. et al., 2018. Systematic Reviews and Meta- and Pooled Analyses Does Strength-Promoting Exercise Confer Unique Health Bene fi ts ? A Pooled Analysis of Data on 11 Population Cohorts With All-Cause , Cancer , and Cardiovascular Mortality Endpoints. *American Journal of Epidemiology*, 187(5), pp.1102–1112.

Stanilov, N. et al., 2010. Advanced Colorectal Cancer Is Associated With Enhanced IL-23 and IL-10 Serum Levels. *Laboratory Medicine*, 41(3), pp.159–163.

Stokes, I. et al., 2002. Enlargement of Growth Plate Chondrocytes Modulated by Sustained Mechanical Loading. *THE JOURNAL OF BONE AND JOINT SURGERY*, 84(10).

Strupler, M. et al., 2007. Second harmonic imaging and scoring of collagen in fibrotic tissues. *Optics Express*, 15(7), pp.4054–4065. Available at: https://www.osapublishing.org/abstract.cfm?URI=oe-15-7-4054.

Sugiyama, T. et al., 2012. Bones' adaptive response to mechanical loading is essentially linear between the low strains associated with disuse and the high strains associated with the lamellar/woven bone transition. *Journal of Bone and Mineral Research*, 27(8), pp.1784–1793.

Sugiyama, T., Galea, G.L., et al., 2010. Mechanical loading-related bone gain is enhanced by tamoxifen but unaffected by fulvestrant in female mice. *Endocrinology*, 151(12), pp.5582–5590.

Sugiyama, T. et al., 2008. Mechanical loading enhances the anabolic effects of intermittent parathyroid hormone (1-34) on trabecular and cortical bone in mice. *Bone*, 43(2), pp.238–248.

Sugiyama, T., Price, J.S. & Lanyon, L.E., 2010. Functional adaptation to mechanical loading in both cortical and cancellous bone is controlled locally and is confined to the loaded bones. *Bone*, 46(2), pp.314–321. Available at: http://dx.doi.org/10.1016/j.bone.2009.08.054.

Suzuki, K. et al., 2003. Impact of a Competitive Marathon Race on Systemic Cytokine and Neutrophil Responses. *Medicine and Science in Sports and Exercise*, 35(2), pp.348–355.

Suzuki, K. et al., 2002. Systemic inflammatory response to exhaustive exercise. Cytokine kinetics. *Exercise Immunology Review*, 8, pp.6–48.

Svensson, E. et al., 2017. Survival after bone metastasis by primary cancer type: A Danish population-based cohort study. *BMJ Open*, 7(9), pp.1–7.

Taaffe, D.R. et al., 1997. High-Impact Exercise Promotes Bone Gain in Well-Trained Female Athletes. *Journal of Bone and Mineral Research*, 12(2), pp.255–260.

Taichman, R.S. et al., 2013. GAS6 Receptor Status Is Associated with Dormancy and Bone Metastatic Tumor Formation. *PLoS ONE*, 8(4), pp.1–10.

Talmage, R. V., 1970. Morphological and Physiological Considerations in a New Concept o f Calcium Transport in Bone. *The American Journal of Anatomy*,

129(4), pp.467–476.

Tanaka, H. et al., 1999. Successful Adoptive Immunotherapy of Murine Poorly Immunogenic Tumor with Specific Effector Cells Generated from Gene-Modified Tumor-Primed Lymph Node Cells. *The Journal of Immunology*, 162(2), pp.3574–3582.

Tang, M. et al., 2018. Interferon-Gamma-Mediated Osteoimmunology. *Frontiers in Immunology*, 9, p.1508.

Tang, W. et al., 2011. Osteoblast-specific Transcription Factor Osterix (Osx) Is an Upstream Regulator of Satb2 during Bone Formation. *THE JOURNAL OF BIOLOGICAL CHEMISTRY*, 286(38), pp.32995–33002.

Tehrani, S. et al., 2006. Cortactin Has an Essential and Specific Role in Osteoclast Actin Assembly. *Molecular Biology of the Cell*, 17(7), pp.2882–2895.

Terpos, E. et al., 2019. Multiple Myeloma Bone Disease. *Encyclopedia of Endocrine Diseases (Second Edition)*, 4, pp.329–340.

Thalmann, N. et al., 1994. Androgen-independent Cancer Progression and Bone Metastasis in the LNCaP Model of Human Prostate Cancer. *Cancer Research*, 54(10), pp.2577–2581.

Thiyagarajan, S. et al., 2007. Role of GLI2 Transcription Factor in Growth and Tumorigenicity of Prostate Cells. *Cancer Research*, 67(22), pp.10642–10646.

Thompson, H.J. et al., 1995. Inhibition of Mammary Carcinogenesis by Treadmill Exercise. *JNCI: Journal of the National Cancer Institute*, 87(6), pp.453–455.

Thudi, N.K. et al., 2011. Dickkopf-1 (DKK-1) stimulated prostate cancer growth and metastasis and inhibited bone formation in osteoblastic bone metastases. *Prostate*, 71(6), pp.615–625.

Tomlins, S.A. et al., 2006. Integrative molecular concept modeling of prostate cancer progression. *Nature Genetics*, 39(1), pp.41–51.

Tomlinson, R.E. & Silva, M.J., 2015. HIF-1 α regulates bone formation after osteogenic mechanical loading. *Bone*, 73, pp.98–104. Available at: http://dx.doi.org/10.1016/j.bone.2014.12.015.

Townsend, N. et al., 2015. Physical activity statistics. *Physical Activity Statistics 2015. British Heart Foundation: London.*, pp.1–128. Available at: http://www.publichealth.ox.ac.uk/bhfhprg.

Turner, C.H. et al., 1991. A noninvasive, in vivo model for studying strain adaptive bone modeling. *Bone*, 12(2), pp.73–79.

Turner, C.H., Forwood, M.R. & Al, T.E.T., 1994. Mechanical Loading Thresholds for Lamellar and Woven Bone Formation. *Journal of Bone and Mineral Research*, 9(1), pp.87–97.

Turvey, S.E. & Broide, D.H., 2010. Innate Immunity. *The Journal of Allergy and Clinical Immunology*, 125(2 Suppl 2), pp.S24–S32.

Ulvestad, M. et al., 2021. Effect of high- - intensity training on bone health and body composition in lung transplant recipients: A secondary analysis of a randomized

controlled trial. *Clinical transplantation*, 35(8), pp.1–9.

Ustione, A. & Piston, D.W., 2011. A simple introduction to multiphoton microscopy. *Journal of Microscopy*, 243(3), pp.221–226.

Uth, J. et al., 2018. Football training over 5 years is associated with preserved femoral bone mineral density in men with prostate cancer. *Scandinavian Journal of Medicine and Science in sports*, 28(1), pp.61–73.

Vaday, G.G. et al., 2005. Expression of CCL5 ( RANTES ) and CCR5 in Prostate Cancer. *The Prostate*, 66(2), pp.124–134.

Vahabi, S., Salman, B.N. & Javanmard, A., 2013. Atomic Force Microscopy Application in Biological Research : A Review Study. *Iranian Journal of Medical Sciences*, 38(2), pp.76–83.

Vainshelboim, B. et al., 2021. Cardiorespiratory fitness and cancer in men with cardiovascular disease : Analysis from the Veterans Exercise Testing Study. *European Society of Cardiology*, 1(28), pp.715–721.

Varambally, S. et al., 2005. Integrative genomic and proteomic analysis of prostate cancer reveals signatures of metastatic progression. *Cancer Cell*, 8(5), pp.393–406.

Verhelle, J. et al., 2009. 3D strain map of axially loaded mouse tibia : a numerical analysis validated by experimental measurements. *Computer Methods in Biomechanics and Biomedical Engineering*, 12(1), pp.95–100.

Verschueren, S.M.P. et al., 2009. Effect of 6-Month Whole Body Vibration Training on Hip Density, Muscle Strength, and Postural Control in Postmenopausal Women: A Randomized Controlled Pilot Study. *Journal of Bone and Mineral Research*, 19(3), pp.352–359.

Vlachopoulos, D. et al., 2018. The effect of a high-impact jumping intervention on bone mass , bone stiffness and fitness parameters in adolescent athletes. *Archives of Osteoporosis*, 13(1), p.128.

Vlaeminck-Guillem, V., 2015. When prostate cancer circulates in the bloodstream. *Diagnostics*, 5(4), pp.428–474.

Walker, C., Mojares, E. & Hernández, A. del R., 2018. Role of Extracellular Matrix in Development and Cancer Progression. *International Journal of Molecular Sciences*, 19(10), p.3028.

Wallace, J.M. et al., 2007. Exercise-Induced Changes in the Cortical Bone of Growing Mice Are Bone and Gender Specific. *Bone*, 40(4), pp.1120–1127.

Walsh, N.P. et al., 2011. Part one: Immune function and exercise. *Exercise Immunology Review (EIR)*, 17, pp.6–63.

Wang, J. et al., 2015. Trabecular Plates and Rods Determine Elastic Modulus and Yield Strength of Human Trabecular Bone. *Bone*, 72, pp.71–80.

Wang, L. et al., 2020. Various pathways of zoledronic acid against osteoclasts and bone cancer metastasis : a brief review. *BMC Cancer*, 20(1059), pp.1–10.

Wang, N., Docherty, F., Brown, H.K., et al., 2015. Mitotic quiescence, but not unique

“stemness,” marks the phenotype of bone metastasis-initiating cells in prostate cancer. *FASEB Journal*, 29(8), pp.3141–3150.

Wang, N., Docherty, F., Brown, H.K., et al., 2015. Mitotic quiescence , but not unique “ stemness , ” marks the phenotype of bone metastasis-initiating cells in prostate cancer. *The FASEB journal*, 29, pp.3141–3150.

Wang, N. et al., 2014. Prostate Cancer Cells Preferentially Home to Osteoblast - rich Areas in the Early Stages of Bone Metastasis : Evidence From In Vivo Models. *Journal of Bone and Mineral Research*, 29(12), pp.2688–2696.

Wang, N., Reeves, K.J., et al., 2015. The frequency of osteolytic bone metastasis is determined by conditions of the soil , not the number of seeds ; evidence from in vivo models of breast and prostate cancer. *Journal of Experimental & Clinical Cancer Research*, 34(124), pp.1–12. Available at: http://dx.doi.org/10.1186/s13046-015-0240-8.

Wang, S. et al., 2021. Moderate tibial loading and treadmill running , but not overloading , protect adult murine bone from destruction by metastasized breast cancer. *Bone*, 153(June), p.116100. Available at: https://doi.org/10.1016/j.bone.2021.116100.

Warburton, D.E.R., Nicol, C.W. & Bredin, S.S.D., 2006. Health benefits of physical activity: the evidence. *Canadian Medical Association Journal*, 174(6), pp.801–809.

Watson, S.L. et al., 2018. High-Intensity Resistance and Impact Training Improves Bone Mineral Density and Physical Function in Postmenopausal Women With Osteopenia and. *Journal of Bone and Mineral Research*, 33(2), pp.211–220.

Weemen, B.K. Van & Schuurs, A.H.W.M., 1971. Immunoassay using antigen—enzyme conjugates. *FEBS Letters*, 15(3), pp.232–236.

Wehrle, E. et al., 2015. The impact of low-magnitude high-frequency vibration on fracture healing is profoundly influenced by the oestrogen status in mice. *Disease Models & Mechanisms*, 8(1), pp.93–104.

Wener, M.H. et al., 2014. A Transient Increase in Eosinophils is Associated with Prolonged Survival in Men with Metastatic Castration-Resistant Prostate Cancer Who Receive Sipuleucel-T. *Cancer Immunology Research*, 2(10), pp.988–999.

Westcott, W.L., 2012. Resistance Training is Medicine : Effects of Strength Training on Health. *Current Sports Medicine Reports*, 11(4), pp.209–216.

de Wet, J.R. et al., 1985. Cloning of firefly luciferase cDNA and the expression of active luciferase in Escherichia coli. *Proceedings of the National Academy of Sciences of the United States of America*, 82(23), pp.7870–7873. Available at: http://www.pubmedcentral.nih.gov/articlerender.fcgi?artid=390871&tool=pmcentrez&rendertype=abstract.

Whyte, M.P., 1994. Hypophosphatasia and the Role of Alkaline Phosphatase in Skeletal Mineralization. *Endocrine Reviews*, 15(4), pp.439–461.

Wiedemeyer, W.R. et al., 2010. Pattern of retinoblastoma pathway inactivation dictates response to CDK4/6 inhibition in GBM. *Proceedings of the National Academy of Sciences of the United States of America*, 107(25), pp.11501–

11506.

Williams, P.T., 2009. Lower prevalence of hypertension, hypercholesterolemia, and diabetes in marathoners. *Medicine and science in sports and exercise*, 41(3), pp.523–529.

Willie, B.M. et al., 2013. Diminished response to in vivo mechanical loading in trabecular and not cortical bone in adulthood of female C57Bl / 6 mice coincides with a reduction in deformation to load. *Bone*, 55(2), pp.335–346. Available at: http://dx.doi.org/10.1016/j.bone.2013.04.023.

Winkler, J., Werb, Z. & Metcalf, K.J., 2020. Concepts of extracellular matrix remodelling in tumour progression and metastasis. *Nature Communications*, 11(5120), pp.1–19. Available at: http://dx.doi.org/10.1038/s41467-020-18794-x.

Wise, D.R. et al., 2020. Dickkopf-1 Can Lead to Immune Evasion in Metastatic Castration-Resistant Prostate Cancer. *JCO Precision Oncology*, 4, pp.1167–1179.

Wong, S.K. et al., 2019. Prostate Cancer and Bone Metastases: The Underlying Mechanisms. *International Journal of Molecular Sciences*, 20(10), p.2587.

Woods, J.A. et al., 2009. Cardiovascular exercise training extends influenza vaccine seroprotection in sedentary older adults: the immune function intervention trial. *Journal of the American Geriatrics Society*, 57(12), pp.2183–2191.

Woods, J.A. et al., 1999. Effects of 6 months of moderate aerobic exercise training on immune function in the elderly. *Mechanisms of ageing and development*, 109(1), pp.1–19.

Wu, A.H.B., 2006. A selected history and future of immunoassay development and applications in clinical chemistry. *Clinica Chimica Acta*, 369(2), pp.119–124.

Xiao, M. et al., 2017. Osteoblasts support megakaryopoiesis through production of interleukin-9. *Blood*, 129(24), pp.3196–3209. Available at: http://dx.doi.org/10.1182/blood-2016-11-749838.

Xu, J.M.D. et al., 2009. Signal transduction in electrically stimulated articular chondrocytes involves translocation of extracellular calcium through voltage-gated channels 1. *Osteoarthritis and Cartilage*, 17(3), pp.397–405. Available at: http://dx.doi.org/10.1016/j.joca.2008.07.001.

Xu, Y. et al., 2015. Downregulation of MicroRNA-152 contributes to high expression of DKK1 in multiple myeloma. *RNA Biology*, 12(12), pp.1314–1322.

Yalow, B.R.S. & Berson, S.A., 1960. IMMUNOASSAY OF ENDOGENOUS PLASMA INSULIN IN MAN. *The Journal of Clinical Investigation*, 39(7), pp.1157–1175.

Yang, H. et al., 2014. Characterization of cancellous and cortical bone strain in the in vivo mouse tibial loading model using microCT-based finite element analysis. *Bone*, 66, pp.131–139. Available at: http://dx.doi.org/10.1016/j.bone.2014.05.019.

Yang, S. et al., 2019. Ankle loading ameliorates bone loss from breast cancer–associated bone metastasis. *The FASEB journal*, 33(10), p.10742–10752.

Ye, L., Kynaston, H.G. & Jiang, W.G., 2007. Bone metastasis in prostate cancer: Molecular and cellular mechanisms (Review). *International Journal of Molecular Medicine*, 20(1), pp.103–111.

Yokota, H., 2021. Mechanical Loading-Driven Tumor Suppression Is Mediated by Lrp5-Dependent and Independent Mechanisms. *Cancers*, 13(267), pp.1–17.

You, L. et al., 2009. Osteocytes as Mechanosensors in the Inhibition of Bone Resorption Due to Mechanical Loading. *Bone*, 42(1), pp.172–179.

Yu, C. et al., 2016. Intra-iliac Artery Injection for Efficient and Selective Modeling of Microscopic Bone Metastasis. *Journal of Visualized Experiments*, 115, pp.1–7.

Yu, G. et al., 2018. Osteoblast-secreted factors mediate dormancy of metastatic prostate cancer in the bone via activation of the TGFβRIII-p38MAPK-pS249/T252RB pathway. *Cancer Research*, 78(11), pp.2911–24.

Yu, G. et al., 2019. Osteoblast-secreted factors mediate dormancy of metastatic prostate cancer in the bone via activation of the TGFβRIII-p38MAPK-pS249/T252RB pathway. *Cancer Research*, 78(11), pp.2911–2924.

Yu, Y.P. et al., 2004. Gene Expression Alterations in Prostate Cancer Predicting Tumor Aggression and Preceding Development of Malignancy. *Journal of Clinical Oncology*, 22(14), pp.2790–9.

Yuan, Y. et al., 2016. The roles of exercise in bone remodeling and in prevention and treatment of osteoporosis. *Progress in Biophysics and Molecular Biology*, 122(2), pp.122–130. Available at: http://dx.doi.org/10.1016/j.pbiomolbio.2015.11.005.

Yue, Z. et al., 2022. RSPO2 and RANKL signal through LGR4 to regulate osteoclastic premetastatic niche formation and bone metastasis. *The Journal of Clinical Investigation*, 132(2), pp.1–19.

Yumoto, K. et al., 2016. Axl is required for TGF- β 2-induced dormancy of prostate cancer cells in the bone marrow. *Scientific Reports*, 6, pp.1–16.

Yunfeng, G. et al., 2017. Exercise overcome adverse effects among prostate cancer patients receiving androgen deprivation therapy. *Medicine*, 96(27).

Zahm, A.M. et al., 2010. Numerical modeling of oxygen distributions in cortical and cancellous bone: oxygen availability governs osteonal and trabecular dimensions. *American Journal of Physiology. Cell Physiology*, 299(5), pp.922–929.

Zayzafoon, M., 2006. Calcium/Calmodulin Signaling Controls Osteoblast Growth and Differentiation. *Journal of Cellular Biochemistry*, 97(1), pp.56–70.

Zekri, J., Mansour, M. & Mustafa, S., 2014. The anti-tumour effects of zoledronic acid. *Journal of Bone Oncology*, 3(1), pp.25–35. Available at: http://dx.doi.org/10.1016/j.jbo.2013.12.001.

Zenobia, C. & Hajishengallis, G., 2016. Basic biology and role of interleukin-17 in immunity and inflammation. *Periodontology 2000*, 69(1), pp.142–159.

Zheng, X. et al., 2008. Inhibitory effect of voluntary running wheel exercise on the

growth of human pancreas Panc-1 and prostate PC-3 xenograft tumors in immunodeficient mice. *Oncology Reports*, 19(6), pp.1583–1588.

Zhong, L. et al., 2020. Intra-arterial injection to create bone metastasis of prostate cancer in mice. *American Journal of Clinical and Experimental Urology*, 8(4), pp.93–100.

Zinn, K.R. et al., 2008. Noninvasive bioluminescence imaging in small animals. *ILAR journal / National Research Council, Institute of Laboratory Animal Resources*, 49(1), pp.103–115. Available at: http://www.ncbi.nlm.nih.gov/pubmed/18172337%5Cnhttp://www.pubmedcentral.nih.gov/articlerender.fcgi?artid=PMC2614121.

Ziouti, F. et al., 2017. Targeted Remodeling of the Tumor Microenvironment Via Mechanical Stimulation Defines a Novel Therapeutic Strategy in Myeloma Bone Disease. *Blood*, 130(1), p.1778.